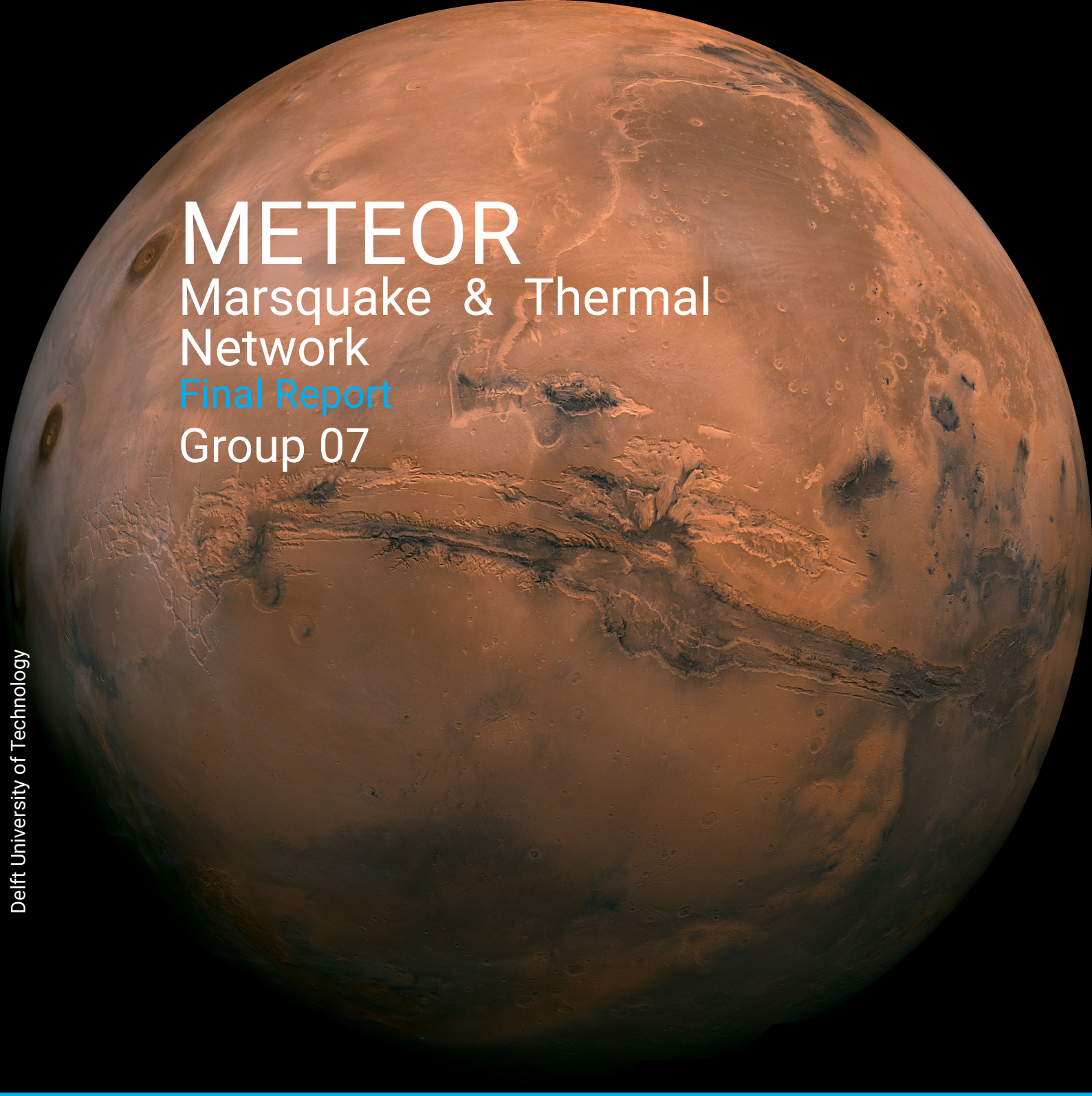

METEOR

Marsquake & Thermal Network

Final Report

Group 07

Delft University of Technology

TU Delft

This page was left blank intentionally.

METEOR

Marsquake & Thermal Network

Final Report

by

Group 07

Name	Student ID
Mees Beumer	4648838
Thijs Bolscher	4656717
Marnix Enting	4659147
Martijn Kanger	4645952
Mohamed Khalifa	4646339
Luigi Maiorano	4431138
Dong-Hyuk Na	4648846
Elrawy Soliman	4684443
Filippo Tagliacarne	4670930
Alexis van Wissen	4676793
Andreas Zafiropoulos	4474538

June 30, 2020

To obtain the degree of Bachelor of Science at Delft University of Technology,

Project duration: April 20, 2020 – July 2, 2020
Supporting Staff: Dr. ir. B.C. Root,
Dr. S.J. de Vet,
B. Rattanagraikanakorn, MSc

Cover image from NASA photo archive [1]

TU Delft

Nomenclature

Physical Constants

μ_{earth}	Earth's standard gravitational parameter	$0.39860 \cdot 10^6$ km^3/s^2
μ_{mars}	Mars' standard gravitational parameter	$0.042828 \cdot 10^6$ km^3/s^2
μ_{sun}	Sun's standard gravitational parameter	$132,712.0 \cdot 10^6$ km^3/s^2
c	Speed of light	299792458 m/s
G	Gravitational constant	$6.67384 \cdot 10^{-11}$ N m^2/kg^2
g_0	Earth surface gravitational acceleration	9.807 m/s^2
g_{mars}	Mars surface gravitational acceleration	3.711 m/s^2
$J2_{mars}$	Mars' oblateness perturbation	$1960.45 \cdot 10^{-6}$ /
k	Boltzmann constant	$1.38064852 \cdot 10^{-23}$ m^2 kg s^{-2} K^{-1}
r_{earth}	Earth's orbital radius around the Sun	$149.6 \cdot 10^6$ km
R_{mars}	Mars' mean radius	3389.5 km
r_{mars}	Mars' orbital radius around the Sun	$227.92 \cdot 10^6$ km
sol	One Mars solar day	88775 s

Symbols

$\dot{q}$	Heat flux	W/m^2
α	Thermal expansion coefficient	m/K
ΔT	Temperature Difference	K
ΔV	Velocity increment	m/s
γ	Flight path angle	°
κ	Main input variable of subsystem design	/
Λ	Latitude	°
λ	Longitude	°
λ	Wavelength	m
r	Position vector	(m,m,m)
μ	Standard gravitational parameter	m^3/s^2
ν	True anomaly	rad
Ω	Right ascension of the ascending node	°
ω	Argument of periapsis	°
ω	Rotational rate	rad/s
ρ	Density	kg/m^3
σ	Standard deviation	/
σ	Stress	Pa
Υ	Sensitivity	/
ε	Elevation	°
ε	Obliquity of ecliptic	°
ζ	Main output of subsystem design	/
a	Acceleration	kg m/s^2
a	Semi-major axis	m
AR	Acquisition rate	1/s
C_D	Drag coefficient	/
d	Distance	m
E	Eccentric anomaly	rad
E	Energy	J

E	Young's Modulus	$(\mathrm{kg/m})/s^2$
e	Orbital eccentricity	/
E_b	Energy per bit	W
F	Force	N
f	Frequency	Hz
$f_{eclipse}$	Fraction of orbit in eclipse	/
G	Antenna gain	/
g	Gravitational acceleration	$\mathrm{kg\,m/s^2}$
H	Scale height	m
h	Height	m
h	Orbit altitude	m
i	Orbital inclination	°
I_{sp}	Specific impulse	s
L	Loss factor	/
l	Length	m
$L_\odot$	Sun's ecliptic longitude	rad
M	Mean anomaly	rad
M	Memory size	bit
m	Mass	kg
n	Mean motion	rad/s
N_0	Noise power	W
P	Orbital period	s
P	Power	W
p	Probability	/
R	Data rate	bit/s
R	Planet radius	m
r	Orbit radius	m
S	Surface area	$\mathrm{m^2}$
s	Slant range	m
T	Period	s
T	Temperature	K
T	Torque	N m
t	Thickness	m
t	Time	s
V	Velocity	m/s

Abbreviations

$\mathrm{HP^3}$	Heat flow and Physical Properties Package
ACS	Attitude Control System
AOCS	Attitude and Orbital Control System
BER	Bit Error Rate
C&DH	Command and Data Handling
CG	Center of Gravity
CNSA	China National Space Agency
COSPAR	Committee on Space Research
CPU	Central Processing Unit
DC	Direct Current
DOT	Design Option Tree
DSE	Design & Synthesis Exercise
DSN	Deep Space Network

EDL	Entry, Descent and Landing
EM	Engineering Model
EOL	End Of Life
EPS	Electrical Power System
ESA	European Space Agency
ESOC	European Space Operations Centre
EUT	Electra UHF Transmitter
FBD	Full Body Diagram
FEM	Finite Element Method
FM	Flight Model
GPS	Global Positioning System
HF	High Frequency
HGA	High Gain Antenna
HiRISE	High Resolution Imaging Science Experiment
InSight	Interior Exploration using Seismic Investigations, Geodesy and Heat Transport
ITU	International Telecommunication Union
JAXA	Japan Aerospace Exploration Agency
KIPS	Thousand Instructions Per Second
LCA	Life Cycle Analysis
LF	Low Frequency
LGA	Low Gain Antenna
LM	Lean Manufacturing
LMO	Low Martian Orbit
METEOR	MarsquakE and Thermal nEtwORk
MGS	Mars Global Surveyor
MIMU	Miniture Inertial Measurement Unit
MLI	Multi Layer Insulation
MR	Mars Reveal
MRO	Mars Reconnaissance Orbiter
MRT	Market
MSL	Mars Science Laboratory
N/A	Not Applicable
NASA	National Aeronautics and Space Administration
OBC	Onboard Computer
OCS	Orbital Control System
PPR	Planetary Protection Rules
PSK	Phase Shift Keying
PSP	Primary Science Phase
QM	Qualification Model
QMR	Quadruple Modular Redundancy
RAMS	Reliability, Availability, Maintainability, and Safety
RDA	Radar Doppler Altimeter
RDT&E	Research, Development, Testing & Evaluation
RF	Radio Frequency
RFDU	Radio Frequency Distribution Unit
RTG	Radioisotope Thermal Generator
S/C	Spacecraft
SDST	Small Deep Space Transponder
SEIS	Seismic Experiment for Internal Structure

SF	Safety Factor
SMAD	Space Mission Analysis and Design (Book)
SNR	Signal-to-Noise Ratio
SP	Short Period
SR	System Requirement
STM	Structural and Thermal Model
STRCT	Structure
SWOT	Strengths, Weaknesses, Opportunities and Threats
TAS-I	Thales Alenia Space - Italia
TBC	To Be Confirmed
TBD	To Be Determined
TCP	Transmission Control Protocol
TDS	Terminal Descent Sensor
TES	Thermal Emission Spectrometer
TFU	Theoretical First Unit
TGO	Trace Gas Orbiter
TL	Top Level
TMR	Triple Modular Redundancy
TRL	Technology Readiness Level
TT&C	Telemetry Tracking & Command
TWTA	Travelling Wave Tube Amplifier
UHF	Ultra High Frequency
VBB	Very Broad Band
WFD	Work Flow Diagram
WTS	Wind & Thermal Shield

Executive Overview

Human colonisation of Earth's neighbouring planet Mars has regained the interest of the industry once again. In the last decade, several missions have been sent to this new frontier to assess numerous aspects of the red planet. Surface missions like the Mars Science Laboratory (MSL) have investigated whether local conditions in the past were suitable to support life [2]. Orbital missions such as the Mars Reconnaissance Orbiter (MRO) have mapped the surface, studied the atmosphere and even have been probing underground in order to understand the past of Mars [1]. These missions all have the aim to ultimately aid in the human exploration of Mars. However known locations for both water and energy sources are considered prerequisites before a human presence can be realised [3]. More recent missions such as InSight continue the study of Martian history [4], however, no mission exists as yet that has its primary focus on locating these specified resources. The MarsquakE and Thermal nEtwORk (METEOR) mission is designed to fill this void, and is expected to reveal a global mapping of both water and thermal resources.

The METEOR Mission

METEOR is a complete system designed to transport scientific instruments to the Martian surface and provide all necessary logistical support for the duration of the mission. Comprised of two main elements, the orbiter and eleven probes, it will travel to Mars as a single spacecraft. The probes will individually be deployed and enter the atmosphere following a short de-orbit burn. The orbiter will remain in a high-altitude circular orbit to relay data between the probes and Earth's Deep Space Network (DSN).
For both the orbiter and the probes, the individual subsystems are designed using primarily off-the-shelf components to meet preliminary mission requirements. This first-order sizing has resulted in a overall design of the METEOR system, as summarised in Table 1.

Table 1: *METEOR System characteristics.*

Characteristic		Value	Unit
Operations	Mission Lifetime	5	years
	Number of Probes	11	-
Exterior Dimensions	Orbiter deployed	6.94 x 2.5 x 3.17	m
	Probe deployed	3.16 x 0.53 x 1.30	m
Mass	Total (orbiter + probes)	5440.0	kg
	Orbiter - operational	418.1	kg
	Probe - entry	211.5	kg

In order to fit in a single Ariane 64 launch, the orbiter and probes have been configured to be as small and light-weight as possible. The probes are connected to the orbiter via the use of a boom, this boom will be ejected after the detachment of the orbiter. The probes will be detached in orbit and begin the entry, descent and landing phase. Once landed, the probes will deploy their subsystems, the fully deployed probe can be seen in Figure 1a. The configuration in orbit around Mars with all the probes can be seen in Figure 1b.
The system will act as a global seismic network covering up to 91.2% of the surface of the planet. Marsquakes of magnitude 3.2 are detected with a probability of 0.99956. The probes all have a landing circle with a 100km radius, ensuring the landing zones are small enough to achieve the above-mentioned coverage. Table 2 shows the percentage of the planet surface that is covered by at least the indicated number of probes. The system will produce 1282.9 bps of data per probe during the scientific phase using a Transmission Control Protocol (TCP), modulated on an Ultra High Frequency (UHF) carrier. The data is transmitted to the orbiter, which in turn relays the data back to Earth over X-band, using the Deep Space Network.

[1] `https://www.jpl.nasa.gov/news/fact_sheets/MRO.pdf` Retrieved: 17/06/2020

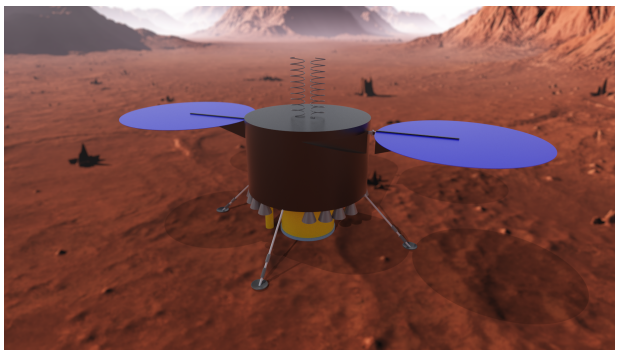

(a)

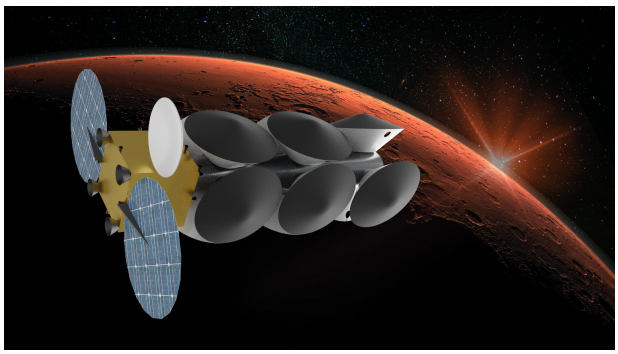

(b)

Figure 1: *METEOR spacecraft renders.*
***(a)**: Lander with deployed solar panels on Mars. **(b)**: Satellite in orbit around Mars.*

Table 2: *System performance.*

Characteristic		Value	Unit
Probe Coverage	No coverage	9.8	%
of Martian Surface	≥ 1 probe	90.2	%
(magnitude 3.0 - 3.1)	≥ 2 probe	81.9	%
	≥ 3 probes	70.3	%
	≥ 4 probes	31.8	%
	≥ 5 probes	0.8	%
Standard scientific data return per probe		22.70	Mbit/sol

Market analysis

Analysing the market, it is clear that more space exploration missions are being launched and planned. There is particular interest in Mars since colonising Mars is seen as the next leap in space exploration. NASA and SpaceX are planning for manned mission to Mars in 2030s and 2024 respectively. Such interest in Mars increases the demand for water and heat sources. Studying the market it was found that there are no other competitors that have searched or planned to search for underground water. However, one mission, Insight, is currently investigating the underground heat sources but it does not represent a risk to METEOR mission as Insight is having problems with the mole.

The METEOR mission provides considerable additional value compared to previous missions or the requirements from the customer:

- No other mission, past or future (except for MetNet), plans to create such a global network of sensor on Mars.
- The system will provide eleven probes instead of the proposed 10, which will allow for more accurate data.
- An additional 1500 kg are available on the launcher, allowing for a ride-share mission, which would cut launch cost, or allow the mission to bring extra scientific payload to increase the value of the mission.

Furthermore, METEOR can be used for other additional functions during and after the lifetime of the mission. The probes can be used as weather stations to inform the inhabitants about the weather. The orbiter can be used as a relay communications satellite after the mission lifetime.

The estimated cost of the mission excluding the launch cost can be seen in Table 3. The heritage reduction factor is related to the TRL level of the components whereas the learning curve factor is to consider the reduction in production cost as the number of manufactured units increase. The cost of the total mission is smaller than the Insight mission's cost. Keeping in mind that METEOR mission is landing eleven probes, the cost of one probe of METEOR is sixteen times less expensive than Insight's.

Table 3: *Estimated cost of the system with reducing factors.*

Cost estimate without reduction [M€]	Cost with heritage reduction factor [M€]	Cost with learning curve reduction factor [M€]	Final cost estimate [M€]
513.2	467.8	479.4	439.6

Risk

Like any other space mission METEOR also has risks. To increase the probability of success of the METEOR mission, different risks are identified and mitigated. Each subsystem has looked into the reliability of the system individually. However, there are other risks to the METEOR mission. Some risks arise due to multiple subsystems interacting with each other.

Some risks are associated with the launch. The launch could be postponed due to weather problem or delay in production. Risks associated with launches are mitigated by planning well ahead of time and by setting up guidelines for the production.

There are risks associated with not meeting the deadline for not meeting the different budgets in the design phases. These risks are mitigated by setting up two limits. Setting up two budget limits and trying to stay inside the first limit, even if the limit is surpassed the design is very likely to still stay under the final budget requirements. This mitigation has been implemented very successfully in the final phase of the design of the METEOR mission.

There is risk associated with the failure of one of the probe due to failure of any of the part of the mission. This risk is mitigated by having eleven probes located such that even if one of the probes is lost the impact is minimised during the landing site selection.

There is risk associated with failure of the orbiter. This is mitigated by first designing all the components in the orbiters to have redundancy such that the reliability of the system is very high. Second, the telecommunication on board on the probes are designed that they will still be able to send data back via orbiters from different missions.

Sustainable design development

The sustainable design development plan was divided into sustainability analysis for three different stages: the production phase, the (prolonged) utilisation phase and the disposal phase. Sustainability in the production phase firstly means a general reduction of emissions, use of clean water, use of energy, and a reduction in the waste of raw resources. More specifically to the METEOR mission, there are more measures to be named. First of all, the fact that the METEOR mission consists of eleven identical landers must be benefited from; the same assets will perform the same actions. Secondly, duly checking for defects prevents more costly repairs later in the production phase. The use of off-the-shelf components generally decreases waste and cost. Moreover, it is made sure that the Planetary Protection Rules (PPR) are met. It is also advised to reuse existing facilities such as the ground station and the clean rooms. For the separate subsystems, sustainability considerations were mainly put into the hands of the off-the-shelf components manufacturers. Where possible, negotiations with separate manufacturers shall be joined to maximise sustainability efforts. The prolonged utilisation phase will possibly take up to 20 years, during which the METEOR system is most likely to keep functioning as a seismic measurement system. On top of this, the system might use its Auxiliary Payload Sensor Suite (APSS) equipment to function as a global meteorological network, a function that adds much scientific worth to the mission. After these twenty years of prolonged mission lifetime, a deorbit burn is still guaranteed to ensure no unacceptable space debris is left behind, which would possibly hinder future Mars missions. It can be guaranteed that the orbiter burns up in the Martian atmosphere after deorbit burn.

Future timeline

NASA plans to launch the first manned mission to Mars in the 2030s, meaning that water locations and thermal sources might be needed before then. Initial estimates place this mission in 2035 if not 2037, which would allow the METEOR mission to launch in February of 2031 and provide valuable intel on the location of underground water and thermal sources. This launch dates gives 11 years to go through phases A to D of

an ESA mission. The timeline for the mission is shown in Figure 2. Phase A is the feasibility study and it is the Design & Synthesis Exercise. Phase B is the preliminary definition, where all the subsystems undergo a detailed design phase. This phase will take 5 years as some instruments will have to be redesigned. Phase C is the detailed definition where several models for the system are built and tested, and will last 3 years. Phase D is the qualification and production phase which lasts 3 years and includes the production and testing of the Flight Model (FM). Phase E is the launch and operations phase and will be described in the next paragraph. Collaboration between NASA and ESA will benefit the mission by lowering development costs and allowing NASA to use the data provided by the METEOR mission to select a landing site for future manned missions.

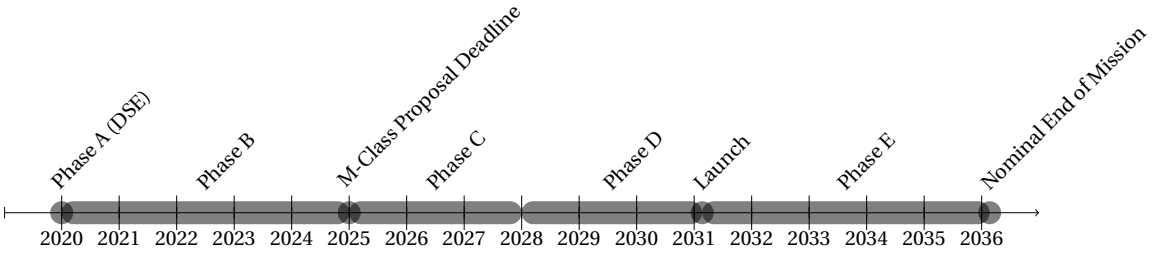

Figure 2: *METEOR mission timeline after DSE*

The system will be designed, manufactured and tested in Europe. Once built, it will be transported to Kourou, French Guiana, where it will be integrated with the European launcher Ariane 64. The mission will launch on February 2, 2031 during the Hohmann transfer window and will spend 258 days in interplanetary travel. The mission will communicate to the European Space Operations Center (ESOC) through the Deep Space Network (DSN) for the majority of the mission and will use European ground stations during launch and the first part of interplanetary travel. The mission will then spend 60 days aerobraking and will deploy the probes once the aerobraking phase has ended provided no global or local dust storm is blocking the landing. Once landed the probes will deploy the instruments and begin the Primary Science Phase which will last a total of 3.73 years. The total mission will last 5 years, with the opportunity to be extended for a longer period of time.

Subsystem design

Planetary science

The main mission of the METEOR mission is to find possible water sources and power source for the future mission on Mars. Finding these sources are going to be done by the usage of the thermal heat flux sensor and seismic sensor. To locate the water source using the seismic activity of Mars, it is very important to place the seismic sensor to the correct location. It is due to the fact that to find the exact location of the seismic source at least three seismic sensor needs to detect the same seismic event.

Furthermore, there exist different constraints and requirements. Some regions are specified by the customer on Mars that needs to be covered. There are different constraints set by different subsystems on altitude, latitude, dust, slope and rock abundance. All of these factors are taken into account and the final location of eleven probes are decided. Using the surface data that the previous missions have collected landing ellipses are determined. An analysis is made for different magnitude of mars quake sizes and it is confirmed that the eleven probes can detect around 240 seismic events per year. Figure 3 shows the locations of the chosen landing sites on Mars.

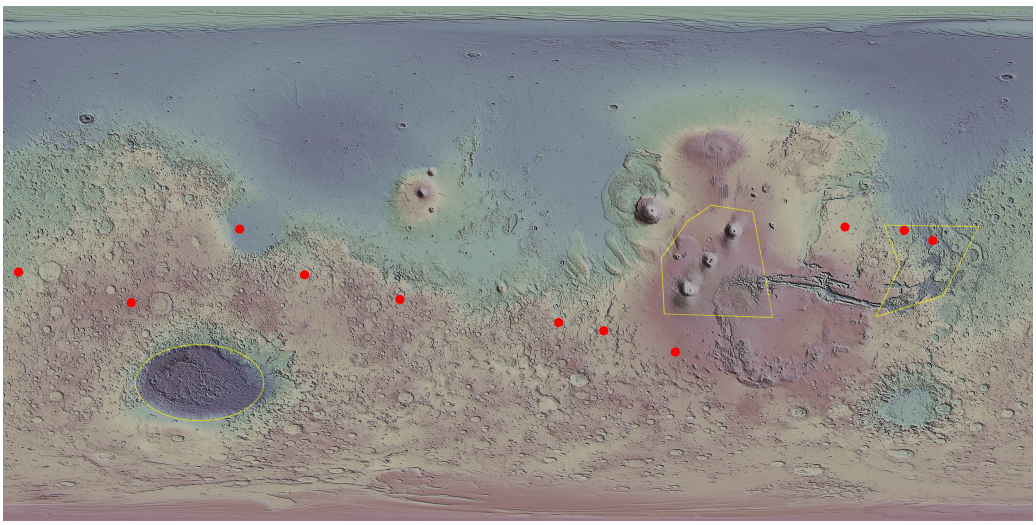

Figure 3: *Probes landing sites drawn on Mars map.*

Scientific payload

The scientific payload ensures that the scientific objectives of the mission can be completed. For this mission, this is detecting water and energy sources on Mars for future colonisation. Two instruments have been chosen to perform this task.
For water detection, a seismometer is used. Seismometers detect water by analysing the seismic waves that run through them. This method is called seismic tomography and works by the same principle as X-ray imaging for medical purposes. Waves are passed through the region of interest and sensors on the other side pick up the waves. Based on the changes to the waves detected by the sensors, a conclusion can be made of the body they have passed through. For seismic tomography, the wave source is not an X-ray but a Marsquake and the sensors are the seismometers. Just like X-ray imaging, a single sensor is not sufficient to provide enough resolution, this is why an array of eleven probes each with their own seismometer will be deployed on the Martian surface. This has the combined effect of increasing resolution and coverage of the planet. Detection capabilities of seismometers are mainly limited by signal noise in their environment. To reduce this, a wind & thermal shield and an environmental sensor suite are used. The sensor suite is composed of a magnetometer, wind speed sensors, air temperature sensors and an atmospheric pressure sensor.

For thermal energy sources, a heat flux probe is used. This instrument burrows itself to a depth of three to five meters and is connected to the lander with a strip covered with temperature sensors at regular intervals. Over time, the temperature measurements will allow scientists to determine the local thermal flux of the ground and detect potential thermal energy sources.

Both instruments will be lowered from underneath the lander once it has landed. The heat flux probe once lowered to the surface will begin its digging procedure which may take up to 44 sols or 45 days. The seismometer may start operations on sol 1 as soon as the Wind and Thermal Shield is lowered.

Structures & Materials

Structures & materials subsystem ensures that all load-bearing structures can perform their function without failing. All designed structures were designed with a 1.4 safety factor to account for experiencing higher than expected loads, degradation, structural deflections and thickness variation. As a result, structures shall be able to withstand 40 % higher loads than expected. The subsystem is also responsible for material selection of all designed components.
The probe was modelled as a hollow cylinder, designed to withstand launch loads and more critically, the entry and descent phase of a peak acceleration of 6.9 g. Moreover, it is equipped with four landing struts accompanied with shock absorbers able to land safely without energy dissipation to the payload. By using carbon-aluminium composites, a structural weight of 12.59 kg is expected. The production costs are not high as eleven probes are being produced.
For the orbiter, modelled as a hollow cube, for easier attachment to the launch vehicle adapter, is also de-

signed to withstand launch loads of peak acceleration of 4.6 g. Stiffness design is also taken into account by keeping the natural frequency, in both longitudinal and lateral direction, higher than the stated excitation frequency caused by random vibrations during launch. However, as only one orbiter is produced, the cost of using composites would be high, thus, Alu-7475-T761 alloy is used, resulting in a structural mass of 50.5 kg.
A challenging part of the design is material selection for the heat shield. Due to high experienced temperatures during descent, most metals would evaporate. Therefore, ablative material with high enthalpy required for vaporisation were considered. This resulted in choosing carbon fibre composite with phenolic honeycomb core filled with a mixture of silica microspheres, cork and silica fibres. Moreover, titanium alloy, Ti6AL-4V was chosen as a propulsion tank material due to high specific strength property.
A solar array support structure was designed to prevent the solar arrays for breaking and safely folding during the worst-case scenario. Lastly, the eleven probes and orbiter were oriented in the launcher compactly to fit together. This resulted in a required beam design to connect them. The beam needs to also withstand the launch loads and support the bending loads introduced by probes and orbiter without failing. The resulting weight of the launch beam is 514 kg.

Astrodynamics
The astrodynamics subsystem determines all the orbital elements related to the mission, from the arrival at Mars, all the way to the End Of Life (EOL) of the orbiter. Due to the preliminary nature of this analysis, all orbits are treated as Keplerian orbits and the Hohmann transfer is calculated using patched conics. The orbits are designed to meet all the requirements from other subsystems, as well as minimising the ΔV requirements for the mission.
The mission will arrive at Mars from a Hohmann transfer from Earth, utilising 1222.0 m/s of ΔV to slow down. It will then make use of aerobraking to reach the required orbit to deploy the probes. The probes will be deployed weather permitting, and the orbiter will then circularise its orbit. The orbiter will require 1545.7 m/s of ΔV for the entire mission, while the probes will require 25 m/s to deorbit.
The orbiter will be placed in a circular orbit 520 km above Mars, with an inclination of 30 ° to ensure communication with all the probes. This orbit ensures that each probe has enough communication time with the orbiter, as well as ensuring a slower decay due to the much thinner atmosphere.

Propulsion
The propulsion system's primary function is to provide the required ΔV. Both the lander and satellite need a propulsion system. The lander needs to perform a propulsive landing to touch down softly on the Martian surface. The satellite needs to perform manoeuvres to change or maintain its orbit. The requirements on the propulsion system vary for the lander and satellite, therefore, they are designed separately. The lander uses high thrust, high I_{sp} thrusters to provide a large deceleration in a short timeframe. The satellite uses the same high thrust, high I_{sp} thrusters for the capture burn, which requires a large acceleration in a short timeframe. Moreover, the satellite has an orbit maintenance propulsion system. Where the capture-burn uses more efficient high I_{sp} bi-propellant, the maintenance is done with more precise monopropellant. By making the conscious design choice to select the same fuel type for the bi-propellant and monopropellant, the infrastructure is partly shared, which makes the design lighter. To ensure the successful completion of the mission, the propulsion system is designed with redundancy in mind. There are two propellant tanks and two oxidiser tanks, such that if one of the tanks fails, the remaining tank can still function and ensure a successful mission.

Entry, Decent & Landing
The EDL subsystem's function is to land the probes with a sufficiently small touchdown velocity on the Martian surface. The EDL sequence is divided into three phases, entry, descent with parachutes and descent with thrusters. The entry vehicle is designed to be stable at an angle of attack = 0° for most of the entry phase. The instability period is controlled using the reaction control system with the onboard control thrusters. The heat shield is designed to withstand the expected max heat flux of 0.255 Mw/m^2. In the descent with parachute phase, the Disk-gap band parachute is deployed using a mortar and the heat shield is jettisoned. A disk-gap band parachute is used due to its capabilities to perform at high Mach numbers and dynamic pressures. The parachute, being deployed at an altitude of 17.87 km for the landing site with the

highest elevation, decelerates the entry vehicle from a velocity of 694.1 m/s to 167.7 m/s. The last phase is the terminal descent with thrusters. The EDL subsystem can land the probes safely on an elevation up to 2800 m with a touchdown velocity less than 0.5 m/s.

Altitude & Orbital control system

Both the orbiter and the probes are equipped with attitude and orbital control subsystems (AOCS), which ensure proper pointing direction during each phase of the mission. Responsible for both orbital guidance and attitude control, it will monitor the trajectory and manoeuvre the spacecraft to execute the necessary burns. During Mars orbit insertion, the attitude of the spacecraft will be essential in controlling the effectiveness of the aerobraking. Once in the final orbit, the AOCS of the orbiter will be 3-axis stabilised, maintaining a nadir pointing attitude as required by the TT&C subsystem. The probes will utilise their AOCS for the entry, descent and landing phase. The single de-orbit burn will be spin-stabilised, and the timing will be coordinated by the orbital control system. Throughout atmospheric entry and descent, the probes will be 3-axis stabilised, which is necessary for the propelled terminal descent.

The orbiter is equipped with four Honeywell HR12 reaction wheels, one of which is for redundancy. These reaction wheels are the primary components responsible for attitude control, and rejection of disturbance torques. Attitude control thrusters will be used for high rate manoeuvres and periodic reaction wheel momentum desaturation. Two Miniature Inertial Measurement Units (MIMUs) from Honeywell will provide coarse attitude determination, and will be supplemented by two Leonardo Systems A-STR star sensors for accurate 3-axis control.

The probe will use eight cold gas thrusters mounted on the aeroshell for stability control during the entry and descent phases. To reduce the necessary propellant mass, the probes will rely primarily on aerodynamic stability to remain within safe pointing deadbands, only firing thrusters if necessary. The attitude sensor suite will rely on data from two of the same MIMUs during these first phases. For the final propelled landing phase, a flight-proven radar Doppler altimeter developed by Thales Alenia Space will provide additional precise ranging data to ensure a soft touchdown.

Telemetry, tracking & Command

The TT&C subsystems for both orbiter and probes are considered critical subsystems as failing to retrieve the scientific data implies mission failure. Both TT&C architectures are based on maximising the reliability by applying active parallel redundancy its components. This redundancy philosophy was applied throughout all mission phases. The reliability regarding the TT&C subsystem for orbiter and probe is 0.9664 and 0.9898 respectively.

The data generated by the probes is transmitted to the orbiter using the Ultra High Frequency (UHF) frequency band. The orbiter can retrieve data from multiple probes simultaneously with the aid of the Transmission Control Protocol (TCP) reaching retrieved data volume of 146.8 Mbit/sol per probe at a SNR of 27.3 dB.

The orbiter collects the data from all probes and transmits this to the Deep Space Network (DSN). This communication link too makes use of radiofrequency carrier waves, however in the X-band domain. This dual functionality of the orbiter happens simultaneously. The orbiter-DSN link transmits 1.77 Gbit each Earth day at a SNR of 12.2 dB which is above the 10dB threshold set by the DSN [5].

Command & Data handling

The C&DH subsystem is there to process all housekeeping and scientific data as well as commands coming from Earth, This subsystem distributes named data across the orbiter and the lander. The software structure, for which the C&DH hardware is mostly responsible is completely drawn out in Figure 17.8. Mission heritage was used to determine housekeeping and command data rates, where more detailed estimations were made for the scientific data rates. These data rates, in turn, were used to calculate required processing power (1.497 MIPS) and mass memory capacity (2.617 GB) for the orbiter and mass memory capacity (2.131 GB) for the individual landers. The orbiter memory capacity was sized for the period of solar conjunction, where the landers were designed to save data for 30 sols. Recommendations for off-the-shelf hardware meeting the requirements were given. Within the hardware structure, numerous reliability considerations come to light, the C&DH being crucial for data return. Firstly, the OBC is designed fully redundantly with cross-coupling between vital functions, one of the reasons the OBC has a reliability value of 0.99 for a 20

year lifetime, thus taking into consideration the possible prolonged utilisation phase. Quadruple modular redundancy was included in the design. Finally, checksum is included within the TCP packages transferred as an extra means of data transmission guarantee.

Electrical power system

Both the orbiter and landers are designed with two solar arrays and secondary batteries. The solar arrays use the UltraFlex solar array technology developed by Orbital ATK. These are circular solar array with much higher mass to area ratios than traditional rigid solar arrays. The solar arrays use quadruple junction solar cells which have a cell efficiency of 32%.
The batteries are NCA Li-Ion batteries developed by Yardney. The batteries have one of the highest specific energy in-class and the technology has successfully been used on Mars. The sizing for the solar array and batteries have been performed for the worst-case scenario. This includes the worst-case power load and the worst-case environmental conditions. The system is designed to provide a constant supply of power during these worst-case conditions.
Lastly, the system was designed around an unregulated bus with a battery charging unit and battery management unit. The battery charging unit and battery management unit were added to reduce the degradation of the battery. An unregulated bus was chosen for its high efficiency and small amount of components.

Thermal control

The orbiter and probe both rely on a combination of passive and active control to keep components within operational temperature range. The passive control of both spacecraft consists of Multi Layer Insulation (MLI) and an array of coatings and paints. The active control of both spacecraft is managed by electrical heaters that are placed near components with strict temperature requirements, such as the batteries.
The orbiter uses MLI on the outside of the structure with a highly reflective coating. A small panel is painted black to radiate heat from the batteries away while a heater is used to heat the batteries during eclipses. The landers use MLI and dark paint on the outside of the spacecraft to capture as much solar heat as possible during the day, while using heaters both during the day and the night to keep the temperatures within the limits.

Sensitivity analysis

To check the robustness of the design, a sensitivity analysis is performed. In a sensitivity analysis, the key input variables are changed to see their effect on the outcome of the design. This way, the most sensitive input variables are determined. In the design phase to come, these input values are determined first to ensure that the design teams work with the most accurate values.
The sensitivity analysis uses a method of partial derivatives, which ensures that the impact of only a single variable can be determined.
The sensitivity analysis revealed an overall robust design, most key input variables have a diminishing impact on the design. Notable exceptions are the large sensitivity of the EDL subsystem and the structural subsystem.

Contents

1 Introduction

Mars is the prime candidate for making human life multi-planetary [6]. It offers in-situ resource utilisation opportunities to produce air and propellant for the astronauts and return vehicles. Space colonisation is considered essential for the survival of the human race. In the past year, over 750 objects have been observed to approach the Earth within ten lunar distances [7], of which the largest is estimated to have a diameter of 220-490 m. The largest terrestrial impact in recorded history is the Tunguska event of 1908, the impact of an asteroid with a diameter of 50-100 m [8]. The event occurred over the sparsely populated Eastern Siberian Taiga, killing three people [9]. An impact of an asteroid of this size can easily destroy a metropolitan area, killing many more people. The impact of an even larger asteroid, such as one of the many catalogued near-Earth objects, will have even more disastrous consequences [10]. To prevent the extinction of the human race, it is paramount that human life becomes multi-planetary and for a human civilisation to live on Mars, liquid water and a source of energy are of the utmost importance. The best place to look for liquid water and energy on Mars is below the surface [11]. This need is answered perfectly by the METEOR mission, which aims to locate water and thermal energy sources on Mars in preparation for future colonisation of the planet [12].

This report details the conceptual design of the previously selected concept [11] and meets all the requirements [13]. Using concurrent engineering, each subsystem is designed by a functional analysis, an analysis of the requirements, the development of a design tool, completing a subsystem trade-off, the analysis of the design risks, verification and validation of the design tool and confirming that all the requirements are met. Besides the conceptual design, the secondary aim of this report is to provide a coherent and complete overview of the total system and the economic aspects of the mission.

Chapter 5 presents the results of the concept trade-off. The budgets as the basis for the conceptual design of the entire mission. Chapter 6 explains the selection of landing sites. Chapter 7 through Chapter 16 cover the conceptual subsystem design of the scientific payload, structures and materials, astrodynamics, propulsion, entry descent and landing, altitude and orbital control subsystem, telemetry tracking and command, electrical power subsystem and thermal control subsystem. How these subsystems combine into a single system is explained in Chapter 17. The performance of the system is analysed in Chapter 18 and Chapter 19 assesses the robustness of the design by performing a sensitivity analysis. The risks are then evaluated in Chapter 4. The economic aspects are analysed in Chapter 2 through Chapter 21, which cover the market analysis, sustainable design development and post-conceptual design development. The report concludes with Chapter 22.

2 Market Analysis

The METEOR mission is designed as a proposal for ESA's Medium class mission. To ensure funding from ESA, the market has to be analysed to assess the future market value. A brief heritage study is performed to estimate the demand on exploration missions to Mars. Furthermore, competitors are identified to ensure that there is a sufficient market share. SWOT analysis needs to be performed to predict the market position of the METEOR mission. Finally, based on the market value, a target cost is estimated.

2.1. Medium class missions

The METEOR mission is designed as a proposal for Medium class missions by ESA. These missions are selected to be part of ESA's Cosmic Vision campaign. The campaign started in 2005 and aims at performing research in different fields including astrophysics, fundamental physics and solar system exploration. The missions selected need to comply with a budget ranging from 50 to 550 million Euros. Since 2010, ESA has had five mission calls. Four M-class missions have been confirmed, these can be seen in Table 2.1. Mars Reveal is to be proposed to ESA's M-class proposals in the post-2025 round.

Table 2.1: *Scheduled ESA M-Class Missions.*

Mission	Project Name	Launch Date
M1	Solar Orbiter	Feb 2020
M2	Euclid	Jun 2022
M3	PLATO	2026
M4	ARIEL	2025

2.2. Heritage Study on Missions to Mars

Since the 1960's there have been interplanetary spaceflights with varying destinations, size and cost. However, in recent times the demand for M-class and Mars exploration missions has increased. This trend can be observed when considering the interplanetary missions since the 1990s. Since then there have been 28 interplanetary missions that have reached their destination, sixteen of which are missions to Mars. These are listed in Table 2.2. From Table 2.2, one can observe that missions to Mars have been planned and launched in a continuous fashion. Also, an increase in the missions' budgets is observed which ensures the increasing interest in Mars exploration. When looking solely at NASA missions one can see a clear focus on Mars. As most of the Mars missions in the list were performed by NASA. This can be explained by their goal to send humans to Mars in the 2030s.

2.3. Competitors

In a market, there are two types of competitors, the ones that perform the same mission, and the ones that achieve the same result using different methods. Both types of competitors are discussed below.

Competitors With Similar Missions

A definition of a similar mission to Mars Reveal needs to be set first. A similar mission to Mars Reveal is therefore defined as a mission aiming at finding water and heat sources on Mars.
Using this definition, numerous past missions have found evidence of water on the surface of the red planet, some as their mission purpose and some found it accidentally. Most notably the Mariner 9 orbiter, which found the first evidence of past water on Mars and the Exploration Rovers which accidentally found water when one of Spirit's wheel broke and scraped off the upper layer of soil, revealing frozen water underneath. However, no past or planned mission aims to locate underground sources of water, meaning the Mars Reveal mission has no direct competitors in that aspect of the mission. Moreover, all previous missions had only one rover or lander, meaning that the search area is limited to a small area around the landing sites.

Table 2.2: *Missions sent to Mars.*

Mission Name	Year	Destination	Total Cost Including Inflation [M€]
Insight	2018	Mars	759.33
ExoMars (TGO) / Schiaparelli EDM	2016	Mars	1340.72
MAVEN	2013	Mars	661.94
Mars Orbiter Mission	2013	Mars	72.02
Mars science laboratory / Curiosity rover	2011	Mars	2558.75
Mars Reconnaissance Orbiter	2005	Mars	848.25
Phoenix Lander	2005	Mars	454.75
Mars Express orbiter / Beagle 2 Lander	2003	Mars	431.28
MER-A/MER-B opportunity (spirit/opportunity rover)	2003	Mars	1025.07
Mars Odyssey orbiter	2001	Mars	386.00
Mars Polar Lander / Deep Space 2 impactor	1999	Mars	151.37
Mars Climate Orbiter	1998	Mars	176.47
Mars Global Surveyor orbiter	1996	Mars	225.17
Mars Pathfinder lander / Sojourner rover	1996	Mars	387.47

Mars Reveal, on the other hand, has eleven probes which can cover most of the planet's surface.

For the heat sources, some past missions were also equipped with a thermal emission sensor to analyse the heat flow of the surface of Mars. However, only one mission, InSight, tried to locate underground heat sources, and so far it has failed to do so due to a malfunction in the heat probe deployment device. From the given definition, InSight is considered a competitor. However, given that InSight has not completed its mission and that it is only one probe, compared to the eleven proposed probes the Mars Reveal mission would deploy, it is not considered to be a threat to the METEOR mission.

Competitors With Similar Results

First, different approaches to obtain water are considered. Since no mission was sent to Mars with the purpose of extracting water, possible future competitors are presented here. Water on Mars is not only present underground, but also on the surface as ice, dissolved in rocks and in the atmosphere as water vapour. There are different methods to produce water on the surface of Mars, some are more feasible than others, and some are more scalable than others.

The first approach is to use water from the poles. This is one of the most obvious methods as there is a very large amount of water frozen and easily accessible. Although this option seems the most feasible, it would require landing near the poles, where the temperature is low enough to cause problems with the electronics. Another issue would be that, just like on Earth, astronauts would be subject to long periods of daytime or nighttime due to Mars's tilted axis.

The second approach is to extract water from rocks by using supercritical CO_2 [14]. This method seems promising as it is not very complicated, however it has the problem of scalability. Furthermore, no further research was provided on this method since 2001.

The third approach is to extract water from the atmosphere [15]. However, Mars' thin atmosphere poses a major scalability problem. The research shows that 480 m^3/min of atmosphere needs to be processed to produce 1 metric ton of water in one (Earth) year which is approximately how much water one astronaut uses on the ISS every year. Even if most of the water would be recycled, a massive amount of atmosphere would have to be processed for a more substantial Mars mission or colony.

For the thermal sources, as mentioned above, Insight is the only mission investigating the heat sources on Mars. Thus no real competition exists for this mission aspect.

2.4. Future Markets

When analysing the market of the manned exploration of Mars, one must consider both the short-term future (20 years) and the long-term future. For the short term, the value of finding water and heat sources can be estimated by considering the option of bringing water and heat to Mars. However, the mission budget will not be underestimated by this approach because finding such sources has an even larger influence on Mars missions and possible inhabitants in the long run. One has to keep in mind that bringing water to Mars is not a sustainable solution in the long run.

Short-Term Future Market

Multiple agencies and companies plan to send humans to the red planet in the near future. Currently, two of them have formally planned manned missions, namely, NASA and SpaceX. NASA plans to send the first manned mission in the 2030s and the SpaceX plans to send the first humans in 2024. Moreover, ESA has already shown interest in Mars with the Aurora program [16] however has not yet planned manned missions. Other agencies such as JAXA and CNSA are following closely. While these goals might seem ambitious, a manned mission to Mars is the next step in the human exploration of the solar system. Since water would be fundamental for these missions, the agencies responsible for them can be considered customers of the scientific data provided by Mars Reveal. To know the value of this scientific data, one must consider the alternative to using water from Mars, bringing it from Earth. With a launch cost of 10,000 $/kg [17] and estimated water mass required of 100 kg per person per year, the cost would be 7.5 million $ for a 1.5-year mission of five people on Mars, which does not include the potential water needed for the fuel needed for the trip back.

Long-Term Future Market

In the long-term future, it is clear that a permanent presence on the surface of Mars comes with an increasing demand for water and heat sources. A method of finding that water and heat source is vital for a colony and its survival. Water is important not only for basic needs but it can be also used as a source of fuel for the habitats of Mars. Mars Reveal mission plans to provide the means to find the needed water and heat source.

2.5. Stakeholder Analysis

In a space mission there are numerous stakeholders, from the ones that invest and fund the project to the scientists that use the data.

The first and most obvious stakeholder is the customer, which requested a Mars mission to locate underground water and thermal sources. The second stakeholder is ESA, which will be the one funding the mission and is therefore interested in the cost and scientific return of the mission. The third stakeholder is the whole scientific community, which will receive all the data provided by the mission and will be able to perform groundbreaking research with the new data. The Ariane group will also be a stakeholder as they will provide the Ariane 64 launcher. There is one final group of stakeholders which includes, but is not limited to, NASA, SpaceX and the Mars Society, which plan to send humans to Mars within the next decade.

2.6. Additional Value

Additional value of the mission is measured in comparison to other past or planned missions, as well as the original requirements for the mission.

The first major additional value provided by the METEOR mission is its planet-wide coverage like no other mission, with the exception of the MetNet landers [18], provides this kind of data. The MetNet lander is not a direct competitor however since it will provide atmospheric data and not thermal and seismic data. The second additional value provided is the presence of eleven landers, compared to the planned ten landers. This will provide more than three probes-coverage along the equator, allowing for more accurate data, as well as redundancy in case one of the probes were to fail. Finally, additional value is provided by the extra 1500 kg available in the rocket, which might allow for a rideshare mission to share the rocket, allowing for savings on launch cost up to 20 M€. The extra mass can also be used to bring some extra payload on the orbiter, to provide more scientific data.

Long-Term Future Market

In the long-term future, it is clear that a permanent presence on the surface of Mars comes with an increasing demand for water and heat sources. A method of finding that water and heat source is vital for a colony and its survival. Water is important not only for basic needs but it can be also used as a source of fuel on the habitats on Mars. Mars Reveal mission plans to provide the means to find the needed water and heat source.

2.7. SWOT Analysis

The Strength, Weakness, Opportunity and Threat analysis can be used to predict the market position of the Meteor mission. This is done by showing the internal and external effect in the rows, and the helpful and harmful aspects in the columns. By building on the strengths of the mission and utilising the given opportunities the company can establish a strong market position. The internal weaknesses will be minimised and a contingency plan will be set up for external threats, to minimise overall risk.

Table 2.3: *SWOT Market Analysis for the METEOR Mission.*

	Helpful	**Harmful**
Internal	- Unique Product - Inexpensive design process - Additional Mass Available	- Conceptual mission design - Small Labour Force - Inexperienced designers
External	- Market Demand for Mars Missions - Market Demand for M-class missions - Space Sector Growth - Increased Interest in Mars - ESA Increased Budget	- Competition for M-class missions - Economic Recession due to COVID-19 Pandemic

The market SWOT analysis for the meteor mission is shown in Table 2.3, where it can be noted that a great opportunity for this mission is the increase in public interest for space missions and an even greater interest in Mars missions. This is at least partially due to SpaceX' plans to send humans to Mars by 2024, and NASA's plans to send the first manned missions to the red planet by the 2030s. Thanks to the uniqueness of the mission and the additional values provided as discussed in section 2.6, the mission has the potential to be very valuable to potential customers. Due to the conceptual nature of this design, and the labour force behind it, the mission could have a lower standing in the market which would be harmful due to the competitive nature of M-class missions.

3 Sustainable Design Development

The sustainable development strategy presents the sustainability of the design and the design process. The life cycle of an ESA space mission is usually approached in five different phases; Design, Production, Launch, Utilisation and Disposal [19]. At this stage, efficiency in the design phase has been discussed elaborately. Therefore, the focus lays on the other four stages. For the production phase, low-waste manufacturing and adhering to the Planetary Protection Rules (PPR) set by COSPAR are discussed. Furthermore, probabilities of and possibilities for a prolonged utilisation phase are discussed. Finally, the disposal of the orbiter and landers is elaborated upon.

3.1. Definition of Sustainability

For a space mission it is hard to use the normal definition of the sustainability on the Earth which focuses on environmental impact as the mission happens outside the Earth. Thus the group has came up with a new definition for the sustainability. Sustainability is defined as "The ability to be maintained at a certain rate or level"[1]. This means for the sustainability of this product, the focus lies on durability. Using this definition, sustainability of the design is achieved.

3.2. Sustainable production phase

Even though METEOR is a space mission, it has implications on Earths' environment. The production of the METEOR satellite and landers needs to be performed sustainably. Numerous methods and guidelines for a sustainable production have been set up, those applicable will be discussed here.

Firstly, it is important to define Lean Manufacturing (LM) [20]. Lean manufacturing is a method of manufacturing that minimises the waste produced during the process and reduces the effects on the environment. One of the most common tools used for LM is Life Cycle Analysis (LCA). LCA allows to fully analyse the environmental impact due to the actions and decisions made during activities like production of goods and services [21]. LCA is applied to ensure that separate producers know and minimise the negative consequences of their actions.

There are different ways to directly reduce the impact on the environment while producing. The following activities would improve sustainability across the entire supply chain:

- Reduction of energy usage
- Reduction of usage of water
- Reduction of emissions
- Reduction of waste of raw resources

These points are the general method that allows the manufacturing of any product to be sustainable. Now more detailed strategies that will be applied to METEORs' production are introduced.

- **Benefit from reproduction**: One of METEOR's most outstanding characteristics is that eleven identical probes have to be produced. This feature will be benefited from; by putting the same assets on set tasks in the production line of the eleven landers, time, cost and material can be saved. This has to do with the learning curve introduced when assets repeat certain operations [20].
- **Prevent the occurrence of defects by testing components regularly**: In the satellite engineering industry, satellites undergo rigorous testing. This is no different for the satellite and landers of the METEOR mission. Defects are very costly to repair, it requires a lot of time and manpower to reproduce (part of) a satellite. By preventing defects, these costly repairs are avoided.
- **Use of off-the-shelf components**: The use of off-the-shelf components has numerous advantages. First of all, larger-scale producers benefit from the effect of the learning curve, by which waste can be

[1] `https://www.lexico.com/en/definition/sustainability`, retrieved 11/05/20

minimised as described under "benefit from reproduction". This is why buying subcomponents from those larger-scale producers decreases waste. Moreover, within the (detailed) design phase itself, the use of off-the-shelf components saves resources on research and development, since these components are readily available. At most, small improvements of the components are required. Finally, using off-the-shelf components reduces transportation wastes and therefore emissions. It is simply easier to reduce transportation distances if the responsibility for the production of subcomponents is spread and full components are shipped to the assembly location together. For both the orbiter and the lander of the METEOR mission, this principle has been applied in abundance. Take for example the mole concept and the SEIS instrument that were taken as sizing/leading components in the design. This is the main reason that the METEOR landers are relatively low in cost.

- **Meeting the Planetary Protection Rules**: Biocontamination of Mars' ecosystem must be limited. Therefore, Planetary Protection Requirements were set up in earlier stages of the design phase. These requirements are set to meet the rules set by the Committee on Space Research (COSPAR) for category IVa missions[22]. Further explanation of the category METEOR belongs to can be found in chapter 18. These requirements are discussed in Chapter 18. As stated there, assembling and testing the system in the appointed clean rooms (class 100000) allows for minimisation of biocontamination. Moreover, the orbiter is guaranteed not to impact the Martian surface, due to the disintegration in the Martian atmosphere, as explained in section 3.3.
- **Reuse of existing facilities**: Besides benefiting from existing production facilities, it is important to reuse facilities for the ground station and cleanrooms. The TT&C subsystem is designed to comply with the Deep Space Network, which means the METEOR mission can fully benefit from the already existing on-earth facilities.
- **Propellant considerations**: Although toxic to humans, as described in Chapter 10, N_2H_4 was chosen as propellant. The advantages of this propellant outweigh the risks linked to N_2H_4, having its implications on safety precautions during loading the propellant on board and preparing for take-off.
- **Other subsystems**: For other subsystems, sustainability considerations often make it hard to meet the requirements, biodegradable materials for example often make it impossible to guarantee the required lifetime. Moreover, off-the-shelf components are only considered when designed to be durable. In most cases sustainable production is left to the separate producers, who will use the LCA tools, mainly because the production is simply in their hands (see "Use of off-the-shelf components"). However, especially because of the relatively large-scale production of the eleven landers, there are possibilities to join negotiations with the separate manufacturers, possibly maximising sustainability efforts during production. Finally, where possible, during the detailed design phase, sustainability considerations shall be part of the trade-off for (sub)components.

3.3. Prolonged utilisation phase

The end-of-life strategy entails (part of) two of ESA's Life Cycle Assessment mission phases: the (prolonged) utilisation phase and the disposal phase. During the prolonged utilisation phase, it is of utmost important to benefit from all assets that function past the utilisation phase to optimise for sustainability.

The prolonged utilisation phase

To be able to analyse this phase optimally, three scenarios are portrayed; the orbiter and/or on-Mars section can work beyond planned mission lifetime separately, or together. Table 3.1 shows the options for the three named situations.

Table 3.1: *Depiction of all possible prolonged utilisation phase purposes in three different scenarios. Green cells mark likely purposes of the system after its set lifetime, red cells mark less likely purposes of the system.*

Only orbiter	Only lander(s)	Combination of orbiter and lander(s)
Relay satellite	On-Mars radio/communication stations	Continue seismic measurements and relay
	Global meteorological system	Global meteorological system, including relay
	Continue seismic measurements	

Note that the orbiter is used for relay purposes in all scenarios shown in Table 3.1. Moreover, all critical

subsystems of both the landers and the orbiter have been designed with redundancy and high-reliability scores. This makes the possibility of the orbiter and landers surviving beyond the planned utilisation phase highly likely. Especially the chance that all landers fail during or just after mission lifetime is nihil, as the landers are designed to exceed the required mission lifetime.
More likely, one of the other two scenarios will unfold, because the assumption that at least one lander will survive is viable. For now, since large spread out populations on Mars are still far ahead and will not happen within 5 years of the mission end, 'On-Mars radio/communication stations' does not seem like a helpful strategy.

Continuing as global seismic network

Most likely, the system will be used to continue its functioning, especially still using its seismic measurement capacity. The thermal measurements can be prolonged mostly to verify the earlier measurements and increase the accuracy of the obtained data (minimising errors induced by external sources such as the Sun). However, the seismic network can be used to discover the interior of Mars far beyond just water pockets and thermal heat sources.

Continuing as global meteorological system

Extending the mission use beyond the mission need could increase the value and therefore the return on investment. The APSS equipment comes with great possibilities here. With measurements being done one wind speed and direction, pressure, temperature and the local magnetic field strength and direction, a very complete, global meteorological system can be put into operation. Of course, a combination of this meteorological functioning with the earlier mission purpose is not unthinkable, however, the downlinked data needs to be selected more carefully, as this is the limiting factor here. Also, in the detailed design phase, when all components and materials have been chosen, it can be decided to invest in some extra weather equipment when the probes are expected to live (far) beyond mission lifetime. This, however, needs an extra trade-off in the detailed design phase as it would increase the mass, volume, power need and cost of the orbiter and landers. A meteorological system with such coverage is not present yet on Mars, meaning this meteorological feature adds greatly to the worth of the mission.
As a final note, the orbiter its expected spare lifetime depends on several factors which will be discussed in the next subsection.

3.4. Disposal phase

Disposal of orbiter

The disposal of the METEOR system consists of that of the orbiter and the landers. For the orbiter, the disposal will mainly entail a deorbit burn allowing for the orbiter to disintegrate in the Martian atmosphere within a month. Such an operation is required because passive deorbiting can take up to twenty years and because of Mars its irregular gravity field it is impossible to predict the orbiter's location. This type of space debris is unacceptable, especially with future Mars missions in prospect. Therefore, a deorbit burn needs to be guaranteed. This implies that propellant needs to be reserved for this deorbit burn. With all margins taken into account in the models described in Chapter 10 and Chapter 9, there is enough propellant onboard to have the METEOR orbiter maintain its orbit for more than 20 years and still deorbit as described in Chapter 9. With total energy absorbed ranging up to $3\,MJ/m^2$ during entry of the Martian atmosphere (see Chapter 11), and the orbiter not being designed for high temperatures at all, the orbiter will burn up completely. Other than for the heat shield, the Aluminium structure of the orbiter has a low enthalpy for evaporation, which means temperatures will amply exceed the melting temperatures of the orbiter.

Disposal of landers

For the landers, getting rid of all the material during the disposal phase is not as viable and/or necessary as for the orbiter. Past and current Mars landers are usually just left on the Martian surface after operation. However, in the PPR and requirements such as **MR-TL-08** measures are taken to disturb Mars' ecosystem as little as possible.

4 Risk

This chapter features technical risk assessment. The technical risk assessment focuses on the risks that are not be handled in the subsystem analysis and design. These risks are summed and assessed in terms of probability of occurrence and impact on the mission. A neat overview of this risk assessment is depicted in Table 4.2. Next, all assessed risks are mitigated and re-assessed in a similar fashion.

4.1. Risk Assessment

Now the METEOR mission is heading into the detailed design phase, several risks have come to the forefront already. It is decided that the risks associated with subsystem will be identified and mitigated during the design phase of each subsystems. In this chapter risks regarding the whole system or those that have to do with the final design phases are shown. By analysing the risks now, it is possible to mitigate the risks as done in section 4.2. The SWOT analysis that was done in the baseline phase of the project which led to several of the analysed risks [13]. Since this was mostly helpful for earlier design stages, this analysis is not repeated here.

In Table 4.1, the probabilities and impacts of risks range from 1 to 5. A probability of 1 indicates 'extremely unlikely' to occur, and 5 indicates 'extremely likely' to occur. For the assessment of impact, the scale also ranges from 1 to 5. Negligible (1), means the impact is just an inconvenience or non-operational impact. Minor (2), means impact is a minor to the operation of the mission. Major (3), means impact is significant to the operation of the mission. Hazardous (4) means that the success of the mission is questionable or there is reduction in the technical performance. And catastrophic (5), means the impact results in mission failure.

Table 4.1: *Risk Assessment overview.*

No.	Risk	Cause	Consequence	Prob	Impact
1	Launch failure.	Launch vehicle destroyed.	Mission failure.	2	5
2	Launch postponed.	Extreme weather, incomplete spacecraft production.	Postponed launch.	2	2
3	Payload destruction during launch.	Launch loads.	Mission failure.	2	5
4	Spacecraft separation failure.	Obstruction by launcher.	Not reaching earth orbit.	1	5
5	Not enough budget to proceed on development of mission.	Cost exceeding the monetary budget limit.	Insufficient resources to realise current design.	3	4
6	Delayed development of the spacecraft design.	Team not meeting the deadlines.	Not possible to launch in the planned launch window.	2	4
7	Spacecraft too heavy to be launched.	Not meeting mass budget requirement.	Need to find an alternative launcher which will cost more.	3	4
8	Spacecraft does not fit in the launcher.	Not meeting volume budget requirement.	Need to find an alternative launcher which will cost more.	2	4

9	System failure of a lander.	Failure of any subsystem (as described in subsystem-related chapters).	Probe being out of service for rest of mission duration, decreasing coverage and scientific return.	3	4
10	System failure of the orbiter.	Failure of any subsystem (as described in subsystem-related chapters).	Orbiter being out of service for rest of mission duration, possibly mission failure.	3	5

To provide a better overview of all risks and their overall impact on the project, a risk map is created in Table 4.2. Using the risk map, it has been decided to try and mitigate all risks that appear in a yellow, orange or red cell (Starting from green to red the risk gets higher in the risk map).

Table 4.2: *Risk map of baseline risk assessment.*

		Impact on the project				
		1	**2**	**3**	**4**	**5**
Probability of occurrence	**1**					4
	2		2		6,8	1,3
	3				5,7,9	10
	4					
	5					

4.2. Risk Mitigation

After identifying different risks of the mission, they are ranked into different category based on the severity. It is important to come up with strategies for the ones that are ranked at higher risk levels. Risk mitigation strategy does not fully mitigate the risk but it is developed to reduce the overall impact they have on the mission. Risk mitigation has been achieved using one of two ways, either by reducing the impact said risk has on the mission or by reducing the probability of the event ever occurring.

A detailed explanation of the risk mitigation is provided in Table 4.3. Even though there are no risks located in red region of the risk map all the risks are tried to be mitigated to reduce the risk level of the entire system.

Table 4.3: *Risk Mitigation.*

No.	Action	Description of measure	Prob	Impact
1	Reduce Probability	Instead using 2 launchers all the system is designed to fit in 1 launcher. Furthermore, by analysing the missions that uses the same launcher before, if there is a critical problem with the launcher there will be higher chance of finding out the problem.	1	5
2	Reduce Probability	Weather conditions are checked and production process is planned carefully. Planning of the production process entails keeping an eye on external producers. Designing the 11 probes to have exact same configuration allowing the components to be ordered together. Using off the shelf components less likely there will be delay in production phase.	1	2
3	Reduce Probability and Impact	The complete spacecraft and its payload are carefully protected within the launcher. Making sure to design the payload configuration such that payloads do not touch each other under vibration	1	5

5	Reduce Probability	Cost manager will have an overview and set a guideline for each subsystem engineers to stay under the cost budget limit. By designing the probes to be universal so the development cost will be development cost of only 1 design. Furthermore, as the landers are designed universally, the production cost of the tooling will also reduce per probe.	1	4
6	Reduce Probability	Project manager will keep track of the team's deadlines via the Gantt chart and each subsystem's chief engineer will meet the deadlines.	1	4
7	Reduce Probability	The system engineer will communicate during the design phase with other subsystem chief engineers to meet the mass budget requirement. For designing process, there will be two limits. the First being the nominal limit and the second being the ultimate design limit. During the design phase the first limit will be considered as the ultimate limit. If due to circumstanced this limit is surpassed, it would not be really critical to the process.	2	4
8	Reduce Probability	Structure subsystem engineer will communicate during the design phase with other subsystem chief engineers to meet the volume budget requirement.	1	4
9	Reduce Probability & Impact	Probes will be located such that there is more than three coverage for different location of Mars. If one of the probes malfunction, there will still be enough coverage to acquire required information. Also, subsystems of the landers will be designed to have very high redundancy to reduce the probability of failure.	2	3
10	Reduce Probability & Impact	The subsystems of the orbiter will be designed to have very high redundancy to reduce the probability of failure. This allows the probes to still transfer data if there is problem with the orbiter. Moreover, in case the orbiter fails to transfer data to Earth, the probes will have the back-up option to communicate with other communication orbiters such as MRO. Since the TT&C subsystem is designed to be compliant with DSN, it is easy to reconnect the landers to an other orbiter.	1	4

Once the risk mitigation has been performed, an updated risk map is constructed in Table 4.4. As observed, the risks that were positioned at higher risk zones are moved to lower risk zones of the risk map.

Table 4.4: *Updated Risk map of baseline risk assessment..*

		Impact on the project				
		1	**2**	**3**	**4**	**5**
Probability of occurrence	**1**		2		5,6,8,10	1,3,4
	2			9	7	
	3					
	4					
	5					

5 Initial system overview

This chapter presents the results from the concept selection phase [11]. These results are the initial values that are used in the design that is detailed in this report.

5.1. Functional Flow Diagram

The system is designed to perform primary functionalities required to full fill the customer need. In order to established these functionalities a functional flow diagram is made and presented in Appendix A.

5.2. Functional Breakdown Structure

To establish a complete set of the functionalities the system is required to perform a functional breakdown is drafted in Appendix B. The diagram contains in a complete set of the required capabilities of the system to perform its mission.

5.3. Budgets

This chapter contains the initial budgets that are used as guidelines and reference data in the design process. The budgets were constructed in the concept selection phase of the METEOR mission design process [11].

Power Budget

The preliminary power budget remains unchanged from the concept selection phase [13] [11]. Based on the total power need previously determined, a preliminary budget was made for each subsystem using a percentage model. This model was estimated using heritage data [23]. This resulted in the peak power budget found in Table 5.1.

Table 5.1: *Preliminary peak power budget.*

Subsystem	Probe	Orbiter	Unit
Propulsion	1	5	W
C&DH	24	91	W
AOCS	28	107	W
TT&C	33	123	W
Payload	40	0	W
Structures & Materials	1	5.3	W
EPS (passive use)	14	53	W
Thermal	40	150	W
Total	182	534.3	W

Cost Budget

The preliminary cost budget has not changed since the concept selection phase and is shown in Table 5.2 [13] [11].

Table 5.2: *Preliminary cost budget.*

Mission stage	Absolute Maximum Cost [M€]	Design Cost [M€]
Development & Implementation	346.3	244.9
Operations	59.1	41.8
Launch	144.6	102.3
Total	550	389.0

Communications Budget

The preliminary budgets for the communications have not changed since the concept selection phase and are shown in Table 5.4[13] [11].

Table 5.3: *Preliminary communication budgets.*

	Minimum [bps]	Maximum [bps]	Allowed frequency bands	
Downlink	40	10	S,X	
Uplink	7.8	0.256	S,X,Ka	
Band	**Use case**	**Frequency [GHz]**	**Bandwidth [MHz]**	**Power [Watt]**
X	Primary link	8	50	100
Ka	Scientific transmission	32	500	35
UHF	Communication to probes	0.3-3	400	20-30
Mission phase	**Communication use**	**Uplink data rate**	**Direction**	
EDL	Essential telemetry on EDL	Low (5-10kbps)	One-way	
Science	Household & scientific data	High (1Mbps)	Two-way	

Computational Budget

The preliminary computational budget remains unchanged from the concept selection phase and is shown in Table 5.4.

Table 5.4: *Preliminary computational budget.*

Function	Estimated data [KIPS]	Budgeted data [KIPS]	% of total
Communications	10	40	4
Attitude sensors	25	100	9
Attitude determination	105	420	29
Autonomy	21	84	8
Fault detection	20	80	7
Power management	5	20	2
Thermal control	3	12	1
Kalman filter	80	320	30
Total	269	1076	100

Volume Budget

A preliminary volume budget is determined using the Ariane 6 User Manual provided by ESA [17]. For a single launch, the maximum usable volume in the fairing of the Ariane 64 is 242 m^3. Applying a 30% contingency means that the design maximum will be approximately 170 m^3. Extra considerations need to be taken as to how this volume is organised. The majority of the volume is made of a cylinder of 4.57 m in diameter and 11.185 m in height. This is approximately 76% of the total volume budget. The other 24% of the volume is a cone that tapers down from 4.47 m to 0.575 m in diameter over a height of 6.815 m [11].

In the initial heritage study percentage model, all the subsystems are well within budget. Table 5.5 shows only the total mission phase volumes, since a very detailed table does not show more relevant information.

Table 5.5: *Volume budget heritage percentage model.*

Mission phase / (Sub)system mass	Percentage model [%]	Absolute maximum [m^3]	Design maximum [m^3]
10 landers & satellite in Hohmann transfer (wet)	100	242	170
10 landers & satellite in LMO	30	72.0	50.4
1 lander in LMO (wet)	1.6	3.80	2.66
1 lander dry mass	1.4	1.58	1.11
Satellite in LMO (wet)	13	30.3	21.2
Satellite in LMO (dry)	10	25.1	17.6

Mass Budget

From the previously performed concept trade-off and heritage study, a more accurate preliminary percentage model mass budget is found in Table 5.6[11].

Table 5.6: *Percentage model of mass budget. The different shades of blue indicate the different mission phases and subsystems.*

Mission phase / (Sub)system mass	Percentage model [%]	Absolute maximum [kg]	Design maximum [kg]
Total mass in transfer (Wet)	100	7000	4900
Circularisation propellant mass	23	1608	1126
Total mass (wet) in LMO	77	5692	3984
Lander in LMO (wet)	100	300	210
Deorbit propellant mass	1.0	40	28
Aeroshell	27.0	70.2	49.1
Landing propellant	24.0	65	46
Propulsion	2.4	6.24	4.37
C&DH	1.9	4.99	3.49
TT&C	1.9	4.99	3.49
Scientific payload	13.9	36.2	25.3
AOCS	3.8	9.98	6.99
Structures & Material	10.1	26.2	18.3
EPS	10.1	26.2	18.3
Thermal	1.4	3.74	2.63
Cabling	2.4	6.24	4.37
Satellite in LMO (wet)	100	2392	1674
Maintenance propellant mass	17	406.6	284.6
Propulsion	5.8	139	97.3
C&DH	3.3	79.4	55.6
TT&C	23.24	556	389
AOCS	5.8	139	97.3
Structures & Material	17.4	417	292
EPS	21.6	516	361
Thermal	2.5	79.4	55.6
Cabling	3.3	59.6	41.7

6 Planetary Science

One of the most critical aspects that affect the design of the space mission is the environment where the operation takes place. In this chapter the landing site selection of the probes of the METEOR mission is presented.

6.1. Requirements

Customer requirements

There are two requirements that are given by the customer on the system that directly affect the landing site selection. These two requirements are the following:

MR-TL–02: The system shall consist of at least 2 probes per terrain: Northern Plains, Southern Highlands, Tharsis Complex, outflow region of Valley Marineris and Hellas Basin.

MR-TL–05: The system shall avoid current and planned landing sites by 100 km.

MR-TL–02 requires the 5 terrains to be covered at least by 2 probes. The 5 terrains are marked with Yellow shapes on the map Figure 6.1.

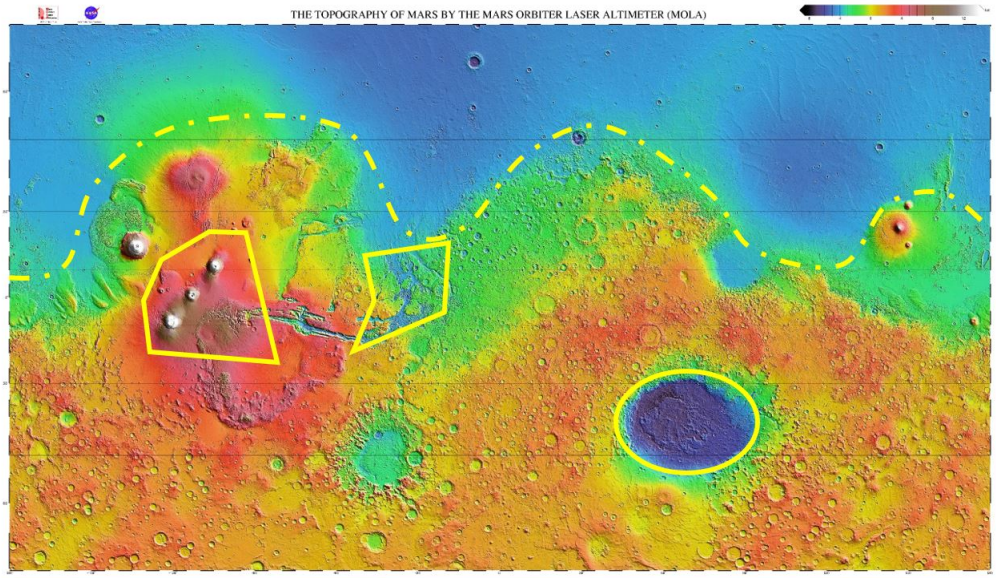

Figure 6.1: *Starting from left solid shaped regions, Tharsis Complex, Outflow region of Valley Marineris and Hellas Basin. Northern Plains and Southern Highlands are separated using a dashed line. Base map : MOLA topography[24].*

The requirement is interpreted, after consulting with the supervisor, in the way that a minimum of 10 probes are required and that the specified regions must be in the coverage zone of at least two probes. The coverage zone is a circular area marked on the surface of Mars wherein the probes can detect any seismic activities. It is very important to note that even though the scientific payload instruments on board of the probes do not change, the coverage zones can vary in size depending on the different magnitudes of seismic activities [25]. Table 6.1 shows the possible detection distance and coverage area for different magnitudes of the Marsquakes based on the SEIS instrument. As the METEOR's probes are using a seismometer that is as accurate as of the InSight SEIS instrument, the distances in angles in Table 6.1 can be used for the coverage mapping numerical model.

Table 6.1: *Possible seismic detection area for different magnitudes of Marsquakes of the InSight SEIS instrument[25].*

Distance [deg]	M_{min}	Fraction of Mars surface
25	2.6	0.07
45	2.9	0.15
60	3.0	0.25
90	3.2	0.50
150	3.5	0.93

Distance that is represented using an angle can be interpreted the following way: If the probe is located on the pole, and, if the distance coverage is 90 °, the probe has coverage until the equator line. M_{min} means the minimum Marsquake magnitude.

MR-TL–05 requires the probes of the METEOR mission to be placed at least 100 km away from all the previous and planned landing sites. All the previous landing sites' geographical locations on Mars are collected and marked on the map a the later stage to make sure there is no overlap of landing locations.

Other subsystem requirements

Apart from the requirements from the customer, there are also other constraints on the landing site selection. In this section, the requirements generated due to constraints from different subsystems of the space mission are discussed.

Dust cover constraint

From background research on landing site selection, one of the issues that can arise during the mission is that dust can cover up the solar arrays, leading to failure of the EPS subsystem of the probes. To avoid this problem, probes must land at a location with a low number of dust particles.
Dust coverage of different location of Mars is indicated by the dust cover index. The dust cover index is generated using thermal emission spectral data from the Mars Global Surveyor Thermal Emission Spectrometer (MGS-TES) [26]. The dust index is a score between 0 and 1, with 1 being the least amount of dust in the area. The threshold value that is used to rule out regions with too much dust is index of 0.94. This index value is based on the InSight mission [27].

Regolith composition constraint

From background research on the landing site selection of the InSight mission, one of the constraints is that the location that the probe will land must have fragmented regolith depth of 3 to 5 meters. Furthermore, the material that composes the regolith must be thicker than dust but not composed out of rocks. This is a requirement generated for the deployment of the HP^3 instrument [27].
Probes of the METEOR mission also need to plant the thermal sensor underground. From the design trade-off phase, a decision was made to use the same concept of the 'Mole' of the HP^3 instrument. There will be some modification to the instrument for better accuracy, but the insertion principle is the same. Thus, the same requirement of regolith is required. In order to look deep into the regolith it is required to analyse the crater projectiles of the region and composition of the projectile materials. However, this is impossible at this stage of the project as there is not any data available. More details will be explained in section 6.6. On the other hand, the particle composition of the first few cm of the surface can be analysed using the thermal inertia values. If the thermal inertia value is above 140 J m^{-2} K^{-1} $s^{-1/2}$, the regolith particles are considered to be bigger than dust particles [27]. The particles are more like the size of sand, which is the optimal compound to dig through. Thus, for the landing site selection, regions with a thermal inertia value lower than 140 J m^{-2} K^{-1} $s^{-1/2}$ are excluded.

Rock abundance constraint

From background research on the landing site selection, one of the constraints is that the location that the probe will land shall have a limited number of rocks. Rocks can be a source of landing sequence failure as it could tip over the lander. Also in the case of the InSight mission, the abundance of rocks can be the problem for the insertion of the HP^3 instrument. As the METEOR mission uses the similar concept, the same constraint for the rock abundance is applied. The constraint is that the landing site must have a lower

rock abundance than 10% [27]. The rock abundance map of Mars is acquired using the Thermal Emission Spectrometer (TES) results [28].

Altitude Constraint
For the probes to safely land on the surface of Mars, deceleration is required. Most the the deceleration happens due to atmospheric drag. The EDL system thus sets a constraint on the maximum altitude where the probes can be placed. For project METEOR, a hard limit of 3000 m is set. This value is deduced from previous missions.

Latitude Constraint
For the probes to operate, the EPS subsystem needs to provide enough power, the primary source of the power is the solar flux. At high latitudes, the incidence angle and magnitude of the solar flux decreases significantly. From the EPS subsystem, the hard limit for the maximum latitude the probes can be placed at are 40 ° North and 40 ° South latitude(13.4). This factor is not counted during the landing zone elimination but is taken into account in the landing site candidate selection part of the numerical model.

Steepness Constraint
For the seismometer to work, the slope of the deployment site needs to be less than 15 °[27]. This is due to the constraint of the seismic instrument that it should be placed below 15 ° angle for the 3-axis sensors to work correctly.

Newly generated requirements on landing sites
These are the newly generated requirements due to constraints from other subsystems, as just described.

MR-LSS–02: Landing sites of all the probes shall have a dust index of more than 0.94
MR-LSS–03: Landing sites of all the probes shall have a thermal inertia value higher than 140 $J\,m^{-2}\,K^{-1}\,s^{-1/2}$.
MR-LSS–04: Landing sites of all the probes shall have a rock abundance of less than 10 %.
MR-LSS–05: Landing sites of all the probes shall be placed in a location with altitude lower than 3000 m.
MR-LSS–06: Landing sites of all the probes shall be place in a location with latitude lower than 40 °.
MR-LSS–07: Landing sites of all the probes shall have a steepness of less than 15 °.

6.2. Model & Results
In this section, the build-up of the numerical model and the way the model is used to locate the final landing locations are presented. As the numerical model is focused on image processing, the run time of the numerical model is significant. Thus, the numerical model is divided into multiple steps. Data sets that are used in the numerical model are all extracted from the 'JMARS' program[29]. To be able to map the data to the correct position of the Martian surface, all data points are extracted together with the corresponding longitude and latitude positions.

Input variables

Table 6.2: *Input variables for landing site selection.*

Input variable	Value	Unit	Input variable	Value	Unit
Maximum altitude	3000	m	Maximum rock abundance	10	%
Maximum latitude	40	deg	Maximum ground slope	15	deg
Minimum dust index	0.94		Minimum thermal inertia value	140	$J\,m^{-2}\,K^{-1}\,s^{-1/2}$
Landing ellipse semi-major axis	100	km	Landing ellipse semi-minor axis	27	km

Landing zone elimination
The first part of the numerical model eliminates the different zones of the Martian surface that do not meet the requirement **MR-TL–05** or the constraints imposed by the different subsystems, as mentioned in section 6.1.
In Figure 6.2 black regions are No-Go regions for the METEOR probes.

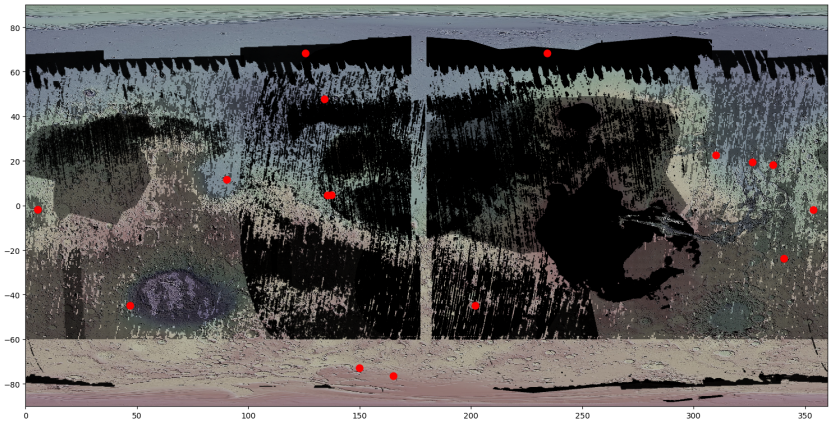

Figure 6.2: *Map of Mars indicating unacceptable landing surfaces in black. Red dots are location of the different missions current and planned. Between 173° longitude and 183° longitude data could not be retrieved.*

Locations on Mars that do not meet the threshold value are coloured black on the base Mars map. Also, there was another requirement on the landing site of the previous missions. Red circles indicate the regions that there is or will be a different Mars mission. Figure 6.2 uses the Mars surface map [30] as the base map to project all the data on. Then, from JMARS [29] different data sets like Altitude MOLA data, Thermal Emission Spectrometer data, TES dust index data, TES rock abundance data are collected. These data had to be collected manually by selecting parts of the surface of Mars. The data sets include longitude, latitude and the numerical value of the selected feature at the given location. For all the data sets, for the latitudes higher than 65, there is simply no data as the satellites that go around Mars did not collect data in the regions near the poles [29]. Unfortunately, for some parts of Mars the data was not complete. Namely the region between 173 degrees longitude and 183 degrees longitude. (This is expected to be problem during the data extraction from JMARS[29]). In the later stage, this region of Mars was excluded from possible landing sites. To rule out the different landing location on Mars, a numerical model is used to iterate through the entire data collected from JMARS. As mentioned in Table 6.1 there are threshold values for different filters.

Landing site candidates selection

After excluding the places that cannot be used for the landing site selection, now possible landing zones are identified. Possible landing sites does not mean all the areas that do not fall in the 'No Landing Zones'. This is because the lander cannot pinpoint the location and fall on the wanted location exactly. Any lander has an area on the planet called the 'Landing Ellipse'. This is a region where, if the probe executes the EDL sequence, it will land somewhere inside the zone. From background research on landing ellipses, the semi-major axis of the landing ellipse of the METEOR mission is decided to be 100 km Chapter 11. However, before the exact positions of the landing sites are selected, the orientations of the landing ellipses are unknown as they depend on the latitude positions of the landing sites. Thus, in this part of the numerical model the landing sites are assumed to be a circular region to make sure any orientation of the landing ellipses can fit once the orientations are known.
To efficiently find the possible landing zones, Figure 6.2 is converted into a black-and-white map of 720 X 360 pixels. With this image file, now the possible landing zones with 100 km diameter can be located. To find a possible location, each pixel is analysed with the following grid.

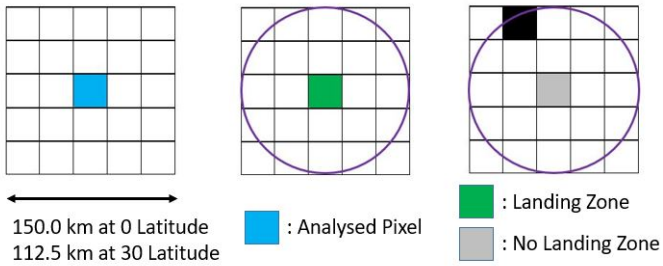

Figure 6.3: *Landing zone verifying pixel grid method.*

As indicated in the Figure 6.3, at different latitudes of the map, the pixel grid indicates a different landing zone size. This was calculated by dividing the circumference at the given latitude by 144. This is because every circumferential distance at different latitudes is divided into 720 pixels and 5 pixels indicate 1 landing zone size. As shown in the Figure 6.3, for a pixel that is getting analysed, if the surrounding grid does not have black pixels (which means that the location is restricted for landing) the pixel is coloured green. Else, it is coloured very light grey (just for clearance in the figure the shade is exaggerated). After this process, it is clear where on Mars the possible landing zones are. In Figure 6.4 the areas with possible landing zones are indicated.
Now that the area where landing zones can lie is clear, it is time to find exact locations where the probes can land. This was done using the JMARS program. In this program very high quality topography data is available. Thus, looking at areas with possible landing zones, possible landing zones are found. This part was done visually by finding where on the surface of Mars a circle with 100 km diameter can fit in. The circle shall not include craters or rough terrain. This is done in order to meet the requirement of 15 ° steepness constraint presented in section 6.1. By looking into areas that possible landing zones can be present, a total of 25 locations on the surface of Mars are chosen as possible landing sites.

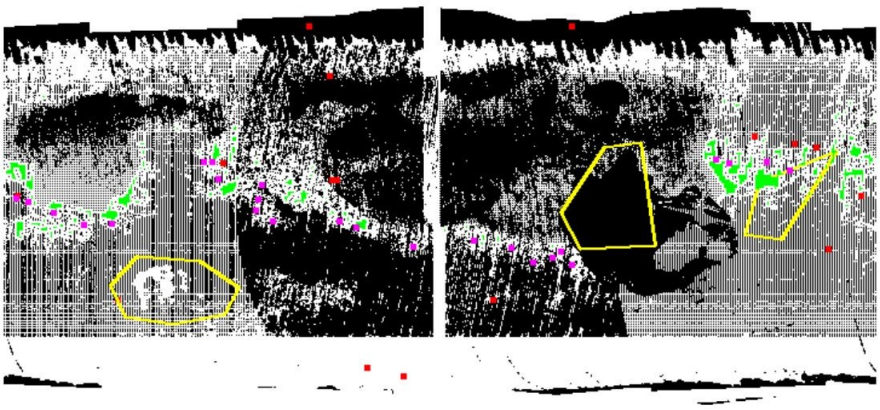

Figure 6.4: *25 landing site locations marked as pink dots. Green zones are an indication of possible areas with landing zones from the pixel analysis. Yellow regions indicate the three interest regions. Red dots indicate other missions.*

Landing site combination selection

In order to select the most optimal combination, background research on the locations of interest is performed outside the requirement of the costumers. The ultimate goal of the METEOR mission is to locate water and power sources for future colonisation of Mars. Looking at the planet's environment, specifically the temperature range and eclipse time, it is clear that if the future human colonisation happens, the location of interest is near the equator. Other locations of Mars are too harsh to start the colonisation. Thus, the coverage of the probes will mainly focus on the equator of the planet. As for finding a possible water source, hydrated mineral maps are used [31]. Hydrated mineral is a mineral that only arises if some time in the past the mineral was in contact with liquid water. Hydrated minerals are abundant near the equator region, especially above the Hellas basin region and the delta region of Valley Marineris. However, the formation of these minerals dates back to millions of years. Thus it may not represent the location where the most recent

water could have been. But still, looking at the geology of the terrains like surface roughness and orientation of the valleys, it can be concluded that near the equator region there is high chance of underground water. Thus, while finding the optimal composition of probes, the mentioned region is prioritised.
To find the best composition of the landers, a numerical model that will help the visualisation of the coverage of the probes is developed. For a given probe location on Mars, it indicates the circular coverage around the location in a 3D model. Then it translates the covered area onto a 2D map. If the coverage area of multiple probes overlap, the overlapping regions are coloured in different colours to indicate the level of coverage.
Form the background research on seismology, in order to locate the exact location of Marsquakes through seismic activity and extract any useful data, it is required to detect the seismic activity from at least three different locations [32]. Thus, the numerical model was used to optimise the regions near the equator to be covered with more than three probes at the same time.
As mentioned in section 6.1, for different magnitudes of seismic activity the coverage region changes. For a selected combination of landing sites the probability of detecting Marsquakes of different magnitudes is calculated. During the integration process, due to communication budget, a maximum of eleven probes can fit in the vehicle, thus two options using ten and eleven probes are analysed. The different results are shown in Table 6.3.

Table 6.3: *Comparison between ten and eleven probes design option detection capabilities.*

Marsquakes magnitude range	Minimum number of Marsquakes for given magnitude range for a year [25]	ten probes Mars more than 3 times or more surface coverage		eleven probes Mars more than 3 times or more surface coverage	
		Fraction of surface of Mars covered	Number of Marsquakes detected	Fraction of surface of Mars covered	Number of Marsquakes detected
2.6 ~2.8	100	0.00	0	0.02	2
2.9	80	0.19	15	0.30	24
3.0 ~3.1	140	0.65	90	0.70	98
3.2 ~3.4	76	0.99	76	0.99	76
3.5 or above	40	1	40	1	40
Total Number of Marsquakes detected per year			221		240

Table 6.3 shows the number of Marsquakes at different magnitude ranges that can be detected using the probes. The detection needs to happen by at least three probes to locate the exact position of the Marsquake. The third and fifth columns give the fraction of the Martian surface covered by at least three probes over the entire Mars surface. The fourth and sixth columns give the actual number of Marsquakes detected per year. These values are calculated by multiplying to number of Marsquakes per year (second column) and the fractions (third and fifth column). The number of occurrences of different Marsquake ranges are calculated from a technical debriefing report of the InSight mission [25]. After performing a trade off between the detection capabilities, redundancy and different budgets, it is decided to have eleven probes for the METEOR mission. The Figure 6.5 shows the coverage maps for two different Marsquake magnitude ranges.

As it can be seen for different magnitude ranges the coverage is very different. However, it is clear that the METEOR mission prioritises the equatorial region and the required area is indicated with a yellow shape. For higher magnitudes of Marsquakes the entire planet is covered. The exact locations of the probes are given in Table 6.4.

The eleven locations are optimised by trying different locations of probes from the possible 25 locations using the same tool that is used to generate Table 6.3.

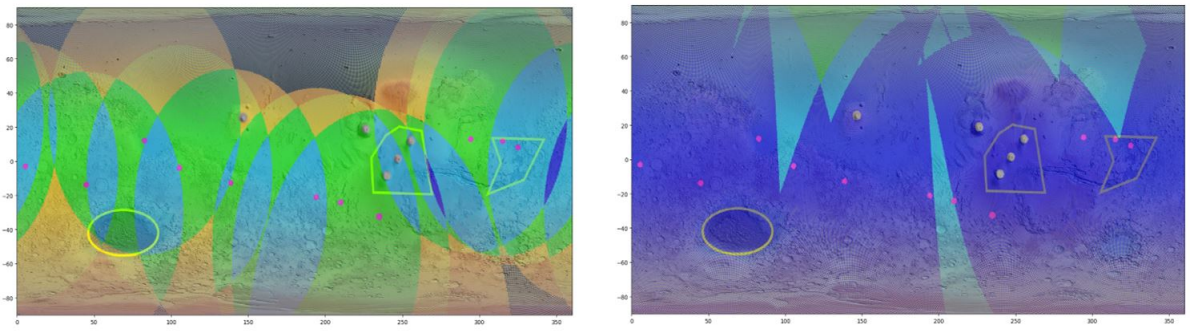

Figure 6.5: *Left : Coverage map for Marsquakes with a magnitude range of 3.0 to 3.1.*
Right : Coverage map for Marsquakes with a magnitude range of 3.2 to 3.4.
Coverage colour scheme Black: No coverage, Orange: 1, Yellow: 2, Green: 3, Light Blue: 4, Dark Blue: more than 5.

Table 6.4: *Selected landing sites of eleven probes.*

Number	Longitude [deg]	Latitude [deg]
1	5.41	-3.00
2	44.84	-13.72
3	82.71	12.00
4	105.37	-3.94
5	138.68	-12.59
6	194.18	-20.62
7	209.93	-23.50
8	234.98	-30.96
9	294.25	12.77
10	324.97	8.02
11	315.00	11.59

Landing Ellipses

After identifying the maximum latitude of the probes, the detachment orbit is designed such that the probe positioned furthest away from the equator can be placed. Knowing the detachment orbit, the exact orientation of the landing ellipses can be identified. As it can be seen in Table 6.4, the probe that is furthest away from the equator is positioned -31 ° latitude. Figure 6.6 presents a number of the landing ellipses on the surface of Mars.

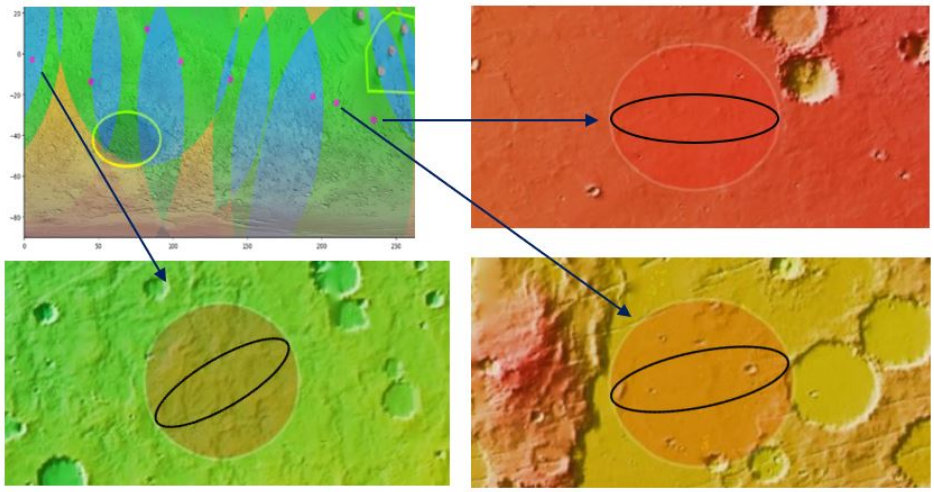

Figure 6.6: *Landing ellipses at different latitude location of Mars. Top left: Part of landing site map ,top right: -30.97 degrees latitude , bottom left: -3.00 degrees latitude , bottom right: -23.50 degrees latitude.*

The different background colour is due to the different altitudes the landing sites are located at. The size of the landing ellipse is determined in section 11.3. The semi-major axis is 100 km and semi-minor axis is 27

km. The inclination of the landing ellipses at different latitude locations are calculated using (6.1)

$$i = 31 \cdot \cos\left(\frac{\pi \cdot \phi}{62}\right) \tag{6.1}$$

6.3. Risk

Once the orientations of the landing ellipses are known, a preliminary risk assessment of the eleven landing ellipses is performed. To quantify the risk two parameters are used. The first parameter is the surface roughness and the second parameter is the crater surface coverage.
The first criterion is scored out of 3. 1 means the surface is smooth and there is low risk. 2 means part of the landing ellipse has rough surfaces. 3 means the entire landing ellipse has rough surface. The second criterion is scored as a percentage and it is based on the percentage of the landing ellipse covered with crater. The two criteria are multiplied to score the final risk and divided by 30. This is done since the maximum of the two criteria combined is 300, but the total risk is more clear if it is taken out of 10. Therefore, the maximum risk value is 10.
From a selecting a landing site candidates low resolution global Mars map was used to avoid the big craters. In the risk assessment higher resolution images are required. There are two Mars surface image data sets that can be used, namely HiRISE data or CTX data. Both of them are from the MRO mission. HiRISE provides very high resolution coloured images with a 30 cm per pixel resolution but due to its resolution, there are not enough data sets for all the landing sites[33]. However, CTX data provides images of the surface of Mars with resolution of 6 m per pixel which is more than enough to assess the craters and there is a very large data set available for the surface of Mars[34]. Thus, using the data from the CTX instrument, high resolution images of the landing ellipses are created.Figure 6.7 shows the high resolution images taken using the CTX instrument which are used for further analysis. the rest of the images can be found in Appendix C

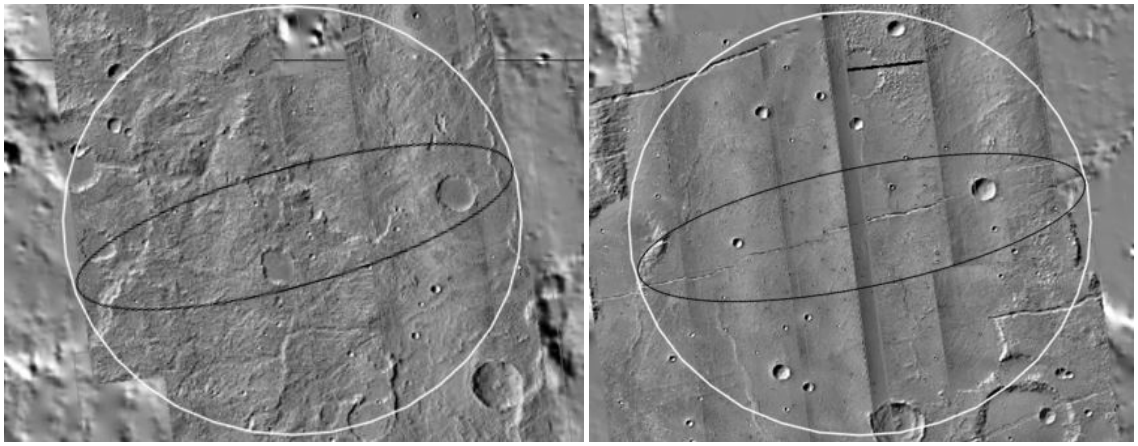

Figure 6.7: *High resolution image of the landing ellipses number 6 and 7 using the CTX instrument of the MRO mission*

Based on the high resolution CTX images of the 11 landing ellipses Table 6.5 is created that presents the different risk values based on roughness of the terrain and crater surface coverage.

Table 6.5: *Risk assessment of 11 landing ellipses*

Landing Ellipses	Roughness	Crater Surface Percentage (%)	Total Risk
1	3	0.41	0.04
2	2	0.92	0.06
3	1	0.36	0.01
4	2	0.20	0.01
5	3	2.17	0.22
6	3	7.95	0.80
7	1	0.56	0.02
8	1	0.52	0.02
9	1	0.54	0.02
10	2	1.23	0.08
11	1	0.96	0.03

As it can be seen in Table 6.5, the risk of the landing ellipses are small. These risks can be further reduced by having more accurate determination of landing ellipses. This means smaller ellipses can be drawn inside the current landing ellipses which can be orientated to avoid rough terrain or craters.

6.4. Verification & Validation

The numerical model is verified using the following method. First, the mapping capability is verified. This is done by getting the coordinates of very characteristic features of Mars like the three mountain peaks in Terras Complex region and Olympus Mons and mapping onto a desired base map. The numerical model is able to put points on the desired locations given the right coordinates.
Second, the coverage contour drawing capability is verified. This is verified by comparing the model with validated software called 'JMARS'. Different coordinates of probes are selected and coverage maps are created in both of the programs. The conversion from 3D coverage contour to 2D of the numerical model matched the circular coverage region that was drawn with the 'JMARS' program.
Third, the pixel analysis capability is verified. This is verified by inputting very simple bitmap of black & white and RGB images. The numerical model is able to analyse each and every pixel without making any errors in interpreting the colour of each pixel.
All the data that is used in the numerical model is validated data that is acquired though the validated software 'JMARS'[29]. The others part of the numerical model are very simple image processing and coordinate converting processes. Thus, it is safe to state that the numerical model is validated.

6.5. Compliance matrix

Table 6.6 shows the compliance matrix for the landing site selection. As it can be seen, all requirements are met.

Table 6.6: *Compliance matrix of landing site selection.*

Requirement ID	Met / Not met / TBD	Justification
MR-TL–02	Met	
MR-TL–05	Met	
MR-LSS–02	Met	
MR-LSS–03	Met	
MR-LSS–04	Met	
MR-LSS–05	Met	
MR-LSS–06	Met	
MR-LSS–07	Met	

6.6. Recommendations

The next phase of the landing site selection would be analysing the terrains in more depth. As stated in section 6.1, more analysis requires very high resolution data of the surface of Mars. This for example is to understand the exact depth of regolith of the landing ellipses. This data can be acquired by using for example the HiRISE camera. If the detailed analysis results in rejection of one of the selected landing sites, different combinations of landing site selection procedures will be iterated.

7 Scientific Payload

With the planetary science constraints presented in Chapter 6 discovered one can look into the characteristics and sizing of the scientific payload.

7.1. Functional analysis

The scientific payload subsystem ensures that the scientific mission objectives can be performed. This means the scientific payload shall be able to detect water and thermal energy sources on Mars. To do this, the scientific payload will consist of a seismometer instrument and a heat flux instrument. The seismometer will detect Marsquakes and use seismic tomography methods to determine the composition of the Mars crust and detect water pockets. The heat flux instrument will measure heat flux at the landing location which will indicate the presence of thermal energy sources.

7.2. Requirements

MR-SCI–01: Each Probe shall detect Marsquakes of minimum magnitude 3.236 in a circular area equivalent to 25% of Mars' surface around the probe.
*This requirement flows down directly from **MR-TL-13***

MR-SCI–01-01: The system shall be isolated from noise sources to ensure a signal to noise ratio (SNR) of 3 in the assigned area.
3 is the minimal SNR required for the payload to measure 3.236 magnitude Marsquakes in the 25% area around the payload.

MR-SCI–01-02: The system shall detect vibrations in the 0.1-5Hz bandwidth. **Replaced** [35]

MR-SCI–01-03: The system shall detect vibrations in the 0.1-20Hz bandwidth. [36]

MR-SCI–02: The system shall operate on Martian soil with a maximum tilt of 0.2 or [TBD] °. **Replaced** [35]
To ensure the nominal operation of the seismometers

MR-SCI–03: The system shall have an acquisition rate larger than 20 samples per second [35]. **Replaced**
To prevent aliasing

MR-SCI–04: The system shall measure temperature differences with a 1-σ uncertainty of 6.5 mK.
[37]

MR-SCI–05: The system shall measure the regolith thermal conductivity with a 1-σ uncertainty of 3.5%.
[35]

MR-SCI–06: The system shall measure the heat flux at a depth range of [TBD] mW/m^2 to [TBD] mW/m^2 meters beneath the surface. **Replaced**
To avoid that the heat flux measurements are influenced by solar heat flux.

MR-SCI–07: The system shall operate on Martian soil with a maximum ground slope of 15 °. [35]
Based on limitations of the short period seismometers.

MR-SCI–08: The system shall have a sampling rate 2.5 times higher than the highest recorded frequency.

To prevent aliasing

MR-SCI–09: The system shall measure the heat flux at a depth range of 3 to 5 meters beneath the surface.

To avoid that the heat flux measurements are influenced by solar heat flux.

MR-SCI–10: The system shall synchronise its on-board time management unit with the orbiter time management unit at least once per sol. **Added**
This is essential to ensure accurate conclusions can be made using the seismic network

Replaced Requirements

MR-SCI–01-02 replaced by **MR-SCI–01-03**: The original frequency range of 0.1-5 Hz was not sufficient to cover the high-frequency Marsquakes.

MR-SCI–02 replaced by **MR-SCI–07**: Tilt was changed to ground slope as this is better defined. The value also has changed as the instrument has been modified.

MR-SCI–03 replaced by **MR-SCI–08**: This new requirement does not require being changed when other requirements change such as **MR-SCI–01-03** while remaining verifiable.

MR-SCI–06 replaced by **MR-SCI–09**: Incorrect units for depth make the requirement unverifiable and a new requirement was made.

7.3. Model & Results

The most recent mission that possesses the same type of instruments that will be used for this mission is the InSight mission. Due to the complexity of fully designing two new instruments, these existing instruments and their performances will be used to size the subsystem.

Seismometer

The Insight seismometer is composed of two systems. Very Broad Band (VBB) sensors and Short Period (SP) sensors. The VBB covers a frequency range from 0.01 to 5 Hz and the SP from 0.1 to 50 Hz. Such a broad range is not necessary for the objectives of this mission. The smallest pockets of water that can be detected depends on the highest frequency that can be detected by a seismometer. In other words, if the water pocket is smaller than the smallest wavelength that can be detected, this water pocket cannot be registered. To estimate this, P and S wave speeds in the crust also need to be known. The current best estimates for the wave speeds in the Martian crust are given in Table 7.1 [36] as well as the smallest wavelengths calculated using (7.1). Where λ is the wavelength, V_{quake} Marsquake wave speed and f wave frequency. Even though the SP sensors can measure up to 50 Hz, their performance has been limited to 20 Hz due to excessive noise past this frequency. This has the added benefit of allowing a reduction of the sampling frequency to 50 Hz and thus overall data generation. To prevent aliasing, a factor of 2.5 has been applied to the 20 Hz limit and therefore the sampling frequency may not go below 50 Hz.

$$\lambda = \frac{V_{quake}}{f} \tag{7.1}$$

Table 7.1: *Seismic Wave Calculations.*

	Wave Speed [m/s]	SP Highest Frequency [Hz]	VBB Highest Frequency [Hz]	SP Smallest Wavelength [m]	VBB Smallest Wavelength [m]
P wave	3979	20	5	198.95	796
S wave	2300	20	5	115	460

The ability to measure high frequency (HF) seismic waves (HF events are higher than one hertz [36]) plays an important role in increasing the resolution of the data that can be gathered. Another reason for detecting HF Marsquakes instead of Low Frequency (LF) Marsquakes is based on one of the fundamentals of seismic tomography. The waves detected by the seismometer have to pass through the region of interest to be able to gather any information. With the Martian crust being the region of interest to find water in, looking at Figure 7.1[36], HF events primarily propagate in the crust and therefore can provide information about its composition.

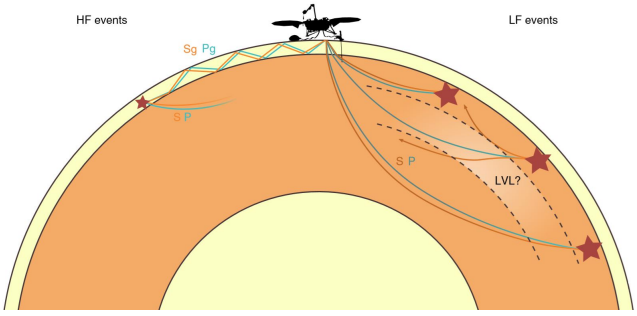

Figure 7.1: *HF and LF Marsquake wave propagation.*

The VBB is highly focused on detecting very low-frequency events, therefore it is considered non-essential for this mission and is removed from the instrument package. Based on data recorded by the SEIS instrument package until the 30th of September 2019, 174 seismic events were recorded, of which 150 are high-frequency events. As the VBB and SP have similar performances over the 3 to 5 Hz range and the VBB does not go above 5 Hz, it is removed as the extra information it provides is not relevant to the mission. This has several positive outcomes such as reducing the subsystem mass and the amount of data produced, reducing requirements for other subsystems.

Removing the VBB also changes the requirements for this subsystem. The remaining SP sensors do not require being level and can perform the mission up to a ground slope angle of 15°. This requirement mainly affects the landing site selection which is covered in Chapter 6. With this change, additional components can be removed. These are the levelling actuators and the legs that the actuators move. The mass savings are shown in Table 7.2. It was decided to keep the levelling sensors as these are useful to calibrate the remaining SP sensors.

Table 7.2: *Scientific Payload Mass Breakdown.*

	Before VBB Removal [kg]	After VBB Removal [kg]
Seismometer Assembly Mass	8.702	6.414
WTS Mass	3.628	3.628
APSS Mass	5	5
Heat Flux Instrument Mass	3.757	3.757
Scientific Payload Total	21.087	18.799

With each SP sensor having a mass of only one gram each[1], making two levels of redundancy would only require an additional six SP sensors and thus six extra grams. Each level of redundancy requires three SP sensors as each sensor can only cover one axis.

Noise reduction

Seismometer performance highly depends on the amount of noise in the environment. Therefore measures are taken to minimise the noise. The payload will feature both passive and active noise reduction features that will be elaborated upon.

Passive noise reduction: Wind & Thermal Shield (WTS). To isolate the seismometer from external noise and the extreme conditions on Mars, the WTS is used. As this mission has a smaller lander and does not have access to a robotic arm as the Insight mission does, the deployment of the instrument and the WTS need to be redesigned. A simple solution for this is to drop the instruments from underneath the probe as well as the WTS.

As the WTS is deployed from the bottom of the lander, it no longer needs a top cover as the original Insight WTS has. An estimate of this new mass can be made by dividing the new WTS surface area by the original WTS surface area and multiplying this ratio with the original WTS mass. In using this method to estimate the new mass of the WTS, it is assumed that it will have the same noise reduction and thermal shielding as the original WTS. Keeping these requirements is essential to the function of the seismometer as noise is the main limiting factor when detecting seismic activity[35].

Active noise reduction: Auxilliary Payload Sensor Suite (APSS)[38]. The APSS is a combination of sensors used to actively reduce the noise in the signal detected by the seismometer. These sensors include a magnetometer, wind speed sensors, air temperature sensors and an atmospheric pressure sensor. As the mass of these sensors could not be found, an initial estimate of five kilograms was allocated to these and added in the scientific payload mass in Table 7.2.

[1] `https://www.seis-insight.eu/en/public-2/seis-instrument/sp-seismometer`, retrieved 13/06/2020

Heat flux probe

For the Heat Flux Probe, the HP^3 instrument concept from the Insight mission fits the needs of this mission perfectly. The HP^3 measures the heat flux by deploying an instrumented tether into the Martian surface [37]. The instruments on this tether are temperature sensors placed at specific intervals. Measuring the temperature at different depths in this way, the heat flux can be calculated. The tether is inserted into the ground with the help of the 'mole' which is a mechanical hammering device. However, reusing the HP^3 instrument would not be possible for this mission as it does not meet the **MR-TL-02** requirement presented in Chapter 18. The accuracy of HP^3 is 5 mW/m^2 whereas the required accuracy is 1 mW/m^2. Redesigning and verifying the new accuracy of the updated instrument is outside of the scope of this design phase and it is assumed it will meet requirements once updated. However, some factors that increase accuracy will be presented.

Accuracy of heat flux measurements increases with measurement time[37]. The HP^3 accuracy is based on a two year measurement time. Looking at Table 21.1 METEOR has a primary science phase of 3.81 years which means the measurement time can be nearly doubled and thus the accuracy will increase. Another option is to increase the accuracy of the temperature sensors placed on the tether. Finally, if both these options do not suffice to meet the requirement, more temperature sensors may be placed on the tether to increase resolution. This is not ideal as it would increase the total data production and impose larger data transfers back to Earth.

The mass of the updated instrument was assumed to be the same as the original HP^3 instrument [37] and is shown in Table 7.2. The physical configuration has been altered to fit within the new lander. The original configuration can be seen in Figure 7.2a [2] and the new configuration in Figure 7.2b. The structural mass for this new configuration is expected to be lighter than the original as it is now incorporated into the lander which means it no longer requires legs to support itself. This means that the mass of the new instrument is likely overestimated and may be reduced during further iterations of the design.

(a) **(b)**

Figure 7.2: *Original (a) and new (b) HP^3 configuration.*

Instrument deployment

The seismometer and WTS can be deployed on sol 1 and start operating as soon as both are deployed. The WTS will first be lowered, then shortly followed by the seismometer.

The heat flux probe however, may take up to sol 44 for it to be fully deployed at the required depth[37].

7.4. Risk

The instruments still need to be developed so calculating their reliability is not feasible at this stage. It is therefore assumed that they will be designed with reliability higher or equal to 99%. Risks related to the Martian environment will be discussed in this section along with the methods used to mitigate these risks.

[2] `https://www.seis-insight.eu/fr/public/la-mission-insight/les-autres-instruments`, retrieved 14/06/2020

1. **Risk**: Ground slope of more than 15°
   ***Mitigation**: Adequate landing site selection*
2. **Risk**: WTS Damage
   ***Mitigation**: Ensure design can survive Martian environment*
3. **Risk**: Rocks blocking deployment of either instruments
   ***Mitigation**: Adequate landing site selection*
4. **Risk**: Mole does not reach sufficient depth
   ***Mitigation**: Adequate landing site selection*

7.5. Verification & Validation

Verification

The sizing of the scientific payload only required calculations of surfaces, volumes, masses, densities and wave properties which have been unit tested through manual verification. Calculations combining all the results have also been verified using manual verification.

Validation

The tools used are only sizing tools that are not modelling anything and therefore do not require validation.

7.6. Compliance matrix

Table 7.3 shows the compliance matrix for the scientific payload subsystem.

Table 7.3: *Compliance Scientific Payload, TBC = To Be Confirmed.*

Requirement ID	Status	Justification
MR-SCI–01	MET	
MR-SCI–01-01	MET	
MR-SCI–01-03	MET	
MR-SCI–04	TBC	Will be met when updated mole instrument is developed
MR-SCI–05	MET	
MR-SCI–07	MET	
MR-SCI–08	MET	
MR-SCI–09	MET	
MR-SCI–10	MET	

7.7. Recommendations

Seismometer

At this stage of the process, it is assumed that removing the VBB does not affect the performance of the seismometer such as coverage. This is done to help select landing sites. It is recommended once this updated seismometer is developed to test its performance indicators such as detection coverage. Large changes in performance may require an extra iteration in the instrument design or change the mission characteristics such as landing site selection.

Further investigation needs to be done concerning the time synchronisation of all the seismometers. Absolute timing is not required for all the landers but relative differences in time need to be minimal. This can be done by synchronising the time management units of the landers with the orbiter time management unit every time they come into contact. Each lander is contacted at least once per sol by the orbiter and therefore may synchronise their time management units. The orbiter time management unit will act a the reference for all landers. The lander time management unit will then simply have to deviate less than a certain amount between orbiter contacts.

Finally, if the mass of the APSS is more than the five kilograms allocated initially, an iteration will need to be made and the total lander wet mass will increase. This is not expected to be problematic as the entire system still may increase by an additional 1500 kg before reaching the maximum launch mass.

Heat Flux Probe

The performance of the HP^3 instrument has proven to be problematic for Insight. The mole initially failed to insert itself into the ground. The current solution to the problem that is providing results is applying 50 N of force to the top of the mole using Insights' robotic arm to get it be fully underground[3]. The mole is expected to be able to continue digging by itself once it is completely underground. The mole for this mission is deployed beneath the lander which means a simple mechanism can be developed to apply the necessary pressure to get the mole to a sufficient depth for it to start digging by itself. The lander would act as an object the mechanism can push against. Extra iterations of the design would therefore be necessary as the mechanism required to apply this force has not been taken into account in the current design iteration.

In the event that the probe still does not work after being pushed fully underground, the heat flux probe either needs to be redesigned with the new acquired knowledge or the method needs to be scrapped and a new method will need to be developed. A redesign could consider changing the outer surface of the mole to give it more friction unidirectionally. This means minimising friction in the direction of motion and maximising it in the opposite direction.

[3] `https://www.dlr.de/blogs/en/all-blog-posts/The-InSight-mission-logbook.aspx`, retrieved 12/06/2020

8 Structures & Materials

Structures and materials subsystem is responsible for designing all load-bearing structures for the METEOR mission and provide certainty it will perform its function without failure. Another responsibility is the choice of materials used throughout the whole mission.

8.1. Functional analysis

The functions for the structures and material subsystem are displayed in Figure 8.1.

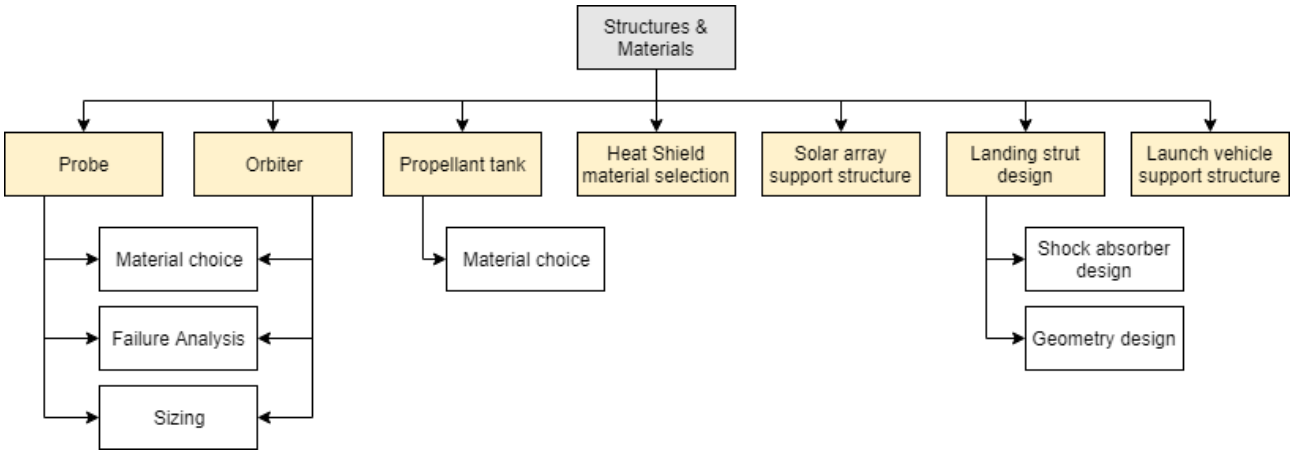

Figure 8.1: *Functional breakdown for the Structures & Materials subsystem.*

As can be seen, both probe and orbiter are provided with the same outputs. First, a material choice trade-off is performed for both the probe and orbiter to allow for further analysis. Afterwards, the loads acting on both the probe and orbiter are set and failure analysis is performed. This entails analysing different possible failure criteria and by iteration figuring out which failure mode is critical. This depends on the probe and orbiter size. Therefore, several iteration cycles were performed were the orbiter size is changed to fit components and then repetitively check if the structure fails or not.

Regarding the EPS subsystem, a rod supporting the solar arrays was designed to prevent failure during extreme conditions as high wind, for example. In addition, for the payload, a shock absorber was designed alongside the landing strut to allow for safe landing without impact loads propagating to the payload. Also, to facilitate landing at angles lower than 15 °. For the propulsion subsystem, a trade-off was performed for materials used for the propellant tank. Moreover, during entry and descent, the heat shield was designed alongside the EDL engineer to satisfy all requirements mentioned in section 8.2 and 11.2. Again based on these requirements, the material choice trade-off was performed. Lastly, to align the probes and orbiter in the launch vehicle, a supporting structure was designed.

8.2. Requirements

Below you can find a list of requirements previously generated during the requirement and concept generation phase of the design process [13].

MR-STRCT-01: The system shall be able to house all spacecraft subsystems.
MR-STRCT-01-01: The system shall be able to unite all subsystems in one structure.
MR-STRCT-01-02: The system shall comply with the mass budget.
MR-STRCT-01-03: The system shall comply with the given launcher dimensions.
MR-STRCT-01-04: The system shall comply with the volume budget.
MR-STRCT-02: The system shall withstand experienced loads during launch phase.

MR-STRCT-02-01: The system shall withstand internal static loads during launch phase of magnitude of [TBD]. **Deleted**
MR-STRCT-02-02: The system shall withstand external static loads during launch phase of magnitude of [TBD]. **Deleted**
MR-STRCT-02-03: The system shall withstand internal dynamic loads during launch phase of magnitude of [TBD]. **Deleted**
MR-STRCT-02-04: The system shall withstand external dynamic loads during launch phase of magnitude of [TBD]. **Deleted**
MR-STRCT-02-05: The system shall withstand longitudinal accelerations in the range from -4.6 g to 3.1 g during launch [17].
MR-STRCT-02-06: The system shall withstand lateral accelerations in the range from -2.0 g to 2.0 g during launch [17].
MR-STRCT-03: The system shall withstand loads during entry, descent and landing procedure.
MR-STRCT-03-01: The system shall withstand loads of magnitude of 6.9 g during descent.
MR-STRCT-03-02: The system shall withstand loads of magnitude of 4.74 g during landing.
MR-STRCT-04: The system shall protect the scientific payload in all mission phases. **Deleted**
MR-STRCT-04-01: The system shall protect the scientific payload from forces with a maximum magnitude of [TBD]. **Deleted**
MR-STRCT-04-02: The system shall provide a maximum vibrational load of [TBD] to the scientific payload. **Deleted**
MR-STRCT-05: The system shall protect the spacecraft from external space threats.
MR-STRCT-05-01: The system shall protect the spacecraft from radiation of 1 Sv.
MR-STRCT-05-02: The system shall protect the spacecraft from impact with foreign objects with a mass of [TBD] kg and velocity of [TBD] kg. **Replaced**
MR-STRCT-05-03: The system shall protect the spacecraft against surface threats.
MR-STRCT-05-04: The system shall protect the spacecraft from Martian atmosphere.
MR-STRCT-06: The system's structural stiffness shall guarantee fundamental frequencies of the spacecraft within requirements of the chosen launch vehicle.
MR-STRCT-06-01: The system shall withstand a minimum longitudinal frequency of 100 Hz. [17]
MR-STRCT-06-02: The system shall withstand a minimum lateral frequency of 100 Hz. [17]
MR-STRCT-07: The materials used in the system shall maintain its performance throughout the spacecraft lifetime.
MR-STRCT-07-01: The materials used shall withstand temperatures with a minimum of 318 K.
MR-STRCT-07-02: The materials used shall have a maximum thermal coefficient of 300 [W/m·K].
MR-STRCT-07-03: The materials used shall be corrosion resistant or equipped with a corrosion protection layer.
MR-STRCT-07-04: The materials used shall be manufacturable.

Deleted Requirements

During the conceptual design phase, requirements were reviewed and some were chosen to be deleted.

- **MR-STRCT-02-01** and **MR-STRCT-02-02** were deleted because they stem from requirements **MR-STRCT-02-05** and **MR-STRCT-02-06**.
- **MR-STRCT-02-03** AND **MR-STRCT-02-04** were deleted because they stem from requirements **MR-STRCT-06-01** AND **MR-STRCT-06-02**.
- **MR-STRCT-04** and its child requirements were deleted as they are not verifiable at this stage of the design.

Replaced Requirements

Requirement **MR-STRCT-05-02** is replaced as the mass and velocity are not the limiting factor but the force exerted by them is. New requirement is

MR-STRCT-05-05: The system shall protect the spacecraft from impact with foreign objects with a maximum experienced force of 5000 kN.

8.3. Model & Results

This section is divided in two different ways based on Figure 8.1. First, on a higher level, it is divided into probe, orbiter, propellant tank, EPS support structure, landing strut design, heat shield material selection and launch vehicle support structure. Afterwards, every part is further broken down into model development and results.

Probe

Material Choice

Before considering the possible options, the trade-off criteria need to be set. The criteria were chosen based on the aforementioned requirements. Also, these choices were recommended in literature [39]. The criteria are:

- Specific Stiffness
- Specific Strength
- Ease of manufacturing
- Thermal expansion coefficient
- Cost

As the structure subsystem needs to withstand all the applied loads and experienced frequencies while being as light weight as possible, specific stiffness and strength are considered. Specific stiffness for a lightweight panel is $\frac{E^{\frac{1}{3}}}{\rho}$ and specific strength is $\frac{E^{\frac{1}{2}}}{\rho}$ [40]. Ease of manufacturing is graded relative to other materials. It entails manufacturing difficulties, possible geometries and availability. Furthermore, the thermal expansion coefficient is a measure of how much the material expands when high temperatures are applied. This is an important criterion as during the EDL procedure, the material experiences high temperatures. Lastly, cost is considered as it is a limiting factor during the design as well according to requirement **MR-MRT-01** [13].

Based on literature [23, 39, 41], Table 8.1 was constructed with the most promising and most widely used options in the aerospace industry.

As can be seen, composites excel in terms of specific stiffness and strength in comparison with other metals. However, they provide difficulty in manufacturing and most importantly, they are expensive to produce. To limit the composite choices, boron composites are excluded as they still have a low TRL despite their potential. This is because boron composites display surface defects that decrease the structural integrity of the composite[42]. Steel-aluminium composites are very heavy compared to other metals and carbon-aluminium composites. Thus, the only remaining viable option is carbon-aluminium composite, where carbon is used as the skin material carrying tension and compression loading and aluminium is the core material providing a higher bending stiffness and withstanding shear loads. For the probes, carbon-aluminium composites can be a viable option as eleven probes need to be produced. Carbon-aluminium composites are cheaper if they are produced in large numbers, thus, this way the production costs can be reduced [23].

Failure Analysis

To start analysing the possible failure modes, the loads acting on the probe are considered first. The most critical loads are the ones experienced during launch. As mentioned in Chapter 11, the maximum experienced loads are 6.9 g vertically. However, the loads experienced during launch are higher, as mentioned in requirements **MR-STRCT-02-05** and **MR-STRCT-02-06**. For the conceptual phase, the probe is chosen to be a cylinder structure to handle internal pressure and fit subsystems easily.

As there is a longitudinal and lateral loads acting on the probe, axial and bending stresses will be induced. These are grouped together and indicated by (8.1). This is done with the underlying assumption of modelling the probe as a beam with its mass concentrated as a point load.

$$\sigma_{tot} = \frac{SF \cdot g_{long} \cdot g \cdot \text{Mass}}{\pi \cdot d \cdot t} + \frac{SF \cdot g_{lat} \cdot g \cdot \text{Mass} \cdot \frac{1}{2} \cdot h}{\pi \cdot r^3 \cdot t} \tag{8.1}$$

Table 8.1: *Possible materials and their respective properties.*

	Material	Specific Stiffness [m^2/s^2]	Specific Strength [m^2/s^2]	Ease of manufacture [1-5]	Thermal Expansion Coefficient [$W/(m \cdot K) \cdot 10^{-6}$]	Cost [1-5]
Aluminium	2014-T6	1.486	7.017	5	154	5
	2024-T36	1.502	7.337	3	120	4
	2195-T84	1.542	7.991	3	130	3
	6061-T6	1.499	5.728	5	167	5
	7075-T6	1.479	7.559	4	196	4
	7475-T761	1.4666	7.532	4	147	4
Composites	Boron-Aluminium	2.329	13.342	1	-	2
	Boron-Magnesium	2.808	16.112	1	-	2
	Carbon-Aluminium	2.723	13.333	2	-	1 or 2
	Steel-Aluminium	1.094	8.808	2	-	3
	Boron-Titanium	1.847	10.842	1	-	1
Titanium	Ti6AL-4V	1.095	6.696	3	7.3	2
Steel	AISI 4340	0.751	2.762	4	15	4
	D6AC	0.755	5.276	4	-	4

The safety factor (SF), is chosen to be 1.4, the value of the flight limit load safety factor, the reasoning behind this will be explained later in section 8.4. This is often used to calculate the maximum load experienced during mission [43]. Both g_{long} and g_{lat} indicate the maximum longitudinal and lateral accelerations experienced during launch [17]. Diameter, radius, thickness and height are indicated by d, r, t and h respectively. Mass here refers to the total mass of the probe.

Furthermore, as the largest load applied is longitudinal, column buckling is an important factor to consider as well. For hollow cylinders, column buckling is indicated by (8.2) where E indicates the material's young's modulus [43].

$$\sigma_c = E \cdot \left[9 \left(\frac{t}{r} \right)^{1.6} + 0.16 \left(\frac{t}{h} \right)^{1.3} \right] \tag{8.2}$$

Previous equations, (8.1) and (8.2), are considered from a design for strength perspective. However, designing for stiffness is a critical aspect as well. Thus, the longitudinal and lateral natural frequencies of the probe are considered and displayed in (8.3) and (8.4) [23].

$$f_{long} = 0.250 \sqrt{\frac{\pi \cdot d \cdot t \cdot E}{\text{Mass} \cdot h}} \tag{8.3}$$

$$f_{lat} = 0.560 \sqrt{\frac{E \cdot \pi \cdot r^3 \cdot t}{\text{Mass} \cdot h^3}} \tag{8.4}$$

As set by requirement **MR-STRCT-06** from [17], both of the natural frequencies need to be higher than 100 Hz to provide sufficient stiffness to the structure.

Sinusoidal excitation affects the launch vehicle during its powered flight, therefore it imposes a natural frequency constraint. However, as specified in the Ariane 64 user manual [17], the maximum excitation frequency in both longitudinal and lateral direction is lower than 100 Hz. Therefore, it was not considered to be

a limiting factor during design. The same applies for acoustic vibrations, which occur due to unsteady aerodynamic phenomena and shock loads, which occur during stage and fairing separation. Thus, the driving requirements are the longitudinal and lateral accelerations and random vibration frequency requirement of 100 Hz. This is also supported by literature [39].

Sizing
The sizing of the probe is done by taking the dimensions of the probe as an input, then the stresses and frequencies previously mentioned are computed and it is checked whether they meet the requirements. The size is iterated to fit all remaining subsystems while being kept as compact as possible. The stresses and frequencies are computed using the material previously selected. The probe assembly with all subsystems fitting is indicated in section 17.2

The final volume of the structure is computed using (8.5)

$$V_{pr} = \left(h(\pi \cdot r^2 - \pi \cdot r_{inner}^2)\right) + 2\left(\pi \cdot r_{inner}^2 \cdot t\right) \tag{8.5}$$

Finally, the structural mass can be computed using (8.6)

$$m_{pr} = \rho \cdot V_{pr} \tag{8.6}$$

Results
Using the aforementioned equations and method, the input and output variables are displayed in Table 8.2.

Table 8.2: *Input and output variables to size the probe.*

Input variable	Value	Unit	Output variable	Value	Unit
r	450	mm	σ_{tot}	6.31	MPa
h	545	mm	σ_c	411.9	MPa
t	2	mm	f_{long}	839.798	Hz
SF	1.4	/	f_{lat}	1098.308	Hz
g_{long}	6.9	/	m_{pr}	12.593	kg
g_{lat}	2	/	V_{pr}	0.005597	m^3
$f_{excitation}$	100	/			
ρ	2250	kg/m^3			
σ_{yield}	900	MPa			
$\sigma_{ultimate}$	900	MPa			
E	230	GPa			
$Mass$	211.487	kg			

Orbiter
The orbiter design approach is very similar to the probe design approach. Thus, in this subsection, the differences are stated.

Material Selection
The same material selection method that is used for the probe applies for the orbiter as well. This also includes trading off materials based on the same criteria. However, the only difference is the number of products produced. As only one orbiter is produced, the cost of choosing composites would be too expensive. This is because for composite materials, if produced in a large volume, the price difference with low-volume production is small because of the equipment and materials purchased [39]. Thus, aluminium is the preferred choice. Seven series aluminum alloy is chosen, as the second series alloy impose difficulty in manufacturing and assembly. In specific, the 7075-T6 aluminium alloys is chosen because of its higher specific properties compared to 7475-T761.

Failure Analysis

Again, the same failure criteria apply. However, as the orbiter would be at the base of the launch vehicle, which would be illustrated later on in section 17.2, the orbiter needs to attach to the launch vehicle adapter. Thus, a cross-section is a square or rectangle [23]. Therefore, the stresses and frequencies equations previously stated would change by changing the cross-section. By having square cross-sections, shear stress plays an important role as well. A commonly used failure analysis method to include shear is Von-Mises stress which is displayed in (8.7) after simplification [44].

$$\sigma_{vm} = \sqrt{\frac{1}{2}\left((\sigma_z - \sigma_y)^2 + \sigma_z^2 + \sigma_y^2\right) + 3\left(\tau_{xy}^2 + \tau_{zx}^2\right)} \tag{8.7}$$

Using Figure 8.2 [45], but with the z-axis pointing upwards, the Von-Mises stress components can be computed using (8.10), (8.10), (8.9) and (8.11).

$$\sigma_z = \frac{SF \cdot g_{long} \cdot g \cdot \text{Mass}}{(2 \cdot t \cdot (l+w)} \tag{8.8}$$

$$\sigma_y = \frac{SF \cdot g_{lat} \cdot g \cdot \text{Mass}}{2 \cdot t \cdot (l+h)} \tag{8.10}$$

$$\tau_{xy} = \frac{SF \cdot g_{long} \cdot g \cdot \text{Mass}}{2 \cdot t \cdot (l+h)} \tag{8.9}$$

$$\tau_{zx} = \frac{SF \cdot g_{lat} \cdot g \cdot \text{Mass}}{2 \cdot t \cdot (l+w)} \tag{8.11}$$

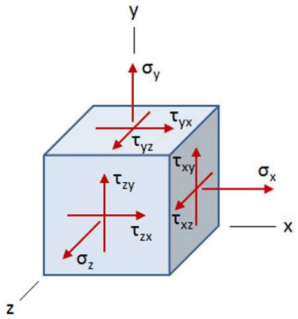

Figure 8.2: *von-Mises stress component direction.*

Furthermore, column buckling is to be considered as well which are given by equation (8.12) [46].

$$\sigma_c = 4\frac{\pi^2 E}{12\left(1-\upsilon^2\right)}\left(\frac{t}{w}\right)^2 \tag{8.12}$$

Lastly, again, the longitudinal and lateral frequencies are indicated by (8.13) and (8.14). The same requirement apply here as well, where they will be higher than 100 Hz.

$$f_{long} = 0.250\sqrt{\frac{2 \cdot t \cdot E \cdot (l+w)}{\text{Mass} \cdot h}} \tag{8.13}$$

$$f_{lat} = 0.560\sqrt{\frac{\frac{1}{12}(w + 2t_o b) \cdot E \cdot h^3 - \frac{1}{12} w \cdot h^3)}{\text{Mass} \cdot h^3}} \tag{8.14}$$

Sizing

The same procedure is again applied here for sizing. The volume can be computed using (8.15) and mass using (8.6).

$$V_{ob} = l \cdot w \cdot h - (l - 2t)(w - 2) \cdot t_o b \cdot h \tag{8.15}$$

Results

The inputs and output parameters for the orbiter are displayed in Table 8.3.

Table 8.3: *Input and output variables to size the orbiter.*

Input variable	Value	Unit	Output variable	Value	Unit
l	1500	mm	σ_{vm}	22.51	MPa
w	1500	mm	σ_c	1.608	MPa
h	1500	mm	$freq_{long}$	269.9	Hz
t	2	mm	$freq_{lat}$	123.311	Hz
SF	1.4	/	m_{ob}	50.513	kg
g_{long}	4.6	/	V_{ob}	0.01798	m^3
g_{lat}	2	/			
$f_{excitation}$	100	/			
ρ	2810	kg/m^3			
σ_{yield}	448	MPa			
$\sigma_{ultimate}$	517	MPa			
E	70	GPa			
$Mass$	481.23	kg			
v	0.33	/			

Propulsion

For propulsion, a material trade-off for the propellant tank was performed. For the tank, one important trade-off criterion is the specific strength, as the material is required to withstand internal pressure while being as lightweight as possible. Commonly used materials are taken from literature [43].

Table 8.4: *Possible materials and their respective properties for propellant tank.*

	Material	Density [kg/m^3]	Yield Strength [MPa]	Specific Yield Strength [m^2/s^{-2}]
Steel	AISI 301	8000	965	0.120625
	AISI 4340	7850	470	0.05987
	D6AC	7870	1724	0.219
Aluminium	AA 2024-T3	2780	345	0.1241
	AL 2219-T87	2840	393	0.1384
	AA 7475-T761	2810	448	0.1594
Titanium	Ti6AL-4V	4430	880	0.1986

Based on the aforementioned table, D6AC and Ti6AL-4V are the best two materials. Ti6AL-4V is chosen over D6AC as it was previously used in several missions, making it more reliable [23]. Also, more test data is available in literature [47].

Heat Shield

The design of the heat shield is mostly covered in Chapter 11. One part that is related to the structures and materials subsystem is the heat shield material choice. This was briefly covered in the Midterm Report [11], but will be elaborated and continued upon. First of all, as the experienced temperatures during landing can evaporate most known materials, two important factors are melting point and enthalpy required for vaporisation. A material comparison is displayed in Table 8.5 which was previously mentioned in [11].

Table 8.5: *List of possible materials with their respective melting point and enthalpy required for evaporation.*

Material	Melting Point [K]	$\Delta H_{evaporate}$ [MJ/kg]
Beryllium	1550	32.5
Carbon	3775	29.7
Copper	1360	4.7
Tungsten	3685	4.5

As can be clearly seen, carbon outweighs remaining materials. Thus, carbon is chosen as the skin material as its melting point is higher than the maximum experienced temperature mentioned in Chapter 11. However, carbon can only be used as a skin material, thus it requires a core. When selecting a core material, ablative properties are a huge upside as ablating materials lead to a reduction in absorbed heat by convection [48]. To properly design a composite structure requires several tests and more in-depth theoretical knowledge regarding composites. Therefore, based on the selection of carbon as a preferred skin material, the core materials used in previous missions are analysed. It is noted that Viking, Mars Pathfinder and MER missions ended up using the same core material which is SLA-561V [48]. The SLA-561V core consists of phenolic honeycomb filled with a mixture of silica microspheres, cork, and silica fibres [49]. Based on available test data and a high TRL, SLA-561V alongside carbon skin is chosen as the heat shield material.

EPS Support Structure

For the EPS subsystem, a structure needs to be designed to connect the solar arrays to the lander and to withstand bending and axial loads during operations. To start off, for the solar arrays it is checked whether they fly off during worst-case weather conditions. For this, lift is computed using (8.16) where V_{wind} is highest expected wind which is assumed to be 100 m/s, A_{SA} is solar array area and c_l is assumed to be 0.5 for a flat plate [50].

$$L = \frac{1}{2} \cdot \rho_{Mars} \cdot V_{wind}^2 \cdot A_{SA} \cdot c_l \tag{8.16}$$

$$D = \frac{1}{2} \cdot \rho_{Mars} \cdot V_{wind}^2 \cdot A_{SA} \cdot c_d \tag{8.17}$$

By comparing the solar array weight with the computed lift, it is concluded that the weight is higher, thus the solar arrays will not fly off vertically during the worst-case scenario. However, they still can break off by bending, so the support structure needs to be designed carefully. Assuming a hollow circle to be the cross-section of the rod and using aluminium 7075-T6 as the material with properties in Table 8.1 for the same reasoning as in the orbiter material selection. The worst-case sc enario is where loads would be highest, this occurs at highest wind speed and maximum angle of 15 ° as specified in landing locations in Chapter 6. Vertical and horizontal forces are then computed using (8.18) and (8.19) respectively where D stands for the experienced drag force expressed in (8.17) and W is the solar array weight. c_d is drag coefficient which is assumed to be 0.2 for a flat plate [50].

$$F_z = L\cos 15 + D\sin 15 - W\cos 15 \tag{8.18}$$

$$F_x = D\cos 15 + W\sin 15 - L\sin 15 \tag{8.19}$$

Afterwards, axial and bending stresses can be computed using (8.20) and (8.21) respectively. These were computed with the assumption that the support structure is a rod with the solar array at the end acting as a point load.

$$\sigma_{axial} = \frac{SF \cdot F_x}{\pi \cdot d \cdot t} \tag{8.20}$$

$$\sigma_{bending} = \frac{SF \cdot F_z \cdot l}{\pi \cdot r^3 \cdot t} \tag{8.21}$$

The geometry of the rod were then iterated until the stresses are lower than the material's yield stress. To summarise inputs and outputs, Table 8.6 is used.

Landing Strut Design

As previously discussed in [11], there are two options for protecting the payload during landing. As the mission is optimising for a soft landing, an impact attenuator option is discarded as during the landing procedure, landing struts will be deployed and will be the first point of contact with Mars's surface. Thus, a shock absorber mounted on the landing strut is a more viable and realistic option. The mechanism of the shock absorber includes a piston and a spring. During landing, the spring is pressed downwards to absorb

Table 8.6: *Input and output variables to size the solar array support structure.*

Input variable	Value	Unit	Output variable	Value	Unit
l	600	mm	L	37.423	N
d	35	mm	D	14.969	N
t	2	mm	F_z	-11.64	N
SF	1.4	/	F_x	18.616	N
ρ	2800	kg/m^3	σ_{axial}	0.1185	MPa
σ_{yield}	448	MPa	$\sigma_{bending}$	290.36	MPa
c_d	0.2	/	Volume	0.0001275	m^3
c_l	0.5	/	Mass	0.3568	kg
M_{SA}	11.85	kg			
A_{SA}	5.26	m^2			
v_{wind}	100	m/s			
Angle	15	deg			
ρ_{Mars}	0.01503	kg/m^3			

the impact energy in the form of mechanical energy. Then, this impact energy is transferred to the piston where this energy presses the rod in the hydraulic system dissipating the shock.

For the shock absorber design, the maximum absorbed force is determined by equating it to the weight of the probe dry mass. The shock absorber can then be sized using (8.22) where $F_{\text{dissipated}}$ is equal to the weight of the probe dry mass. P_{exert} stands for pressure exerted and d_{shock} for diameter [51].

$$F_{\text{dissipated}} = (P_{\text{exert}} \times d_{\text{shock}} \times 0.785) \times 10^{-3} \tag{8.22}$$

Furthermore, for the landing strut configuration, due to the presence of sixteen thrusters, as will be explained in Chapter 10, four landing legs are chosen as a design with three is not possible without the problem of asymmetry. Also, as required by the payload engineer, the probe needs to be at a height of 36 cm from Mars's surface. Thus, two aspects of the design are remaining, which are the angle with respect to the horizontal and the length of the landing strut required.

The angle is affected by the moment induced by both lift and drag computed at worst-case scenarios, at high wind speeds. It was concluded that by iteration 45 ° is a suitable angle. Afterwards, the landing strut cross-section is designed by considering the axial stress experienced during landing. This is displayed in (8.23).

$$\sigma_{\text{axial}} = \frac{SF \cdot \text{W}_{\text{probe}} \cdot \sin(45)}{\pi \cdot d \cdot t} \tag{8.23}$$

By using aluminium 7075-T6, radius and thickness are iterated to keep the axial stress lower than the yield stress. In addition, using the 36 cm requirement, using simple trigonometry, the length is determined. The final dimensions of the landing strut are displayed in Table 8.7.

Table 8.7: *Input and output variables to size the landing strut.*

Input variable	Value	Unit	Output variable	Value	Unit
$Number$	4	/	r	10	mm
$Weight_{probe}$	140.763	kg	t	2	mm
ρ	2800	kg/m^3	l	509	mm
σ_{yield}	448	MPa	$Angle$	45	deg
ρ	2800	kg/m^3	σ_{axial}	4.115	MPa
SF	1.4	/	Mass	0.1634	kg
Min height	36	cm			

Launcher Support Structure

The probes and the orbiter need to be assembled in the launch vehicle. For this, a configuration is determined, which is discussed in section 17.2. The configuration involves a beam structure to which eleven probes are attached. To properly size this launch vehicle, a circular cross-section was assumed to allow for more efficient attachment surface area for the probes. Aluminium 7075-T6 is used here as well. As the structure needs to withstand launch loads as well, the same approach as previously mentioned for the probe is followed here. Thus, (8.1) is used again here. The mass used is the mass of the orbiter as it is the mass acting on the beam longitudinally.

The probes create a moment which acts on the beam. To model the worst-case scenario, the eleven probes are assumed to be modelled as a point masses creating a moment around the beam. To compute the bending stress, (8.24) is used.

$$\sigma_{\text{bending}} = \frac{SF \cdot \text{Mass}_{\text{probe}} \cdot 11 \cdot g \cdot g_{lat} \cdot h}{\pi \cdot r^3 \cdot t} \tag{8.24}$$

Again, iteration over the cross-sectional diameters and height is performed. Thereafter, the stress is computed and it is checked whether it exceeds the yield stress. The final input and output table is be displayed in Table 8.8.

Table 8.8: *Input and output variables to size the launch vehicle support structure.*

Input variable	Value	Unit	Output variable	Value	Unit
r	480	mm	σ_{tot}	11.79	MPa
h	5.67	m	$\sigma_{bending}$	103.64	MPa
t	10	mm	Mass	514.515	kg
SF	1.4	/			
g_{long}	4.6	/			
g_{lat}	2	/			
ρ	2810	kg/m^3			
σ_{yield}	448	MPa			
E	70	GPa			
$Mass$	514.52	kg			

8.4. Risk

Risk is taken into account during failure analysis by the inclusion of the safety factor term. The value of 1.4 is chosen as it entails [52]:

- Experiencing service loads higher than designed for
- Structural deflections above limit load that could compromise vehicle structural integrity
- As-built part thickness within tolerance, but less than that assumed in the stress analysis
- Degradation of material properties due to environmental effects

Degradation is taken into account in the safety factor as concluded by a recent study on effect of Mars's environment on materials [53], a non-conclusive degradation factor is present.

8.5. Verification & Validation

Verification

Verification is done following the verification plan previously introduced in [11]. First the code is checked for syntax and logic errors. This is done by both code debugging and performing the calculations again by hand. Afterwards, calculation verification is performed by changing the input parameters with examples from [43] and [46], as all equations are derived from both sources. Then it is checked whether the accuracy of both results is within acceptable limits.

Validation

Furthermore, for validation, comparison with available FEM and real-life testing results is performed. However, only the calculations for the probe and orbiter design are validated as no test data is found for the remaining calculations. As the probe and orbiter are designed with the same approach but different equations, that are previously verified, due to different geometries, if one set of equations is validated, the other can be deemed validated as well.

A FEM analysis on a CubeSat [54] is compared to the model. From the results, it is observed that the maximum experienced stress was 29 MPa and an experienced frequency range from 0-750 Hz in both directions. Based on the developed numerical model, the results conclude the maximum experienced stress is 31.4 MPa and lateral and longitudinal frequencies are 29.7 and 176 Hz, respectively. The frequency can be observed to be within range. The stress is 8.3 % off. This difference can be justified because in the FEM model, the accurate structural satellite model was tested, including thickness variations and different materials. However, for the numerical model a series of flat panels of constant thickness and the same material are assumed. As a result, the difference is deemed to be within an acceptable range, meaning the developed model is validated.

8.6. Compliance matrix

To check all requirements are met, Table 8.9 is generated.

8.7. Recommendations

Possible recommendations for further design phases would entail:

- More in-depth consideration of composites where the layup can be optimised at different locations. At this phase, the layup is assumed and the core thickness is assumed to be the same everywhere. However, it is not required as a thicker and different layup can be designed where higher stress is experienced.
- A FEM model can be generated to accurately estimate the locations of high-stress concentrations. Then geometry changes could stem from that. For this, a more higher level of detail would be required for the CAD model.
- Substructures holding and separating components and subsystems inside both the lander and orbiter. This would add more loads and may require changing the component arrangement.
- Testing using a shaker to validate the developed FEM model and increase the confidence level of the design.

Table 8.9: *Requirement compliance matrix for structures and materials subsystem.*

Requirement ID	Met / Not Met / TBC	Justification
MR-STRCT-01	Met	Designed to meet
MR-STRCT-01-01	Met	Designed to meet
MR-STRCT-01-02	Met	Designed to meet
MR-STRCT-01-03	Met	Designed to meet
MR-STRCT-01-04	Met	Designed to meet
MR-STRCT-02	Met	Designed to meet
MR-STRCT-02-01	Deleted	Stemming from different requirements
MR-STRCT-02-02	Deleted	Stemming from different requirements
MR-STRCT-02-03	Deleted	Stemming from different requirements
MR-STRCT-02-04	Deleted	Stemming from different requirements
MR-STRCT-02-05	Met	Designed to meet
MR-STRCT-02-06	Met	Designed to meet
MR-STRCT-03	Met	Designed to meet
MR-STRCT-03-01	Met	Designed to meet
MR-STRCT-03-02	Met	Designed to meet
MR-STRCT-04	Deleted	Requirement not verifiable
MR-STRCT-04-01	Deleted	Requirement not verifiable
MR-STRCT-04-02	Deleted	Requirement not verifiable
MR-STRCT-05	TBC	Further analysis is required on the possible future Mars missions and debris impacting the landers.
MR-STRCT-05-01	TBC	Further analysis is required
MR-STRCT-05-02	Replaced	Replaced by **MR-STRCT-05-05**
MR-STRCT-05-03	TBC	Further analysis is required
MR-STRCT-05-04	TBC	Further analysis is required
MR-STRCT-05-05	Met	Designed to meet
MR-STRCT-06	Met	Designed to meet
MR-STRCT-06-01	Met	Designed to meet
MR-STRCT-06-02	Met	Designed to meet
MR-STRCT-07	Met	Ease of manufacturing was taken into account in the material trade-off. However, whether it is possible to manufacture the geometry using the chosen material is something to be investigated in the detailed design phase.
MR-STRCT-07-01	Met	Designed to meet
MR-STRCT-07-02	Met	Designed to meet
MR-STRCT-07-03	Met	Designed to meet
MR-STRCT-07-04	Met	Designed to meet

9 Astrodynamics

The astrodynamics subsystems is essential in a space mission as it designs all the orbits for the mission. In this chapter the models used to determine these orbits will be discussed, along with the obtained results.

9.1. Functional analysis

The astrodynamics subsystem designs all the orbits in the mission, starting from the arrival at Mars and ending with the final deorbiting orbit for the orbiter. Because of the preliminary nature of this analysis, all orbits are treated as Keplerian orbits with Keplerian Elements and the Hohmann transfer is modelled using the patched conics technique. The mission is divided into seven main phases as indicated in Figure 9.1. Phase one is the arrival at Mars and it is followed by the second phase which is the walk-in phase of the aerobraking manoeuvre where the periapsis height is dropped from 400 km to the required 100 km which corresponds to the beginning of phase three. Phase three is the main phase of the aerobraking manoeuvre which is followed by phase four, or the aerobraking walkout phase. The entire aerobraking manoeuvre will take 60 days. Phase five is the probe deployment phase, which will take 6 days, weather permitting. At this point, the periapsis is slightly increased to an altitude of 150 km to allow for a more stable orbit. This is then followed by phase six, where the orbit is circularised. Once the mission has ended, the last phase, the deobrit phase will start. This is in place to reduce space debris. This is not shown as it is identical to phase phase four.

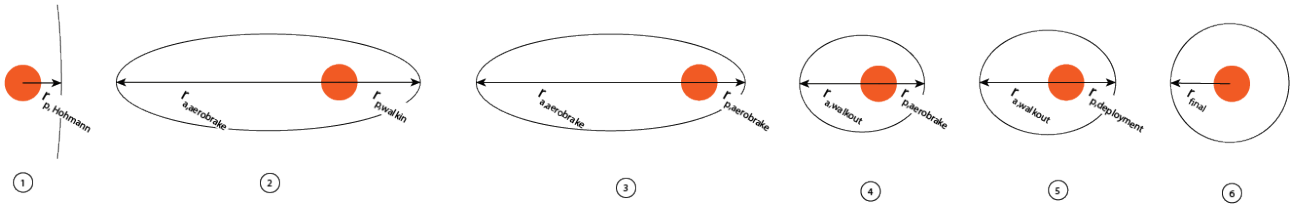

Figure 9.1: *Astrodynamics mission phases.*

9.2. Requirements

No requirements were directly set for the astrodynamics subsystem during the requirement & concept generation phase of the design phase [13], however, some requirements came to light when designing the astrodynamics subsystem, and some planetary protection requirements have been taken into consideration when designing this subsystem. These requirements are provided below. Requirements **MR-ASTR-01** and **MR-ASTR-02**, originate from other subsystems and, since they originate before the astrodynamics subsystem is established, they are unbiased toward the final design. Requirement **MR-ASTR-03** is similar to **MR-PPR-03** as it ensures that nothing crashes into one of Mars' moons, potentially contaminating them. From these requirements it is clear that the largest impact on the astrodynamics subsystem originates from the TT&C and EDL subsystems.

MR-ASTR-01: The orbiter shall be in contact with each probe for 4444 s per sol. **Added**
MR-ASTR-02: The orbiter shall be able to deploy all the probes to their EDL orbit. **Added**
MR-ASTR-02-01: The orbiter shall have an orbital inclination of no less than 30°. **Added**
MR-ASTR-02-02: The probes shall have an altitude of at most 100 km to begin the EDL phase. **Added**
MR-ASTR-03: The probability of crash on Phobos or Deimos for an orbiter or an orbiter system shall be <0.01 for the first 20 years of the mission. **Added**

MR-PPR-03: The probability of crash on Mars for an orbiter or an orbiter system shall be <0.01 for the first 20 years of the mission.

9.3. Model & Results

In this section, the development of the tool is discussed, along with its results.

Tool development

The astrodynamics model is built to generate a suitable orbit for the orbiter and calculate the ΔV requirements during the mission both for the orbiter and the probes. The five major outputs of the program are:

1. Orbital elements (a, e, ω, Ω, P)
2. ΔV required for the mission
3. Atmospheric entry velocity for the probes
4. Data of each pass, for each probe, once on the ground
5. Eclipse time

The driving parameter for the program is the average time of contact between each probe and the orbiter. This requirement originates from the Telemetry, Tracking & Command (TT&C) subsystem, and it means that the model has to iterate different orbital elements until the required contact time is met.

Method

To start the iteration process, an initial estimate for the orbital elements is made. The initial estimate is an altitude of 200 km and eccentricity of 0 (circular orbit), as well as 0 ° for both the longitude of the ascending node Ω and the argument of periapsis ω. The orbital period P is then calculated using (9.1).

$$P = 2\pi\sqrt{\frac{a^3}{\mu_m}} \tag{9.1}$$

Once these parameters have been established, the ΔV requirements are calculated. These are divided into the different phases illustrated in Figure 9.1. To calculate the ΔV , the program takes two orbits as input, checks if there is one point in common, and outputs the ΔV by measuring the velocity of both orbits at the common point with the use of (9.2)

$$V = \sqrt{\mu_m\left(\frac{2}{r} - \frac{1}{a}\right)} \tag{9.2}$$

The atmospheric entry velocity can be computed with the same equation, as long as the entry altitude is known from the EDL subsystem.

To calculate the data of each pass once the probes are on the ground a more iterative solution must be used. The program simulates the position of the satellite for a given time, then evaluates the position of the probe in Cartesian coordinates, which changes due to the rotation of the planet, and finally calculates if the probe is in view of the orbiter or not. This is done for all the probes at intervals of 1 minute over a specified number of orbits. To calculate the position of the satellite the following equation (9.3) is used.

$$\begin{aligned}\mathbf{r}_{\text{sat}} = &([\cos\Omega\cos(\nu+\omega) - \sin\Omega\cos i\sin(\nu+\omega)]\mathbf{i} \\ &+ [\sin\Omega\cos(\nu+\omega) + \cos\Omega\cos i\sin(\nu+\omega)]\mathbf{j} + \sin i\sin(\nu+\omega)\mathbf{k}\big)\, r\end{aligned} \tag{9.3}$$

Where ω, Ω, i and ν are the Keplerian elements and r is the distance between the probe and the planet's centre. Both r and ν are calculated using an iterating method using equations (9.4) through (9.6).

$$E_{n+1} = E_n - \frac{E_n - e\sin E_n - M}{1 - e\cos E_n} \tag{9.4}$$

Where M is the mean anomaly, E is the eccentric anomaly and starting with $E_0 = M = nt$. Once E has been found, ν can be computed using the equation below (9.5).

$$\nu = 2\tan^{-1}\left(\sqrt{\frac{1+e}{1-e}}\tan\frac{E}{2}\right) \tag{9.5}$$

With the true anomaly calculated, the position r can be computed with the use of (9.6)

$$r = a\frac{1-e^2}{1+e\cos\nu} \tag{9.6}$$

Once the position of the satellite is known, the position of each probe can be calculated by using its latitude and longitude, along with Mars' rotation rate, to convert the position to 3D Cartesian coordinates using the following equation (9.7).

$$\mathbf{r}_{\text{probe}} = R_{mars}\left(\cos(\omega_{mars}t+\lambda)\cos(\Lambda)\mathbf{i}+\sin(\omega_{mars}t+\lambda)\cos(\Lambda))\mathbf{j}+\sin(\Lambda)\mathbf{k}\right) \tag{9.7}$$

Where ω_{mars} is the sidereal rotational rate, λ is the longitude and Λ is the latitude. With these two vectors, a third vector from the probe to the orbiter, $\mathbf{r}_{\text{probe-sat}}$, can be obtained by subtracting the probe vector from the satellite vector. For the probe to be in view it must satisfy the following condition, where ε_{min} is the minimum elevation required for the satellite to be visible by the probe.

$$\cos^{-1}\left(\frac{\mathbf{r}_{\text{probe-sat}}\cdot\mathbf{r}_{\text{probe}}}{|\mathbf{r}_{\text{probe-sat}}||\mathbf{r}_{\text{probe}}|}\right) \leq 90^\circ - \varepsilon_{min} \tag{9.8}$$

With this model, data about each pass can be determined, including but not limited to, average time of contact per orbit per probe, maximum number of probes in contact at the same time and average number of probes in contact with orbiter. This model can also be used to calculate when the probes can be deployed. If the orbit passes over the landing location, the probes can be deorbited in such a way that they land in the selected landing site. This calculation of the pass data has some limitations as it is based on a simplified model that makes three assumptions. First, there is no resonance between the orbital period and Martian rotation period. Second, the spacecraft is in a (nearly) circular orbit. Third, the Martian rotational variations are sufficiently small. Since the code iterates over numerous orbits and checks if a probe is in line of sight or not, it does not assume that there is resonance between the orbital period and martian rotational period. The orbit is circular, or idealised as such without disturbances, and therefore that assumption is also valid. Finally, since Mars is a planetary body, its rotational variations are much smaller than the procession rate of the orbit and therefore the assumption is valid.

To calculate the eclipse time, a similar process as the one used to calculate the time of each pass can be used, this time by checking if the angle between the satellite and the vector defining the anti-Sun direction $\rho = -\mathbf{r}_{\text{sun}}$, is less than β, where β is defined as follows [55, p.120].

$$\beta = \sin^{-1}\left(\frac{R_{\text{mars}}}{r}\right) \tag{9.9}$$

The Mars-Sun vector $\mathbf{r}_{\text{sun}}$ is defined using the following equation.

$$\mathbf{r}_{\text{sun}} = \cos L_\odot \mathbf{i} + \sin L_\odot \cos\varepsilon \mathbf{j} + \sin L_\odot \sin\varepsilon_{mars}\mathbf{k} \tag{9.10}$$

where $L_\odot$ is the Sun's ecliptic longitude, measured East along the ecliptic from the vernal equinox (**i** axis), ε_{mars} is the obliquity of the ecliptic.

Once all these parameters are computed, it can be checked if it complies with all the requirements, and if not, changes to the orbital altitude can be made.

Results

With the method described before, the final outputs for the astrodynamics subsystem can be calculated. The inputs for these calculation can be found in Table 9.1. The height of periapsis for the arrival at Mars, $h_{p,hohmann}$, is set to 400 km similarly to MRO [56] to allow the orbiter to evaluate the atmospheric conditions as the periapsis is lowered to the required 100 km height. The minimum elevation for contact, $\varepsilon_{elev,min}$, is chosen to allow for some ground features like valleys or mountains. The periapsis height for probe deployment is chosen such that the orbit is more stable and the system has enough time to deploy all the probes. The periapsis height for the aerobraking manoeuvre is obtained by the aerobraking manoeuvre performed by the MRO [56]. The third row is given by other subsystems, with $t_{contact}$ originating from the TT&C subsystem and h_{entry} coming from the EDL subsystem. The last five rows of Table 9.1 are set values about Mars except for $V_{\infty,mars}$ which is a result of the Hohmann transfer to Mars and therefore cannot change as the transfer is set by the launcher.

The final results of the subsystem, obtained after iteration, can be found in Table 9.2.

Table 9.1: *Input variables to compute required astrodynamics subsystem outputs.*

Input variable	Value	Unit	Input variable	Value	Unit
$h_{p,hohmann}$	400	km	$\varepsilon_{elev,min}$	5	deg
$h_{p,deployment}$	150	km	$h_{p,aerobraking}$	100	km
$t_{contact}$	4444	s	h_{entry}	100	km
$V_{\infty,mars}$	2.649	km/s	μ_{mars}	$0.042828 \cdot 10^6$	km^3/s^2
R_{mars}	3389.5	km	$J2_{mars}$	$1960.45 \cdot 10^{-6}$	-
$t_{sid,mars}$	24.6229	hr	$t_{sin,mars}$	24.6597	hr
ε_{mars}	25.19	deg	i_{mars}	1.85	deg
$t_{year,mars}$	668.59	sol	H_{mars}	11.1	km

Table 9.2: *Output variables from astrodynamics subsystem.*

Output variable	Value	Unit
h	520	km
e	0	-
i	30	deg
P_{orbit}	7421.6	s
$T_{pass,avg}$	1122.1	s
$T_{pass,sol}$	13422	s
$f_{eclipse}$	0.33416	-
$V_{atm,entry}$	4.2304	m/s
s_{max}	1675.1	km
$\Delta V_{probe,deorbit}$	25	m/s
$T_{deployment}$	6	sol
$h_{a,aerobraking}$	10700	km
$T_{aerobraking}$	60	days

Orbiter ΔV Budget		
Phase	Event	ΔV [m/s]
Hohmann Transfer	Obit Insertion	1222.0
	Trim	10
Aerobrake	Walk-in	36.603
	Control	33
	Pop-Up	20
	Walkout	12.064
Primary Mission	Orbit Circularisation	83.248
	Maintanance	33.5
Deorbit	Deorbit	95.312
Total		1545.7

On the left table all the variables connected to the orbits can be found, as well as some other parameters directly related to the final obit like probe contact time per sol, $T_{pass,sol}$, velocity of atmospheric entry, $V_{atm,entry}$, and maximum slant range, s_{max}. The aerobraking apoapsis height, $h_{a,aerobraking}$, is selected based on the time it takes to perform the aerobraking manoeuvre, $T_{aerobraking}$. Since an atmospheric model for Mars at high altitudes is not readily available, the aerobraking time was found by using heritage data from the MRO [57] and ExoMars [58]. On the right table, all the required ΔV for the mission can be found. All the data displaying five significant figures was calculated by the astrodynamics model, the remaining data was obtained from heritage data [57] [58]. The trim ΔV is used to change the trajectory of the system while in Hohmann transfer. This also includes the ΔV for trajectory biasing to comply with category IVa of COSPAR planetary protection requirements **MR-PPR-03**. The control ΔV is used to control the spacecraft during the aerobraking manoeuvre, while the pop-up ΔV is used in case of emergency to raise the periapsis and terminate the aerobraking manoeuvre.

9.4. Risk

The two risks for the astrodynamics subsystem are failure to aerobrake correctly and for the orbiter to crash into one of Mars' moons. The first risk is mitigated by performing the walkin phase of aerobraking which allows to delay the manoeuvre if necessary. The second risk is mitigated by lowering the apoapsis of the aerobraking orbit below Phobos' orbit.

9.5. Verification & Validation

In this section, the verification and validation of the astrodynamics model will be performed.

Verification

Verification of the program is done in parallel with tool development. If the function does not use iteration to solve the problem, the results are checked against calculations made with a graphical calculator and the results were always found to match exactly with the expected output, up to the smallest significant figure of the calculator. These functions used the same input parameters as for validations, which can be found in Table 9.3. The obtained outputs are also equivalent to validation for the above mentioned functions. The functions to calculate the eclipse and pass data only adds the results of two other functions that are verified, and therefore by adding the results of the root functions, these two are verified. The function used to update the satellite's position relies on iteration and therefore would be hard to verify by hand. Since the function works by taking time as input and giving position as output, the reverse was done by hand, since it only requires a simple formula. This allows to easily verify the function which has a maximum position error of 10^{-6} rad which is when the program considers the position to have converged.

Validation

To validate the functions, data from previous missions is used. Since most missions with a lot of known data are around Earth, those missions are used to validate the functions. This can be done since no function differs between Earth and Mars.

Table 9.3: *Validation of astrodynamics functions.*

Function Name	Input	Expected Output	Obtained Output	Deviation
calculateEclipse	(h, i) (200 km, 28°)	$T_{eclipse}$ 2238 s	$T_{eclipse}$ 2234 s	0.18%
orbitTime	(h_p, h_a, i) (408 km, 410 km, 51.64°)	P_{orbit} 5561 s	P_{orbit} 5556 s	0.09 %
calculateV	(h_p, h_a, i) (408 km, 410 km, 51.64°)	V 7.66 km/s	V 7.67 km/s	0.15 %
updateOrbit	(h, i) (200 km, 28°)	($\dot{\Omega}$, $\dot{\omega}$) (-7.35°/day, 12.05°/day)	($\dot{\Omega}$, $\dot{\omega}$) (-7.39°/day, 12.12°/day)	(0.6%, 0.6%)
inView	(h, λ_{sc}, Λ_{sc}, λ_{gr}, Λ_{gr}) (35793 km, 180°, 0°, 150°, -44)	inView True	inView True	N/A

As can be seen in Table 9.3 all the functions that underwent validation procedures, can be said to be validated, however, some of the functions used did not undergo validation procedures. The function *inEclipse*, is not validated because its parent function is, and therefore it would have been impossible for the *calculatEclipse* function to be correct if *inEclipse* was not. *calculateDeltaV* is not validated as it only subtracts one velocity from the other, and its child function, *calculateV* is validated. Finally, *calculatePassData* is not validated due to the difficulty in finding real world validation data. Instead, its child function, *inView* is validated. Since *calculatePassData* only sums the result from *inView* over a period of time, it is assumed to be valid, although a better validation method can be used in the future. The small deviations from the real world data, can be explain by some potentially different inputs such as the standard gravitational parameter or some gravitational disturbances not accounted for.

9.6. Compliance matrix

Table 9.4 shows the compliance matrix for the astrodynamics subsystem. As it can be seen, some requirements are met from the start by designing the system for that, some other requirements were initially not met, and iteration of the design was necessary in order to meet these requirements.

9.7. Recommendations

Due to the low amount of atmospheric data for high altitudes, it was impossible to build an accurate atmospheric model for orbits. This makes it impossible to simulate the aerobraking procedure, as well as calculating the maintenance ΔV required during the mission. Future analysis can use of NASA's GRAM2000 model [59] only available upon request.

A better simulation including at least the Sun, Phobos and Deimos (Mars' moons), and Jupiter shall be modelled to calculate gravitational disturbances, solar flares, Earth-Mars opposition and other events that might

Table 9.4: *Compliance of astrodynamics subsystem requirements.*

Requirement ID	Met / Not Met / TBC	Justification
MR-ASTR-01	Met	Iterated until met
MR-ASTR-02	Met	Designed to meet
MR-ASTR-02-01	Met	Designed to meet
MR-ASTR-02-02	Met	Designed to meet
MR-ASTR-03	Met	Designed to meet

have a significant impact on the mission. This simulations was not built during this design phase due to the extensive time and theoretical knowledge needed to build such a tool.
This model uses the function used to calculate pass data, which is used to calculate the probe deployment time. However, since a probe will only be deployed if the previous probe has landed successfully, the deployment procedure in case of emergency should be analysed. By looking at the available time in between probe deployment, and the expected time required to fix any potential EDL failures, a better estimation for the deployment time can be performed.

10 Propulsion

This chapter discusses the design considerations and sizing of the propulsion system. The functional analysis and the given requirements are the leading factors in the design. A tool is developed to size the propulsion system. The methodology and, verification and validation is described in this chapter as well. Finally, the compliance of the requirements is checked and requirements for the next design phase are made.

10.1. Functional analysis

The functions of the propulsion system are to provide ΔV and handle and store propellants. The spacecraft and lander both have a propulsion system. There is also a propulsion system that will deorbit the landers. The spacecraft propulsion system will provide the ΔV required for the orbit circularisation manoeuvre, as well as for orbit maintenance. The lander propulsion system will slow down the lander to perform a soft landing.

10.2. Requirements

The requirements for the propulsion subsystem were derived in the requirement and concept generation phase of the design process [13].

MR-PROP-01: The system shall provide a velocity increment throughout all mission phases - including transfer - of 1.572 km/s.
MR-PROP-02: The system shall be designed to be operable in any operational spacecraft attitude.
MR-PROP-03: The system shall be designed such that all wetted surfaces remain at least 7K above the freezing point of onboard propellant.
MR-PROP-04: The system shall be restartable.
MR-PROP-05: The system shall store 2118 kg of propellant.
MR-PROP-06: The system shall be used for mid-course corrections during transfer.
MR-PROP-07: The system shall measure the thrust it provides.
MR-PROP-07-01: The system shall detect deviations from the expected thrust of magnitude 0.5 N.
MR-PROP-08: The system shall measure the propellant expended.
MR-PROP-09: The system shall contain a sustainable end of life strategy for the satellite in orbit.
MR-PROP-10: The system shall have built-in redundancy for all critical subelements in case a subelement fails, an extra subelement performing the same function is present.

10.3. Model & Results

Tool development

To design the propulsion subsystem, a Python tool was developed. Given a required ΔV and an estimate for the wet mass, the tool computes the propellant mass and volume. This is used to size the propellant tanks. Using the material properties of the tank material, previously introduced in section 8.3, the tank thickness and tank mass are computed.

Method

Given a wet mass, M_0, and a ΔV requirement, (10.1) is used to compute the dry mass, M_1. The difference between the wet and dry mass is the propellant mass, M_p.

$$\Delta V = I_{sp} g_0 \ln\left(\frac{M_0}{M_1}\right) = I_{sp} g_0 \ln\left(\frac{M_0}{M_0 - M_p}\right) \tag{10.1}$$

Given the propellant mass, M_p, and propellant density, ρ_p, (10.2) is used to compute the usable propellant volume, V_p. In the equation, the factors λ_{error} and $\lambda_{trapped}$ are included. These factors account for a loading error and the fuel trapped in valves, fuel lines etc respectively.

$$V_p = \frac{M_p}{\rho_p} \cdot \lambda_{\text{error}} \cdot \lambda_{\text{trapped}} \tag{10.2}$$

The propellant volume is used to size the propellant tanks. The propellant tanks are chosen to be spherical. This is the most efficient shape for pressure vessels, which reduces the propellant tank mass. The radius of the propellant tanks is determined using (10.3).

$$V = \frac{4\pi r^3}{3} \tag{10.3}$$

For spherical pressure vessels, the tank wall thickness is dictated by the hoop stress, which does not exceed the tank material yield strength. The tank wall thickness is then calculated using (10.4), where SF, is the safety factor and p, is the propellant pressure.

$$\sigma_h \cdot SF = \frac{pr}{2t} \tag{10.4}$$

Knowing the propellant tank wall thickness and the density of the tank material ρ_t, (10.5) gives the propellant tank mass.

$$M_t = \rho_t \left(\frac{4\pi (r+t)^3}{3} - \frac{4\pi r^3}{3} \right) \tag{10.5}$$

Using (10.1) through (10.5), the propellant and tank masses are computed for several propellant types. The propellant types and relevant characteristics are listed in Table 10.1 [60] [23].

Table 10.1: *Propellant characteristics.*

Propellant	Abbreviation	Vacuum I_{sp} [s]	Thrust range [N]	Mean density [kg/m^3]
Cold gas N_2	N_2	50	0.05-200	280
Solid motor	Solid	280	50-5$\cdot 10^6$	1800
Monopropellant H_2O_2	Mono H_2O_2	150	0.05-0.5	1440
Monopropellant N_2H_4	Mono N_2H_4	225	0.05-0.5	1000
Dual mode N_2O_4 / N_2H_4	Dual N_2O_4 / N_2H_4	340	3-200	1559

Aside from the propellant tank mass, the propulsion subsystem dry mass is taken into account as well. The dry mass is composed of the tanks, diaphragms, valves, filters, fuel lines, temperature and pressure transducers, heaters and thrusters. The mass of these components is estimated based on literature [61, p.203]. However, the mass of a thruster is estimated using (10.6) [61, p.203]. In this equation, T is the thrust provided by the thruster.

$$M_{th} = 0.4 + 0.0033T \tag{10.6}$$

The thruster mass is multiplied by the amount of thrusters to obtain the total thruster mass. Then, the total propulsion subsystem mass is computed using (10.7).

$$M_{\text{prop-sys}} = N_{th} \cdot M_{th} + M_{\text{dry-excl. thrusters}} + M_t \tag{10.7}$$

Thrust range

Apart from the dry mass, another important criterion is the thrust range. Different manoeuvres require different thrust levels. For example, for maintenance, a relatively low thrust is required, while for landing, high thrust is required. Thus, different propellant types are more suitable for different scenarios. These different scenarios are elaborated upon in Table 10.2

Table 10.2: *Thrust requirements per mission scenario.*

Scenario	Thrust requirement	Reasoning
Circularization burn	High	The ΔV required is really large. For high thrust, the efficiency is larger than for low thrust. Therefore, high thrust is required.
Landing burn	High	The ΔV required is quite high, and its needs to be provided very fast, therefore high thrust is required.
Maintenance burn	Low	The ΔV required is low. Moreover, the burns need to be accurate, this means that low thrust is required.
De-orbit burn	Medium	The ΔV required is not that high, but the burn will be executed reasonably quick. Therefore a medium thrust level is required.

Results

Using the method described before, combined with the considerations on thrust level, a propellant type and propulsion system dry mass are determined. The input variables used to compute the propulsion system total mass are given in Table 10.1 and Table 10.3.

Table 10.3: *Input variables to compute the total propulsion system mass.*

Input variable	Value	Unit	Input variable	Value	Unit
σ_{yield}	880	MPa	$m_{filters}$	0.6	kg
ρ_t	4430	kg/m^3	$m_{fuellines}$	5	kg
p	7.00	MPa	$m_{Ttransducers}$	3	kg
SF	1.25	/	$m_{Ptransducers}$	1.2	kg
OF	1.64	/	m_{heater}	0.5	kg
λ_{error}	1.005	/	$M_{wet-circularisation}$	5440	kg
$\lambda_{trapped}$	1.03	/	$M_{wet-landing}$	159	kg
$T_{circularisation}$	200	N	$M_{wet-maintenance}$	482	kg
$T_{landing}$	200	N	$M_{wet-deorbit}$	212	kg
$T_{maintenance}$	0.1	N	$\Delta V_{circularisation}$	1573	m/s
$T_{deorbit}$	1	N	$\Delta V_{landing}$	150	m/s
$N_{th-circularisation}$	4	/	$\Delta V_{maintenance}$	300	m/s
$N_{th-landing}$	16	/	$\Delta V_{deorbit}$	25	m/s
$N_{th-maintenance}$	16	/	$N_{tanks-circularisation}$	4	/
$N_{th-deorbit}$	1	/	$N_{tanks-landing}$	4	/
$m_{pressurant}$	1	kg	$N_{tanks-maintenance}$	2	/
$m_{diaphragm}$	3	kg	$N_{tanks-deorbit}$	1	/
m_{valves}	7	kg			

Using inputs from Table 10.3, the program outputs are documented in Table 10.4.

Trade-off

With the results from Table 10.4, a trade-off is performed. As stated before, the subsystem mass and required thrust levels are the main considerations for choosing a propellant type. The cells highlighted in green show the propellant type that is chosen for that specific manoeuvre.

Circularisation manoeuvre

The circularisation manoeuvre requires a lot of ΔV. Naturally, this means you require a large propellant mass. Dual N_2O_4 / N_2H_4 is chosen because of its low propulsion subsystem mass. This low mass is because of the high I_{sp} that this propellant type has. Another advantage of dual N_2O_4 / N_2H_4 is the fact that is has high thrust. For a high ΔV requirement, it is more efficient to have high thrust.

Landing manoeuvre

The landing manoeuvre requires high thrust and a significant amount of ΔV. Therefore, dual N_2O_4 / N_2H_4 was chosen. This propellant type provides the ΔV in the short time required. This propellant type also

Table 10.4: *Propulsion design results.*

	Propellant type					
Result	N_2	Solid	Mono H_2O_2	Mono N_2H_4	Dual N_2O_4 / N_2H_4	Unit
Circularisation Manoeuvre						
M_p	5404	2455	3698	2870	2118	kg
V_p	19.3	1.36	2.58	2.87	1.36	m^3
r	1.05	0.433	0.535	0.555	0.433	m
M_t	1281	90.56	170.5	190.6	90.17	kg
$M_{prop-sys}$	1309	116.1	196.0	216.1	115.7	kg
Landing Manoeuvre						
M_p	66.41	10.91	23.45	14.56	8.22	kg
V_p	0.255	0.00884	0.0198	0.0196	0.00848	m^3
r	0.248	0.0808	0.106	0.105	0.0797	m
M_t	16.95	0.5870	1.312	1.299	0.5631	kg
$M_{prop-sys}$	55.20	38.85	39.57	39.56	38.82	kg
Maintenance Manoeuvre						
M_p	228.3	51.64	92.05	63.43	42.93	kg
V_p	0.8155	0.02869	0.06392	0.06343	0.02754	m^3
r	0.460	0.151	0.197	0.196	0.149	m
M_t	54.15	1.905	4.245	4.212	1.829	kg
$M_{prop-sys}$	81.86	29.61	31.95	10.62	29.53	kg
Deorbit Manoeuvre						
M_p	10.88	1.984	3.688	2.466	1.635	kg
V_p	0.0389	0.00110	0.00256	0.00247	0.00105	m^3
r	0.210	0.0641	0.0849	0.0838	0.0630	m
M_t	2.580	0.07319	0.1701	0.1638	0.06964	kg
$M_{prop-sys}$	2.981	0.4735	0.5704	0.5641	0.4700	kg

has the lowest subsystem mass. Moreover, this propellant type is deemed highly reliable, as it has been successfully used in previous Mars landers [1].

Maintenance manoeuvre

The maintenance manoeuvres require low thrust, which leaves N_2 and both monopropellants as viable options. Mono N_2H_4 is chosen because the circularisation manoeuvre propellant is dual N_2O_4 / N_2H_4. This means there is already a N_2H_4 tank onboard the satellite. By selecting mono N_2H_4 as propellant, the two systems share the same infrastructure. This is excellent for the mass budget. Moreover, mono N_2H_4 has great performance characteristics.

Deorbit manoeuvre

A solid rocket motor is chosen for the deorbit manoeuvre. This was done for several reasons. Firstly, a solid rocket motor provides the required thrust, which is is important to ensure the deorbit burn is as efficient as possible. Secondly, because a solid rocket motor does not need plumbing, heaters, fuel tanks, fuel lines, etc. the dry mass is lower compared to the other options. Thirdly, a solid rocket motor is a simple, reliable system. This means it is less risky than the other options. Lastly, because of its simplicity, a solid rocket motor is a cheaper option.

Subsystem configuration

Figure 10.1 and Figure 10.2 [61, p.163-164] show the configuration of a dual mode propellant system and a solid rocket motor propellant system. These propellant systems are used in the METEOR mission. The dual mode propellant system has 16 thrusters. 12 of these are spaced such that there are 2 on each face of

[1] `https://www.rocket.com/article/aerojet-rocketdyne-has-insight-every-step-way`

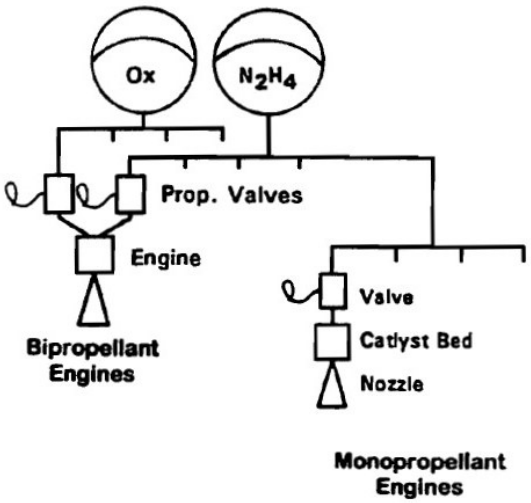

Figure 10.1: *Dual mode propulsion subsystem configuration.*

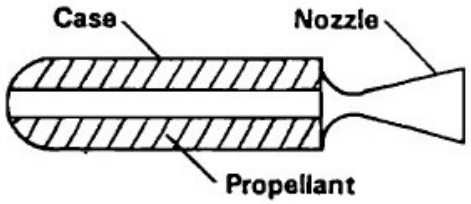

Figure 10.2: *Solid rocket motor propulsion subsystem configuration.*

the satellite. The thrusters are placed such that if two thrusters that are diagonally opposite are fired simultaneously, this produced a pure torque. This allows the satellite to have full 3-axis control. If translational manoeuvres are required, two thrusters that are on the same face of the satellite fire simultaneously, resulting in a pure translation. The 4 redundant thrusters are placed on 4 corners of the satellite. This ensures that in the event of a thruster failure, the satellite maintains full 3-axis control.

10.4. Risk

To prevent catastrophic propulsion subsystem failures, the subsystem is designed with redundancy. This redundancy is to be found in the design choice to have multiple propellant tanks. If one of the tanks would start to leak, or one of the valves would break, the other tank and/or plumbing system is used. Moreover, as explained in Chapter 12, for maintenance only twelve thrusters are needed for full 3-axis control. The satellite has sixteen thrusters to accommodate for thruster failure. Moreover, the propellant tanks are designed to hold reserve propellant. This reserve propellant is accounted for in the 300 m/s maintenance ΔV. The propellant used is toxic to humans. Therefore, it is paramount that the appropriate protocols and regulations are followed when the propellant is loaded into the tanks. The desirable properties of N_2H_4 outweigh the inherent risks of this propellant.Another risk is that the solid rocket motor has an uncertainty in the delivered ΔV or in the thrust vector direction. This risk can be mitigated by performing experiments on the solid rocket motor to verify that the ΔV and thrust it provides is within acceptable margins.

10.5. Verification & Validation

Verification

Verification of the developed tool was done in parallel with the development. The verification results are shown in Table 10.5.

Table 10.5: *Propulsion design tool verification results.*

Input	Output	Expected	Deviation
$(\Delta V, M_0, I_{sp}, \lambda_{error}, \lambda_{trapped})$ = (1000, 300, 250, 1.01, 1.008)	M_p = 102.300	M_p = 102.300	0%
(M_p, ρ) = (250, 1800)	V_p = 0.13889	V_p = 0.13889	0%
$(V_p, N_{tanks}, SF, p, \sigma_{yield}, \rho_t)$ = (0.5, 2, 1.1, 10, 900, 3800)	(r, t, M_t) = (0.3908, 0.002388, 35.05)	(r, t, M_t) = (0.3908, 0.002388, 35.05)	(0%,0%,0%)

Table 10.5 clearly shows that the tool computes what it is designed to compute, with perfect accuracy.

Validation

The nature of the tool is to automatically calculate very simple equations. There is no validation model that is available to use to validate the results. However, the equations used and their derivations have been validated. Therefore, the tool is said to be validated for its intended use.

10.6. Compliance matrix

To check that all propulsion subsystem requirements are met, a compliance matrix is constructed. The compliance matrix for the propulsion subsystem is found in Table 10.6.

Table 10.6: *Compliance matrix propulsion subsystem requirements.*

Requirement ID	Met / Not met / TBC	Justification
MR-PROP-01	Met	Designed to meet
MR-PROP-02	Met	Designed to meet
MR-PROP-03	Met	Designed to meet
MR-PROP-04	Met	Designed to meet
MR-PROP-05	Met	Designed to meet
MR-PROP-06	Met	Designed to meet
MR-PROP-07	Met	Met by AOCS MIMU sensor
MR-PROP-07-01	Met	Met by AOCS MIMU sensor
MR-PROP-08	Met	Designed to meet
MR-PROP-09	Met	Met by implementing section 3.3
MR-PROP-10	Met	Designed to meet

From Table 10.6 it is clear that all the propulsion subsystem requirements are met. This is because the subsystem is designed to meet all these requirements. In the design process, it was discovered that requirements **MR-PROP-07** and **MR-PROP-07-01** are actually requirements for the AOCS.

10.7. Recommendations

For the preliminary and detailed design phase it is recommended to perform a more detailed analysis on the redundancy of the propellant system to ensure that in case of a tank leak, the remaining tank can still function properly. Moreover, the placement of the redundant thrusters may need to be revisited to ensure full 3-axis control is preserved. A more detailed analysis of the solid rocket motors that will perform the deorbit burn is recommended too. A literature study may reveal a suitable off the shelf solid rocket motor. Otherwise, a solid rocket motor may need to be designed.

11 Entry, Descent & Landing

The EDL phase is one of the most critical phases of the mission. In this chapter, a model used to determine the trajectory, the design approach, and the results are presented. Furthermore,

11.1. Functional analysis

The EDL system consists of the entry, descent and landing phases of the mission. This includes calculation of trajectory, loads, aerothermal heating, the heat shield and the sizing of the entry vehicle to ensure its stability during entry. The EDL subsystem is designed to decelerate the entry vehicle from an entry velocity of 4230 m/s to a safe touchdown velocity of 0.5 m. This is achieved through a sequence of three phases, starting with entry with the complete entry vehicle where most of the kinetic energy is lost, a descent with a parachute, and finally the landing.

11.2. Requirements

The requirements for The EDL subsystem are shown below as derived in [13]. Some additional requirements are formulated to ensure that the subsystem performs as required.

MR-EDL-01: The system shall provide the surface element with a ΔV of [4230] m/s required for EDL.
MR-EDL-01-01: The parachutes shall delivers a ΔV of 500 m/s. **Added**
MR-EDL-01-02: The thrusters shall deliver a ΔV of 250 m/s. **Added**
MR-EDL-02: The system shall maintain control of the surface element during entry.
MR-EDL-03: The system shall maintain control of the surface element during descent.
MR-EDL-04: The system shall execute the landing sequence.
MR-EDL-05: The system shall provide a touch-down velocity of [0.5] m/s.
MR-EDL-06: The system shall detect touch-down.
MR-EDL-07: The system shall communicate touch-down.
MR-EDL-08: The system shall maintain control of the surface element during landing.
MR-EDL-09: The system shall deliver the surface element to an elevation up to 2800 m. **Added**
MR-EDL-10: The parachutes shall deploy at a maximum dynamic pressure of 900 Pa. **Added**

The two child requirements item **MR-EDL-01-01** and item **MR-EDL-01-02** were added to assess the performance of the different decelerators of the EDL sequence. Requirement item **MR-EDL-09** is added to ensure that the subsystem is capable of landing safely in the most demanding landing sites, the ones with the highest elevation. Finally, requirement item **MR-EDL-10** is added as the landing sites have different elevations, the parachute will be deployed at a different altitude and hence a different dynamic pressure.

11.3. Model & Results

Tool Development

An EDL design tool is developed to compute the trajectory during the entry, descent and landing. The tool provides the following outputs:

- The max deceleration load during EDL
- The heat flux during EDL
- The parachutes deployment altitude and velocity
- The number of thrusters needed for the last phase of EDL
- The ΔV required by the thrusters and their starting altitude

Method

The EDL phase is divided into three phases. The first phase is the entry, starting at an altitude of 100 km as mentioned in Chapter 9 where the entry vehicle enters the atmosphere with the heat shield experiencing the highest heat flux. The second phase is the descent with parachutes where the heat shield is jettisoned.

The third phase is the powered terminal descent using thrusters. The model presented here is based on [62].

The model uses some simplifications. The atmosphere is assumed to be isothermal, chemically homogeneous, non-rotating, and in hydrostatic equilibrium at some temperature T. Using this assumption, the density at an altitude z is calculated using (11.1)

$$\rho = \rho_0 \exp\left(-\frac{z}{H}\right) \tag{11.1}$$

where the density scale height is defined as shown in (11.2), with m_{mol} referring to the molar mass.

$$H = \frac{kT}{m_{mol} g} \tag{11.2}$$

Another assumption is the absence of gravitational force due to its negligible contribution compared to the drag force. The deceleration is then calculated using (11.3).

$$\frac{\mathrm{d}V}{\mathrm{d}t} = -\frac{\eta V^2}{H} \tag{11.3}$$

where η is defined using (11.4)

$$\eta = \frac{\rho(z) S H C_{\mathrm{D}}}{2m} \tag{11.4}$$

Neglecting the gravity contribution results in a straight trajectory where the flight path angle γ is constant and thus the vertical velocity of the entry vehicle is defined as shown in (11.5)

$$\frac{\mathrm{d}h}{\mathrm{d}t} = -V \sin\gamma \tag{11.5}$$

Combining (11.1) to (11.5), the deceleration and the velocity at each point in the trajectory are calculated using (11.7) and (11.6), respectively.

$$\frac{V}{V_0} = \exp\left(\frac{-\eta}{\sin\gamma}\right) \tag{11.6}$$

$$\frac{\mathrm{d}V}{\mathrm{d}t} = -\frac{\eta V_0^2}{H} \exp\left(\frac{-2\eta}{\sin\gamma}\right) \tag{11.7}$$

where V_0 is the entry velocity.

During the entry phase, the maximum heat flux is experienced by the entry vehicle. A first-order estimation of the heat flux was calculated using (11.8) [63], with R_n referring to the radius of curvature .

$$\dot{q}(z) \cong 1.83 \times 10^{-4} V(z)^3 \sqrt{\frac{\rho(z)}{\mathrm{R_n}}} \tag{11.8}$$

The second phase of EDL is the descent using the parachutes. The parachutes deployment altitude is very critical. Deploying the parachute at high altitudes can cause the parachute to fail due to the high dynamic pressure. On the other hand, if the parachutes are deployed at lower altitudes where the dynamic pressure is lower, there will not be enough time to decelerate the probes before touchdown. To tackle this problem, the parachutes are deployed at the highest possible altitude while maintaining a suitable dynamic pressure not exceeding 900 Pa and then the remaining required deceleration is provided by the thrusters. The only penalty of this approach is the high inflation load experienced due to high dynamic pressure. However, this load is still smaller than the maximum deceleration load experienced during the entry phase. The advantage of this approach is that the thrusters don't need to provide high thrust level and hence they are lighter and less complex. The drag force generated by the parachutes is calculated using (11.9).

$$F_{\mathrm{drag}}(z) = \frac{1}{2} \rho(z) V(z)^2 S_{\mathrm{para}} C_{d,\mathrm{para}} \tag{11.9}$$

where S_{para} and $C_{d,\text{para}}$ refer to the area and drag coefficient of the parachute, respectively.
The last phase of EDL is the descent using thrusters and touchdown. The thrusters are needed because the parachutes alone cannot provide enough deceleration due to Mars' thin atmosphere. Given a parachute deployment altitude, the model considers using a different number of thrusters and starting at different altitudes to minimise the required ΔV. The deceleration provided by the thrusters can be easily calculated using (11.10), where the mass here is the probe mass after jettisoning the heat shield, the back shell and the parachutes.

$$a = g_{mars} - \frac{N_{\text{thrusters}} F_{\text{thrust}}}{m_{\text{probe}}} \tag{11.10}$$

It has to be mentioned that EDL subsystem is using a ballistic trajectory with an angle of attack of 0 °. This means that there is no lift component used to control the vehicle as it is the case in the lifting trajectory. Although the lifting trajectory can result in a smaller footprint than the ballistic trajectory, it requires a more complex and a heavier system. Therefore a ballistic trajectory is used. This results in a footprint of an ellipse with a semi-major axis of 100 km and a semi-minor axis of 27 km as predicted by Phoenix mission [64]. This is a 3-σ meaning that the probability of probe landing inside the ellipse is 99.8 %. The values are decided based heritage missions which had the similar EDL vehicle configuration and trajectory.

Results

Since there are different landing sites with different elevations, the altitude at which the descent with a parachute and the descent with thrusters phases start will differ per landing site. The most critical case, in terms of the experienced loads, is the landing site with the highest elevation (2800 m) where the parachute is deployed at higher altitude experiencing high dynamic pressure. Furthermore, the thrusters have less time to decelerate the probe before hitting the surface of Mars. Therefore, the result presented here is regarding the landing site with the highest elevation. The input parameters are the same for all probes and shown in Table 11.1.

Table 11.1: *Input variables to compute the EDL trajectory.*

Input variable	Value	Unit	Input variable	Value	Unit
h_{entry}	100	km	γ	13.2	deg
v_{entry}	4.23	km/s	R_{n}	0.5	m
$C_{d,\text{capsule}}$	1.6	-	$C_{d,\text{parachute}}$	0.62	-
S_{capsule}	7.787	m^2	$D_{\text{parachute}}$	4.36	m
Thrust	200	N	parachute inflation factor	1.3	-

First, the complete EDL sequence is presented then each phase is discussed in detail. After the entry burn, the vehicle reaches an altitude of 100 km with a velocity of 4.23 km/s. The vehicle is provided with 8 cold gas thrusters to overcome the disturbances during the entry phase as explained in Figure 11.3. Then, the parachute is deployed using a mortar when the g load measured by the IMUs corresponds to the parachute deployment altitude. After the parachute deployment, the heat shield is jettisoned allowing for the final phase of EDL to start. Radar is used to measure the velocity and the altitude at this phase. The radar used can detect the surface from an altitude of6.5 km above the surface level. The thrusters ignite 1200 m above the surface level, allowing for a touchdown velocity less than 0.5 m/s.

The details of each phase of EDL are now presented. The deceleration and the velocity during the first and second phases of the EDL is shown in Figure 11.1a and 11.1b, respectively. The max deceleration load is experienced during the entry phase, with a maximum deceleration of 67.70 m/s^2 (6.9 earth g). The maximum deceleration caused by the parachute inflation is 46.46 m/s^2 (4.74 earth g).

The parachute is deployed at an altitude of 17.87 km where the dynamic pressure is 835.19 Pa to ensure that the dynamic pressure does not exceed the maximum allowed value of 900 Pa. This dynamic pressure constraint is represented by the red line in Figure 11.1b. The parachute used is a disk-gap band parachute due to its capabilities to operate at high Mach numbers and high dynamic pressures. It was tested and

deployed successfully at a dynamic pressure of 972 Pa [65]. The parachute is deployed using a mortar to ensure reliable inflation. The deployment altitude of the parachute is large compared to other missions, such as used by the Phoenix Lander where the parachute deployed at 12.9 km [64]. This is due to the high elevation of the highest landing site, with an elevation up to 2800 m compared to −4100 m in the Phoenix mission.

One more consideration regarding the deployment altitude of the parachute is the Mach number. Although deploying the parachute at a lower velocity decreases the dynamic pressure, there is a limiting factor to this approach, namely to avoid being at or near a transonic condition at parachute deployment. As the vehicle approaches Mach number 1, it enters a dynamic instability region. This aerodynamic instability causes the angle of attack to oscillate at an increasing rate [64]. This constraint is represented by the green line in Figure 11.1b where the minimum Mach number is set to be Mach 1.5.

With this in mind, it has to be ensured that for the other landing sites, the vehicle does not enter a transonic regime. The most critical case for this constraint is the landing site with the lowest elevation of −3900 m. The result of this analysis is shown in Figure 11.2. It is clear that the parachute deployment satisfies the mach number constraint, meaning that the mach number is higher than 1.5 at the deployment altitude. For this case, the vehicle velocity before starting the terminal descent is 97.43 m/s at an altitude of −3000 m, meaning that the 12 thrusters can easily decelerate the vehicle to a safe landing velocity before touchdown.

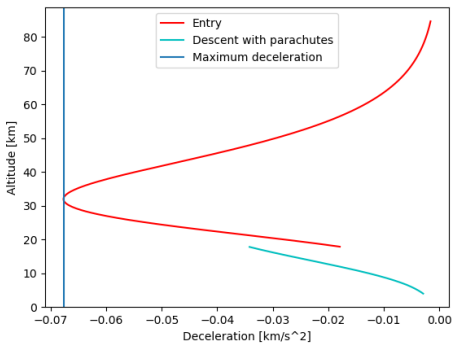

(a) *Deceleration during entry and descent with parachute.*

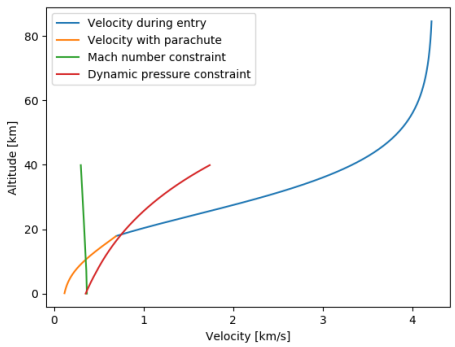

(b) *Velocity during entry and descent with parachute.*

Figure 11.1: *Deceleration and velocity during entry and descent with parachutes phases.*

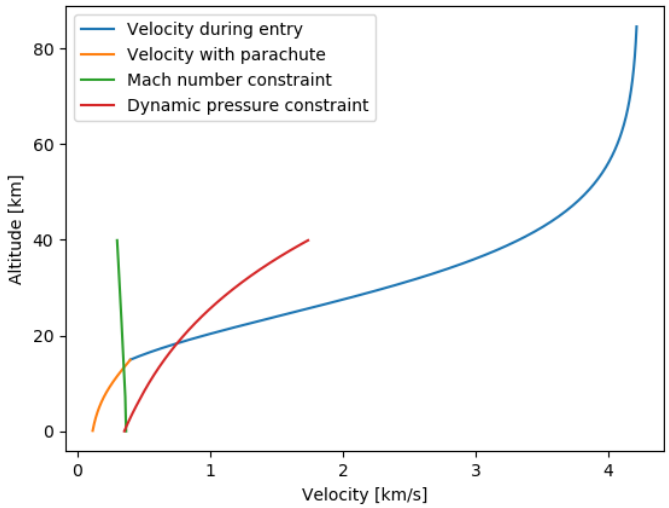

Figure 11.2: *Velocity during entry and descent for the landing site with the lowest elevation*

Next, the terminal descent starts at an altitude of 4.0 km. This is a higher altitude than usually done in other missions such as Phoenix [64]. The thrusters decelerate the probe to a landing site of an elevation up to 2800 m. This the highest elevation amongst all the landing sites and thus represents the most critical case. The thrusters provide a constant deceleration of 11.45 m/s^2. The trajectory during this phase is shown in Figure 11.3. The main results of the EDL design tool can be summarised as shown in Table 11.2.

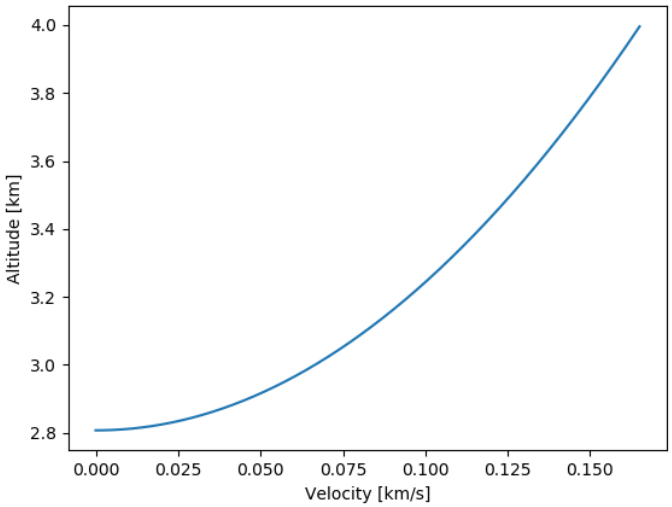

Figure 11.3: *Velocity during the terminal descent with thrusters.*

Table 11.2: *Output results for the EDL.*

Input variable	Value	Unit	Output variable	Value	Unit
Maximum deceleration	67.70	m/s^2	Parachute deployment altitude	17.87	km
Maximum parachute deceleration	46.46	m/s^2	Thrusters starting altitude	3.98	km
Maximum heat flux	0.255	MW/m^2	Highest elevation touchdown	2.80	km
Deceleration of thrusters	11.45	m/s^2	Maximum dynamic pressure for parachute	835.19	Pa

The heat flux is only calculated during the entry phase since it's the phase with the highest thermal loads; after this phase, the heat shield is discarded since it has already protected the vehicle from the highest heat load. Figure 11.4 shows the heat flux, with a maximum of 0.255 MW/m^2. Based on these heat flux values, the heat shield materials are chosen. During the design of the heat shield materials, the Viking mission heat shield was investigated since it was designed to withstand a similar maximum heat flux of 0.200 MW/m^2. Similar to the Viking and Pathfinder missions, carbon fibre with a core of Phenolic honeycomb filled with a mixture of silica microspheres, cork, and silica fibres is used for the heat shield, as mentioned in Chapter 8. This composite can withstand even higher heat flux loads, greater than 1 MW/m^2 [62].

Hardware Sizing

The sizing of the entry capsule and the heat shield are discussed in this subsection. The entry capsule is designed to be aerodynamically stable for most of the entry phase. The entry vehicle has a natural trim angle of zero degrees, but the radial CG location is not on the axis of symmetry. The stability requirements is met when $C_{m,cg} = 0$ and $\partial C_{m,cg}/\partial\alpha < 0$. These stability conditions are generally satisfied by using a 70 ° spherically-blunted conical forebody such as the Phoenix entry capsule [64]. However, in Pathfinder and Phoenix trajectory, it was predicted and noticed that there is an area of instability when the vehicle velocity is between 3 and 4 km/s. This instability is not of concern since the aerodynamic disturbances are small and the reaction thrusters are designed to keep the capsule pointed in the correct orientation.

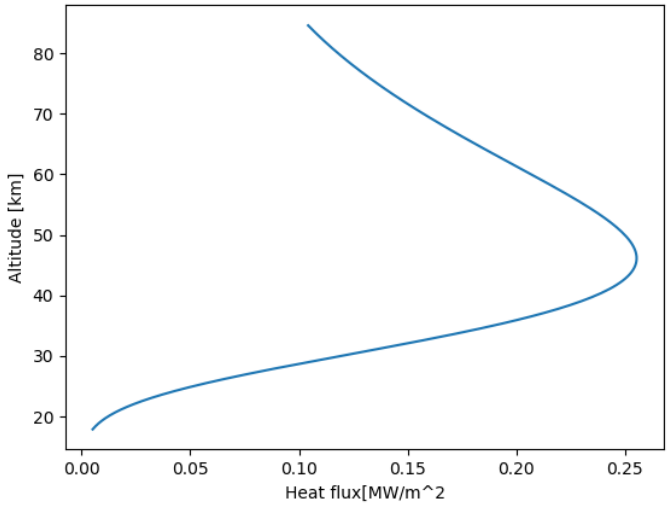

Figure 11.4: *Heat flux during the entry phase.*

The mass of the parachute, the heat shield and the back shell and support structure estimated using [66]. The mass breakdown is shown in Table 11.3.

Table 11.3: *EDL Hardware Mass estimation.*

Component	Percentage %	Mass [kg]
Heat shield	11	20.16
Back shell & support structure	9.7	17.77
Parachute	1.7	3.11

11.4. Risk

During the design of the EDL subsystem, some risks were identified and a mitigation strategy was considered for them. Some of these risks are:

1. Performing EDL in unsuitable weather conditions.
2. Landing with some of the lander's legs on a rock that could cause the lander to tip over.
3. Landing on a landing site with high elevation.
4. Entanglement of the parachute during deployment.

The mitigation strategy of these risks are as follows:

1. Mars Reconnaissance Orbiter data can be used to obtain the temperature and dust activity of the atmosphere.
2. The landing sites were chosen to have low rock abundance.
3. The EDL subsystem designed to operate properly for the worst-case scenario of the highest altitude
4. Mortar is used to deploy the parachute with sufficiently high velocity.

11.5. Verification & Validation

The verification of the deceleration load is done by using equations to estimate the maximum deceleration. These equations are based on the same model implemented in Python, however, the implementation in Python uses numerical integration where the deceleration and the heat flux is calculated at each point in the trajectory. These equations, on the other hand, calculate only the maximum value. The maximum heat flux was also verified by using ρ and V values corresponding to the maximum heat flux. The results are shown in Table 11.4.

The validation is performed using available data from similar missions and comparing the output. For the

Table 11.4: *EDL tool Verification results.*

Input	Output	Expected	Deviation
(h_{entry}, v_{entry}, R_{n}, S, γ, $c_{d,\text{capsule}}$)= (100, 4.23, 0.50, 7.787 ,-13.2, 1.6)	max heat flux = 0.255 Mw/m^2	max heat flux= 0.255 Mw/m^2	0.0 %
(h_{entry}, v_{entry}, S, γ, $c_{d,\text{capsule}}$) = (100, 4.23 ,7.787, -13.2 , 1.6)	max deceleration = 6.9 g	max deceleration = 6.9 g	0.0%

heat flux verification, the Viking mission is used since in this mission the entry vehicle started entry from an orbit around Mars. The entry altitude, entry velocity, radius of curvature and other parameters were changed to Viking's values and the max heat flux was calculated as shown in Table 11.5. For the deceleration load, the Phoenix mission was used since Mars Reveal entry capsule has a similar shape to Phoenix's and hence similar aerodynamic characteristic. The input parameters and the results are shown in Table 11.5.

Table 11.5: *EDL tool validation results.*

Input	Output	Expected	Deviation
(h_{entry}, v_{entry}, R_{n}, S, γ, $c_{d,\text{ capsule}}$)= (88, 4.6, 0.50, 11.23 ,-17, 1.6)	max heat flux = 0.262	max heat flux = 0.20	31.0 %
(h_{entry}, v_{entry}, S, γ, $c_{d,\text{capsule}}$) = (100, 5.5 , 8.34 , -13.2 , 1.6)	max deceleration = 11.68 g	max deceleration = 9.30 g	25.6%

As seen in Table 11.5, there are large deviations between the model results and the validation data. This is partially due to the simplifications in the model. It can also be due to some parameters that were estimated and not obtained exactly because of their non-availability. This applies to the area of the entry vehicle and the entry altitude. Furthermore, the atmospheric model used is not very accurate at high altitudes which contributes to this large deviation. It should be noted that the EDL design tool always overestimates the expected loads which are acceptable at this phase of the design.

11.6. Compliance matrix

Table 11.6 shows the compliance matrix for the EDL subsystem.

Table 11.6: *Compliance matrix of EDL subsystem requirements.*

Requirement ID	Met / Not met / TBC	Justification
MR-EDL-01	Met	Met by the entry vehicle, parachute and thrusters deceleration.
MR-EDL-01-01	Met	Designed to meet
MR-EDL-01-02	Met	Designed to meet
MR-EDL-02	Met	Designed to meet by designing entry vehicle shape
MR-EDL-03	Met	Designed to meet using the reaction control system
MR-EDL-04	Met	Designed to meet
MR-EDL-05	Met	Designed to meet using the thrusters
MR-EDL-06	Met	Designed to meet using the radar and IMU sensor
MR-EDL-07	Met	Designed to meet
MR-EDL-08	Met	Designed to meet
MR-EDL-09	Met	Designed to meet
MR-EDL-10	Met	Designed to meet by deploying the parachute at the correct altitude and velo

11.7. Recommendations

An accurate atmospheric model at high altitudes needs to be implemented to have a more accurate estimation of the density at the high altitudes during the start of the entry phase. Furthermore, a more detailed

aerothermal heating model can be implemented in the future where not only convective heating is considered, but also phenomena such as the variation of the heating rate with the flow regime, being turbulent or laminar, and real-gas properties of the atmosphere are implemented.

Another recommendation related to the stability of the entry vehicle is to have the centre of mass on the symmetry axis of the vehicle. This ensures better stability of the vehicle during EDL at an angle of attack = 0°. This can be achieved during the next iteration of the design by moving the different masses around or adding a balance mass if necessary.

12 Attitude & Orbit Control System

The Attitude and Orbit Control System (AOCS) consists of two primary elements. The Attitude Control System (ACS) ensures that the spacecraft remains oriented in the proper direction, as defined by mission and sub-system requirements. The Orbit Control System (OCS) is responsible for determining the spacecraft's position and controlling manoeuvres to change its orbit. These changes may originate from station-keeping requirements or mission objectives [11]. The following design is a first-order sizing of the most critical AOCS components. The mass, power and volume estimates driven by the specific hardware selection contribute to the overall configuration of the spacecraft.

12.1. Functional analysis

The METEOR mission has two applications of the AOCS: on board the orbiter, and on each of the probes. For each probe, the system is responsible for maintaining a specified pointing orientation during the de-orbit burn, and to keep the probe within required attitude deadbands during the entry, descent and landing phases. This is designed using heritage and trajectory requirements [67]. Concerning the orbiter, the AOCS is responsible for maintaining and modifying the pointing direction throughout all phases of the mission. During the nominal operation in a circular orbit around Mars, the UHF antenna must always be nadir pointing. Any disturbing torques on the orbiter must, therefore, be accounted for to prevent deviations.

12.2. Requirements

The requirements specified in the baseline report[13] are reiterated below, with possible updates or additions. The compliance of all requirements are summarised in Table 12.6. Requirements **MR-AOCS-02-01**, **MR-AOCS-02-03**, **MR-AOCS-02-04**, and **MR-AOCS-02-05** have been deleted because the orbital determination will be conducted using JPL's HORIZONS service, which does not use Keplerian elements[1].

MR-AOCS-01: The system shall be able to determine the orientation and position of the spacecraft throughout all phases of the mission.
MR-AOCS-01-01: The system shall have a maximum angular rotation error of 0.5 °/sec. **Updated**
MR-AOCS-01-02: The system shall have a maximum pointing excursion of 23.5 °. **Updated**
MR-AOCS-01-03: The system shall have a minimum positional accuracy of 0.2 milliarcseconds [68]. **Updated**
MR-AOCS-01-04: The orbiter shall maintain a nadir pointing attitude during the operational phase of the mission. **New**
MR-AOCS-02: The system shall provide navigation for the spacecraft.
MR-AOCS-02-01: The system shall determine the semi-major axis, eccentricity and true anomaly of the orbit of the spacecraft. **Deleted**
MR-AOCS-02-03: The system shall detect deviations from the intended semi-major axis to an accuracy of [TBD]. **Deleted**
MR-AOCS-02-04: The system shall detect deviations from the intended eccentricity to an accuracy of [TBD]. **Deleted**
MR-AOCS-02-05: The system shall detect deviations from the intended true anomaly to an accuracy of [TBD] rad. **Deleted**
MR-AOCS-03: The system shall control the attitude of the spacecraft.
MR-AOCS-03-04: The system shall be able to generate a torque around all three axes of 0.1 Nm. **Updated**
MR-AOCS-04: The system shall control the path of the spacecraft.
MR-AOCS-05: The system shall have the capability to detect hazardous foreign objects with at least one dimension larger than 3m. **Updated**
MR-AOCS-06: The system shall limit generated vibrations to a maximum of 9.81 m/s^2. **Updated**
MR-AOCS-07: The system shall limit generated accelerations to a maximum of 9.81 m/s^2. **Updated**

[1] `https://ssd.jpl.nasa.gov/?faq#B06`, retrieved 19/06/2020

MR-AOCS-08: The system shall incorporate failure detection, isolation and recovery.
MR-AOCS-08-04: During Safe Mode, the system shall maintain a thermal environment within a temperature range of 253 K to 333 K. **Updated**
MR-AOCS-08-06: The system shall have a lifetime probability of success of 98%. **Updated**
MR-AOCS-09: The critical subsystems of the system shall be designed with redundancy.

12.3. Model & Results

OCS Architecture

The orbit control system is most relevant in coordinating the manoeuvres of the orbiter. Its architecture is based on similar missions, in which the onboard sensor suite measures the inertial data of the orbiter and combines it with estimations from the star trackers. This information is periodically sent to mission control on Earth, which utilises JPL's HORIZONS system to accurately determine the ephemeris data[2]. The corresponding necessary trajectory corrective manoeuvres (TCMs) are then sent back to the orbiter and executed by the AOCS.

Onboard the probes, the OCS is primed prior to detachment from the orbiter [64]. Because it only provides guidance for the de-orbit burn, the precise timing and relative pointing are initialised based on the orbital trajectory of the orbiter.

ACS Design Tool

The ACS design process consists of six distinct steps: requirements determination, attitude control method selection, quantification of disturbance torques, hardware selection, budget updates, and finally control logic selection. This process is based on the steps described in *Space Mission Analysis and Design (SMAD)* [23, ch 11.1] and *Elements of Spacecraft Design* [61, ch 5].

A parametric tool written in python is used to size the AOCS and select specific actuator hardware to meet the functional requirements. The sizing is based on worst-case conditions, to ensure that the requirements will always be met. A worst-case condition would be one with the orbiter in a configuration having the greatest possible moment of inertia (full propellant mass, all probes onboard, and solar arrays deployed), and requiring the least effective control actuators to be used.

The tool uses inputs as described in Table 12.1. The left column contains mission operation parameters, based on heritage data and driving requirement. The right column consists of physical spacecraft parameters that are needed to calculate mass moments of inertia and the effect of torques on the spacecraft.

Table 12.1: *AOCS Sizing Tool Inputs.*

Mission Ops Parameter	Variable	Value	Unit	Spacecraft Parameter	Variable	Value	Unit
Appendage slew angle	θ_{app}	90	deg	Drag coefficient (Cd)	C_d	3	-
Appendage slew time	t_{app}	120	sec	Mass orbiter w/ probes	m_{max}	5439	kg
Momentum dump burn time	t_{md}	1	sec	Reflectance factor	q	0.6	-
Momentum dump interval	f_{md}	48	hrs	Residual magnetic dipole	D	1	$A \cdot m^2$
Number slew manoeuvres	n_s	100	-	Solar array mass (per side)	m_{SA}	12.5	kg
Pointing accuracy	θ_{acc}	0.5	deg	Solar array radius	r_{SA}	1.12	m
Slew manoeuvre angle	θ_s	135	deg	Solar array thickness	r_{th}	0.05	m
Slew manoeuvre time	θ_t	1200	sec	Solar incidence angle	i_{SA}	5	deg
Spacecraft lifetime	yr	5	years	TTC earth array height	h_{ttc}	0.5	m
				TTC earth array radius	r_{ttc}	0.75	m
				TTC earth array mass	m_{ttc}	45.3	kg

Attitude Control Method

The AOCS sizing process for the orbiter is based primarily on its nominal mission phase, where it will function as a communications relay in a circular Martian orbit. Except for a couple of large slewing manoeuvres during orbit insertion, it will need to maintain a reliable nadir pointing direction throughout the duration of its operation. Due to pointing accuracy requirements along each of its axes, a 3-axis stabilised system

[2] `https://ssd.jpl.nasa.gov/?horizons`, retrieved 10/6/2020

is selected for the orbiter. This design choice is reinforced by performance tables found in SMAD, as well as previous similar missions such as the Mars Reconnaissance Orbiter (MRO) [23, 69]. The lack of frequent slewing manoeuvres allows the system to utilise momentum wheels for primary attitude control. Attitude control thrusters are included for periodic momentum wheel desaturation and initial high-torque slews when the probes are attached to the orbiter.

For the probe, the AOCS is only active during the EDL phase. It must perform accurate pointing for the de-orbit burn and attitude control during the atmospheric entry. Needing less pointing accuracy than the orbiter, and experiencing greater disturbance torques, the probe will rely on cold-gas thrusters for attitude control. For the de-orbit burn, it will utilise spin-stabilisation to rotate the entire probe about its roll axis, effectively fixing the angular momentum vector in inertial space [23]. This removes the need for vectored thrust control and minimises the overall mass of the probe. The overall disk shape of the probe further ensures that the roll axis will have the greatest moment of inertia, guaranteeing stability. Prior to atmospheric entry, the probe is de-spun, changing the control type to 3-axis stabilised. This is necessary for the propelled descent as described in Chapter 11. The aeroshell is designed such that it will be inherently stable throughout the hypersonic phase, and will need few corrective inputs from the attitude control thrusters. This is supported by the design of the MSL lander, which required limited active control to remain within the specified dead bands [70]. Upon reaching the transonic phase, the ACS will become more active due to the instability around Mach 1 [67].

Disturbance Torques

Having selected the attitude control methods, the magnitude of the disturbance torques are needed to determine the sizing of the hardware. For the probe, the primary disturbance torque would be the aerodynamic loads, but due to the shape of the aeroshell, there is little need for active control. The thruster propellant estimation is therefore based primarily on heritage data, referencing the MSL and Phoenix lander which utilised similar EDL profiles [64, 70–73].

For the orbiter, both internal and external disturbance torques are analysed. These can be divided into cyclic and secular torques, where “the cyclic torques will cause cyclic rates, while secular torques cause gradual divergence” [23, p.369]. These secular torques will accumulate momentum throughout the orbit necessitating periodic momentum desaturation of the reaction wheels.

A rough parametric model of the orbiter is generated based on the locations and masses of major components. The model calculates the centre of gravity of the orbiter and the resulting moments of inertia about each axis. Additionally, the centre of pressure for a worst-case configuration is estimated, which is used for external disturbance torque calculations. These physical properties are updated and recalculated with each iteration of the overall design, such as the addition of an eleventh probe.

$$T_{gg} = \frac{3\mu}{2R^3}\left|l_z - l_y\right|\sin(2\theta_{gg}) \tag{12.1}$$

$$T_a = 0.5\rho C_d A_s V^2\left(c_{pa} - cg\right) \tag{12.2}$$

$$T_{sp} = \frac{F_s}{c} A_s(1+q)\cos(i)\left(c_{ps} - cg\right) \tag{12.3}$$

$$T_m = D\frac{M}{R^3} \tag{12.4}$$

$$T_{app} = \frac{4\theta_{app} I_{app}}{{t_{app}}^2} \tag{12.5}$$

The modelled external torques are: gravity gradient using (12.1), aerodynamic using (12.2), solar radiation using (12.3), and magnetic torque using (12.4). Major internal torques generated by actuation of the solar arrays or antenna gimbals are also calculated (12.5). The tool identifies the maximum torque that the orbiter may be subjected to, and calculates the momentum of the reaction wheels necessary to overcome this. By utilising momentum wheels, the orbiter will be stable throughout the orbit without the need for active manoeuvres to counteract each disturbance.

Hardware Selection

The sizing of the momentum wheels is based on three criteria. First, disturbance rejection, where the torque of the reaction wheels must at a minimum be able to counteract the worst-case disturbance torque. Second, slew torque where the reaction wheels on the orbiter will be required to slew the spacecraft during

manoeuvres, using (12.6). The largest will be after the aerobraking, when the orbiter needs to rotate from a maximum-drag attitude to a minimum-drag attitude, fully loaded with all probes on board. This is a 90 deg rotation in 50 min window. Third, momentum storage, which is calculated by integrating each cyclic torque over half its period, and summing with the maximum secular momentum that can be accumulated, using (12.7). Based on heritage data, the momentum wheels will be desaturated once every 48 hours [23].

Table 12.2: *AOCS Technical results.*

Parameter	Variable	Value	Unit
Max external disturbance torque	T_D	$1.24{\cdot}10^{-5}$	N m
Max internal disturbance torque	T_{app}	$1.03{\cdot}10^{-1}$	N m
Momentum storage for disturbance rejection	h	$3.20{\cdot}10^{-2}$	N m s
Secular momentum buildup per 48hrs	h_{secular}	$5.53{\cdot}10^{-11}$	N m s
Thrust force for momentum dump	F_{md}	$3.68{\cdot}10^{-11}$	N
Thrust force for slew manoeuvre	F_s	$5.00{\cdot}10^{-3}$	N
Torque for slew manoeuver	T_s	$1.00{\cdot}10^{-3}$	N m
Total lifetime thruster pulses	n_p	2768	-
Total propellant mass	m_p	8.72	kg

The sizing of the thrusters is dependent on the thruster placement and manoeuvre requirements. As further detailed in section 12.4, the thrusters are sized to be able to counter any disturbance torque or to execute a worst-case slew manoeuvre; using (12.9) and (12.10) respectively. Using the calculated centre of gravity from the geometric model, the effective moment arm (L) of each thruster is calculated and the least-effective thruster pair is used for sizing. Assuming an acceleration of 5% of the total manoeuvre time [23] the minimum force of each thruster is calculated. Combining the thruster pulse life calculated using (12.12), with the specific impulse creates an estimation of minimum propellant mass required (12.13). This is then added to the propellant mass required for high-torque slews for a total propellant mass.

$$T_s = 4\theta \frac{I}{t^2} \tag{12.6}$$

$$h = (T_D)\,\frac{T_{orb}}{4}(0.707) + h_{\text{secular}} \tag{12.7}$$

$$F_{md} = \frac{h}{L t_{md}} \tag{12.8}$$

$$F_d = \frac{T_D}{L} \tag{12.9}$$

$$F_s = \frac{I \cdot \theta_s}{0.05 {t_s}^2 L} \tag{12.10}$$

$$n_{md} = 3 \cdot 365 \cdot yr \cdot \frac{24}{f_{md}} \tag{12.11}$$

$$n_p = 2 \cdot 2 \cdot n_s + n_{md} \tag{12.12}$$

$$m_p = \frac{t_{md} F_{md} n_{md} + 4 n_s \cdot 0.05 t_s}{9.81 I_{sp}} \tag{12.13}$$

The third type of hardware to be selected is the sensor suite. The detailed selection will be done in a later design phase when precise requirements are known, however, in this phase, flight-proven off-the-shelf components have been selected based on comparable missions. The orbiter AOCS will utilise two Miniature Inertial Measurement Units (MIMUs) from Honeywell [61] (one for redundancy) and two A-STR high-resolution star trackers from Leonardo Systems [74]. The need for a 3-axis stabilised system mandates that at least two star trackers are used, although more may provide additional accuracy. Inertial measurement units are included for initial stabilisation when the angular rates are too high for the star sensors to function accurately.

Table 12.3: *AOCS Hardware results.*

Component	Name	Mass [kg]	Quantity	Spacecraft
Reaction wheel	Honeywell HR12 [75]	9.50	4	Orbiter
Star sensor	Leonardo A-STR	3.55	2	Orbiter
Inertial measurement unit	Honeywell MIMU	4.70	2	Orbiter, Probes
Attitude control thrusters	See Chapter 10			Orbiter, Probes
Terminal descent sensor	TAS-I RDA	6	1	Probes

The probe will be equipped with cold gas thrusters mounted to the aeroshell for attitude control during entry and descent [76]. As summarised in Table 12.3, the sensor suite will consist of two MIMUs, and a Terminal Descent Sensor for ranging during the final landing phase. This is based on the flight-proven landing designs of the ExoMars and Mars Science Lander[3]. The terminal descent sensor will be a Radar Doppler Altimeter (RDA)[77], manufactured by Thales Alenia Space - Italia (TAS-I). This is the only non-standard hardware component, but the development costs will be minimal due to it being TRL 8+ technology.

12.4. Risk

For both the orbiter and the probe, a non-operational AOCS will guarantee mission failure. Being unable to provide correct pointing direction or sufficient pointing accuracy will prevent the solar arrays from generating power or the communications system from transmitting/receiving data. The probe must execute its de-orbit burn manoeuvre properly to ensure a correct landing, and the terminal guidance system must prevent the probe from impacting the surface.

To mitigate these risks, as per industry norm the AOCS is designed with multiple levels of redundancy [61]. All attitude sensors such as the star trackers and MIMUs are installed in pairs; data from only one sensor meets requirements. One reaction wheel is installed for each of the three axes of control, plus one for redundancy in case of failure. As an additional level of redundancy to ensure that all critical manoeuvres can be executed, the orbiter is fitted with 16 attitude control thrusters (four redundant), each of which are sized to be able to perform a worst-case manoeuvre. This configuration is standard practice for similar spacecraft such as the MRO [78].

On the probe, both the sensors and attitude control system incorporate component-level redundancy. The cold gas thrusters mounted on the aeroshell are installed in parallel pairs for each thrust axis, which provides immediate backup in case of failure. As with the orbiter, dual inertial measurement units are selected to measure attitude changes and keep the probe within the specified dead bands.

Relying on component-level redundancy for nearly all hardware significantly increases the mass of the system. Additionally, hardware is selected to exceed the minimum performance requirements, resulting in additional mass. Nevertheless, the complete AOCS mass of both the orbiter and probe falls well within the allocated budgets.

12.5. Verification & Validation

All sizing functions in the AOCS tool were verified using python unit tests to guarantee no computational or syntax errors. In addition, because the tool is developed based on the AOCS design process described in *Space Mission Analysis and Design (SMAD)* [23] and *Elements of Spacecraft Design* [61], each of these functions is independently validated using the provided data for the fictional FireSat mission. Since the reference literature provides rough values as input and output of each function, the same number of significant figures is used during the validation. This results in an error of 0% for each function, as summarised in Table 12.5.

For a first-order sizing of the AOCS, this accuracy is considered sufficient [61]. The FireSat mission in earth-based, and therefore used an extensive set of parameters as listed in Table 12.4. For the Mars mission, a uniform standardised set of parameters is used by all numerical models in this report.

12.6. Compliance matrix

The AOCS has been designed to meet all the requirements as listed in the baseline report [13]. Requirements **MR-AOCS-02** and **MR-AOCS-05**, which respectively specify that the system shall provide navigation for the spacecraft, and have the capability to detect hazardous foreign objects, have been met by analysing ephemeris data provided by JPL HORIZONS. Requirement **??** will be met in the detailed software design phase, such that the system will automatically switch to safe mode in the event of failure.

[3] `https://exploration.esa.int/web/mars/-/47852-entry-descent-and-landing-demonstrator-module`, retrieved 10/06/2020

Table 12.4: *FireSat parameters used for validation.*

Parameter	Symbol	Value	Unit	Parameter	Symbol	Value	Unit
Num. high-rate manoeuvres	n_s	60	-	Orbit radius	R	7078	km
Angle long axis to vertical	θ_{gg}	30	deg	Orbital period	t_{orb}	98.9	min
Angle of incidence	i	0	deg	Reflectance factor	q	0.6	-
Atmospheric density	ρ	1e-13	kg/m^3	Residual dipole of spacecraft	D	1	Am^2
Centre of gravity	cg	0	m	Slew angle	θ_s	30	deg
Centre of solar pressure	$c_p s$	0.3	m	Slew manoeuvre time	t_s	600	sec
Centre aerodynamic press.	$c_p a$	0.2	m	Solar Constant	F_s	1367	W/m^2
Drag coefficient	C_d	2.0	-	Spacecraft velocity	V	7504	m/s
Earth's gravity constant	μ	3.986×10^{14}	m^3/s^2	Speed of light	c	3×10^8	m/s
High-rate manoeuvre time	$t_{s_{hr}}$	60	sec	Stored momentum	h	0.4	Nms
Magnetic field (earth)	B	7.96×10^{15}	tesla m^3	Surface area	A_s	3	m^2
Mass moments of inertia	I_z	90	kgm^2	Thruster force	F	0.8	N
Maximum disturbance torque	T_d	4.5×10^{-5}	Nm	Thruster moment arm	L	0.5	m
Mission lifetime	yr	5	years	Thruster pulse time	t_p	1	sec
Momentum dump frequency	f_{md}	24	hrs	Thruster specific impulse	I_{sp}	200	sec

Table 12.5: *AOCS tool validation results.*

Function	Input Parameters	Output	Expected	Deviation
Gravity gradient disturbance torque	μ, R, I_z, θ_{gg}	4.4×10^{-5}	4.4×10^{-5}	0%
Solar radiation disturbance torque	F_s, c, A_s, q, i, $c_p s$, cg	6.6×10^{-6}	6.6×10^{-6}	0%
Magnetic field disturbance torque	D, B	4.5×10^{-5}	4.5×10^{-5}	0%
Aerodynamic disturbance torque	ρ, V, C_d, $c_p a$, cg	3.4×10^{-6}	3.4×10^{-6}	0%
Reaction wheel torque for slew	θ_s, t_s, I_z	5.2×10^{-4}	5.2×10^{-4}	0%
Momentum storage	t_{orb}, T_d	4.7×10^{-2}	4.7×10^{-2}	0%
Thruster force for slew	θ_s, L, $t_{s_{hr}}$, I_z	0.52	0.52	0%
Thruster force for momentum dump	t_p, h, L	0.8	0.8	0%
Thruster pulse life	yr, n_s, f_{md}	5715	5715	0%
Propellant mass estimate	I_{sp}, F, yr, n_s, f_{md}	2.43	2.43	0%

12.7. Recommendations

In each of the primary steps, more precise requirements stemming from other subsystems and mission planning will allow the model to more accurately reflect the necessary performance of the AOCS. These improvements will be applied in the next design iterations as follows:

Manoeuvre Planning

A predefined list of all manoeuvres to be executed, including their respective rates and slew angles, is necessary for designing a mission-specific attitude control system. Working in partnership with mission control, these manoeuvres can be planned such that the vehicle is minimally impacted, allowing for less momentum storage and lighter overall AOCS design. This may include prohibiting full-body slew manoeuvres and antenna pointing to occur together or planning them such that the generated torques balance out.

Spacecraft Geometry

Detailed knowledge of mass distributions and configurations of both the orbiter and probe will facilitate a higher resolution geometric model. More accurate CG and moment of inertia calculations provide an essential basis for torque estimations. This will most notably have an impact on the estimation of aerodynamic torques generated during the aerobraking phase. The exact location of the centre of pressure and a better drag coefficient will greatly affect the calculated disturbance torque.

The exact placement of thrusters, and possible nominal utilisation of the four redundant thrusters, can result in new thruster pairs that require less individual force for the planned manoeuvres.

The incorporation of specific hardware may also lead to additional internal disturbance torques, not limited to: thruster misalignment, rotating machinery such as pumps, propellant sloshing, probe detachment forces, dynamics of flexible structures, or thermal shocks [23].

Hardware Selection
As mentioned previously, the sensor suite hardware can be refined once the specific performance requirements are known. The current design is based on heritage data, but a detailed configuration of the orbiter will allow for a more specific selection. The 3-axis stabilised system mandates the need for at least two star trackers, but the exact accuracy and thus component selection will be affected by the physical space available for placement. Naturally, the sensors will need to face away from mars to function properly.

Control Logic
Finally, the exact control logic can be defined, which will drive the selection of computational hardware and data processing. In contrast to the data handling system which must excel in storage, the command and control computers must be capable of rapid computations, further described in Chapter 14. The control algorithms will likely use quaternions to determine the spacecraft attitude and the data from the sensors will require Kalman filters minimise errors. The precise design of control software will be developed in the following phases.

Table 12.6: *AOCS Requirements compliance (TBC = To Be Confirmed)*

Requirement ID	Status	Justification
MR-AOCS-01	MET	
MR-AOCS-01-01	MET	
MR-AOCS-01-02	MET	
MR-AOCS-01-03	MET	
MR-AOCS-01-04	MET	
MR-AOCS-02	MET	
MR-AOCS-02-02	MET	Met using ephemeris data from JPL HORIZONS
MR-AOCS-02-06	MET	Met using ephemeris data from JPL HORIZONS
MR-AOCS-02-07	MET	
MR-AOCS-03	MET	
MR-AOCS-03-01	MET	
MR-AOCS-03-02	MET	
MR-AOCS-03-03	MET	
MR-AOCS-03-04	MET	
MR-AOCS-03-05	MET	
MR-AOCS-04	MET	
MR-AOCS-04-01	MET	
MR-AOCS-04-02	MET	
MR-AOCS-04-03	MET	
MR-AOCS-05	MET	Met using ephemeris data from JPL HORIZONS
MR-AOCS-06	MET	
MR-AOCS-07	MET	
MR-AOCS-08	TBC	Met by monitoring health and selecting appropriate mode
MR-AOCS-08-01	MET	
MR-AOCS-08-02	TBC	Will be met when control software is developed
MR-AOCS-08-03	TBC	Will be met when control software is developed
MR-AOCS-08-04	TBC	Will be met when control software is developed
MR-AOCS-08-05	TBC	Will be met when control software is developed
MR-AOCS-08-06	MET	Uses flight proven hardware from similar missions
MR-AOCS-09	MET	

13 Telemetry, Tracking & Command

This chapter is focused on the TT&C subsystem design for both orbiter and probe. The hardware selection is mainly based on off the shelf components with the redundancy aspects in mind. Furthermore, the subsystem is sized according to the data transfer needs of the system.

13.1. Functional analysis

The TT&C subsystem for both orbiter and probes have similar top-level functionality, namely to provide a link to another entity over which data can be transmitted in both directions. However, as the METEOR system has two different types of elements within the space segment (probe and orbiter) the TT&C system its design is tailored to the different functionalities as described below.

Probe functionality

The probe TT&C subsystem its main functional flow consists of two modes. The first is when the orbiter is not in sight, the second is when the orbiter is in sight and a connection is established. During mode 1 the probe stores the data to be transmitted to the probe using the C&DH subsystem. In this mode the TT&C will be in low power mode and will be able to detect a hailing signal from the orbiter to switch modes. In mode 2 the probe will transmit the queued data and receive commands from the orbiter. When the orbiters' overpass ends, the probe TT&C will terminate the connection and switches back to mode one.

Orbiter functionality

The orbiter TT&C compared to the probe TT&C is more intricate. Its core functionality is to gather the probe data from the Martian surface and transmit it to earth whenever it has a chance to setup a connection with the DSN. Because of this dual functionality, the TT&C will have to run the two interfaces simultaneously as illustrated by the high-level functional flow presented in Figure 13.1.

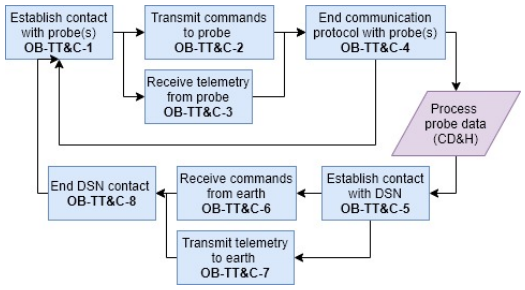

Figure 13.1: *High level functional flow of orbiter TT&C . NOTE: purple indicates interaction with other subsystem.*

13.2. Requirements

With the functionality of the TT&C established, one can assess if its performance on these functionalities satisfies customer needs by assessing the previously discovered [13] high-level subsystem requirements, presented below.

MR-TT&C–01: The system shall have a maximum downlink data rate of 10 Mbps.
MR-TT&C–02: The system shall have a maximum uplink data rate of 256 kbps.
MR-TT&C–03: The system shall use the X radio frequency band for communication to earth.
MR-TT&C–04: The system to earth communication shall have a comply with the ITU prescribed bandwidth of 6000 Hz.
MR-TT&C–05: The system its antenna shall be pointed to earth with a 0.008 rad pointing accuracy.
MR-TT&C–06: The system shall transmit signals with a minimum power upon arrival at earths antenna of 10 dB.
MR-TT&C–07: The system shall enable the space segment to switch operator selected flight modes upon request including the EOL procedures.

MR-TT&C–08: The system shall handle commands received on the up-link from earth.
MR-TT&C–09: The system shall transmit space segment data upon request.
MR-TT&C–09-01: *moved to chapter 14*
MR-TT&C–09-02: The system shall be available for communication with earth for 30000 s per day.
MR-TT&C–09-03: The system downlink data transmission shall have a minimum duration of 4000 s.
MR-TT&C–10: The critical subsystems of the system shall be designed with redundancy.

13.3. Model & Results

The model of the TT&C consists of three main elements. The TT&C subsystem architecture, the link design and the communication protocol. Note that both the probe and orbiter each have their TT&C subsystem tailored to their functional needs. Also, the level of detail for both subsystems will vary as some aspects are deemed more relevant to the conceptual design phase. An example of this is the subsystem architecture of the orbiter, this architecture is more detailed compared to its link design because of the required reliability estimation.

TT&C subsystem architecture

The TT&C subsystem architecture for both the probe and orbiter are based on the preliminary estimations featured in the midterm [11]. The most notable of these is the selection of the UHF and X-band for the probe-orbiter and orbiter-DSN communication links respectively. Looking at the presented subsystem architectures in Figure 13.2 one can observe that the selection of these carrier frequency bands has driven the architecture design. Another aspect that has driven the architecture design is associated with the subsystem its reliability. This will be elaborated further upon in section 13.4.

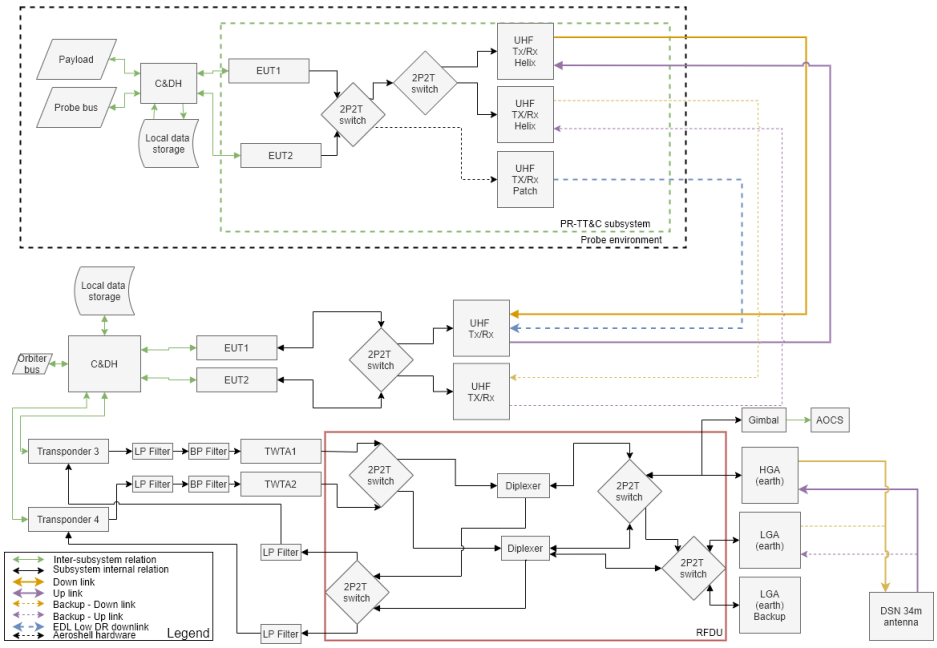

Figure 13.2: *TT&C subsystem architecture of both probe and orbiter.*

This figure indicates both the relations with other subsystems and the internal relations between components. Also it contains the communications diagram, indicating the communications flow throughout the system. Note that the communications diagram shows the relation between a probe and orbiter as a representation of all probe-orbiter communication. The presented architecture will be elaborated upon in three main steps. First, the probe and its TT&C subsystem will be explained, then the UHF part of the orbiter, and lastly the X-band related hardware on the orbiter. Communication between orbiter and probe will follow the Transfer Control Protocol (TCP). TCP data packets contain unique source IDs. The protocol allows for multiple probes to communicate to the orbiter at the same time. Also TCP features several software redundancy measures which will be elaborated upon at later stage.

Probe architecture

The components featured in the probe TT&C architecture are presented in Table 13.1 along with their respective masses, volumes and power usages. Most notable is the Electra UHF Transceiver (EUT) which combines the functionalities of the diplexer, transponder and amplifier. This hardware was used on the MSL mission for all UHF related communication [79]. Note that these values were retrieved from heritage [79] or literature [23, p.571].

Table 13.1: *Overview of hardware components in the TT&C subsystem of the probe.*

Hardware item	Quantity	Unit mass [kg]	Mass [Kg]	Power use [W]	Size [m]	Volume [m^3]
EUT	2	10.1	20.2	71	0.2x0.4x0.4	0.032
UHF Tx/Rx	2	1.4	2.8	0	0.2x0.2x0.42	0.0168
2P2T switch	2	0.1	0.1	0	-	0
Total						
TT&C PR			23.2	71		0.0976

The two UHF Tx/Rx will be helical antennas with a diameter of 0.2 m and height of 0.42 m and will have the ability to transmit signals from both EUT devices by means of the 2P2T switch. Note that the TT&C subsystem of the probe will feature hot redundancy for all main components (further explained in section 13.4). For the probe, its communication hardware will be in a standby mode when not transmitting. In this mode, it will only be able to receive an empty TCP packet containing a synchronise bit. Upon arrival, the probe TT&C mode switches and an empty TCP packet is returned with the synchronise and acknowledge bit. The orbiter ends then concludes the three-way handshake by acknowledging and the data transmission is initiated. During EDL the probe will transmit decent data in a low data rate UHF uplink. While the probe is inside the aeroshell it will be tethered to a UHF patch on the aeroshell. Upon separation a switch triggered the TT&C to switch to the two main helical antennas for the remainder of the mission.

Orbiter UHF architecture

As presented by Figure 13.2 the orbiter TT&C subsystem features an UHF compatible interface comparable to the TT&C subsystem present in the probe. These subsystems are quite similar, except for their operational time. The UHF interface will be active most of the orbiter its time as it collects the data from all eleven probes. The physical characteristics of the hardware can be observed in Table 13.2 together with the hardware of the orbiter its X-band interface.

Orbiter X-band architecture

The X-band architecture is mostly based on classical TT&C subsystem design [23, p.391]. Both transponders have modulating and demodulating capabilities conform the SDST, featured in the MRO [80]. The signal from the SDSTs is amplified by the TWTA and then passed to the RFDU which in turn directs the signal to the appropriate antenna (HGA or LGA on gimballed TWTA panel). The X-band interface too features hot redundancy in all vital components for all mission phases (for instance during coast when HGA cannot pointed at earth). Table 13.2 features all TT&C subsystem components present in the orbiter. These values were obtained through heritage [79] [80] and literature [23, 571].

Table 13.2: *Overview of hardware components in the TT&C subsystem of the orbiter.*

Hardware item	Quantity	Unit mass [kg]	Mass [Kg]	Power use [W]	Size [m]	Volume [m^3]
HGA	1	10.6	10.6	0	1.5x1.5x0.5	1.76
LGA	2	0.8	1.6	0	0	0
UHF Tx/Rx	2	1.4	2.8	0	0.2x0.2x0.42	0.0168
Diplexer	2	1.8	3.6	0	0	0
2P2T switch	4	0.1	0.4	0	0	0
2 axis gimbal	1	30	30	15	0.3x0.3x0.3	0.027
LP filter	4	0.2	0.8	0	0	0
BP filter	2	0.2	0.4	0	0	0
TWTA	2	1.9	3.8	160	1x1.5x0.2	0.3
Transponder	2	5.8	11.6	16	0	0
EUT	2	10.1	20.2	71	0.2x0.4x0.4	0.032
Totals						
TT&C OB			85.8	176		2.4846

These components will be arranged such that cable loss is minimised, therefore the two interfaces are mounted apart from each other very close (on the exterior) to their respective antenna assemblies, similar to the MRO TWTA panel behind the HGA [80, p.2].

Link model

All link estimations were drafted to achieve the required data rates at a sufficient signal to noise ratio (SNR). The SNR was determined using(13.1) [23, p.551].Note that the most significant loss factors: space loss(L_S) and multi-path loss(L_m), were incorporated, in the detailed design phase this will be refined by including more loss factors such as cable loss.

$$\frac{E_b}{N_0} = \frac{P_{Tx} G_{AT} L_S L_m G_{AR}}{k T_s R} \tag{13.1}$$

Several factors such as L_m and T_s were assumed or retrieved from numerical studies [23] [81] (to be estimated with more precision in the detailed design phase). L_S was determined (13.2) with the maximum possible distance between orbiter and probe for the probe-orbiter link(d), and maximum distance between Earth and Mars for the orbiter-DSN link. For which f resembles the centre frequency of the link.

$$L_S = \left(\frac{c/f_c}{4\pi d}\right)^2 \tag{13.2}$$

The gain effects of the two used antenna types, parabolic and helix (LGA not considered for sizing) are computed using (13.3) and (13.4) respectively. The gain effects are computed as peak performance, in later design stages, this is to be detailed further. The antenna efficiency μ was assumed 0.55 for the parabolic and 0.70 for the helix [23, p.571].

$$G_{peak} = \mu \cdot \left(\frac{\pi D}{c/f_c}\right)^2 \tag{13.3}$$

$$G_{peak}[dB] = 10.3 + 10\log_{10}\left(\frac{c^2 L}{(c/f_c)^3}\right) \tag{13.4}$$

Lastly the data rate. The data rate is driven by the available bandwidth for each link and the modulation type. The bandwidth is selected to limit the noise, the modulation type reduces the BER and while increasing the data rate. The type of PSK used will be 8-PSK, which allows the data rate to increase up to four times the available bandwidth. Any modulation reduces the radiated power by splitting the signal over double-sided frequency spectrum [82]. Therefore the modulation will increase the data rate while lowering the SNR. The

described link model is employed per connection and assessed on its performance. The link is sized such that it is "closed".

Model inputs & outputs

As mentioned before the METEOR system features two sets of links, one for the probe-orbiter connection and the other for orbiter-DSN connection. Table 13.3 and Table 13.4 show the inputs for these links.

Table 13.3: *Input variables to compute the probe-orbiter uplink and downlink.*

Input variable uplink	Value	Unit	Input variable downlink	Value	Unit
P_{Tx}	8.5	W	P_{Tx}	10	W
B	2	kHz	B	7.5	kHz
f_c	390	MHz	f_c	435	MHz
l_m[dB]	-0.85	-	l_m[dB]	-0.85	-
L	0.4	m	L	0.4	m
T_S	530	K	T_S	530	K
d	1675	km	d	1675	km
Command generation rate	125	bps/probe	Data generation rate	1282.9	bps/probe
TCP packet header	2.27	Mbit	TCP packet header	2.31	Mbit
Modulation type	8-PSK	-	Modulation type	8-PSK	-

Table 13.4: *Input variables to compute the orbiter-DSN uplink and downlink.*

Input variable uplink	Value	Unit	Input variable downlink	Value	Unit
P_{Tx}	100	W	P_{Tx}	100	W
B	1	kHz	B	6	kHz
f_c	7.6	GHz	f_c	8.4	GHz
l_m[dB]	-0.85	-	l_m[dB]	-0.85	-
D_{Tx}	34	m	D_{Tx}	1.5	m
D_{Rx}	1.5	m	D_{Rx}	34	m
T_S	210	K	T_S	200	K
d	2.5	AU	d	2.5	AU
Command generation rate: probe	125	bps	Data generation rate: probe	1282.9	bps
Command generation rate: orbiter	500	bps	Data generation rate: orbiter	2000	bps
Modulation type	8-PSK	-	Modulation type	8-PSK	-

With these input parameters the link models predicted the outcomes presented in Table 13.5 and Table 13.6.

Table 13.5: *Output parameters for the probe-orbiter uplink and downlink.*

Output parameter uplink	Value	Unit	Output parameter downlink	Value	Unit
G_{AT}[dB]	3.7	-	G_{AT}[dB]	5.2	-
G_{AR}[dB]	3.7	-	G_{AR}[dB]	5.2	-
L_S[dB]	-148.7	-	L_S[dB]	-149.7	-
P_{Rx}	-131.9	dBW	P_{Rx}	-129.3	dBW
P_e	-162.3	dBW	P_e	-156.6	dBW
SNR[dB]	30.4	-	SNR[dB]	27.3	-
Data rate	8.0	kbps	Data rate	30	kbps
Data volume transmitted	39.1	Mbit	Data volume transmitted	146.8	Mbit
Contact time required	4785.4	s	Contact time required	4712.31	s
Link status	**Closed**		Link status	**Closed**	

Table 13.6: *Output parameters for the orbiter-DSN uplink and downlink.*

Output parameter uplink	Value	Unit	Output parameter downlink	Value	Unit
G_{AT}[dB]	66.1	-	G_AT[dB]	39.8	-
G_{AR}[dB]	38.9	-	G_{AR}[dB]	66.9	-
L_S[dB]	-281.5	-	L_S[dB]	-282.4	-
P_{Rx}	-156.5	dBW	P_{Rx}	-155.6	dBw
P_e	-175.4	dBW	P_e	-167.8	dBW
SNR[dB]	18.9	-	SNR[dB]	12.2	-
Data rate	4	kbps	Data rate	24	kbps
Data volume transmitted	295.6	Mbit	Data volume transmitted	1.77	Gbit
Link status	**Closed**		Link status	**Closed**	

As can be observed from these outcomes both connections have "closed" links with sufficiently high SNR with respect to **MR-TT&C–06** which is in line with the minimum threshold SNR of the DSN [5, p.7].

13.4. Risk

Both TT&C subsystems will feature redundancy measures to mitigate risk as per **MR-TT&C–10** and achieve reliability comparable to heritage[81]. This is achieved using both hardware and software redundancy.

Hardware redundancy

As depicted in Figure 13.2 both TT&C subsystems contain parallel component in hot redundancy. The reliability of hot redundant components is computed using (13.5) [81]. For which λ is the failure rate of a component per 10^9 Hr, t the mission duration in years and n the number of identical components in hot redundancy.

$$R(t) = \sum_{i=0}^{n} (1 - e^{-\lambda t})^i (e^{-\lambda t})^{n-i} \tag{13.5}$$

After, the reliability of the component types is multiplied to obtain the reliability of the subsystem. The failure rates [81] and the results are presented in Table 13.7 and Table 13.8 for orbiter and probe subsystems respectively.

Table 13.7: *Reliability estimation of orbiter TT&C subsystem. NOTE: n = 2 for all components but "Pointing" (additional factor) and "Antenna" (n=5).*

	TWTA	Diplexer	Transponder	EUT	Antenna	Pointing	Total
Failure rate [10^{-9}Hr]	558.2	0.3	1.6	10	5	203	-
Reliability [-]	0.9764	0.9999	0.9995	0.9999	0.9991	0.9911	0.9664

Table 13.8: *Reliability estimation of probe TT&C subsystem. NOTE: n = 2 for "EUT", "Pointing" is additional factor and n = 5 for "Antenna".*

	EUT	Antenna	Pointing	Total
Failure rate [10^{-9}Hr]	10	5	203	-
Reliability [-]	0.99999	0.9991	0.9911	0.9898

Software redundancy

Next to the hardware the TT&C subsystems also will be equipped with communication protocols that ensure additional reliability for data transfer. This protocol is mostly based on the Transmission Control Protocol

(TCP) [1] from which the most useful aspects were cherry-picked. Redundancy in TCP can be found in the re-sending of packets if not received. Also TCP handles packets arriving out of order. TCP is adopted for the probe-orbiter connection and will feature packets as described in Figure 13.3.

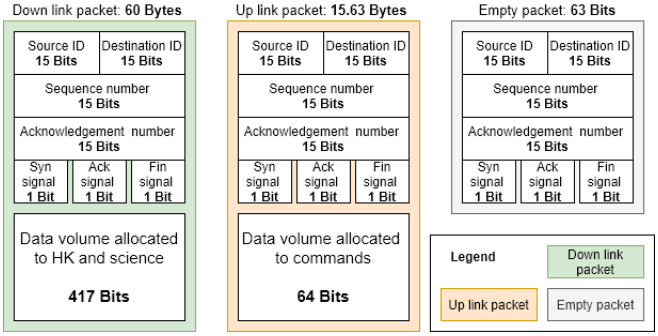

Figure 13.3: *TCP packet types & bit allocation.*

13.5. Verification & Validation

The verification model originates from an AE2235-II exam question regarding link budget. The validation model consists of a known GPS link budget [83, p.70]. The verification and validation results are presented in Table 13.9.

Table 13.9: *Link tool verification & validation results.*

Verification input	Output	Expected	Deviation
(P_{Tx},G_{AT},G_{AR},d,f_c)	$P_{Rx} = -121.525$[dBW]	-121.519[dBW]	0.0049%
(225 w,1,0.8,350 km,1090 MHz)	$P_e = -135.589$[dBW]	-135.591[dBW]	0.0014%
	SNR[dB] = 14.064	14.071	0.0497%
Validation inputs from GPS: (P_{Tx},d,G_{AT},G_{AR},f_c) (27 w, 20200 km, 10, 1, 1.57542 GHz)	$P_{Rx} = -158.1891$[dBW]	-158.2[dBW]	0.0%

Deviations are on the conservative side and suspected to be caused by the number of included significant digits of the Boltzmann constant. Note that the validation currently does not cover all aspects involved in the model explained in section 13.3.

13.6. Compliance matrix

Table 13.10 shows the compliance of the subsystems with respect to the requirements drafted in the baseline report [13] and presented in section 13.7.

[1] `https://www.khanacademy.org/computing/computers-and-the-internet/xcae6f4a7ff015e7d:the-internet/xcae6f4a7ff015e7d:transporting-packets/a/transmission-control-protocol--tcp` retrieved: 08/06/2020

Table 13.10: *Compliance of TT&C requirements.*

Requirement ID	Met / Not Met / TBC	Justification
MR-TT&C–01	Met	Designed to meet
MR-TT&C–02	Met	Designed to meet
MR-TT&C–03	Met	Designed to meet
MR-TT&C–04	Met	For downlink this is the case (uplink not covered by requirement)
MR-TT&C–05	Met	Met by AOCS & gimbal system
MR-TT&C–06	Met	Designed to meet
MR-TT&C–07	TBC	Requirement not relevant for conceptual design phase
MR-TT&C–08	Met	Handled by software diagram
MR-TT&C–09	TBC	Requirement not relevant for conceptual design phase
MR-TT&C–09-01		Covered in chapter 14
MR-TT&C–09-02	Met	Depending on Astrodynamics
MR-TT&C–09-03	Met	Depending on Astrodynamics
MR-TT&C–10	Met	Depending on Astrodynamics

13.7. Recommendations

Throughout the conceptual design phase there have been aspects that could be explored in more detail to provide a more accurate model to size the TT&C subsystems.

- **Include reliability input for architecture**: the architecture presented in this chapter was drafted before a reliability study was performed. However drafting the architecture with reliability as main input employing a Generic Algorithm is expected to lower the number of redundant components whilst maximising the reliability, this leads to lower cost, mass & volume [84].
- **Include more loss factors**: The current model only includes the most significant loss factors effecting the SNR. However a more precise estimate is required in the detailed design phase. This can be acquired by re-estimating loss factors currently present while also including the other loss factors.
- **GNU validation model**: Currently the validation model applied to the link tool does not fully cover all aspects involved in the connection parameter estimation. Therefore a validation model could be drafted from GNU software which is considered validated.
- **Account for Dopler shift**: The current design does not yet take into account the Dopler shift. The velocity by which the orbiter passes by the probes is expected to shift the centre frequency of the UHF carrier waves. This will effect the EUT and its ability to correctly demodulate the transmitted information. Therefore this Dopler shift will have to be addressed in further design phases. The Dopler shift though is very predictable, provided the relative velocity between probe and orbiter is known. It is recommended to correct for the shift on the orbiter side of the link, as the orbiter contains the exact location of the probes and is able to determine its own exact velocity by means of the AOCS. Additionally, the orbiter's relative velocity this way also is not required to be estimated by each probe individually. The shift can be computed using (13.6) [85].

$$f_d = \frac{f_c v_t}{c} \tag{13.6}$$

For which f_d is the resulting Dopler shift due to relative velocity v_t, also f_c resembles the centre frequency.

14 Command & Data Handling

The Command & Data Handling subsystem of the METEOR mission is there to process the scientific and housekeeping data for the downlink on the one hand, and to process the uplink commands on the other. In this chapter, the general design of the subsystem is discussed, meant to meet the requirements stated in section 14.2. A model developed to calculate required mass memory and processing rates is described in section 14.3, after it is verified in section 14.5. Hardware recommendations are given, also taking into account reliability considerations.

14.1. Functional analysis

The processing of data and commands entails the conversion of analogue to digital signals and vice versa, saving data for possible long-term use, using and distributing obtained data and commands for housekeeping or scientific purposes. Often the C&DH subsystem needs to be able to urge the concerning space segment to act autonomously, meaning without interference by the Earth Segment, The C&DH is vital to the scientific return and therefore mission purpose, meaning reliability considerations are of high importance.

14.2. Requirements

In the Baseline Report [13], several requirements are marked as TT&C requirements. For traceability purposes, these requirements will keep their original codes, although they are more related to the C&DH subsystem.

MR-TT&C-09-01: The system its downlink data transmission shall have a household and scientific data ratio of [TBD]. **Deleted**

MR-TT&C-09-04: The system shall accommodate the temporary storage of the household data for up to a period of [TBD] s. **Replaced**

MR-TT&C-09-05: The system shall accommodate the temporary storage of the scientific data for up to a period of [TBD] s. **Replaced**

MR-TT&C-09-06: The system shall accommodate the temporary storage of the household and scientific data for up to a period of 14 Earth days. **Orbiter, Added**

MR-TT&C-09-07: The system shall accommodate the temporary storage of the household and scientific data for up to a period of 30 sols. **Lander, Added**

MR-TT&C-09-08: The system shall be able to send 186.9 MB downlink per sol. **Added**

MR-C&DH-01: The system shall have a processing capacity of 1.497 MIPS. **Added**

MR-C&DH-02: The critical subsystems of the system shall be designed with redundancy. **Added**

MR-C&DH-03: The system shall track the time of the mission on the orbiter and the probes.

MR-C&DH-04: The system shall include magnetometers on board of all probes.

Replaced Requirements

Requirement **MR-TT&C-09-01** is deleted because this requirement does not set any unreasonable constraint on the design. The requirements **MR-TT&C-09-06**, **MR-TT&C-09-07** and **MR-C&DH-01** are put in place to design the system for any worst-case data rates and amounts of data, now it is up to the Earth segment or data team to decide what household data and what scientific data is requested downlink. The requirements **MR-TT&C-09-04** and **MR-TT&C-09-05** are replaced by the more elaborate requirements **MR-TT&C-09-06** and **MR-TT&C-09-07**.

14.3. Model & Results

The following section will describe the main program development and highlights all calculations required to meet all the requirements as stated in section 14.2. The calculation of the depicted minimum memory capacities and processing power of the orbiter is being discussed in the following three subsections.

C&DH Architecture

An overview of the CDH hardware is given in Figure 14.1, clearly depicting the different mentioned flows of data. The rates of the most important data are depicted on the concerning arrows.

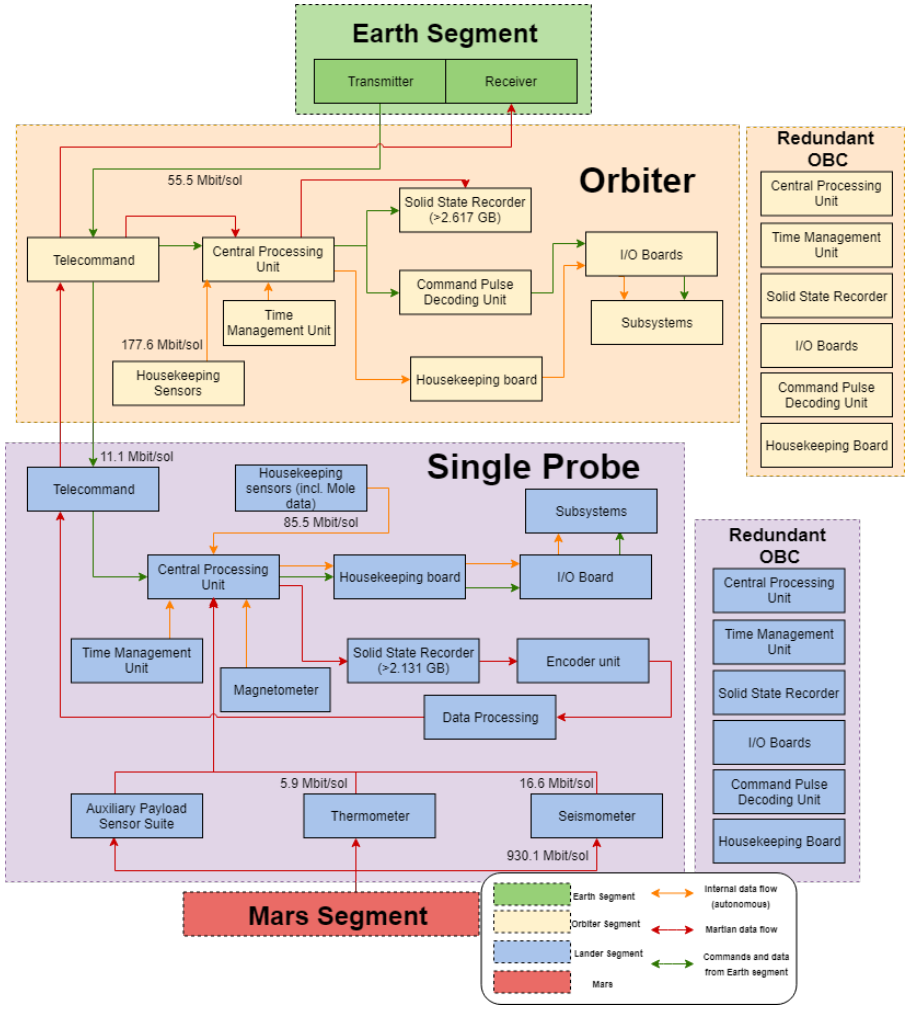

Figure 14.1: *The Data Handling block diagram, depicting all hardware and data flows within the CDH subsystem. The numbers on the arrow depict the data rates belonging to that flow of data. The required SSR capacity is also included.*

The OnBoard Computer (OBC), the device that entails all hardware as depicted in Figure 14.1, is the brain of both the orbiter and the lander section. It contains the mass and volatile memory of the spacecraft, but also the CPU, the processor that makes the autonomous decisions within the spacecraft. Moreover, the OBC contains a time management unit, encoding/decoding units and interfaces with all subsystems. Magnetometers are present within the OBCs of all landers for noise determination purposes. As will be described in section 14.4, the OBC will be designed to be completely redundant, with cross-coupling between vital functions. The redundant OBCs are depicted on the right-hand side of the figure, the depicted components are actually connected to the other components consistently with the connections on the left-hand side.
Only a compressed version of a selection of data is sent downlink. First of all, on the landers themselves, digital filters are used to reduce the sample rate and the OBC decides whether the data is interesting enough to send a (compressed) version downlink. In the first place, only a compressed version of the seismic data is sent downlink to the orbiter and the Earth segment. However, because all landers are given the memory capacity to store all data for 30 sols, interesting data can be requested by both the Earth segment or the orbiter autonomously.
The functioning of the C&DH subsystem becomes even more clear once one studies the software diagram in Chapter 17. The separate data flows are dismantled in further detail. Note that all functions outside of the dashed boxes in the diagram are performed by the C&DH subsystem.

Required mass memory for the orbiter

The first step in setting the requirements for the METEOR C&DH subsystem is setting the required onboard memory capacity for both the orbiter and the lander. This memory capacity (Mem_{orb}) is calculated using (14.1).

$$\text{Mem}_{orb} = t_{st_{orb}} \cdot \sum R_{max} \tag{14.1}$$

$t_{st_{orb}}$ is the required storage time and $\sum R_{max}$ the sum of worst-case compressed scientific data rates, worst-case housekeeping data rates of both the orbiter and all the landers and worst-case command rates for the eleven landers. For the orbiter, the longest period that contact between Earth and the orbiter segments is disrupted, is taken as a leading factor in the required orbiter memory capacity. This period is known to be the period of solar conjunction. The path from Mars to the Earth is blocked by the Sun once every two years. For a maximum period of fourteen Earth days [86], only simple commands can be sent uplink, and downlink data needs to be stored. The downlink data contains all received seismic, thermal and housekeeping data as well as data recovered from the mole, from all landers for the set period. The determined memory capacity can be found in Table 14.2.

Required mass memory for the landers

Secondly, the onboard memory required per lander is determined. The memory capacity of the landers is determined using (14.2).

$$Mem_{land} = t_{st_{land}} \cdot \sum R_{max} \tag{14.2}$$

$\sum R_{max}$ is the sum of worst-case, non-compressed data rates of the scientific instruments and mole, and the estimated housekeeping data of each lander. $t_{st_{land}}$ is the maximum time the data needs to be stored onboard. As for the InSight mission, the time that all full-temporal-resolution data needs to be stored on the separate landers is taken to be 30 sols [35]. Once again, all data rates are taken to be at their maximum estimates. With all this in mind, the required memory capacity per lander is 2.2 GB as depicted in Table 14.2.

Required processing power Orbiter OBC

Finally, the required processing power for the landers and orbiter can be determined, simplifying a hardware trade-off in the detailed design phase. Once again, in these estimations, worst-case data rates are considered, so that the theoretically maximum required processing powers are calculated. For the processing power of the orbiter, several possibly limiting scenarios are accounted for in the simulation. Only the most limiting scenario is described here. In this scenario, the maximum uplink command rates and maximum downlink data rates are received by the orbiter simultaneously. For the downlink, the model is integrated with the astrodynamical model as described in Chapter 9, facilitating the orbital information needed to determine the contact times and moments of the landers. From the orbital information, the minimum contact time between a lander and an orbiter (36 180 s) and the maximum amount of landers ever in contact with the orbiter simultaneously (four landers) are taken as constants. This computes to a required processing power for the worst scenario possible. Again, to be able to meet orbiter processor requirements, it is assumed all data needs to be able to be sent downlink once every sol. This way, the Earth segment is updated on every lander's performance every sol.

Model inputs and outputs

The developed model requires the inputs listed in Table 14.1.

Table 14.1: *Input variables of the C&DH model.*

Input variable	Value	Unit	Input variable	Value	Unit
$R_{\text{seis},DL}$	16.557	Mbit/sol	f_{thermal}	10	Hz
R_{thermal}	5.9	Mbit/sol	R_{mole}	5.9	Mbit/sol
$R_{HK,LD}$	1000	bps	$R_{HK,ORB}$	2000	bps
$R_{com,LD}$	125	bps	$R_{com,ORB}$	500	bps
$t_{st_{orb}}$	14	days	$t_{st_{land}}$	30	sols
T_{astr}	100	sols			

Note that on top of the above inputs, orbital parameters are used to determine contact durations and moments of all probes with the orbiters. Numbers of 100 sols is taken into account and the outcomes of the model as described in Chapter 9 are integrated with this model. The HK data rates for the orbiter and landers as well as the orbiter command rate are taken to be equal as those of Mars Global Surveyor, Viking and Mars Global Surveyor, respectively [61]. The command data rate for the landers is taken to be equal to that of the Phoenix mission [87]. The scientific data rates from the seismic[1], thermal (including acquisition rate) and mole health-monitoring [35] data rates are taken equal to the worst-case data rates of InSight. $t_{st_{orb}}$ and $t_{st_{\text{land}}}$ are the period of solar conjunction and $30 sols$, respectively.

The four most important outcomes of the C&DH model are presented in Table 14.2.

Table 14.2: *Most important output variables of the C&DH model.*

Requirement	Value	Unit
Downlink data rate from orbiter	186.9	MB/sol
Mass memory orbiter	2.7	GB
Mass memory per lander	2.2	GB
Processing power orbiter	1.5	MIPS

The downlink data rate per sol is simply a sum of the worst-case data rates as stated in Table 14.1, and is an important input to the model discussed in chapter 13.

Notes on scientific data rates

For both the thermal and seismic data, some small considerations need to be mentioned. Firstly, the obtained thermal data. The data rates originate from Insight [37], where the worst-case scenario features the thermal instrument is in conductivity mode. However, compared to the InSight mission, the driving requirement **MR-TL-02** requests a 5 times higher accuracy is required for the thermal conductivity measurements of the METEOR mission. Therefore, the daily amount of thermal measurement sets is computed using (14.3) and results in the maximum acquisition rate $f = 10 Hz$ [37].

$$N_{\text{Bits}} = \frac{DR}{t_{sol} \cdot f} \tag{14.3}$$

Here N_{Bits} is the amount of bits per thermal measurement set, DR is the worst-case data rate in MBit/sol, t_{sol} the time per sol in s. Now, to account for the increase in accuracy, N_{Bits} is increased by three bits per measurement set.

For the seismic measurements, there is a large discrepancy between the data obtained by each lander and its share in the downlink data rate. The difference mainly lies in the excluded VBB data rates[35]. It has to be mentioned that compared to the InSight mission, the acquisition rates for the seismic measurements is reduced to 50 Hz. Since only seismic waves up to 20 Hz need to be measured and the sampling frequency needs to be more than 2 times higher [88], including a safety margin, the sampling frequency is determined to be $2.5 \cdot 20 Hz = 50 Hz$.

[1] `https://mars.nasa.gov/insight/spacecraft/instruments/seis/`, retrieved: 05/06/20

14.4. Risk

The scientific return is crucial to the success of the METEOR mission. Since all data requires processing by the C&DH subsystem, this subsystem is designed for high reliability. Both the hardware and software have several design features in place that lead to a high reliability of this subsystem.

Failure-safe Hardware

The OBC its design is completely internally redundant, with cross-coupling between vital functions and with one computer remaining dormant at all times. Command and acquisition interfaces are separated into failure-isolated blocks. The present non-volatile memory allows the OBC to maintain data, even when the power supply fails. All interface electronics are fully redundant, so if one route fails, the main computer can switch to the other. Additionally, the mass memory shall be split into two modules, allowing to be united to one if required. The reliability factor of the OBC is therefore 0.99 during a lifetime of 20 years[89], exactly matching the maximum expected operational lifetime of the mission.
Now, the memory operation architecture is chosen to be quadruple modular redundant (QMR). Compared to triple modular redundancy (TMR), the overhead area only increases by 47531 μ m^2, while the failure rate due to bit-flips (radiation-related memory degradation) is lower by 6 orders of magnitude. QMR even allows for correction -not only detection- of bit-flips, an advantage over TMR [90]. The overhead area penalty is considered smaller than the advantage of increased reliability. On the InSight mission, not designing with TMR or QMR had its consequences and was regretted [2]. Since the mass memory requirements are still a factor 100 lower than what can be implemented on state-of-the-art computers, duplicating the memory up to four times is expected not to pose a problem and is accounted for in the budgeting.

Software

First of all, external and internal offsets can trigger the OBC's alarm functions, allowing for an autonomous reboot of the system. Secondly, the TCP, as described in Chapter 13, allows for integrated checksum software. Part of the 100-bit message that is filled by the C&DH system is reserved for a checksum verification code. The checksum generated by the OBC software will be matched against the checksum included in the message [91]. Finally, the METEOR mission is required to connect to other Mars orbiting communication satellites when the orbiter fails in some way, or when critical communication with Earth is blocked, by Mars for example.

14.5. Verification & Validation

Verification

Verification of the developed tool is done in parallel with the development using hand calculations. The verification results are shown in Table 14.3.

Table 14.3: *Propulsion tool verification results.*

Input	Output	Expected	Deviation
(acc,f,DR_{in})= (5,10,5.9)	DR_{therm}=96.5 bps	DR_{therm}=96.5 bps	0%
(t_{storage},N_{land}, $DR_{\text{HK,orb,bps}}$,$DR_{\text{HK,land,bps}}$, DR_{therm},DR_{seis}, DR_{mole}) = (14,11,2000,1000,5.9,930,5.9)	Mem_{orb} = 2.407 GB	Mem_{orb} = 2.407 GB	0%
GB (t_{storage}, DR_{HK}, DR_{therm}, DR_{seis}, DR_{mole}) = (30,1000,5.9,930,5.9)	Mem_{land} = 2.131 GB	Mem_{land} = 2.131 GB	0%
(N_{land},$N_{\text{land,in,cont,sim}}$, $N_{\text{orb,per,sol}}$) = (11,4,13)	Orbiter processing power = 1.50 MIPS	Orb. proc. power = 1.50 MIPS	0%

[2] `https://www.dlr.de/blogs/en/all-blog-posts/The-InSight-mission-logbook.aspx`, retrieved 11/06/2020

Validation

The nature of the tool described in this chapter is to perform relatively simple calculations, automatically integrating changes in astrodynamics and the different data rates. No validation model can be used, however, methods are checked against comparable missions. The solar conjunction phase, for example, is often used as a sizing factor for the memory capacity [86].

14.6. Compliance matrix

As can be seen in Table 14.4, almost all set requirements can be met already by selecting hardware comparable to what is advised in section 14.3 and section 14.4. Since the hardware is available and meets all budgets, these requirements are said to be 'met'.

Table 14.4: *Compliance matrix for C&DH subsystem.*

Requirement ID	Met / Not Met / TBC	Comment
MR-TT&C-09-06	Met	Designed to meet
MR-TT&C-09-07	Met	Designed to meet
MR-TT&C-09-08	Met	Designed to meet
MR-C&DH-01	Met	Designed to meet
MR-C&DH-02	Met	Designed to meet
MR-C&DH-03	Met	Designed to meet
MR-C&DH-04	Met	Designed to meet

14.7. Recommendations

Hardware considerations - Onboard intelligence and bus

Now the main requirements of the C&DH subsystem have been set and the hardware possibilities have been explored in the process, it is time to look into the hardware possibilities. For both the lander and the orbiter design, the same OBC and processing unit is selected for sizing purposes. Additionally, it is selected to see whether meeting the requirements is viable. Following the set requirements, taking into account the complexity of each segment, the processing capacities and the memory requirements, preferences for the onboard computer and its processing unit can be given.

First of all, the OBC. The Next Generation On Board Computer [89] is considered to meet all the set requirements. This OBC is a state-of-the-art, fully redundant computer, including all hardware features required. The system meets TRL 9 by ESA standards [89], being used on several interplanetary missions. The computer ensures high performance meeting the (memory) requirements in combination with low mass, volume and power consumption. With abundant interface capabilities all subsystems can be coupled. The RAD750 processor [92] is used as a reference for the processing unit, as its proven architecture guarantees performance in high-radiation environments. On top of this, the volatile memory and processing performance specifications fit the requirements of the C&DH subsystem. This processor can handle 2.1 MIPS at 132 MHz.

15 Electrical Power System

The electrical power system is used for power generation, storage, distribution and regulation. In this chapter, the power system will be designed and sized.

15.1. Functional analysis

The EPS has four major functions, these are power generation, power storage, power distribution and power regulation & control. The EPS system shall be able to supply the system with a continuous source of electrical power. Hence, the power generation shall be able to generate enough for both eclipse and in sunlight. The energy required for the eclipse shall, therefore, be stored in batteries. The system shall also be able to provide the average and peak power needs of the system. The latter will be provided by the batteries. The worst case peak power will be when the TT&C, C&DH, AOCS and Thermal are all operational at the same time.

The distribution system shall be reliable and be protected against failures in the EPS. Lastly, the regulation and control system shall keep the bus voltage within the designed range. The more sensitive equipment in the C&DH and TT&C subsystems shall have additional converters to provide a more precise voltage.

15.2. Requirements

The requirements for the EPS system were determined in the baseline report [13]. All requirements relating to the EPS system can be found in this section. In the baseline report, some requirements were not specified for the orbiter or lander. Therefore, in this section a distinction was made for the power requirements of the orbiter and lander.

General

MR-EPS-03-01: The system shall be capable of charging the secondary power source.
MR-EPS-04: The system shall monitor the status of the solar arrays. [S1.4.1]
MR-EPS-05: The system shall monitor the status of the secondary power source.
MR-EPS-06: The system shall control the spacecraft's subsystem power.
MR-EPS-07: The system shall detect faults in EPS.
MR-EPS-08: The system shall correct faults in EPS.
MR-EPS-09: The system shall have a reboot function.
MR-EPS-10: The system shall have redundancy built in in the solar arrays.
MR-EPS-11: The system shall have redundancy built in in the secondary power source.

Orbiter

MR-EPS-01-ORB: The system shall provide a total power of 681.5 W in sunlight to the spacecraft throughout the lifetime of the mission. **Updated**
MR-EPS-02-ORB: The system shall provide a total power of 437.9 W for worst case eclipse. **Updated**
MR-EPS-03-ORB: The orbiter shall be able to store total energy of 1.12 kWh. **Updated**
MR-EPS-03-02-ORB: The system shall not discharge the secondary power source more than 30% of its total capacity. **Updated**

Lander

MR-EPS-01-LDR: The system shall provide a total power of 179.8 W in sunlight to the spacecraft throughout the lifetime of the mission. **Updated**
MR-EPS-02-LDR: The system shall provide a total power of 63 W for worst case eclipse. **Updated**
MR-EPS-03-LDR: The orbiter shall be able to store total energy of 1.47 kWh. **Updated**
MR-EPS-03-02-LDR: The system shall not discharge the secondary power source more than 70% of its total capacity. **Updated**

15.3. Model & Results

The sizing of the EPS system consists of three elements. These are the solar array sizing, the secondary battery sizing and design and the power regulation and control design. This is done for both the probe and the orbiter. The variables used are explained in Table 15.4.

Method

To calculate the power the solar arrays need to produce, the shortest sunlight duration needs to be determined. For the orbiter, this is calculated in Chapter 9. For the probe, given the latitude and declination angle, the shortest daytime duration in hours can be computed using (15.1) [93]. Using the shortest sunlight duration and power required by each subsystem during both sunlight and eclipse and their respective path efficiency, the power that shall be generated by the solar arrays can be computed using (15.2) [23].

$$T_d = \frac{2}{15}\cos^{-1}(-\tan\phi\tan\delta) \tag{15.1}$$

$$P_{sa} = \frac{\frac{P_e T_e}{X_e} + \frac{P_d T_d}{X_d}}{T_d} \tag{15.2}$$

This equation can be used for both the lander and the orbiter. To size the solar arrays, the areal power density of the solar arrays will be estimated. This power density is based on the worst case conditions for both the orbiter and lander. These are EOL efficiencies for the solar array, which can be estimated using (15.3). For the lander, L_d will also include dust accumulation. It also includes the worst case incidence angle. For the orbiter, this is be based on heritage [23]. The lander's average incidence angle was computed using (15.4).

$$L_d = (1-d)^{yr} \tag{15.3}$$

$$\theta = \arccos(\sin\phi\sin\delta + \cos\phi\cos\delta\cos\omega) \tag{15.4}$$

The average incidence angle is defined as the incidence angle at which the power is equal to the average power generated during the day [93]. Lastly, the inherent degradation due to manufacturing and temperature losses are estimated. Given these parameters the power generated by the solar array can be computed using (15.5). Area is then computed using (15.6).

$$P_o = E_s \eta L_d I_d \cos\theta \tag{15.5}$$

$$A_{sa} = \frac{P_{sa}}{P_o} \tag{15.6}$$

Once the solar arrays have been sized, the batteries can be sized. The batteries are sized around the total energy storage that is required. Afterwards, the battery configuration can be made. This is based on the voltage and current of specifications of the battery. The required battery cell capacity can be computed using (15.7). From this the number of battery cells can be calculated using (15.8).

$$C_r = \frac{P_e T_e}{(DOD)n} \tag{15.7}$$

$$N = \frac{C_r}{C_{bat}} \tag{15.8}$$

Hardware Selection

For hardware selection, there are three subsystems to consider. These are the power generation, power storage and power regulation & control.

Starting with the power generation, there are two technologies to consider, these are the solar cell technology and the solar array technology. The current state of the art technologies for solar cells are triple junction and quadruple junction cells. These technologies offer efficiencies of 30% and 32% respectively, both are based on solar cells from Azur Space[1]. The quadruple junction cells have a TRL of 7 compared to the TRL

[1] `http://www.azurspace.com/index.php/en/products/products-space`, retrieved on 11/06/2020

of 9 for the triple junction cells. Although the TRL of the quadruple junction is lower, the quadruple junction cells offer better efficiencies and lower degradation rates than its counterpart. For this reason, it was selected as the solar cell technology.

For the solar array technology, there are four options available, these are; body-mounted rigid solar arrays, deployable rigid arrays, flexible fold-out arrays and flexible roll-out arrays. These can be seen in Table 15.1. All, except for the latter technology, have a TRL of 9. The flexible roll-out array has a TRL of 7 [94]. Body mounted arrays are the simplest as these are simply attached to the body of the spacecraft. These will, therefore, be the light option. However, these will have a limited area and thus can only be used for very low power requirements. The power that is needed for this mission will be too large to use this technology.

Table 15.1: *Current state of the art solar array technologies.*

Array Technology	Specific Power at 1AU [W/kg]	Areal Density at 1AU [W/m^2]	TRL
Body mounted array	N/A	314	9
Deployable rigid array	80	330	9
Flexible fold-out	150	338	9
Flexible roll-out	150	338	7

The remaining three options are all viable. The flexible fold-out arrays were selected for the design. These arrays offer the best in class performance and have a higher TRL than the flexible roll-out arrays.

For power storage, various secondary battery types have been used in space missions. These include; Silver-Zinc (Ag-Zn), Nickel-Hydrogen ($Ni-H_2$), Nickel-Cadmium (Ni-Cd) and Li-Ion. The latter is the state-of-practise for aerospace applications. There are various types of Li-Ion batteries, the most common are NCA ($LiNiCoAlO_2$), NCO ($LiNiCoO_2$)and LCO ($LiCoO_2$)[95], the performance of these batteries can be seen in Table 15.2. LCO are the smallest batteries, they have lower specific energy and are generally used for missions that do not require a lot of energy storage. NCO is the predecessor of NCA, it has lower specific energy, efficiency and energy density than NCA. Hence, NCA batteries were deemed as the best option for power storage.

Table 15.2: *Performance of Li-Ion batteries used in space missions [95].*

Battery technology	Specific energy [Wh/kg]
LCO	80-95
NCO	90-110
NCA[2]	140-160

Lastly, the power regulation and control system will be selected. There are two techniques used for power regulation these are Peak Power Tracking (PPT) systems and Direct Energy Transfer (DET) systems. The former option uses a DC-DC converter in series with the solar array. It tracks the peak power point of the solar array and allows it to operate at its peak power point. Since the converter is in series it has a much lower efficiency than its counterpart. The efficiency is generally 4-7% [23]. The DET system uses a shunt regulator. This regulator is in parallel with the solar array and can, therefore, influence the voltage of the solar arrays. It is much more efficient than the PPT as it only shunts away the excess power. The DET has fewer parts and a lower mass than the PPT. It also has better performance than the PPT at EOL. For these reasons, it was selected for the power regulation system for the solar array.

For the batteries, a similar trade-off is performed between an unregulated and a (partially) regulated bus. An unregulated bus is chosen as this offer much better performance when the bus does not need to be highly regulated. Since only the TT&C and C&DH require specific voltage inputs they will have their own dc-dc converter. Further, the batteries will have a BCU, as this will significantly increase the battery lifetime. This results in the electrical power system which is seen in Figure 15.1. The shunt regulator module, is based on

Terma space S3R module[3]. It includes an additional shunt cell for redundancy. For the linear, current charge control (LC^3), a second LC^3 is added for redundancy. This LC^3 charger is added with a transfer switch.

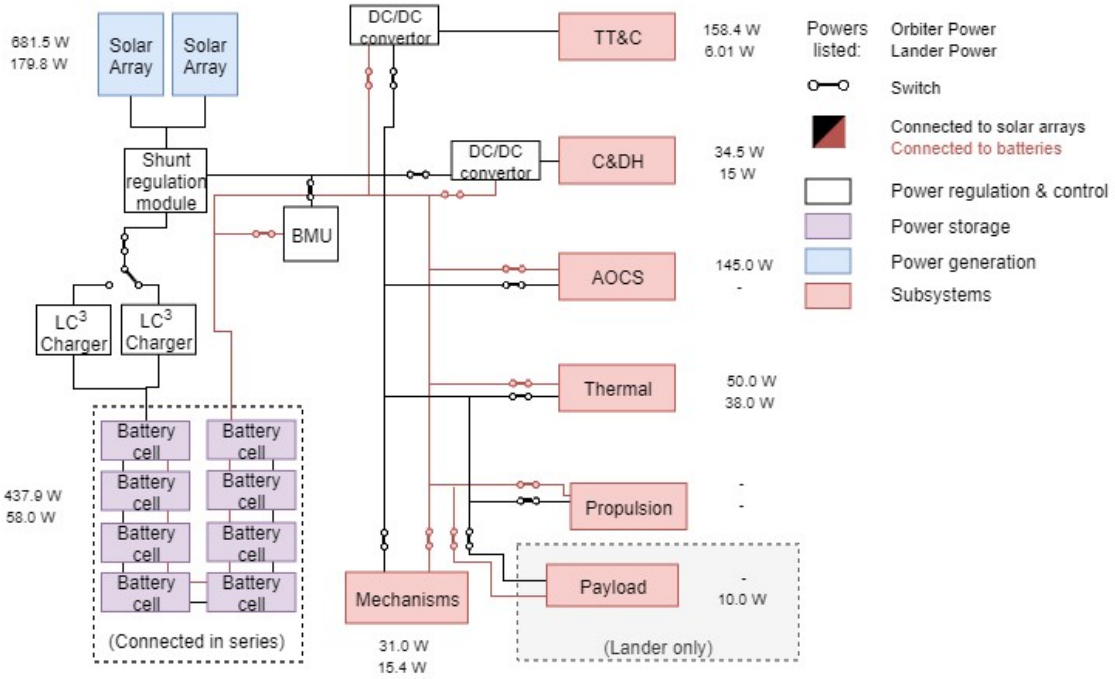

Figure 15.1: *The electrical block diagram with all components and power needs.*

Results

The solar array sizing is based on the average power required by each subsystem. The power needs of each subsystem can be seen in Table 15.3. These are based on specific hardware in each subsystem and their operational time per day and eclipse.

Table 15.3: *Average power required by each subsystem for the orbiter.*

Subsystem	P_d (Orbiter) [W]	P_e (Orbiter) [W]	P_d (Lander) [W]	P_e (Lander) [W]
C&DH	34.5	34.5	15.0	15.0
TT&C	158.4	158.4	6.01	0
AOCS	145	145	-	-
Thermal	5	50	38.0	38.0
Payload	-	-	10.0	10.0
Total	387.9	437.9	69.1	63.0

The inputs can be seen in Table 15.4. The degradation rate is estimated using standard degradation rates for multi-junction cells. The inherent degradation, Depth of Discharge and system path efficiency are estimated using SMAD [23]. Lastly, during the design, a constraint was set on the latitude. This is due to the harsh winter conditions present at higher latitudes. At 40° latitude the average areal power density is 73.8% of the average at 30° latitude. This is still within limits. However, when increasing the latitude further the power output becomes too low. At 50° latitude, the average areal power density is only 45.3% and at 60° latitude, it is only 15.4%. This low areal power density, combined with the higher power needs of the thermal system make these latitudes unsuitable as landing locations.

Once the initial outputs have been computed, the solar arrays and batteries can be sized. The solar array configuration is based on Azur Space quadruple junction solar cells[4] and it uses the UltraFlex array technology developed by Orbital ATK. The UltraFlex arrays are circular solar arrays. Because of this, they require

[3] `https://www.terma.com/media/177722/s3r_shunt_regulation_module.pdf`, Retrieved on 30-06-2020.
[4] `http://www.azurspace.com/index.php/en/products/products-space/space-solar-cells`, retrieved on 12/06/2020

Table 15.4: *Input variables for the EPS system.*

Name	Input variable	Value	Unit	Name	Input variable	Value	Unit
Cell efficiency	η	0.32	-	Battery efficiency	n	0.9	-
Latitude	ϕ	30	deg	Power daytime	P_d (orbiter)	387.9	W
Declination angle	δ	24.96	deg	Power daytime	P_d (lander)	59	W
Hour angle	ω	20.4	deg	Power eclipse	P_e (orbiter)	437.9	W
Inclination angle	θ (orbiter)	23.5	deg	Power eclipse	P_e (lander)	58	W
Inclination angle	θ (lander)	54.94	deg	Power required	P_{sa} (orbiter)	681.5	W
Degradation rate	d	0.035	-	Power required	P_{sa} (lander)	179.8	W
Depth of Discharge	DOD (orbiter)	0.3	-	Duration day	T_d (orbiter)	4941.6	s
Depth of Discharge	DOD (lander)	0.7	-	Duration day	T_d (lander)	35725.7	s
Solar Irradiance	E_s	586.2	W/m^2	Duration eclipse	T_e (orbiter)	2480.0	s
Inherenet degredation	I_d	0.77	-	Duration eclipse	T_e (lander)	52894.2	s
Life time degredation	L_d (orbiter)	0.84	-	Path efficiency day	X_d	0.85	-
Life time degredation	L_d (lander)	0.66	-	Path efficiency eclipse	X_e	0.65	-
Capacity required	C_r (orbiter)	1117.3	Wh	Mission duration	yr	5	years
Capacity required	C_r (lander)	1469.3	Wh				

customised solar cells. The solar array modules are not designed in this report, this will be done in the detailed design phase. The batteries are sized around Yardney batteries[5]. They offer a wide variety of NCA battery sizes, the sizing characteristics are given in Table 15.5.

Table 15.5: *The specific energy of the different battery options.*

Capacity [Wh]	Specific Energy [Wh/kg]
133.95	141
194.31	153
256	160

The optimal battery size depends on the battery configuration. The bus voltage is 28V, this is the standard in space applications and most components are designed around this voltage [23]. All batteries have the same voltage range of $3.0-4.1\,V$, therefore, at least eight batteries are required in series to achieve the bus voltage of 28V. This means that the battery cells will be designed in sets of eight. This results in the outputs for the EPS system, these can be seen in Table 15.6. An overview of the design options can be seen in Table 15.7. An overview of the system with all components can be found in Figure 15.1

[5] `https://www.eaglepicher.com/about-us/our-divisions/yardney/`, retrieved on 12/06/2020.

Table 15.6: *Outputs for the EPS system.*

Output Orbiter	Value	Unit	Output lander	Value	Unit
C_{bat}	194.31	Wh	C_{bat}	194.31	Wh
A_{sa}	10.9	m^2	A_{sa}	6.03	m^2
r_{sa}	1.31	m	r_{sa}	0.98	m
V_{bus}	24-32.8	V	V_{bus}	24-32.8	V

Table 15.7: *EPS system overview.*

Element	Value	Output lander	Value
Configuration	8s1p	Configuration	8s1p
Battery type	NCA (43Ah)	Battery type	NCA (43Ah)
Array technology	UltraFlex	Array technology	UltraFlex
Power regulation and Control	Unregulated, with BCU	Power regulation and Control	Unregulated, with BCU

15.4. Risk

Designing around risk is important in the design of a spacecraft subsystem. Failure in the EPS system can be caused by the regulation & control units, the battery, the solar array or the distribution system. The latter will be designed in the detailed design phase and will therefore not be included in the risk analysis. For the EPS system, the risk is minimised in three ways. First, for the hardware selection, only space-grade hardware is used. The battery, the solar cells and the power regulation system have a TRL of 9. Meaning that they have both been used on a space mission with success. Hence, they have proven reliability and the risk will be minimal. Second, the system is designed for end-of-life conditions. A worst case degradation rate of the specific component was used in the sizing and hardware selection. Third, the number of critical components was minimised in the EPS design. An unregulated bus has fewer components than a regulated bus. The system uses an unregulated bus, which has fewer components than a regulated system. This decreases the probability of failure within the EPS system.

15.5. Verification & Validation

The verification of the EPS sizing model is done in conjunction with the development and done using unit testing. The results of the unit tests can be seen in Table 15.8. For the validation, there is no validation model available. However, the tool was designed using a validated EPS design process [23].

Table 15.8: *EPS tool verification results.*

Input	Output	Expected	Deviation
$(\phi, \delta) = (0, 20)$	$P_o = 12$	$T_d = 12$hr	0%
$(P_d, X_d, T_d, P_e, X_e, T_e,) = (500, 0.9, 3600, 250, 0.8, 1800)$	$P_{sa} = 711.8$W	$P_{sa} = 711.8$W	0%
$(\phi, \delta, \omega) = (10, 15, 20)$	$\theta = 20.14°$	$\theta = 20.14°$	0%
$(E_s, \eta, L_d, I_d, \theta) = (1000, 0.25, 0.9, 0.9, 20)$	$P_o = 190.28$W	$P_o = 190.28$	0%
P_e, T_e, DOD, n = (1000, 1, 0.3, 10)	$C_r = 333.3$	$C_r = 333.3$	0%

15.6. Compliance matrix

In this chapter the compliance matrix is given, it can be seen in Table 15.9. All requirements have been met for the EPS design.

Table 15.9: *Compliance of EPS requirements.*

Requirement ID	Met / Not Met / TBC	Justification
MR-EPS-01-ORB	Met	Designed to meet
MR-EPS-01-LDR	Met	Designed to meet
MR-EPS-02-ORB	Met	Designed to meet
MR-EPS-02-LDR	Met	Designed to meet
MR-EPS-03-ORB	Met	Designed to meet
MR-EPS-03-LDR	Met	Designed to meet
MR-EPS-03-01-ORB	Met	Designed to meet
MR-EPS-03-01-LDR	Met	Designed to meet
MR-EPS-04	Met	Designed to meet
MR-EPS-05	Met	Designed to meet
MR-EPS-06	Met	Designed to meet
MR-EPS-07	Met	Designed to meet
MR-EPS-08	Met	More information in the Chapter 14.
MR-EPS-09	Met	More information in the Chapter 14.
MR-EPS-10	Met	Designed for worst case conditions
MR-EPS-11	Met	Designed for worst case conditions

15.7. Recommendations

During the design phase, there have been aspects of interest that can be explored more in detail. These are either newer concepts, which can offer better performance than the concepts explained in this chapter, or concepts can be explored more in detail.

- **Inverted Metamorphic Multi-junction (IMM) Cells:** These cells have demonstrated efficiencies of up to 35%. However, they are yet to be space-qualified.
- **Optimising solar arrays for Martian atmosphere:** The solar radiance spectrum on the Martian surface is modified by the atmosphere. By optimising for the spectra available, the power output can be improved by as much as 7% [94].
- **Concentrator solar arrays:** Concentrator solar arrays are currently still in development. However, these arrays are interesting for Mars as they show potential in mitigating the losses associated with Low Irradiance, Low Temperate (LILT) conditions. These arrays could allow for probes to be placed at higher latitudes. Thereby, increasing the coverage of the Martian surface.
- **Power distribution system:** The power distribution system was not designed in this design phase. The mass and losses of the power distribution system were included and estimated using SSE [55].
- **Optimising the hardware selection batteries:** The hardware was based on the manufacturers mentioned in the NASA state of the art report [94]. The batteries were based on Yardney batteries by Eaglepitcher. Because it was based on a single manufacturer the battery selection was limited. This combined with the required battery configuration caused the batteries to be overdesigned. Hence, choosing a different manufacturer with batteries that closer fit the required capacity would optimise the EPS design.

16 Thermal Control

The thermal control subsystem is presented right after the EPS as the subsystems are closely connected. The thermal subsystem uses a significant portion of the power budget while its main objective is to keep the temperature of the spacecraft and especially the electronics within a certain temperature range.

16.1. Functional analysis

The thermal subsystem can be divided into two main parts: passive and active thermal control. Functions the passive control part are similar to the functions of the active control part as they both are intended to keep the temperatures of the spacecraft components within survivable or operational limits. Passive control uses radiators, coatings and multi-layer insulation (MLI) to capture heat from the sun, the planet the spacecraft orbits around and other spacecraft components but also to reject heat by radiating into space or other spacecraft components and exchanging heat with the atmosphere of a planet. These functions are usually executed with little power required, making them methods of passive control. Active control, on the other hand, relies on heaters, moving fluids or moving spacecraft components to keep the temperatures within the desired range. Heaters are used mostly around components that have a small operational temperature window and components with windows of relatively high temperatures, such as batteries.

16.2. Requirements

MR-THE–01: The system shall maintain operable internal OB temperatures between min 170 K and max 348 K.

MR-THE–02: The system shall maintain operable internal LD temperatures between min 170 K and max 348 K.

MR-THE–02-01: The system shall maintain internal LD temperatures between min 150 K and max 348 K during descent. This will be checked for the final version of the report.

MR-THE–02-02: The system shall maintain operable internal LD temperatures between min 170 K and max 348 K during the scientific phase.

MR-THE–02-03: The system shall maintain the payload operation temperature of [TBD] +/-[TBD]K. **DELETED**

MR-THE–02-04: The system shall generate heat to increase the internal temperature to nominal 293 K conditions.

MR-THE–02-05: The system shall radiate heat to decrease the internal temperature to nominal 293 K conditions.

MR-THE–02-06: The system shall maintain the electronics temperature between 253 K and 333 K.

MR-THE–03: The system shall prevent thermally induced distortions higher than 0.0096 m.

MR-THE–04: The critical subsystems of the system shall be designed with redundancy.

MR-THE–02-03 is deleted as the payload has its own thermal control system.

16.3. Model & Results

The environment on the surface of Mars is less harsh than in the space around it, leading to two different models for each system. While the orbiter thermal control is more general, the subsystem of the probe has been developed more in-depth. This is done because the probes are the central part of this project, while orbiters have been sent to Mars successfully many times before.

Tool development

The first model represents the probe landed on the surface of Mars. The temperature of the electronics box is then computed every second during one sol to ensure the temperature range is within acceptable limits. The second model represents the orbiter in orbit around Mars. The required radiator area is computed to ensure the temperature of the electronics box is within acceptable limits.

Method

The probe is divided into four nodes, numbered from 0 to 3. The nodes represent the outer MLI and coating, the inside of the probe minus the electronics box, the inner MLI and coating of the electronics box, and the electronics box itself respectively. The temperature is uniform throughout the entire node. The masses and surface areas of the electronics box and MLI layers are estimated from the battery mass, the battery dimensions and the probe dimensions. It is assumed the MLI covers the entire surface of the electronics box and the outside of the probe. The specific heat capacity for this first estimate is assumed to be 1000 J kg^{-1} K^{-1} as this is a typical value for spacecraft[96]. The outer emittance is based on the coatings "Parsons Black paint"[97], white paint, aluminised Kapton and the stainless steel battery case, respectively. The inner emittance is based on the coatings white paint, white paint and "Z93" white paint, respectively [23]. The starting temperature is estimated by running the model with different starting temperatures and matching them to the ending temperatures, as this would mean a new cycle with the same temperature ranges.

Since node 0 is on the outside of the structure, it is in contact with the air and receives planetary and solar radiation. To compute their influence, several more properties are defined for this node only, namely the solar absorbance, area receiving sunlight and radiation, and the convective heat transfer coefficient. The solar absorptance is based again on the "Parsons Black paint "[97], while the areas receiving sunlight and radiation are the top and bottom surfaces of the probe. The convective heat transfer coefficient is based on CFD simulations for the SEIS windshield [35]. For this model, the electronics box has its own node, as it is driving for the design of the thermal control because of its small operational temperature window. The properties of the batteries are chosen as the properties of the entire box since the batteries make up most of the electronics. The electronics are encased by MLI, which is surrounded by the rest of the probe components. These components are encased by the outer MLI, which is in contact with the Martian atmosphere.

$$\begin{aligned} m_i \cdot c_i \cdot \frac{dT_i}{dt} =& Q_{\text{dissipation},i} + Q_{\text{solar},i} + Q_{IR,i} + Q_{\text{albedo},i} - Q_{\text{radiated},i} \\ &+ Q_{\text{convection},i} + Q_{\text{conduction},i} + Q_{\text{radiated},in,i} + Q_{\text{heater}} \end{aligned} \tag{16.1}$$

The model computes the temperature of each of the four nodes every second during one sol, starting at dawn. (16.1) is used to compute the temperature change of every node at every time step. This is the heat balance equation for node i. The temperatures are computed inwards starting from node 0. As node 0 is on the outside, it experiences solar radiation, planetary radiation, albedo, convection, conduction and radiation from other spacecraft components. Since the Martian atmosphere is cold and heat escapes the spacecraft by convection, black paint, a highly absorptive coating, is applied to the spacecraft. This influences the solar radiation, planetary radiation, albedo and heat radiation from the spacecraft as both the solar absorbance α_i and the emittance ε_i are then high. Their relationships are shown in (16.2), (16.3), (16.4) and (16.5), respectively. The view factor F_i in (16.3) is computed using (16.6).

$$Q_{\text{solar}} = J_{\text{s,ground}} \cdot \alpha_i \cdot A_s \tag{16.2}$$

$$Q_{IR} = \varepsilon_i \cdot A_p \cdot F_i \cdot \varepsilon_{\text{Mars}} \cdot \sigma \cdot \tag{16.3}$$

$$Q_{\text{albedo}} = \alpha_i \cdot A_p \cdot F_i \cdot \rho_{\text{Mars}} \cdot J_s \tag{16.4}$$

$$Q_{\text{radiated}} = \varepsilon_i \cdot A_{\text{total}} \cdot \sigma \cdot {T_i}^4 \tag{16.5}$$

$$F_i = \frac{1}{\left(\frac{R_m+h}{R_m}\right)^2} \tag{16.6}$$

Heat is also transferred out of node 1 by convection. The transferred heat is computed at shown in (16.7), where h_c represents the mean convective heat transfer coefficient, and ΔT represents the difference in temperature between the outer MLI and the martian atmosphere.

$$Q_{\text{convection}} = h_c \cdot A_{\text{total}} \cdot \Delta T \tag{16.7}$$

For all four nodes, the radiative heat transfer to adjacent nodes is computed. Every node radiates to the

nodes directly inside and outside of the current node. This relationship is given by (16.8). In this equation, F_{ij} represents the view factor, while ε_{ij} represents the effective emittance between two surfaces, with emittance ε_i and ε_j, respectively. This relationship is shown in (16.9).

$$Q_{\text{radiated},in} = \varepsilon_{ij} \cdot A_i \cdot F_{ij} \cdot \sigma \cdot (\Delta T)^4 \tag{16.8}$$

$$\varepsilon_{ij} = \frac{\varepsilon_i \cdot \varepsilon_i}{\varepsilon_i + \varepsilon_j - \varepsilon_i \cdot \varepsilon_j} \tag{16.9}$$

For node 3, also the conductive relationship is taken into account, as this is the most crucial node and has a relatively high temperature compared to the other nodes. The conductive heat transfer is computed using (16.10). h_{ij} represents the conductive heat transfer coefficient and is based on the thermal conductivity, area and length of the conductive path. These depend on the material the heat travels through, in this case, the outer and inner MLI. ΔT is the difference in temperature between the electronics box and the temperature of the atmosphere.

$$Q_{\text{conduction}} = h_{ij} \cdot \Delta T \tag{16.10}$$

The above-mentioned equations are repeated for every node at every second during 1 sol. During the day, the solar radiation received changes depending on the time of day to incorporate the influence of the rotation of the planet as seen in (16.11), where θ is the angle between the Sun and the horizon, as seen in (16.12). t is the time of sol in seconds, starting at dawn. It is assumed the probe is in sunlight for half a sol for this estimate.

$$J_{s,\text{ground}} = J_{s,\text{Mars}} \cdot cos(\theta) \tag{16.11}$$

$$\theta = \frac{\pi}{44388} \cdot (t - 22194) \tag{16.12}$$

For the orbiter, the model is kept very simple. The first computation of radiator and heater sizes is performed using the worst-case hot scenario to determine the radiator size and the worst-case cold scenario to determine the heater size for the orbiter. It is assumed the electronics box is placed on the side of the orbiter that is continuously facing the planet. This ensures that the dark-coated surface of the probe will radiate heat towards Mars while reducing the absorbed heat from the Sun. (16.1) can then be used, where the mass of the batteries, the solar intensity, convection, conduction, radiation to other components and heater power is neglected. This results in a balance of heat flowing in and out of the radiative surface. As it is the hot case, the highest battery temperature is taken. After the radiator area is computed, (16.1) is used again. For the cold case, the dissipated heat and albedo heat are both set to 0, while Q_{heater} is added as seen in (16.13).

$$Q_{\text{heater}} = -Q_{IR} + Q_{\text{radiated}} \tag{16.13}$$

For the cruise phase, the aeroshell and probe are assumed to be one node together. Using (16.2) and (16.5), ε and α are determined based on the minimum and maximum survival temperatures of the batteries. Since the orbiter spins while in cruise all parts of the aeroshell must be able survive the solar radiation

Results

The previously mentioned method is used together with the input variables found in Table 16.1, to compute the battery temperature at each second as seen in Figure 16.1. The horizontal lines show the maximum and minimum allowable temperatures of 333 and 253 K, respectively. A sharp change from increasing temperature to decreasing temperature can be seen, this is due to the model switching abruptly from outside air temperature. This greatly increases the heat loss due to convection. The model is then used with different

power inputs for the heater, both during the day and during the night until the battery temperature range is within the allowable limits. The batteries function optimally at 293K, but heating the batteries enough to achieve this temperature would require more batteries and again more heating. The solar intensity is determined with the median solar intensity and the average optical depth of the atmosphere. For the worst case hot scenario, the lowest optical depth, 0.3, and highest solar intensitiy, 718 are used [93, 98]. On the other hand, for the worst case cold scenario, the lowest solar intensity, 518, and the highest optical depth, 3.2, which occurs during dust storms, are used [93, 98]. The temperature of the electronics The final power requirements are found in Table 16.2. For the heatshield betacloth is used as the outer layer of the MLI to keep the temperature of the probe within survival limits during the Hohmann transfer [97, p.801].

Table 16.1: *Input variables for the thermal control subsystem.*

Input variable	Value	Unit	Input variable	Value	Unit
$\alpha_{\text{heatshield}}$	0.40	-	c_3	1000	J kg^{-1} K^{-1}
α_0	0.98	-	F_{0-1}	1	-
α_{radiator}	0.08	-	F_{1-2}	$\frac{5}{6}$	-
$\varepsilon_{\text{heatshield}}$	0.86	-	F_{2-3}	1	-
$\varepsilon_{\text{inner,0}}$	0.9	-	h	520	km
$\varepsilon_{\text{inner,1}}$	0.9	-	h_{0-3}	0.279	W/(m^{2}K)
$\varepsilon_{\text{inner,2}}$	0.92	-	h_c	2.59	W/(m^{2}K)
$\varepsilon_{\text{inner,3}}$	0	-	$J_{s,\text{ground}}$	530	W/m^2
$\varepsilon_{\text{Mars}}$	0.950	-	$J_{s,\text{Mars,max}}$	718	W/m^2
$\varepsilon_{\text{outer,0}}$	0.91	-	m_0	1.520	kg
$\varepsilon_{\text{outer,1}}$	0.9	-	m_1	117.688	kg
$\varepsilon_{\text{outer,2}}$	0.3	-	m_2	0.132	kg
$\varepsilon_{\text{outer,3}}$	0.14	-	m_3	12.610	kg
$\varepsilon_{\text{radiator}}$	0.75	-	$P_{d,\text{lander,thermal}}$	37	W
ρ_{Mars}	0.250	-	$Q_{\text{dissipated,orbiter}}$	144	W
σ	$5.67 \cdot 10^{08}$	W/(m$^2 K^4$)	$Q_{\text{dissipated,probe}}$	5.5	W
A_0	2.815	m^2	R_m	3389.5	km
A_1	2.815	m^2	t	0 - 88776	s
A_2	0.244	m^2	T_0	115	K
A_3	0.222	m^2	T_1	165	K
A_{planet}	0.503	m^2	T_2	183	K
A_{solar}	0.503	m^2	T_3	269	K
$A_{\text{solar,heatshield}}$	4.15	m^2	$T_{\text{air,max}}$	190	K
$A_{\text{total,heatshield}}$	7.79	m^2	$T_{\text{air,min}}$	115	K
c_0	1000	J kg^{-1} K^{-1}	$T_{\text{battery,max}}$	333	K
c_1	1000	J kg^{-1} K^{-1}	$T_{\text{battery,min}}$	233	K
c_2	1000	J kg^{-1} K^{-1}	$T_{\text{mean,Mars}}$	217	K

Table 16.2: *Outputs of the thermal control subsystem.*

Input variable	Value	Unit
$P_{d,\text{lander,thermal}}$	37	W
$P_{e,\text{lander,thermal}}$	38	W
$P_{e,\text{orbiter,thermal}}$	58	W
A_{radiator}	0.42	m^2
$T_{\text{battery,max}}$	302	K
$T_{\text{battery,min}}$	268	K

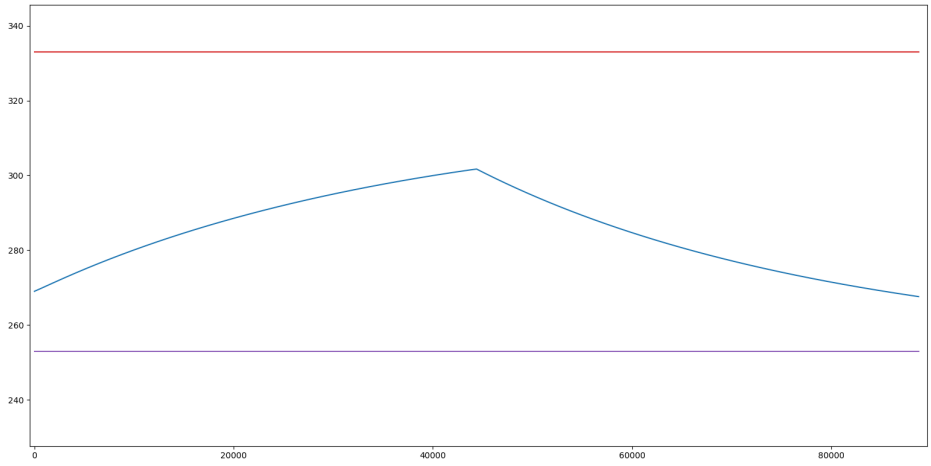

Figure 16.1: *In blue: Temperature range of the batteries during one sol. In purple and brown: The maximum and minimum operational temperatures of the batteries, respectively.*

16.4. Risk

The thermal control subsystem is important as the power supply and operation of large fraction of spacecraft components depend on it working correctly. There are a number of risks the thermal subsystem will prepare for. The most pronounced ones are the complete failure of the heaters and the failure of the MLI. Typical fail rates for active thermal control such as heaters is 0.32 per year. As this is a high failure rate, with a very high impact, a mitigation plan is necessary. It is advised to break the heaters up in multiple smaller heaters and add extra heaters that can take over if the others fail. The battery is still within operational limit if 83% of the planned heaters function. Typical fail rates of passive thermal control such as MLI and coatings is 0.084. The specific failure modes need to be investigated to determine a possible mitigation plan, however, as the probability of failure is much smaller than with active control, this is not the priority.

16.5. Verification & Validation

The model verification is started by performing unit tests on the used functions. The results can be seen in Table 16.3. It is recommended that for the next phase, the model is also verified using thermal modelling software such as ThermXL.

Table 16.3: *Thermal control model verification results*

Input	Output	Expected	Deviation
$(J_s, \alpha_i, A_{\text{solar}})$ = (520,0.93,5.392)	Q_{solar}=2607.5712 W	Q_{solar}=2607.5712 W	0%
(T_i, T_j, h) = (157,236,0.257)	Q_{cond}=-20.303 W	Q_{cond}=-20.303 W	0%
$(\sigma, A_i, F_{ij}, \varepsilon_{ij}, T_i, T_j)$ = $(8.23{\cdot}10^{-8}$,0.05,0.8,0.2,217,218)	$Q_{rad,in}$=-0.0271 W	$Q_{rad,in}$=-0.0271 W	0%
$(\varepsilon_{\text{outer,0}}, A_{\text{planet}}, F_0, \varepsilon_{\text{Mars}}, \sigma, T_{\text{mean,Mars}})$ = $(0.1,3,0.1,0.1,8.23{\cdot}10^{-8}$,236)	Q_{IR}=0.7659 W	Q_{IR}=0.7659 W	0%
$(\alpha_i, A_{\text{planet}}, F_0, rho_{\text{Mars}}, J_s)$ = (0.1,5,0.6,0.9,679.73)	Q_{albedo}=183.5271 W	Q_{albedo}=183.5271 W	0%
$(\varepsilon_0, A_0, \sigma, T_0)$ = $(0.4,7.36,8.23{\cdot}10^{-8}$,251)	Q_{radiated}=961.684 W	Q_{radiated}961.684 W	0%
(h_c, T_i, T_j) = (3.5,397.3,276.8,3.69)	Q_{conv}=1556.2575 W	Q_{conv}=1556.2575 W	0%
$(\varepsilon_i, \varepsilon_j)$ = (0.7,0.3)	ε_{ij}=0.265822784 W	ε_{ij}=0.265822784 W	0%

There are a number of assumptions used in the thermal mathematical model. The first is that the day and night are of the same length. In reality, this will vary per season depending on the latitude of the probe. The influence of the solar intensity changing with the seasons is small enough for the battery temperature

to remain within the acceptable limits. Next, the influence of the individual components of the probe is neglected. For this phase of the project, it was decided that it is acceptable to group the components in one node for the analysis, in order to focus on the electronics box. This is also done in an example of a valid thermal mathematical model [55]. Lastly, the current model consists only of four nodes. Again, this is done to investigate the driving requirement that is the battery temperature. For the orbiter, a very simplified model is used where the radiator and heater are computed for the electronic box only [23]. This was decided to be acceptable as the focus of the project is on the probes. All equations used for both models are valid and widely used [96].

16.6. Compliance matrix

Table 16.4: *Compliance matrix for the thermal subsystem*

Requirement ID	Met / Not met / TBD	Comment
MR-THE–01	TBD	Assumed to be met based on heritage. Needs more analysis
MR-THE–02	TBD	
MR-THE–02-01	TBD	This will be checked for the final version of the report
MR-THE–02-02	Met	
MR-THE–02-04	Met	
MR-THE–02-05	Met	
MR-THE–02-06	Met	
MR-THE–03	TBD	Material was chosen to limit this. Needs more analysis
MR-THE–04	Met	

16.7. Recommendations

For future models, the analysis will focus more on the specific probes and a decision will be made to either customise the subsystem for each probe environment or design for the worst-case scenarios, resulting in some over designing. Some recommendations for future development are listed below:

- **Increase the number of nodes.** Adding more nodes will more accurately estimate the heat exchange between the different components while allowing individual MLI and coatings where needed.
- **Make the day/night cycle more accurate.** Improving the day and night cycle will result in more extreme situations where the spacecraft has more time to warm up during the day but also where the night is longer than the day and the temperature may drop significantly.
- **Incorporate the influence of latitude.** This will influence the solar intensity received but also the day and night time.
- **Incorporate the influence of altitude.** This will change the outer air temperature, influencing the convective heat transfer.
- **Incorporate the influence local albedo and IR.** Now, the albedo is computed assuming the Sun is directly over the probe during the day, this will be a function of the position of the Sun. Furthermore, the emittance of Mars is not uniform all over the planet, the emittance at each landing location will be investigated.
- **Perform a specific material analysis.** The specific heat coefficient and temperature requirement of each component can then be accurately determined, resulting in a more reliable thermal model.
- **Investigate the convective coefficient.** The current coefficient is a mean value from a similarly shaped windshield for SEIS. However, the coefficient will be determined at different locations on the spacecraft according to the selected number of nodes.

In conclusion, a first thermal mathematical model indicates it is possible to design a thermal control subsystem using passive and thermal control within the decided budget.

17 System Overview

This chapter will contain an overview of the entire subsystem after the subsystem design. It will consist of an overview of the mission, the system configuration and an overview of the key system characteristics.

17.1. Mission Overview

Launcher

The chosen launcher is the Ariane 64. Its selection took place in the midterm report [11]. The Ariane 64 was selected on three aspects. First, it features the lowest cost of the options. Second, it can bring the most mass to Martian orbit and third, it has a lower risk than the other suitable options.

Table 17.1: *The Ariane 64 specifications.*

Cost [M€]	Mass in orbit [kg]	Volume [m^3]
115	7000	128.2

Ground station

As explained in Chapter 13, the system will use the DSN. The DSN is a worldwide network of ground stations that supports NASA's interplanetary missions. All facilities are equipped with steerable, high gain antennas and ultra-sensitive receivers. They were designed for deep space tracking. The DSN facilities are:

- Goldstone Deep Space Communication Complex (California)
- Madrid Deep Space Communication Complex
- Canberra Deep Space Communication Complex

Based on previous Mars missions that did use the DSN, namely; Magellan, Mars Global Surveyor, Mars Reconnaissance Orbiter and Mars Odyssey, the DSN is assumed for this design stage to be available for usage. In addition, based on these missions, the DSN is assumed to take around 3.8 % of total misison budget [11, 99].

The spacecraft will transit from Earth orbit to Mars on a Hohmann transfer trajectory. Spinning slowly about its longitudinal axis, it will coast through the cruise phase making any necessary trajectory correction manoeuvres en route. Upon arrival, the spacecraft will perform a capture burn, and subsequently rely on aerobraking to gradually lower the apoapsis to the desired altitude. The spacecraft will then perform a final circularisation burn to arrive in the intended parking orbit. The orbiter will remain in this circular 520km orbit to allow for a communications link with all probes and the DSN for the duration of the mission.

The probes will be detached from the orbiter and individually perform a de-orbit burn manoeuvre. The probes are encapsulated within an aeroshell, which is aerodynamically stable throughout the hypersonic flight. As the spacecraft approaches transonic speeds, the parachute will be deployed to increase its rate of deceleration. At 700m above the surface the propelled landing phase will begin, using 16 retro thrusters. Onboard terminal guidance will select an appropriate landing location, and gently set the probe down on the surface.

The two solar panels on the probe will unfurl and provide power to all subsystems. A communications link will be established with the orbiter, allowing the transmission of telemetry and scientific data to earth. The scientific payload then is deployed to the surface from the underside of the lander. The heat probe will utilise a telescoping tube to guide the initial burrowing process. The seismometer will be lowered from the centre of the probe to the surface, with a protective shield surrounding it from external wind and other environmental disturbances.

After the primary scientific phase is concluded, the probes and orbiter will not be shut down. Both will

continue their planned function of taking seismic measurements, but they can also be used as weather measurement stations. When the orbiter runs out of propellant for station keeping, it will be deorbitted to burn up in the Martian atmosphere. The probes will remain on the Martian surface after they are no longer operable.

17.2. Configuration

Orbiter

The configuration of the orbiter can be seen in Figure 17.1

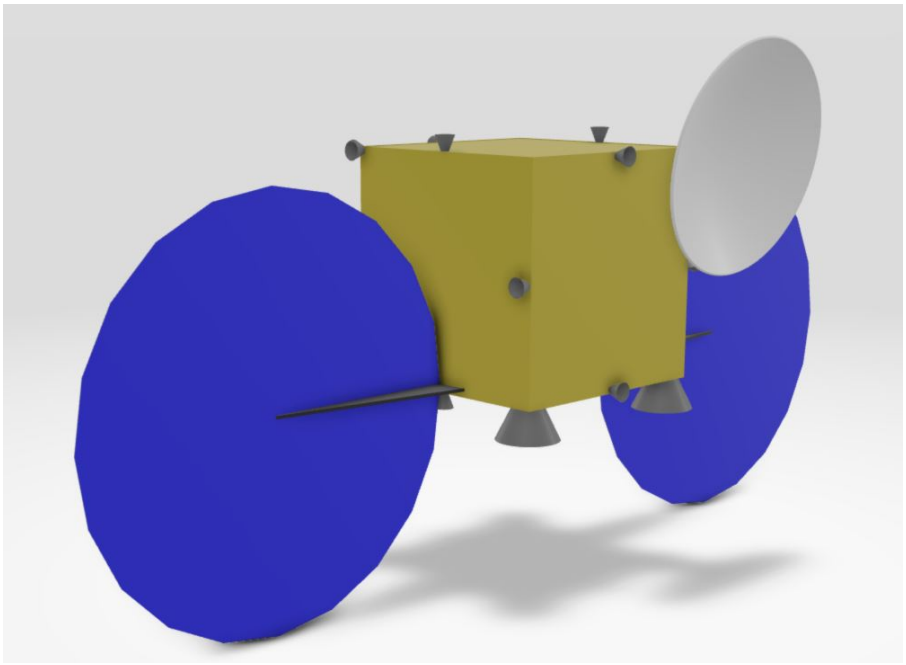

Figure 17.1: *Orbiter configuration with deployed solar panels and gimballed antenna.*

The internal configuration development of the orbiter does not take place in this report. This will be done at the detailed design phase. There are various constraints on the external configuration of the orbiter. First, there was a constraint on the shape of the orbiter coming from the launch vehicle. For the launch vehicle adaptor, a square probe is required. Second, the solar array and antennae are placed on the orbiter. They are placed in such a way that the solar arrays are always sun pointing with a maximum inclination angle of 23.5 °. The antenna is always pointing to the earth. Both the solar arrays and the antenna have a gimbal to allow for rotation. The solar arrays will be deployed as can be seen in Figure 17.5.

Lander

The configuration of the lander can be seen in Figure 17.2 and Figure 17.3.

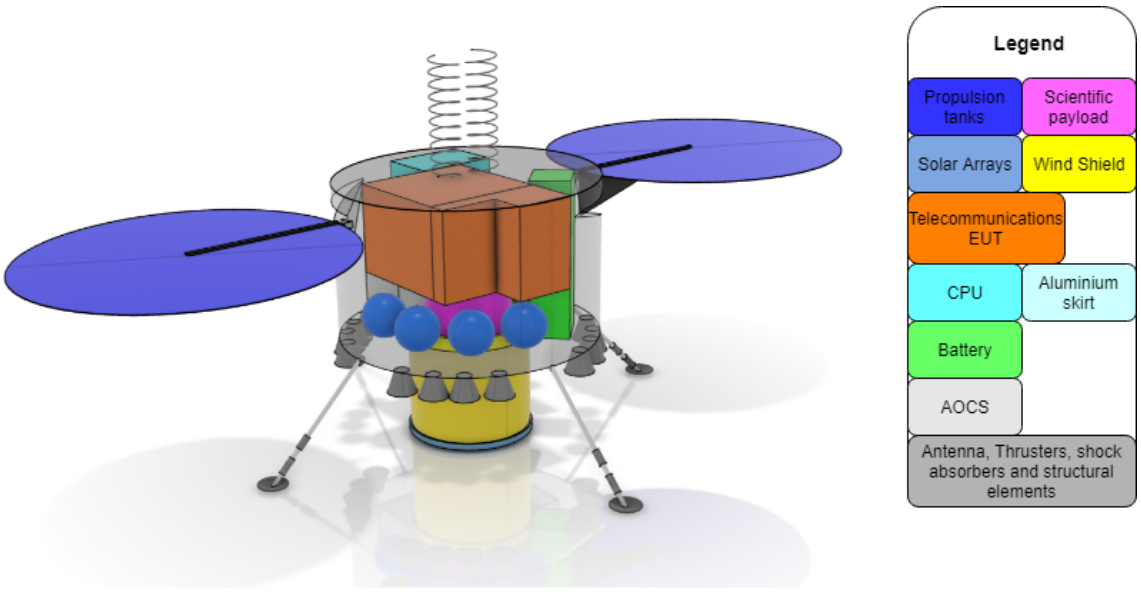

Figure 17.2: *Lander assembly side view.*

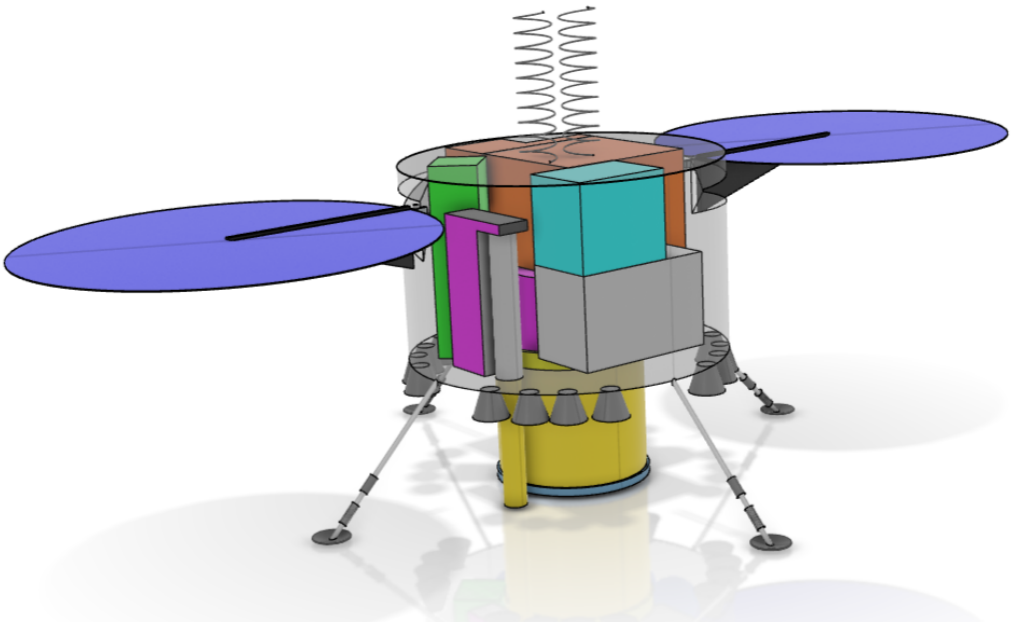

Figure 17.3: *Lander assembly opposite side view.*

The internal and external configuration are determined using constraints from various subsystems. For the internal configuration, there was a constraint on the battery location from the thermal subsystem. The batteries require placement at the centre of the probe for better temperature regulation. All components have dimensions as dictated by the relevant subsystem. They are placed around the battery and configured in such a way as to minimise the volume.

The external structure is a cylinder, this shape is chosen to minimise the volume of the probe. Furthermore, a cylinder also fits more tightly in the entry vehicle. Another constraint from the EDL subsystem is that the probe is required to be made less slender. This increases the ballistic coefficient of the entry vehicle. The resulting entry configuration can be seen in Figure 17.4.

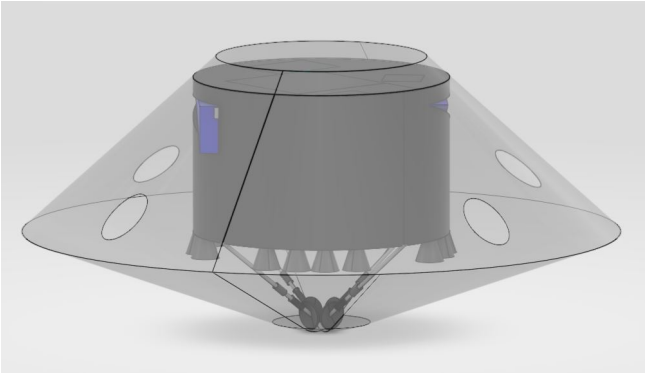

Figure 17.4: *Lander in aeroshell configuration*

The solar arrays are stored partially inside the body. This is done to minimise the volume the solar arrays occupy. The root of the solar array is connected to a hinge which will rotate 90 ° during deployment. After which the solar array will unfold as can be seen in Figure 17.5.

Figure 17.5: *Deployment mechanism of the solar arrays.*

Launch configuration

The launch configuration can be seen in Figure 17.6.

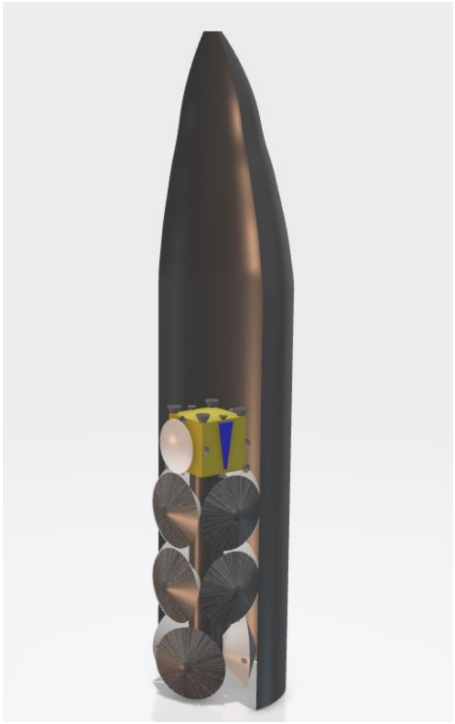

Figure 17.6: *Launch vehicle configuration.*

The orbiter connects to a single large boom. This boom connects to all probes. Four probes are mounted

to each segment of the boom, with an angle of 90 ° between them. Since there are eleven probes the last probes will have an angle of 120 ° between them as can be seen in the figure. The boom will detaches after deployment of all the probes.

System Hardware

The main components of the system and the interactions between them are presented in Figure 17.7. Only the main components were shown, smaller and more specialised components can be found in Chapter 6-Chapter 16.

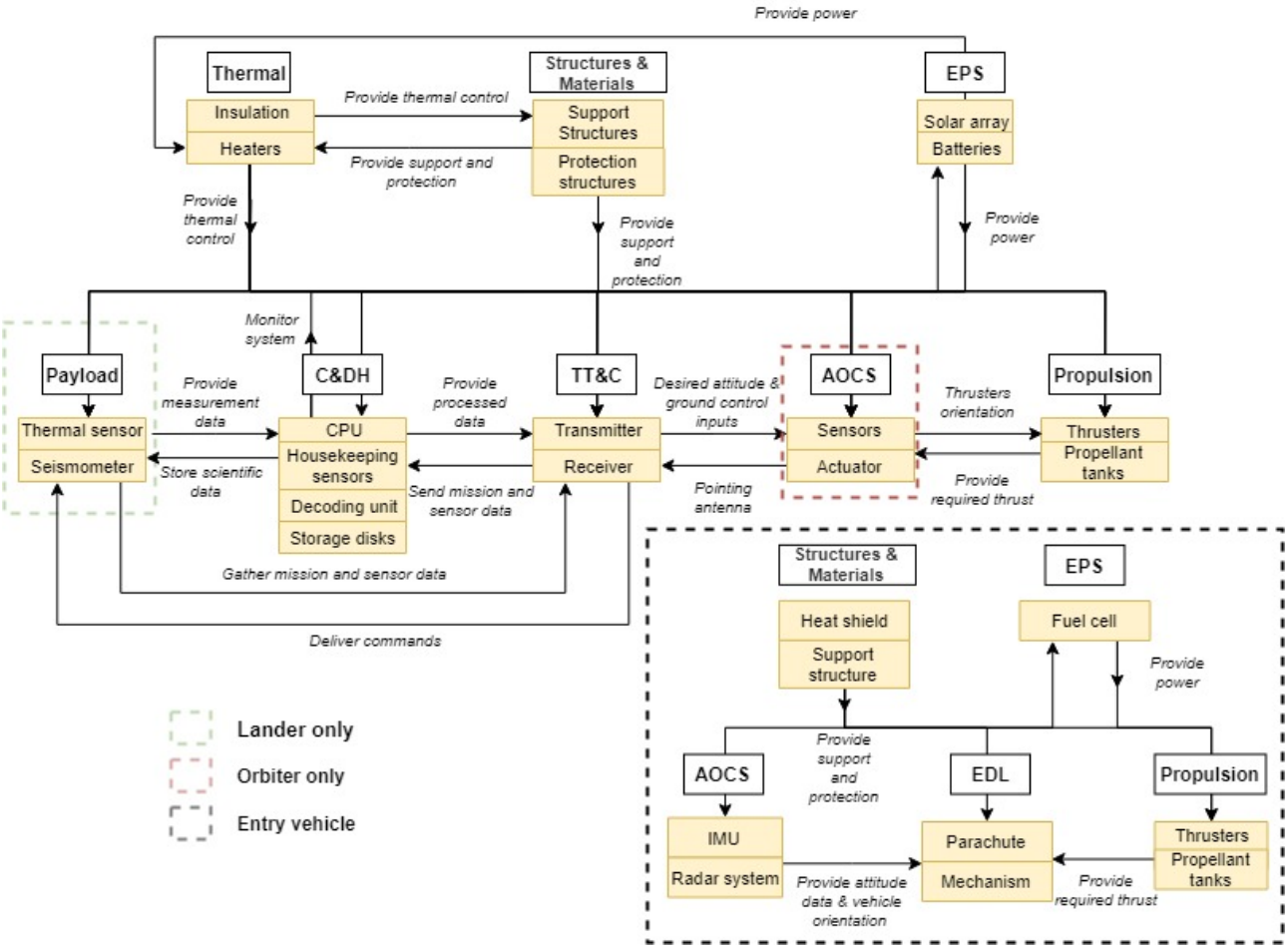

Figure 17.7: *The hardware block diagram.*

System Software

To depict the software of the complete system, a flow diagram is created for the orbiter depicting the flow of internal health monitoring data, scientific data and commands received from the Earth segment. The colour of the arrows in Figure 17.8 marks to what type of data flow the arrow is related. It features only design a complete software diagram for the orbiter, since the lander software diagram would be very similar. An important difference is that the landers will not receive scientific data from the TT&C subsystem, but rather directly from the measuring payload. Moreover, commands -the green-coloured flow- are received from the orbiter, not from Earth directly. The TCP connection is established from the orbiter's initiative, so the landers are 'woken up' by the orbiter first. Finally, the lander needs to convert the obtained scientific data from analogue to digital before it can be processed and eventually sent downlink. In Figure 17.8, thermal HK and health monitoring data are treated separately for clarity purposes. Moreover, to be able to "determine offsets" and "select HK data to be transmitted to Earth" thresholds need to be decided upon in the final design phases. As a final note, "Commanding subsystems" may entail rebooting the entire subsystem or some of its components. Now, to link the required software to the hardware in place, as depicted in Figure 14.1 and Figure 11.3, indicating letters are included in each box containing a software function. These letters indicate the hardware that will have to perform each function. It is important to note that all

connections with both the probes and the Earth segment are initiated by the Time Management Unit and CPU of the orbiter cooperatively. With other words, the three-way handshake as described in chapter 13 always starts at the orbiter.

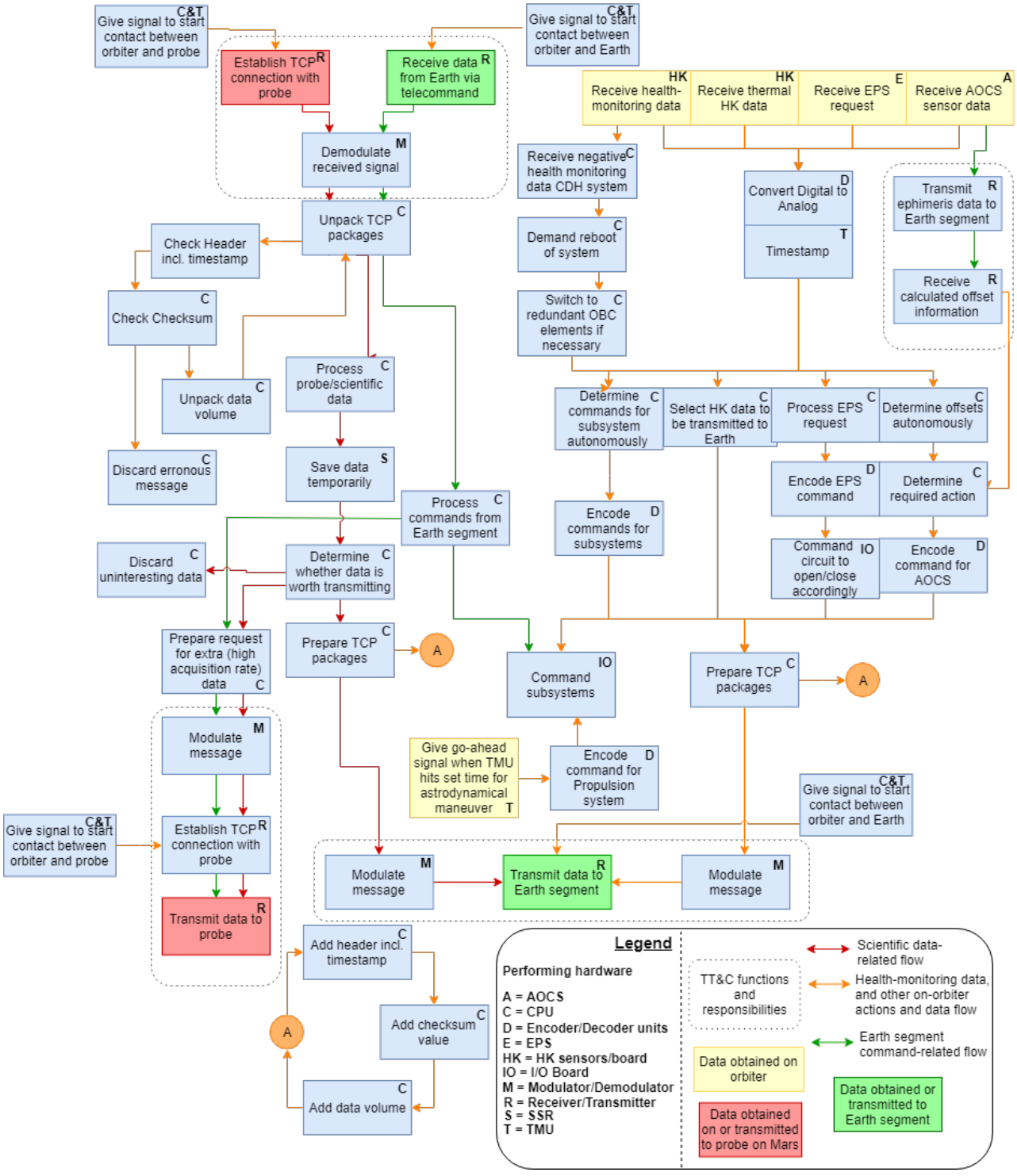

Figure 17.8: *Orbiter Software Diagram, the diagram should be read from top to bottom.*

The dashed boxes indicate functionalities performed by the TT&C subsystem, where the rest are performed by the C&DH subsystem.

17.3. System Characteristics

The main characteristics of the system are given in Table 17.2. The values in between the orbiter and the probe indicate that the value does not apply to a specific system. More detailed characteristics relating to

each subsystem can be found in Chapter 6 to Chapter 16. Moreover, the data rates are the highest possible.

Table 17.2: *Overview of METEOR system characteristics.*

Characteristic (operational phase if unspecified)		Orbiter	Probe	Unit
Exterior Dimensions	Deployed Configuration	6.94 x 2.5 x 3.17	3.16 x 0.53 x 1.30	m (L x W x H)
Mass	Total (@ launch)	3112.1	211.5	kg
	Total (operational)	418.1	145.3	kg
	Propellant (@ launch)	2180.0	15.7	kg
	Propulsion	126.3	38.8	kg
	CD&H	6.5	6.6	kg
	TT&C	85.8	23.1	kg
	AOCS	54.5	15.3	kg
	EPS	72.7	30.0	kg
	Thermal	21.8	4.4	kg
	Structures	50.5	13.4	kg
	Probe Mount Structure	514.0	-	kg
	Scientific Payload	-	18.8	kg
	EDL	-	45.4	kg
Electrical Power	Solar Array Radius	1.12	0.9	m
	Power Generated	681.5	179.8	W
	Storage Capacity	194.3	194.3	Wh
Data Rates	Probe → Orbiter	30		kbps
	Orbiter → Probe	8		kbps
	Orbiter → DSN	24		kbps
	DSN → Orbiter	4		kbps
Operations	Mission Lifetime	5		years
	Final Orbiter Altitude	520		km
	Total Number of Probes	11		-
Probe Coverage of Mars Surface (magnitude 3.0 - 3.1)	No coverage	9.8		%
	≥ 1 probe	90.2		%
	≥ 2 probe	81.9		%
	≥ 3 probes	70.3		%
	≥ 4 probes	31.8		%
	≥ 5 probes	0.8		%

17.4. Cost estimation

The cost budget is presented in this subsection. A cost budget is estimated for each subsystem. This budget is divided into two categories, non-recurring and recurring cost. The non-recurring cost includes all the costs related to the research and development of the subsystem, namely, costs related to design, drafting, engineering unit, ground support equipment and a portion of the program management and the systems engineering cost. On the other hand, the recurring cost includes the costs associated with flight hardware manufacturing, part of the program management and the systems engineering cost, and finally integration, assembly and testing (AI&T). The non-recurring cost is also referred to as RDT&E (research, development, testing and evaluation) and the recurring cost is referred to as TFU (theoretical first unit). Using [23], Table 17.3 shows the budget for each subsystem for both the lander and the orbiters. Furthermore, there are some additional costs that are defined as follows [23]:

- AI&T (Assembly, Integration and Testing) cost: refers to labor and material costs for integrating the spacecraft subsystems and the payload into an operational space vehicle.
- Program level: refers to costs for system engineering, program management, planning, quality assurance, and the costs that can not be assigned to an individual subsystem.
- GSE (Ground Support Equipment) cost: refers to costs of test and support equipment that is needed for assembly, development and testing. This equipment are also used for the integration of spacecraft subsystems and the spacecraft to the launch vehicle.
- LOOS (Launch and Orbital Operations Support) cost: refers to cost of planning and operations related to the launch and orbital checkout of the space system.

The cost of TT&C and C&DH can be obtained separately using 0.45/0.55 split [23].

Table 17.3: *Estimated cost of the system.*

Cost component	RDT&E [M€]	TFU [M€]
1. Payload	0.000	0.500
2. Probe	29.322	13.249
2.1 Structure	1.825	0.237
2.2 Thermal	5.974	1.010
2.3 EPS	2.529	2.016
2.4 TT&C and C&DH	10.367	5.864
2.5 AOCS	8.256	3.987
2.6 Propulsion	0.372	0.136
3. Orbiter	96.438	34.820
3.1 Structure	40.578	9.941
3.2 Thermal	3.749	0.601
3.3 EPS	6.132	3.962
3.4 TT&C and C&DH	25.103	11.156
3.5 AOCS	19.975	8.801
3.6 Propulsion	0.9020	0.358
4. AI&T	9.805	39.805
5. Program level	5.027	127.209
6. GSE	0.775	0.000
7. LOOS	0.000	18.754
8. LV	0.000	0.000
Total	141.367	371.827
Combined total	513.194	

For the final estimated cost, a reduction based on use of heritage and already existing components and a reduction based on the learning curve is applied. The factors are 0.8 for the heritage as the mission is redesigning major components of an already existing mission, InSight [23]. The learning curve slope is 95 % for the probe components [23], meaning that the average cost of a unit is 95% of the first unit cost. The heritage factor is applied to the RDT&E costs, while the learning curve factor is applied to the TFU costs, and hence the manufacture cost. The result of this is shown in Table 17.4.

Table 17.4: *Estimated cost of the system with reducing factors.*

Cost estimate without reduction [M€]	Cost with heritage reduction factor [M€]	Cost with learning curve reduction factor [M€]	Final cost estimate [M€]
513.2	467.8	479.4	439.6

18 Performance Analysis

This performance assessment explores system successfulness in preforming the primary functions. It also checks the compliance of all requirements not covered by the subsystems. Finally, the life cycle of the system is assessed.

18.1. Performance assessment of primary functions

The METEOR mission is designed with the following four main functionalities in mind.

1. Provide global seismic & thermal measurements
2. Land the eleven probes on the allocated Martian surface
3. Retrieve the scientific data
4. Maintain the system for a minimum duration of the mission design life

The abovementioned system functionalities are assessed once the conceptual design has been drafted.

Global seismic network

The conceptual design features a global seismic and thermal network covering the entire Martian surface with at least three or four probes (depending on the magnitude of the Marsquake). The network is capable of detecting quakes with magnitudes of 3.0 with a probability of detection of 0.70257. As Marsquake magnitudes increase, the probability of detection increases too, for a magnitude of 3.2 the probability reaches 0.99956. The seismic system does not have an upper limit on Marsquake magnitudes and as magnitudes exceed 3.5 there is a 100% certainty it will be detected.

EDL estimations require a landing ellipse with semi-major axis of 100km. However, the chosen landing sites are circles with a 100km radius to ease the selection procedure. The landing sites of the probes is determined by taking into account multiple surface aspects that would prohibit the probe to operate. Previous surface missions are avoided by at least a radius of 100 km. Dust coverage of all landing sites is identified lower than the dust cover index threshold of 0.94. In addition to the dust constraints, the minimum depth of fragmented regolith was accounted for by excluding any landing site with less than 3m depth of fragmented regolith which has a thermal inertia value lower than 140 $\mathrm{J\,m^{-2}K^{-1}s^{-1/2}}$. Furthermore, the landing sites have a rock abundance of at most 10%. The maximum landing altitude, driven by EDL constraints, is 2700m. Additionally, the landing sites have both north and south latitudes lower than 40 °. Lastly, the slope of the landing site is lower than 15°. The landing site allocations is chosen from the remaining options as to maximise the coverage of the seismic network.

Landing probes

The manoeuvre to land probes on the Martian surface is similar between all probes, except for the final landing phase due to the variation in altitude of the landing sites (-3920m to +2700m). The descent is initiated by a solid rocket motor which provides 25 m/s lowering the periapsis from the 440km altitude circular orbit to 100km. At this entry altitude, the probe is decelerated using the aeroshell. At 22.7 km altitude, the parachute deploy. The thrusters then initiate propulsive landing at an altitude of 4km. The number of thrusters used for this operation varies between sixteen and four depending on the landing site altitude.

Retrieving data

The METEOR mission will produce 1282.9 bps of data per probe throughout the scientific phase of the mission. This data contains both scientific and housekeeping data and requires to be transmitted back to Earth. The transmission occurs via TCP modulated on a UHF carrier at 390MHz uplink and 435 MHz downlink centre frequencies. This carrier is received by the orbiter at a maximum rate of 30 kbps for a duration of 4900 sec per sol. Per probe 146.8 Mbit/sol are transmitted to the orbiter, which collects the data and relays it back to Earth when it is in view. This is done over X-band (at 7.6 GHz uplink and 8.4 GHz downlink frequencies) and will be received by the DSN at a max rate of 24 kbps, transferring 1.77 Gbit per

sol.

Maintenance aspects
The METEOR mission features several maintenance aspects that play a role in the design. Higher maintenance capabilities are expected to prolong the mission duration past its design life. Conservative estimates are made in the AOCS and orbit design concerning ΔV budget. 300 m/s of ΔV are allocated to counteract perturbations from the moons and other celestial bodies and for orbital manoeuvres. These manoeuvres include reaction wheel desaturation.

Furthermore, the probes feature an EPS fitted with a battery capacity of 194.31 Wh to account for power consumption during night time (14.6 hr). This is replenished by a pair of circular solar arrays with a combined area of 6.03 m^2. These arrays also provide the consumed power during day time (9.9 hr).

18.2. Requirements compliance
The compliance of most of the requirements imposed on the system is determined in the chapters presenting the subsystems. However, some of the requirements of the system do not fall under a specific subsystem. These are evaluated in this section. An overview of the compliance with the system requirements is given in Table 18.1.

Stakeholder requirements
The stakeholder requirements are partly discussed in the respective subsystems but will be repeated here.

MR-TL–01: DELETED
MR-TL–02: Heat flow measurements made by the system shall have an accuracy of 1 mW/m^2.
MR-TL–03: The system shall consist of at least 2 probes per terrain: Northern Plains, Southern Highlands, Tharsis Complex, outflow region of Valley Marineris and Hellas Basin.
MR-TL–04: The system shall have a mission life of 5 years including transfer and descent, of which 3 years in scientific phase.
MR-TL–05: The system shall avoid current and planned landing sites by 100 km.
MR-TL–06: The system shall comply with international space laws.
MR-TL–07: For the system an Earth-based microbe contamination reduction strategy shall be developed.
MR-TL–08: The system shall not use RTGs as power source.
MR-TL–09: The system communication system of surface and/or orbital elements shall be compliant with the DSN system.
MR-TL–10: The system shall be viable for a proposal to M-class missions of the European Space Agency.

MR-TL–11: The mission shall be compliant with European Space Agency mission policies.
MR-TL–12: The mission shall be able to be submitted to the European Space Agency call for M-class mission proposals of 2025.
MR-TL–13: The system shall have a sensitivity of 60% of the Insight SEIS system when measuring Marsquakes.

As discussed in Chapter 7, the required accuracy for the heat flow measurements is achieved. Furthermore, as mentioned in Chapter 6, every required region is covered by at least 3 probes, while current and planned landing sites are avoided by at least 100 km. The system complies with international space laws as defined by the United Nations Office for Outer Space Affairs (UNOOSA) [100]. However, it is advised to check this also at later design steps. The microbe contamination reduction strategy was introduced in the requirement and concept generation phase of the mission [13], and will be discussed further in Chapter 3 and Chapter 21. This requirement is met. As discussed in section 21.2, the planned mission lifetime is 5 years, including 3.81 years of Primary Scientific Phase, which meets **MR-TL–04**. In Chapter 15 it is mentioned the system uses solar arrays to generate power. Therefore, no RTGs are used as a power source. The telecommunications subsystem communicates with earth using the DSN, meeting requirement **MR-TL–09**. The last three requirements are met as requirement **MR-TL–12** implies that **MR-TL–10** and **MR-TL–11** are met as well. This requirement is met since the design is within the specified boundary conditions. Namely, the cost of the

design is estimated at 439.6 M£ as will be shown in section 17.4, while the proposed time from mission proposal until launch is seven years. This is within the allowed eight years as specified by ESA. Furthermore, the TLR of all used components is expected to be 6 by 2030.

Market and legal requirements

The market requirements and legal requirements are shown here and briefly discussed.

MR-MRT–01: The mission shall cost no more than 550 Million €.
MR-MRT–02: The system shall launch on an Ariane 5, Ariane 6, Vega, Vega C or Soyuz Rocket.

MR-LGL–01: The mission shall not be used to lay claim on Mars.
MR-LGL–02: The mission shall not place weapons of mass destruction in space.
MR-LGL–03: The mission shall make all its orbit known to the UN.
MR-LGL–04: The mission shall assist any manned missions in need.

The market requirements are met as the estimated cost of the mission is 439.6 M£ and the system will launch on an Ariane 64.

The legal requirements are met as well. No claim will be laid on Mars and no weapons of mass destruction are to be placed in space. Moreover, the mission will make all of its orbits known to the UN and if possible assist manned missions in need.

Planetary Protection requirements

The Planetary Protection requirements set in earlier stages[13], are found below. These requirements can be confirmed now that the category to which the METEOR mission belongs can be confirmed. First of all, the landing sites do not include any critical regions such as the poles - the latitude of the landing sites is limited to 40° above and below the equator. Secondly, the maximum depth of the HP^3 instrument is limited to 5 m. These two design choices lead to a classification of the METEOR mission into category IVa as set by COSPAR.

MR-PPR–01: The spacecraft shall be assembled in a cleanroom of class 100000.
MR-PPR–02: The spacecraft shall be tested in a cleanroom of class 100000.
MR-PPR–03: The probability of crash on Mars for an orbiter or an orbiter system shall be <0.01 for the first 20 years of the mission.
MR-PPR–04: The ground segment(s) shall be restricted to an average bioburden level of $\leq 300\,\mathrm{m}^{-2}$.
MR-PPR–05: The ground segment(s) shall be restricted to a surface bioburden level of $\leq 3 \times 10^5$ spores for every ground segment.
MR-PPR–06: Any other equipment of the lander system whose entry into the Martian atmosphere is not planned shall have a probability of crash $< 10^{-4}$.
MR-PPR–07: Equipment able to transfer life to Mars shall be sterilised.
MR-PPR–08: Other equipment that is part of the probe that will crash on Mars separately shall be decontaminated both on its surfaces and inside until a maximum level of 5×10^5 bacterial spores per system is met. **Replaced**
MR-PPR–09: The final surface bio-contamination result shall be obtained by performing 5 sample tests per square meter of exposed lander surface, each on $25\,\mathrm{cm}^2$.
MR-PPR–10: The heat shield shall be decontaminated both on its surfaces and inside until a maximum level of 5×10^5 bacterial spores per system is met. **Added**
MR-PPR–11: The back shell shall be decontaminated both on its surfaces and inside until a maximum level of 5×10^5 bacterial spores per system is met.**Added**
MR-PPR–12: The parachute shall be decontaminated both on its surfaces and inside until a maximum level of 5×10^5 bacterial spores per system is met.**Added**
MR-PPR–13: Other equipment that is part of the probe that will crash on Mars separately shall be decontaminated both on its surfaces and inside until a maximum level of 5×10^5 bacterial spores per system is met.**Added**

Most planetary protection requirements are met by assembling and testing the system in a cleanroom of class 100000 while confirming the required bioburden using sample tests. The METEOR mission its orbiter

has a negligible probability of crash on Mars of the orbiter system in the first 20 years upon arrival. If the orbiter an uncontrollable state its orbit would decay by about 9.5 m/s (the amount of scheduled maintenance ΔV). Note that this decay is assumed constant through most of the decay period, only if the altitude drops below a 100 km threshold the decay significantly varies. At this constant rate, it would take 20.4 years to sufficiently lower the orbital velocity from 3.5 to 3.3 km/s leading to a crash into Mars. Therefore the orbiter is designed to meet the planetary protection requirement.

Other requirements

MR-LSS–01: Weather conditions at all landing sites shall be measured at all times during probe descent.

MR-TRL–01: The system shall not be composed of any technology below TRL 6 in the year 2030 based on ESA standards.

MR-SR–01: The System Space Segment shall not exceed the Ariane 64 fairing usable volume limit for single spacecraft launch.

Measuring the weather conditions at all landing sites during probe descent will be done by the orbiter. The specific sensors for this have not been chosen, however, there is mass, power and volume available for the instruments on the orbiter. As mentioned before, the TRL of all technology is 6 or higher, as defined by the ECSS standards [101]. Furthermore, the volume of the system in launch configuration does not exceed the Ariane 64 fairing usable volume.

Table 18.1: *Compliance matrix of system requirements.*

Requirement ID	Met / Not met / TBD	Justification
MR-TL–02	Met	
MR-TL–03	Met	
MR-TL–04	Met	
MR-TL–05	Met	
MR-TL–06	Met	
MR-TL–07	Met	
MR-TL–08	Met	
MR-TL–09	Met	
MR-TL–10	Met	
MR-TL–11	Met	
MR-TL–12	Met	
MR-TL–13	Met	
MR-MRT–01	Met	
MR-MRT–02	Met	
MR-LGL–01	Met	
MR-LGL–02	Met	
MR-LGL–03	Met	
MR-LGL–04	Met	
MR-SR–01	Met	
MR-PPR–01	Met	
MR-PPR–02	Met	
MR-PPR–03	Met	Decay rate of the orbit without maintenance suggests crashing into the planet after 20.4 years
MR-PPR–04	Met	
MR-PPR–05	Met	
MR-PPR–06	Met	
MR-PPR–07	Met	
MR-PPR–09	Met	
MR-PPR–10	Met	
MR-PPR–11	Met	
MR-PPR–12	Met	
MR-PPR–13	Met	
MR-LSS–01	Met	

18.3. Mission life cycle

The METEOR mission features several phases within its operational lifetime. The design of this mission is mainly focused on the scientific phase (with a duration of 3 years). Figure 18.1 shows the different phases present in the mission along with some aspects specific to the presented phases. Most of these aspects have been covered in section 18.1.

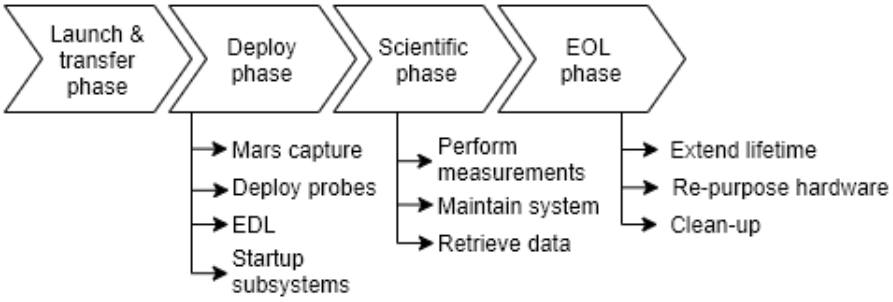

Figure 18.1: *The METEOR mission life cycle.*

The mission life cycle consists of the four main phases: launch & transfer, deployment, scientific and the EOL phase. The last three, feature notable events that take place for that specific phase. In case of the EOL phase, the events are optional as to suit the need of the operator at the end of the mission design life. As mentioned in section 18.1 there is a large contingency in the ΔV budget, therefore a mission lifetime extension can be similar to the Cassini mission [102, p.725-p.744].

Re-purposing the hardware is another option. One option would be to use the orbiter as a communication platform for future missions. At the end of the mission, both the orbiter and the probes will still be highly valuable assets. The former as a communications relay, and the latter as global weather stations.

Lastly, the system can be disposed of in a way that impacts sustainability to a minimum level.

19 Sensitivity Analysis

To identify which subsystem design is most sensitive to changes in input, a normalised sensitivity analysis is performed. This process compares the percent change in result with the percent change in primary input variable. The resulting value is normalised to make them non dimensional. Using these normalised values allows the relative sensitivities of different subsystems to be compared directly [103].

19.1. Method

The process is conducted in the following manner. First, for each subsystem, the main input(s) and output(s) are defined. These are selected on basis of which inputs have the greatest effect on the design, as most of the minor inputs do not have a significant effect; exhaustively testing all inputs is also infeasible at this design stage. Each respective subsystem engineer is consulted to ensure that the in- and outputs are defined correctly. The input values used in the current design are recorded as nominal values. To measure the sensitivity of the result with respect to the input variable, the input variables are changed by 10%. This percentage was chosen because it roughly estimates the changes between design iterations. Also, 10% is a rather large change, the consequence of this is that if the design is still viable after a 10% increase, the design is robust.

For each subsystem, the percentage change in the main output is recorded. By dividing the input variable percent change by the output variable percent change, the sensitivity is obtained. Because the sensitivity can be both positive and negative, the absolute value is taken. This process is shown in (19.1).

$$\Upsilon = \left| \frac{\left(\frac{\zeta_2 - \zeta_1}{\zeta_1}\right)}{\left(\frac{\kappa_2 - \kappa_1}{\kappa_1}\right)} \right| \tag{19.1}$$

Here, κ is the main input variable for the subsystem design, ζ is the main output of the subsystem design, and Υ is the sensitivity. The subscripts denote whether the original (ζ_1) or the 10% change value (ζ_2) is used.

If the output does not change at all, the sensitivity is 0. This method ensures that when the percentage change of the output is less than 10%, the sensitivity has a value between 0 and 1. For sensitivity values larger than 1, the percentage change of the output is larger than the percentage change of the input. This means that the output is very sensitive with respect to the input.

19.2. Results

Table 19.1 shows the results of the sensitivity analysis. It is clear that some changes do not influence the design at all, for example the Signal-to-Noise-Ratio does not change when the data generation rate is changed. Moreover, it is apparent that some subsystems are more sensitive than others. The Electrical Power Subsystem is quite sensitive to changes in the input variables, with a sensitivity of 2.21 for the lander solar array area, while the thermal subsystem is less sensitive, with a sensitivity of 0.28 and 0.36.

From the sensitivity analysis, it is concluded that if subsystems have a sensitivity value between 0 and 1, they have a robust design. Changes in the input variables have a diminished impact on the design. The subsystems with sensitivity values larger than 1 are sensitive. A change in the input variables will have large repercussions for the design. It is paramount that these input variables are determined precisely and accurately at the start of the design process and iteration cycle.

Table 19.1: *Sensitivity analysis results.*

Subsystem	**Main Input Variables (κ)**	**Main Output Variables (ζ)**	**Sensitivity (Υ)**
Propulsion	Delta V	Mass	0.76
AOCS	Total spacecraft mass	Mass	0.00
TTC	Data generation rate	Contact time	0.81
		SNR	0.00
CDH	Data rates	Processing power	0.98
		Mass memory storage	0.98
EPS (lander)	Latitude, Average power	Solar array area	2.21
		Battery capacity	0.00
EPS (orbiter)	Altitude, Average power	Solar array area	0.83
		Battery capacity	0.00
EDL	Entry velocity, Flight path angle	Max deceleration	3.29
		Max heat flux	3.88
Thermal	Available power	Min temp	0.38
		Max temp	0.26
Structures (probe)	Radius, Height, Thickness	Mass	3.31
		Max stress	0.00
		Natural frequency	0.49
Structures (orbiter)	Length, Width, Height, Thickness	Mass	3.31
		Max stress	2.23
		Natural frequency	0.49
Astro	Communication contact time	Altitude	1.40

It is clear from Table 19.1 that most parameters have a robust design. Those parameters with a sensitivity greater than 1 have an increased risk of not meeting their respective design requirements. These requirements are identified in Table 19.2. It should be noted that while the sensitivity is high, a red colour does not directly indicate that the requirement will not be met.

Table 19.2: *Most sensitive requirements*

System	Output variable	Sensitivity	Requirement
EPS lander	Solar array area	2.21	**MR-EPS-01-LDR**
EDL	Max deceleration	3.29	**MR-STRCT-03**
EDL	Max heat flux	3.88	**MR-STRCT-03**
Structures (probe)	Mass	3.31	**MR-STRCT-01-02**
Structures (orbiter)	Mass	3.31	**MR-STRCT-01-02**
	Max stress	2.23	**MR-STRCT-07**
Astro	Altitude	1.40	**MR-ASTR-01**

Because these requirements will be impacted the most by a small change in the design, they will be added as additional driving requirements for the next design iteration. Following the determination of improved design results, this sensitivity analysis will be performed again, and new driving requirements will be identified. This iterative process will ensure that the final design will remain robust, guaranteeing all requirements are met.

20 RAMS

The RAMS analysis is the main part of the dependability study featured in the conceptual design phase. It consists of three main parts, namely, assessing safety critical functionalities, evaluating reliability & redundancy and assessing the system with regard to availability & maintainability.

20.1. Safety critical functionality

The METEOR mission features two types of safety. First is the safety considering the interaction of the system with the construction crew. During development, construction and testing, the crews safety is of vital importance. The system design features several potential hazardous aspects in this regard. An example of this is the handling of hypergolic fuel in all probes. Similar to this, all probes are fitted with a solid rocket motor intended to deorbit the probes upon deployment. Special attention is required in planning the order of operations to minimise these potential hazards.

Another safety type to consider, is the safety of the system and its environment throughout the mission. For instance the safety of other missions is to be guaranteed by landing 100 km away from other landing sites as a minimum required by **MR-TL-05**. Below one finds a list of other safety critical functionalities in this regard.

- **Deorbiting probes**: Mars features several satellites both natural and artificial, the deorbiting procedure primarily focuses on landing the probes on the desired landing site. However, the safety precautions on the surface (landing 100 km away from other mission) equally applies for orbiting missions.
- **Landing probes**: The system requires 11 landings to be performed on a substantial part of Mars. The landing capability is safety critical as failure might impact the Martian environment. Deorbiting a single probe at the time reduced this as the software supports maintenance before deploying the next one.
- **Deorbiting the orbiter at EOL**: Similar to the deorbit procedure of the probes the orbiter deorbit at EOL will have to ensure the safety of other missions both in orbit as on the surface.
- **Shutting down probes at EOL**: As mentioned before, the probes contain potentially hazardous chemicals that affects the surrounding. This is especially the case at the EOL of the probes, the design is made such that safety is ensured even if it is not actively maintained. This is achieved through venting the oxidiser in very small quantities upon landing.

20.2. Redundancy & reliability

Reliability in the case of the METEOR system is defined as the probability of mission success at EOL. The need for reliability originates from the very costly and limited resources available to maintain the spacecraft hardware post-launch. The design featured in this conceptual design phase aims to maximise the system reliability, redundancy is used regularly as a mean to ensure this. Throughout the design, two types of redundancy have been employed, namely hot and cold redundancy [81].

Critical subsystems for which subsystem failure results in mission loss, such as TT&C , EDL and C&DH feature this redundancy for which there is no down-time as the subsystem architectures feature parallel components that are activated instantly. As an example, the TT&C system features parallel TWTAs that are used in case the other fails. Section 13.4 goes in more detail regarding this aspect. Similarly, the propulsion subsystem features several tanks in series, such that a rupture in one tank does not lead to complete failure.

Cold redundancy features redundancy measures that are not in operational mode when the operational hardware fails. Therefore, there is down-time associated with this redundancy, this down-time however is very limited (≈10-60 sec). Cold redundancy is found in, for example, the AOCS which has a redundant reaction wheel that is activated when one other fails to resume the AOCS its functionalities.

Reliability is directly related to the level of redundancy in each subsystem. The reliability estimates in the

conceptual design phase are considered rough, also the inter subsystem dependability is not yet explored. Therefore, the reliability of the entire system is not accurately established using the classical means of multiplying the individual reliabilities.

20.3. Maintainability

The maintainability is defined for both hardware and software. Maintenance of hardware is unrealistic in case of the METEOR mission as expressed before. Thus, this dependability parameter is mostly set by the designed margins in the design and the software update capabilities. Note that the maintainability aspect in the dependability study is only assessed for the scientific phase of the mission and possible extensions after the nominal mission duration.

As mentioned in Chapter 10, the orbiter is sized with 300 m/s ΔV budget for correcting manoeuvres. This enables the orbiter to maintain the designed orbit to provide the intended functionalities. Maintainability aspects are observed in the TT&C HGA assembly. It features a gimbal system to be able to maintain the appropriate pointing towards Earth. Similarly the AOCS features procedures to desaturate its reaction wheels. These features thereby also assist in counteracting ageing effects on hardware.

The aforementioned maintainability aspects will be executed autonomously, whereas, the software maintainability will have to be scheduled in great detail. Updates will enable correction of non-critical software featuring unanticipated errors. Also, it redefines the system its behaviour. However, the updates requires a peak in human resources. The update is limited by transmission windows and DSN availability. Furthermore, the implementation of the software on the system side will induce down-time which will have to occur in several phases maintain critical functionalities.

20.4. System availability

Two of the previously mentioned aspects, namely reliability and maintainability, impact the system availability. In this conceptual design phase, availability is defined by the time the system is able to perform its scientific measurements compared to the total time the system spends in the scientific mission phase. Time not spend on performing measurements is referred to as down-time (20.1). For which, A is the system availability and T_{up} and T_{down} refer to the up-time and down-time respectively. The down-time is affected by the design choices made in regard of the aforementioned dependability characteristics.

$$A = \frac{T_{up}}{T_{up} + T_{down}} \tag{20.1}$$

Redundancy significantly affects the system availability by reducing the down-time with backup components present. Though the availability hugely benefits from a high degree of redundancy it comes at a mass penalty. When comparing hot and cold redundancy, it is observed that hot redundancy has less down-time than cold redundancy and therefore hot redundancy provides higher system availability though this comes at penalty in terms of power need as two components have to be kept in operational conditions at all times.

Availability of the system is impacted by maintainability. With as low maintenance time as possible the down-time will be kept to a minimum. Nonetheless, the system is designed to have the maintenance capability as a contingency measure against unanticipated changes to. Having the system consist of eleven probes and an orbiter also provides the capability of phasing the maintenance such that the system is never fully disengaged from the science in down-time. Also, the level of automation in maintenance procedures increases the system its availability.

In addition to these dependability aspects, there are external factors impacting the system's availability. Mainly the availability of the DSN is limiting. Furthermore, throughout the mission duration at least two solar conjunctions will occur, in these periods of about nine days the RF signals are blocked by the sun. The memory systems in the probes are suitable to store the data generation up till 30 sol, the orbiter in turn stores data up till fourteen Earth days. Therefore no additional downtime is to be expected form the solar conjunction.

21 Post Conceptual Design Development

This chapter focuses on planning future steps of this project after the conceptual design phase.

21.1. Project design and development logic

NASA has as objective to send humans to Mars by the 2030s[1], this provides an estimate on the desired development time for the METEOR mission.

Considering a human Mars mission can still be launched in 2037 to fulfil NASAs' objective and METEOR having a mission time of 5 years, launching the mission in 2031 would be sufficient to provide the scientific findings a human mission would require. The importance of completing the METEOR mission in this timeframe is that the information it will provide might prove to be critical in selecting landing sites for manned Mars missions. This is why the launch window in February 2031[2] has been selected for this mission.

The time until launch is therefore 11 years yet the Insight mission went from preliminary design to launch in only seven years[3]. This is achieved by using an existing lander platform which reduced development time. METEOR has three extra years available for development. METEOR mostly makes use of technologies used in other space missions which drives development time down. However, the novelty of the mission and the redesign of the heat flux probe may drive development time back up. Therefore the three extra years have been assigned to Phase B of the process to account for possible delays in development.

To make sure that subsystem technologies are ready for launch, the **MR-TRL-01** [13] requirement is defined to make sure all technologies used in the 2031 launch are at least TRL 6 by the year 2030. Therefore, the development of the METEOR mission will be in-line with the timeline presented in Figure 21.1. This timeline is shown in greater detail in the Gantt chart in Figure D.1.

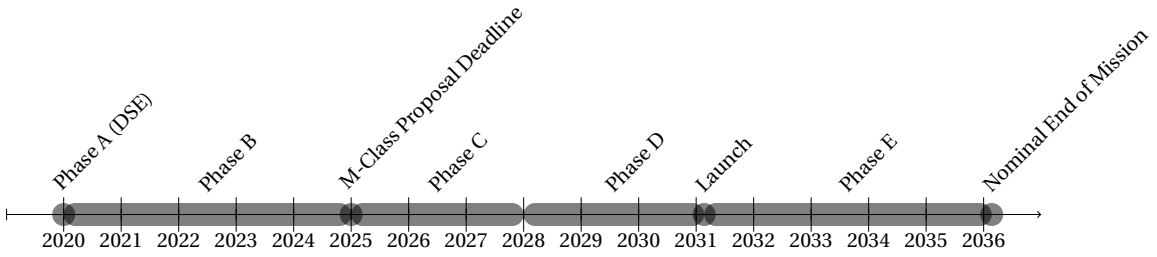

Figure 21.1: *Project timeline after DSE*

Phase A : Feasibility

Based on ESA standards, Phase A investigates the feasibility of a mission. This phase will be covered by the DSE.

Phase B : Preliminary definition

Phase B mainly consists of a detailed design phase where the subsystems and instruments designs are defined. In this design phase, the driving requirements are reidentified based on the sensitivity analysis in Chapter 19. For METEOR, this design phase consists of a detailed design of the landing segment, orbital segment and all other supporting structures. Development time for the scientific payload varies per instrument. The seismometer technology will be reused from the Insight mission and will, therefore, require minimal development time. Development time for the heat flux probe entirely depends on the success of

[1] `https://www.nasa.gov/content/nasas-journey-to-mars`, retrieved 15/05/2020
[2] `http://clowder.net/hop/railroad/EMa.htm`, retrieved 16/06/2020
[3] `www.seis-insight.eu/en/public-2/the-insight-mission/calendar`, retrieved 04/05/2020

the HP[3] probe on the Insight mission and the lessons learned from it. In the worst-case scenario where the instrument needs to be fully redesigned, the allocated five years for Phase B will be sufficient for this.

Phase C : Detailed definition

During Phase C, several models of the system are built to perform tests. These are the Structural and Thermal Model (STM) and the Engineering Model (EM). The STM will be used for tests that replicate for example the launch loads. The EM will be used mainly to make sure all the subsystems work together.

Towards the end of this phase, a Qualification Model (QM) can be built for environmental testing which tests the spacecraft in all possible environmental conditions. For METEOR this requires tests to be made in the vacuum of space as well as simulated Martian environments. Phase C ends with a critical design review.

Phase D : Qualification and production

Phase D includes the production of the Flight Model (FM) which will be used for the mission. Final tests are performed, these include testing that all generated electric signals are received by the appropriate systems, software testing, navigation testing and pointing testing.

Location of the manufacturing process cannot be determined yet as ESA works with a geographical return[4] system that awards manufacturing contracts depending on the funding provided by a member state.

Phase D will conclude with a flight acceptance review which the system needs to pass before it is delivered to the launch site.

Phase E : Launch and operations

An overview of this phase is detailed in Figure 21.2.

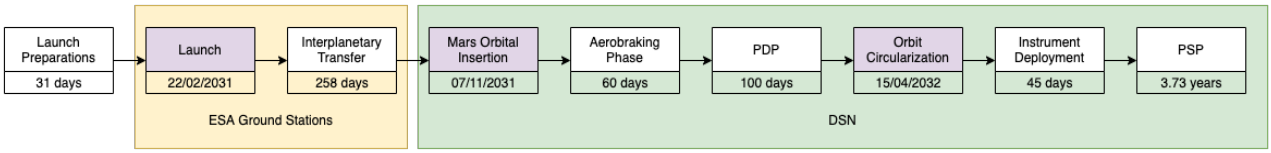

Figure 21.2: *Phase E: Launch and operations (colours indicate ground station used)*

Collaboration

The success of this mission requires the use of instruments designed for the Insight mission funded by NASA. Therefore, a collaboration between ESA and NASA would be required. Collaborations are easier to organise when both sides get extra value from it. From this collaboration, ESA would reduce costs and development time. NASA would use the information collected by METEOR to better select their landing sites for future manned missions to Mars planned in the 2030s.

Other services that NASA provide may be requested to help the project. AOCS will make use of the JPL Horizons system for navigation and landing site selection for the mission might require high-resolution imagery provided by the HiRISE camera on the Mars Reconnaissance Orbiter built by NASA.

21.2. Operations and logistic concept description

The METEOR mission will be developed and constructed across different facilities in Europe to accommodate for geographical return[5]. Once all the parts have been assembled, the final integration of the system will be done at ESA ESTEC located in Noordwijk, Netherlands. Once there, the system will be thoroughly tested and once the testing is complete the system will be transported across the Atlantic to Kourou, French Guiana on a plane. Upon arrival, final integration with the Ariane 64 launcher will be performed in preparation for the launch. Table 21.1 shows the different missions phases, from launch until the end of the mission.

[4] `https://www.esa.int/About_Us/Business_with_ESA/How_to_do/Industrial_policy_and_geographical_distribution` retrieved 02/06/2020

[5] `https://www.esa.int/About_Us/Business_with_ESA/How_to_do/Industrial_policy_and_geographical_distribution` retrieved 02/06/2020

Table 21.1: *Mission Phases of the METEOR mission*

Mission Phase	Timeframe
Launch	22/02/2031
Interplanetary Transfer	258 days
Mars Orbital Insertion	07/11/2031
Aerobraking Phase	60 days
Probe Deployment Phase	100 days
Orbit Circularisation	15/04/2032
Instrument Deployment Phase	45 days
Primary Science Phase	3.73 years
Total Mission Duration	5 years

The launch will occur on February 2, 2031 to accommodate the Earth-Mars launch window [6]. At launch, the mission will be operated from the ESA ground stations located in French Guiana, Australia and Sweden as it can be seen in Figure 21.2. However these ground stations do not provide enough data rates when in orbit around Mars, and therefore the spacecraft will start communicating with the Deep Space Network (DSN) during the interplanetary voyage. The aerobraking manoeuvre requires a lot of monitoring as if the attitude or orbital altitude is incorrect, the final orbit might differ significantly from the intended one. Therefore, this manoeuvre cannot be performed when Earth and Mars are in conjunction as it would prevent communication. Fortunately, this is not the case, as conjunction occurs on July 2032 [7]. Therefore, this manoeuvre can be performed upon arrival at Mars, and will require extensive monitoring from the ground station to ensure that it is successfully executed. The monitoring will be provided by the European Space Operations Centre (ESOC) in Germany.

Once the aerobraking phase is completed, the probes can be deployed during the Probe Deployment Phase (PDP). This phase requires extensive monitoring as weather conditions must be monitored for atmospheric entry and the entry protocol can be delayed for some probes in case one were to fail during entry. This phase can last 6 days, however the process can be halted for up to 100 days if a global dust storm is present, given that the probes are unable to land in such conditions. Once the probes have touched down, the instruments have to be deployed. The seismometer can be deployed on sol 1, however, the heat probe will take 24 to 44 sols (25 to 45 days) to reach a depth of three meters and become operational. After the instruments have been deployed, the Primary Science Phase (PSP) can start, and at this point, the operational requirements are reduced. However, a large amount of data will be generated by the probes and therefore this data will have to be stored at one of ESA's eight data centres[8].

21.3. Manufacturing, Assembly and Integration plan

The Manufacturing, Assembly and Integration (MAI) plan can be found in Appendix E. This plan includes the manufacturing of all components that need manufacturing and the assembly & integration of the landers, entry vehicles, orbiter and the launch configuration. Manufacturing of all these components will be done before assembly. The most expensive components or components that require expensive storage will be manufactured closest to the assembly. The manufacturing will be done in batches. This will minimise the inventory at the start of the production. The inventory will gradually be increased during the production. For the assembly, the landers will be assembled first. After the first lander is assembled, the entry vehicle will be assembled and the lander integrated. This will be repeated 11 times for all probes. Following this process will be the assembly of the orbiter. This process will follow a similar approach to that of the lander. Once all the orbiters, landers and entry vehicles have been built they will be assembled in the launch configuration.

[6] `http://clowder.net/hop/railroad/EMa.htm`, retrieved 16/06/2020
[7] `http://www.alpo-astronomy.org/jbeish/2031_MARS.htm`
[8] `https://sci.esa.int/web/cluster/-/33308-mission-operations`, retrieved 15/05/2020

21.4. Return On investment

As with most space missions, this system is designed for a specific purpose: to deliver a global seismic and thermal measurement system to Mars. However, it can be used to perform other functions during and after the mission life time. The return on investment is highlighted in this section. An overview of the expected costs is given in Appendix F

Sustainable Human Presence on Mars

The system will lead to knowledge of the locations of underground water and thermal heat sources on Mars. Finding usable sources of water will greatly increase the possibilities of human travel to the planet. By enabling potable water extraction from the subsurface, missions to Mars can be longer, as astronauts no longer just depend on the water brought from Earth. Moreover, colonisation of the planet will be a step closer. Human settlements require water not only to drink but also to grow food and for many industrial purposes. Moreover, water can be used to generate rocket fuel. Finding underground heat sources makes travel to Mars less dependent on solar power and RTGs. This is a benefit as solar arrays deteriorate significantly over time and RTGs remain radioactive for a very long time. Establishing a colony on Mars will be of incredible scientific value and will ensure the survival of the human race.

Extra functions of the system

Although this system is designed for the purpose of delivering a global seismic and thermal measurement system to Mars, it can performed other functions during and after its life time. During life time, the network of probes can be used as weather station to warn possible inhabitants about the Martian weather or simply return weather data back to Earth. After life time, the orbiter can be used as a communications relay satellite. Moreover, the seismic network can be used for further subsurface exploration. These additional functionalities adds to the mission value and increases the return on investment.

ESA's Lead in Space Exploration

ESA funding this mission is a great endeavour. ESA focuses its resources mostly on Earth observation with a limited presence in the space exploration domain. Now, with the increase in budget in 2019 came great opportunity to change that. ESA's budget for space exploration was increased in 2019 to 1.95 B€ and the budget for science was increase to 1.15 B€ [9] to be spent in the next 3 years. Finding sustainable sources of water and heat on Mars will ensure that ESA leads the next phase of space exploration. Furthermore, leading such an ambitious project will inspire the next generation of scientists and engineers, not only in Europe but worldwide.

[9] http://www.esa.int/About_Us/Corporate_news/ESA_ministers_commit_to_biggest_ever_budget, retrieved on 18/06/2020

22 Conclusion

This report aimed to perform the conceptual design of the previously selected concept [11] while meeting all the requirements [13], and to provide a coherent and complete overview of the total technical and the economic aspects of the mission. The final conceptual design is confirmed to comply with all the requirements. This means the mission can be performed adequately, and water & thermal sources can be located on Mars, paving the way for humans to colonise the planet.

The design consists of eleven landers and one orbiter. The landers have the following characteristics:

- The landers are equipped with triple redundant 3-axis short period seismometers to measure 3.0 magnitude Marsquakes within a radial distance of 60°, enabling the METEOR mission to measure an estimated 214 Marsquakes of magnitude 3.0 or higher per year.
- The landers are spaced such that they form a Global Seismic & Thermal Network, creating a triple or quadruple overlap in the coverage regions of landers to triangulate underground water and thermal sources.
- The landers have a wet mass of 211.5 kg. After the EDL phase, the heat shield and aeroshell are jettisoned. A propulsive landing ensures a soft touchdown of the 145 kg dry mass landers.
- The landers use two 3.0 m^2 unregulated UltraFlex circular solar panels to generate an average 180 W per sol.
- The landers use Electra UHF Transceivers helical antennas to communicate with the orbiter.

The orbiter has the following characteristics:

- The orbiter performs an aerobrake capture manoeuvre to get into a stable Martian orbit.
- The orbiter has two 5.5 m^2 circular solar panels to generate an average 682 W per sol.
- The orbiter is equipped with a similar UHF architecture as the landers to communicate between lander & orbiter. Also the orbiter features an X-band gimballed High Gain Antenna to communicate with the DSN.

The risks that jeopardise the successful completion of the METEOR mission are assessed and mitigation strategies have been conceived. The mission will be proposed for the ESA M-class mission call. This gives very strict limitations on the budget, which cannot exceed 550 Million EUR. The budget required to successfully execute the mission is 440 Million EUR. Which means the mission is 20% under budget. As part of the sustainability plan, at the end of the mission, there are opportunities for a mission extension or the hardware can be repurposed. The orbiter can be repurposed as a communications relay satellite, while the probes can serve as weather stations to warn the Martian colonists about incoming weather.

Bibliography

[1] NASA/JPL-Caltech. Valles marineris: The grand canyon of mars, July 2013. https://solarsystem.nasa.gov/resources/683/valles-marineris-the-grand-canyon-of-mars/.

[2] *NASA facts - Mars Science Laboratory/Curiosity*. Jet Propulsion Laboratory - California Institute of Technology, Pasadena, California, jpl 400-1537 edition, February 2018.

[3] Horneck, G. Astrobiological aspects of mars and human presence: Pros and cons. *Hippokratia*, 12(Suppl 1)(PMC2577400):49–52, August 2008.

[4] *NASA facts - InSight Into the Early Evolution of Terrestrial Planets*. Jet Propulsion Laboratory - California Institute of Technology, Pasadena, California, October 2018.

[5] Yuen, J. Deep space communications - an introduction. Technical report, Pasadena California, 2016.

[6] Williams, D. and Shaw, M. A crewed mission to mars..., September 2015. https://nssdc.gsfc.nasa.gov/planetary/mars/marswhy.html.

[7] Near earth orbit earth close approaches, June 2020. https://cneos.jpl.nasa.gov/ca/.

[8] Lyne, J. and M.Tauber. Origin of the tunguska event. *Nature*, 375:638–639, June 1995.

[9] Gritzner, C. Human casualties in impact events. *Journal of the International Meteor Organisation*, 25: 222–226, October 1997.

[10] G.Longo. *18: The Tunguska Event, Comet/Asteroid Impacts and Human Society, An Interdisciplinary Approach*. Sprigner, October 2007.

[11] Beumer, M., Bolscher, A., Enting, M., Kanger, M., Khalifa, M., Maiorano, L., Na, D., Soliman, E., Tagliacarne, F., van Wissen, A., and Zafiropoulos, A. Midterm report mars reveal. Technical report, Delft, The Netherlands, May 2020.

[12] Beumer, M., Bolscher, A., Enting, M., Kanger, M., Khalifa, M., Maiorano, L., Na, D., Soliman, E., Tagliacarne, F., van Wissen, A., and Zafiropoulos, A. Project plan mars reveal. Technical report, Delft, The Netherlands, April 2020.

[13] Beumer, M., Bolscher, A., Enting, M., Kanger, M., Khalifa, M., Maiorano, L., Na, D., Soliman, E., Tagliacarne, F., van Wissen, A., and Zafiropoulos, A. Baseline report mars reveal. Technical report, Delft, The Netherlands, May 2020.

[14] Debelak, K. and Roth, J. Recovery of minerals in martian soils via supercritical fluid extraction. page 164, 02 2001.

[15] Sergio, E. and Pascal, L. Fog on mars: Potential implications for water extraction from the martian atmosphere. In *49th Lunar and Planetary Science Conference 2018*, volume 2083, Texas, 2018.

[16] Messina, P., Gardini, B., Sacotte, D., and DiPippo, S. The aurora programme - europe's framework for space exploration. Technical report, may 2016.

[17] Arianespace. *Ariane 6 User's Manual*. Arianegroup, Moulineaux, France, 1 edition, March 2018.

[18] Harri, A., Schmidt, W., Linkin, V., Alexashkin, s., and Vázquez, L. New lander generation for martian in situ surface observations. In *MetNet Mars Mission*, volume 7, 2012.

[19] Austin, J. Developing a standardised methodology for space-specific life cycle assessment. In *CEAS2015*, pages 228–231, 52 Rue Jacques Hillairet Paris 75012, 2015.

[20] Sinke, J. Lecture notes ae3211-ii: Production of aerospace systems, 2020.

[21] Nageswara, P. Sustainable manufacturing: Principles, applications and directions. *Efficient Manufacturing*, May 2018.

[22] Kminek, G., Conley, C., Hipkin, V., and Yano, H. *COSPAR's Planetary Protection Policy*. COSPAR, December 2017.

[23] Wertz, J. and Larson, W. *Space Mission Analysis and Design*. Microcosm Press and Kluwer Academic Publishers, 401, Coral Circle, El Segundo, CA 90245-4622 USA and 101, Philip Drive, Norwell, MA 02061 USA, 3 edition, 2005.

[24] Astrogeology. Mars MGS MOLA Global Color Shaded Relief 463m v1. USGS Astrogeology Science

Center, Goddard Space Flight Center, NASA, February 2014.

[25] Banerdt, W., Smrekar, S., Banfield, D., Giardini, D., Golombek, M., Johnson, C., Lognonné, P., Spiga, A., Spohn, T., Perrin, C., Stähler, S., Antonangeli, D., Asmar, S., Beghein, C., Bowles, N., Bozdag, E., Chi, P., Christensen, U., Clinton, J., and Wieczorek, M. Initial results from the insight mission on mars. *Nature Geoscience*, 13:1–7, 02 2020. doi: 10.1038/s41561-020-0544-y.

[26] Steven W. Ruff, P. R. C. Bright and dark regions on mars: Particle size and mineralogical characteristics based on thermal emission spectrometer data. *Journal of Geophysical Research*, VOL. 107(NO. E12), December 2002.

[27] Golombek, M., Kipp, D., and Warner, N. Selection of the insight landing site. *Space Science Reviews*, December 2016.

[28] S. A. Nowicki, P. R. C. Rock abundance on mars from the thermal emission spectrometer. *AGU Journals*, May 2007.

[29] Christensen, P., Engle, E., Anwar, S., Dickenshied, S., Noss, D., Gorelick, N., and Weiss-Malik, M. JMARS – A Planetary GIS, February 2014. URL `http://adsabs.harvard.edu/abs/2009AGUFMIN22A..06C`.

[30] NASA. Interactive Mars Data Maps. URL `https://marsoweb.nas.nasa.gov/globalData/`.

[31] Paris-Sud, E. Mars hydrated mineral map. Online ESA webpage on Mars exploration, september 2019. https://sci.esa.int/web/mars-express/-/51857-mars-hydrated-mineral-map.

[32] Wookey, N. T. Seismic detection of meteorite impacts on mars. *Physics of the Earth and Planetary Interiors*, Volume 186, Issues 1–2:Pages 70–80, May 2011.

[33] Hirise. `https://mars.nasa.gov/mro/mission/instruments/hirise/`.

[34] Ctx. `https://mars.nasa.gov/mro/mission/instruments/ctx/`.

[35] Logonné, P., Banerdt, W., and Giardini, D. Seis: Insight's seismic experiment for internal structure of mars. *Space Science Reviews*, 215(12), December 2019.

[36] Giardini, D., Lognonné, P., and Banerdt, W. e. a. The seismicity of mars. *Nature Geoscience*, March 2020.

[37] Spohn, T., Grott, M., Smrekar, S., Knollenberg, J., Hudson, T., Krause, C., Müller, N., Jänchen, J., Börner, A., Wippermann, T., Krömer, O., Lichtenheldt, R., Wisniewski, L., Grygorczuk, J., Fittock, M., Rheershemius, S., Spröwitz, T., Kopp, E., Walter, I., Plesa, A., Breuer, D., Morgan, P., and Banerdt, W. The heat flow and physical properties package (hp^3) for the insight mission. *Space Science Review*, 214(5), August 2018.

[38] Banfield, D., Rodriguez-Manfredi, J., Russel, C., and et. al. Insight auxiliary payload sensor suite (apss). *Space Science Reviews*, 215(4), December 2019.

[39] *Spacecraft Systems Engineering*. A John Wiley & Sons, Ltd, John Wiley & Sons Ltd, The Atrium, Southern Gate, Chichester, West Sussex, PO19 8SQ, United Kingdom, fourth edition, 2011. ISBN 9780470750124.

[40] *Materials: Engineering, Science, Processing and Design*. Butterworth-Heinemann, Butterworth-Heinemann Elsevier Ltd, Oxford, United Kingdom, third edition, 2014. ISBN 9780080977720.

[41] Wijker, J. *Spacecraft Structures*. Dutch Space BV, NL-2303 DB Leiden, The Netherlands, 2008.

[42] Fridlyander, J. *Metal Matrix Composites*. Springer International Publishing, first edition, 1996. ISBN 9789401045520.

[43] Zandbergen, B. *Aerospace Design & Systems Engineering Elements I Part: Spacecraft (bus) design and sizing*. Faculty of Aerospace Engineering - Delft University of Technology, P.O. Box 50302600 GB Delft, The Netherlands, August 2017.

[44] Herrera-Arroyave, J., Pérez, J., Colín, A., and Bermúdez-Reyes, B. Cubesat system structural design. page 4. International Astronautical Federation, May 2017.

[45] Patel, R., Riveros, G., Thompson, D., Perkins, E., Hoover, J., Peters, J., and Tordesillas, A. A transdisciplinary approach for analyzing stress flow patterns in biostructures. *Mathematical and Computational Applications*, April 2019.

[46] Rans, C. and Melkert, J. Ae2135-i structural analaysis & design. Online Delft University of Technology BrightSpace, January 2019.

[47] Tam, K. G., W.H. Design and manufacture of a propellant tank assembly. *American Institute of Aero-*

nautics and Astronautics, August 2016.

[48] Ball, A., Garry, J., Lorenz, R., and Kerzhanovich, V. *Planetary Landers and Entry Probes*. Cambridge University Press, The Edinburgh Building, Cambridge CB2 8RU, UK, 2009.

[49] Lockheed Martin. Ablative heat shield materials. Print, Bethesda, MD 20817 U.S.A, 1996.

[50] Zhang, Z., Martin, N., Wrist, A., and Hubner, J. Geometry and prestrain effects on the aerodynamic characteristics of batten-reinforced membrane wings. *Journal of Aircraft*, 2(53), August 2015.

[51] Biswal, M. and Naidu, R. A novel entry, descent and landing architecture for mars landers. *Department of Physics, Pondicherry University, Puducherry*, September 2018.

[52] Zipay, J., Modlin, T., and Laren, C. The ultimate factor of safety for aircraft and spacecraft – its history, applications and misconceptions. *NASA Engineering and Safety Center*, 2016.

[53] Calle, M. Corrosion on mars: Effect of the mars environment on spacecraft materials. *NASA Kennedy Space Center*, June 2019.

[54] Alhammadi, A., Al-Shaibah, M., Almesmari, A., Vu, T., Tsoupos, A., Jarrar, F., and Marpu, P. Quasi-static and dynamic response of a 1u nano-satellite during launching. *European Conference for Aeronautics and Space Sciences*, July 2019.

[55] Fortescue, P., Swinerd, G., and Stark, J. *Spacecraft Systems Engineering*. John Wiley & Sons Ltd., John Wiley & Sons Ltd, The Atrium, Southern Gate, Chichester, West Sussex, PO19 8SQ, United Kingdom, fourth edition, 2011.

[56] Long, S. M., You, T.-H., Halsell, C. A., Bhat, R. S., Demcak, S. W., Graat, E. J., Higa, E. S., Highsmith, D. E., Mottinger, N. A., and Jah, M. K. Mars reconnaissance orbiter aerobraking daily operations and collision avoidance. 2007.

[57] Lyons, D. Mars reconnaissance orbiter: aerobraking reference trajectory. In *AIAA/AAS Astrodynamics Specialist Conference and Exhibit*, page 4821, 2002.

[58] Guilanya, R. and Companys, V. Operational approach for the exomars aerobraking. In *23rd International Symposium on Space Flight Dynamics (ISSFD)*, 2012.

[59] *Mars Global Reference Atmospheric Model 2000 Version (Mars-GRAM 2000): Users Guide*. NASA, May 2000.

[60] Haynes, W., Lide, D., and Bruno, T. *CRC Handbook of Chemistry and Physics*. CRC Press, Boca Raton, FL, 97 edition, 2017.

[61] Brown, C. D. *Elements of Spacecraft Design*, chapter Attitude Control. AIAA, 2002.

[62] A. Ball, R. L., J. Garry and Kerzhanovich, V. *Planetary Landers And Entry Probes*. Cambridge University Press, The Edinburgh Building, Cambridge CB2 8RU, UK, isbn-13 978-0-511-28461-8 edition, 2007.

[63] Justus, C. G. and Braun, R. D. Atmospheric environments for entry, descent and landing (edl). 2007.

[64] Grover III, M. R., Cichy, B. D., and Desai, P. N. Overview of the phoenix entry, descent, and landing system architecture. *Journal of Spacecraft and Rockets*, 48(5):706–712, 2011.

[65] R.Cruz and Stephen, J. Aerodynamic decelerators for planetary exploration: past, present, and future. In *AIAA Guidance, Navigation, and Control Conference and Exhibit*, page 6792, 2006.

[66] Otero, R. E. and Braun, R. D. The planetary entry systems synthesis tool: A conceptual design and analysis tool for edl systems. In *2010 IEEE Aerospace Conference*, pages 1–16, 2010.

[67] Grover III, M. R., Cichy, B. D., and Desai, P. N. Overview of the phoenix entry, descent, and landing system architecture. *Journal of Spacecraft and Rockets*, 48(5):706–712, 2011.

[68] Folkner, W. M. and Border, J. S. Linking the planetary ephemeris to the international celestial reference frame. *Proceedings of the International Astronomical Union*, 10(H16):219–220, 2012. doi: 10.1017/S1743921314005493.

[69] You, T., Graat, E., Halsell, A., Highsmith, D., Long, S., Bhat, R., Demcak, S., Higa, E., Mottinger, N., and Jah, M. Mars reconnaissance orbiter interplanetary cruise navigation. 2007.

[70] Brugarolas, P. B., San Martin, A. M., and Wong, E. C. Entry attitude controller for the mars science laboratory. In *2007 IEEE Aerospace Conference*, pages 1–6. IEEE, 2007.

[71] Portock, B., Kruizinga, G., Bonfiglio, E., Raofi, B., and Ryne, M. Navigation challenges of the mars phoenix lander mission. In *AIAA/AAS Astrodynamics Specialist Conference and Exhibit*, page 7214, 2008.

[72] San Martin, A. M., Lee, S. W., and Wong, E. C. The development of the msl guidance, navigation, and

control system for entry, descent, and landing. 2013.

[73] Brugarolas, P. B., San Martin, A. M., and Wong, E. C. The rcs attitude controller for the exo-atmospheric and guided entry phases of the mars science laboratory. In *International planetary probe workshop*, 2010.

[74] Leonardo Airborne & Space Systems. A-STR amd AA-STR Star Trackers. Digital pdf, Campi Bisenzio, Italy, 2017.

[75] Honeywell Aerospace Electronic Systems. Constellation series reaction wheels. Electronic pdf, Phoenix, Arizona, dec 2003.

[76] Dyakonov, A., Schoenenberger, M., Scallion, W., Van Norman, J., Novak, L., and Tang, C. Aerodynamic interference due to msl reaction control system. In *41st AIAA Thermophysics conference*, page 3915, 2009.

[77] Ornella, B. *Planetary Radars Course*. Thales Alenia Space, L'Aquila, Italy, sep 2016.

[78] Lee, S. and Skulsky, E. Mars reconnaissance orbiter design approach for high-resolution surface imaging. 2003.

[79] Makovsky, A., Ilott, P., and Taylor, J. Descanso design and performance summary series - mars science laboratory telecommunications system design. Technical report, Pasadena, California, November 2009.

[80] Taylor, J., Lee, D., and Shambayati, S. Descanso design and performance summary series - mars reconnaissance orbiter telecommunications. Technical report, Pasadena, California, September 2006.

[81] Demircioglu, E. and Nefes, M. Reliability-Based TT&C Subsystem Design Methodology for Complex Spacecraft Missions. Konya Yolu 40.km Golbasi/Ankara 06839 TURKEY, March 2008.

[82] Ziemer, R., Tranter, W., and Fannin, D. *Signals and systems: Continuous and Discrete*. Prentice Hall, upper saddle River, NJ 07458, 4 edition, 1998.

[83] Tiberius, C. *Signal modulation and detection*. Faculty of Aerospace Engineering - Delft University of Technology, P.O. Box 50302600 GB Delft, The Netherlands, May 2015.

[84] Tavokkoli-Moghaddam, R., Safari, J., and Sassani, F. Reliability optimization of series-parallel systems with a choice of redundancy strategies using a genetic algorithm. *Reliability Engineering & System Safety*, 93:7, March 2007.

[85] Amiri, S. and Mehdipour, M. Accurate doppler frequency shift estimation for any satellite orbit. *3rd International Conference on Recent Advances in Space Technologies - Istanbul, Turkey.*, 2007.

[86] Hastrup, R. and Morabito, D. Communicating with mars during periods of solar conjunction. March 2002.

[87] Taylor, J., Butman, S., Edwards, C., Ilott, P., Kornfeld, R., Lee, D., Shaffer, S., and G.Signori. Phoenix telecommunications. *Design and Performance Summary Series*, page 32, August 2010.

[88] Tan, L. and Jiang, J. *Digital Signal Processing: Fundamentals and Applications*, volume 1. Elsevier B.V., 3 edition, 2019.

[89] RUAG Space. Next generation on board computer. Print, Switzerland, Schaffhauserstrasse 580, 8052 Zurich, May 2019.

[90] Wong, W. and Zhu, T. *Computer Engineering and Networking, Proceedings of the 2013 International Conference on Computer Engineering and Network (CENet2013)*, volume 1. Springer International Publishing, 1 edition, 2014.

[91] Tan, L. and Jiang, J. *The TCP/IP GUIDE*. William Pollock, 2 edition, 2005.

[92] Bae Systems. RAD750 radiation-hardened PowerPC microprocessor. Print, 9300 Wellington Road, Manassas, Virginia, 20110-4122, Jan 2019.

[93] Joseph Appelbaum, D. J. F. Solar radiation on mars. 1990.

[94] Jet Propulsion Laboratory. Solar power technologies for future planetary science missions. Technical Report JPL D-101316, Pasadena, Dec 2017.

[95] Jet Propulsion Laboratory. Energy storage technologies for future planetary science missions. Technical Report JPL D-101146, Pasadena, Dec 2017.

[96] Isidoro, M. Spacecraft thermal modelling and testing. Online Polytechnic University of Madrir Webserver, 2020. Document explaining spacecraft thermal modelling and testing.

[97] Gilmore, D. *Spacecraft Thermal Control Handbook*, volume 1. The Aerospace Press, 2350 E. El Se-

gundo Boulevard, El Segundo, California 90245-4691, 2 edition, December 2002.

[98] Relch, G. and Scoon, G. E. N. Thermal environment and thermal control aspects for mars landers. Technical report, 400 Commonwealth Drive, Warrendale, PA 15096-0001 USA, 1993.

[99] Spencer, D. and Tolson, R. Report on the loss of the mars polar lander and deep space 2 missions. *Aerobraking Cost/Risk Decisions*, page 2, March 2000.

[100] International space law: United nations instruments, May 2017. `https://www.unoosa.org/res/oosadoc/data/documents/2017/stspace/stspace61rev_2_0_html/V1605998-ENGLISH.pdf`.

[101] *Technology readiness level (TRL) guidelines*. European Cooperation for Space Standardization, ESTEC, P.O. Box 299, 2200 AG Noordwijk, The Netherlands, 1 edition, March 2017.

[102] Dougherty, M., Esposito, L., and Krimigis, S. *Saturn from Cassini-Huygens*. Springer, New York, 2009.

[103] Weck, O. and Willcox, K. *Multidisciplinary System Design Optimization (MSDO): Gradient Calculation and Sensitivity Analysis Lecture*. Massachusetts Institute of Technology: MIT, esd.77 edition, 2010.

A Functional Flow Diagram

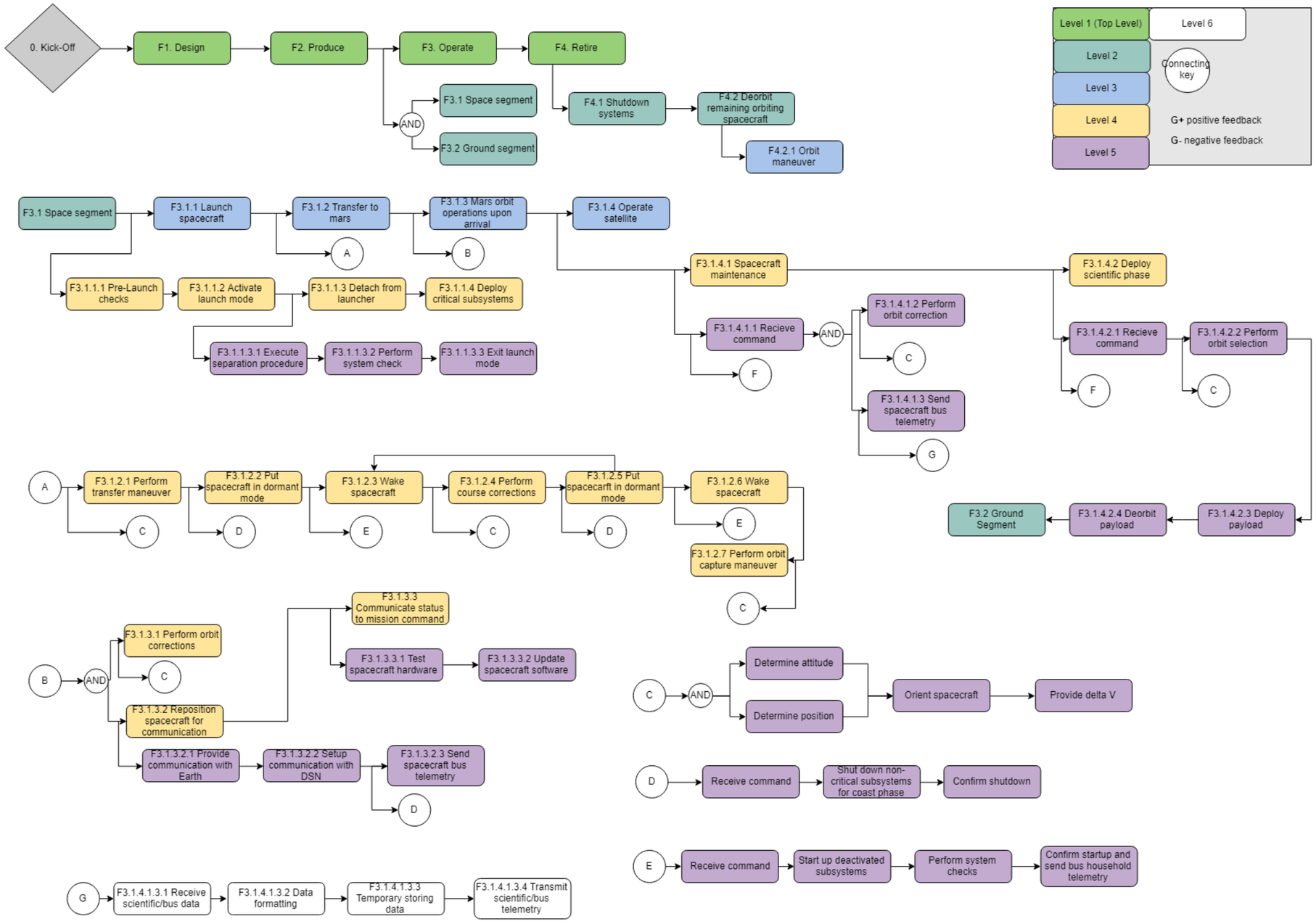

Figure A.1: *The Functional Flow Diagram*

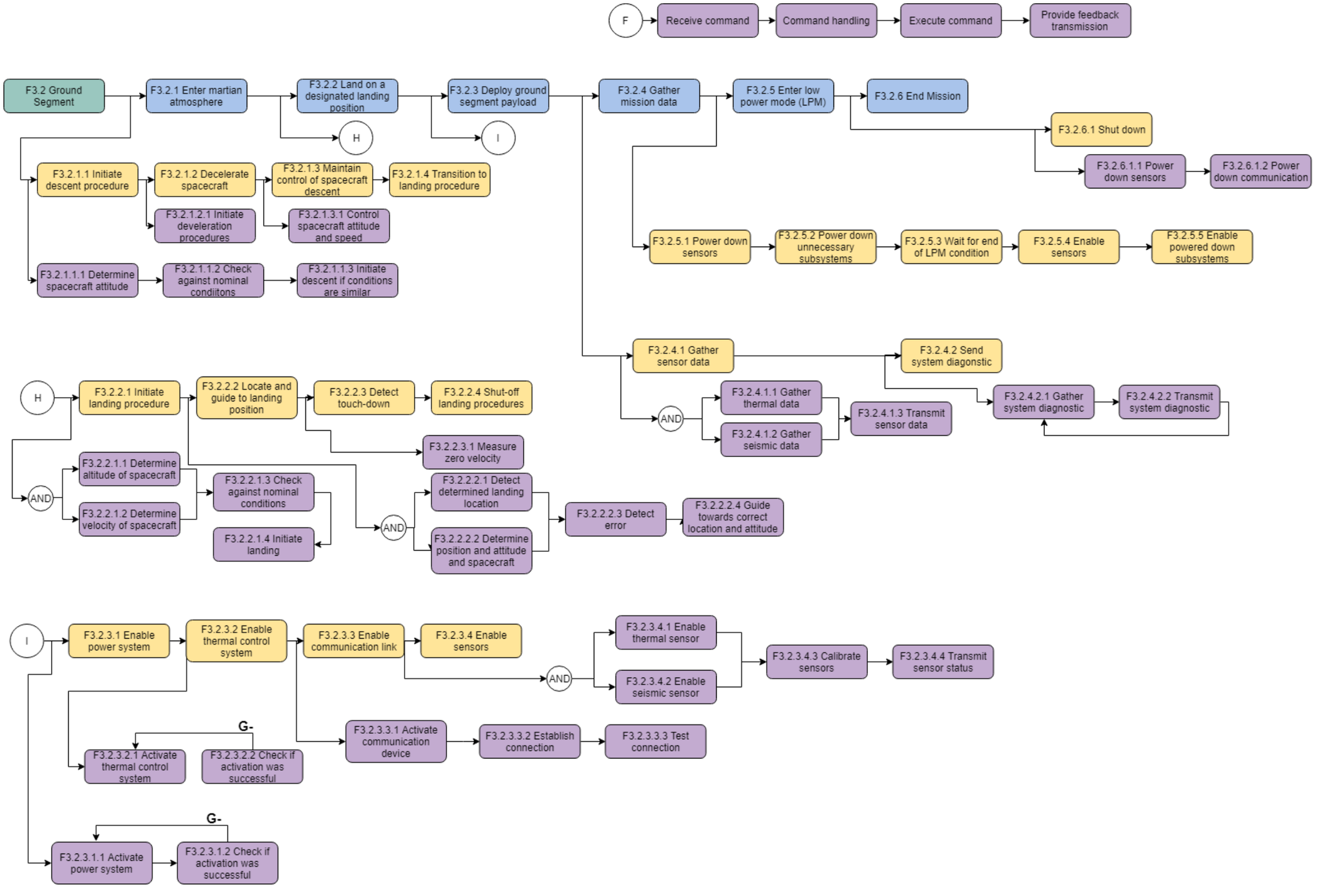

Figure A.2: *The Functional Flow Diagram*

B Functional Breakdown Structure

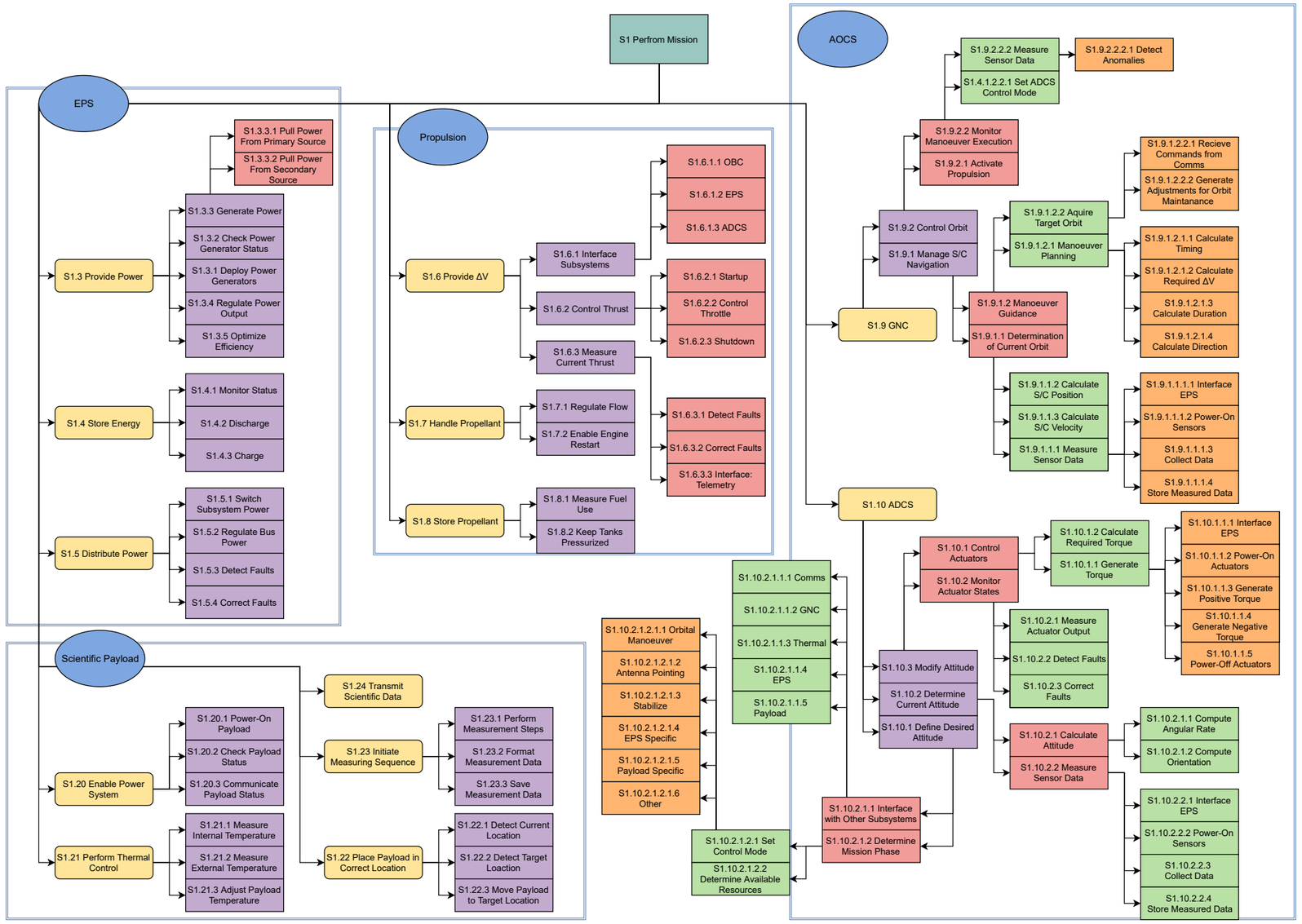

Figure B.1: *The Functional Breakdown Structure*

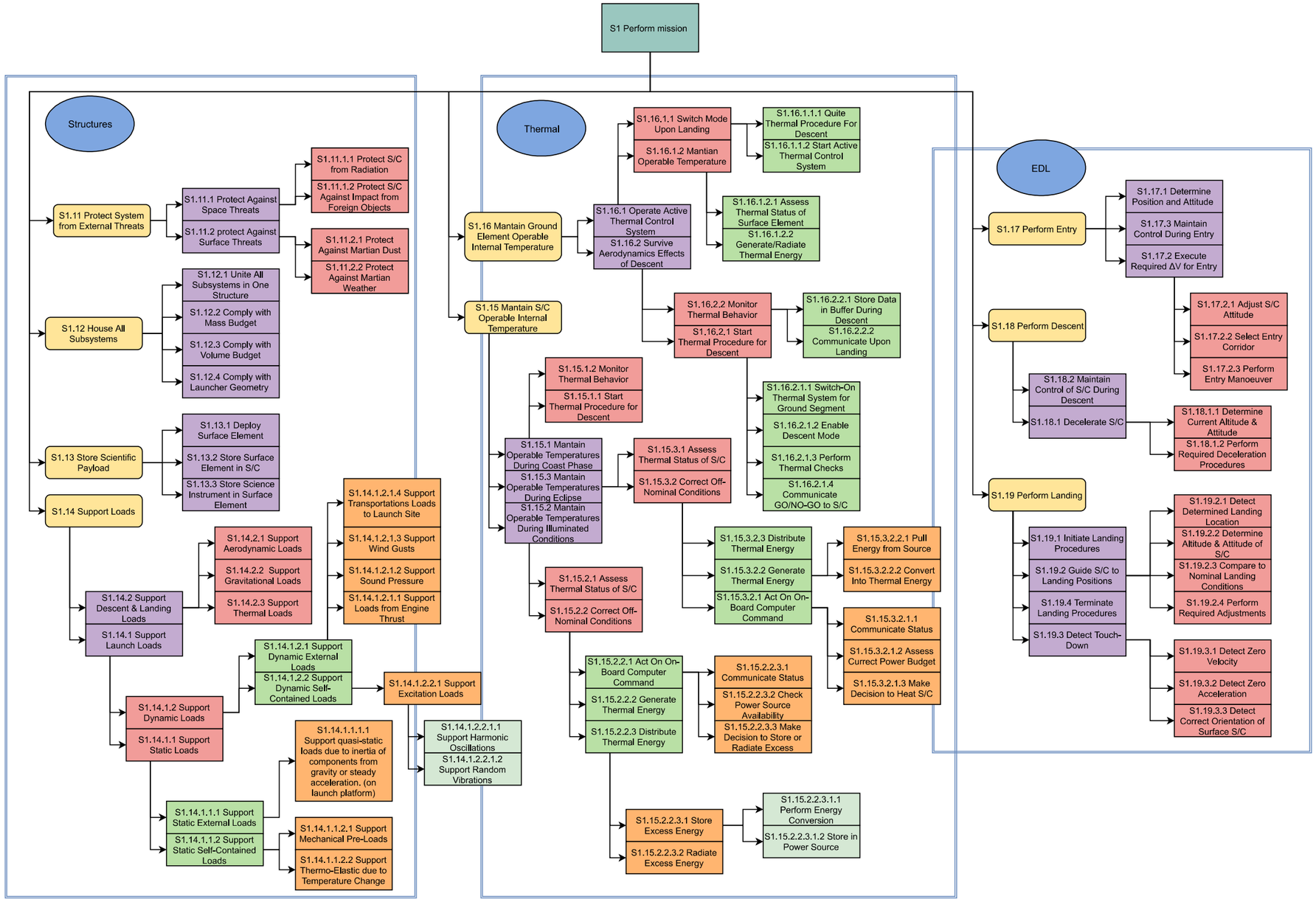

Figure B.2: *The Functional Breakdown Structure*

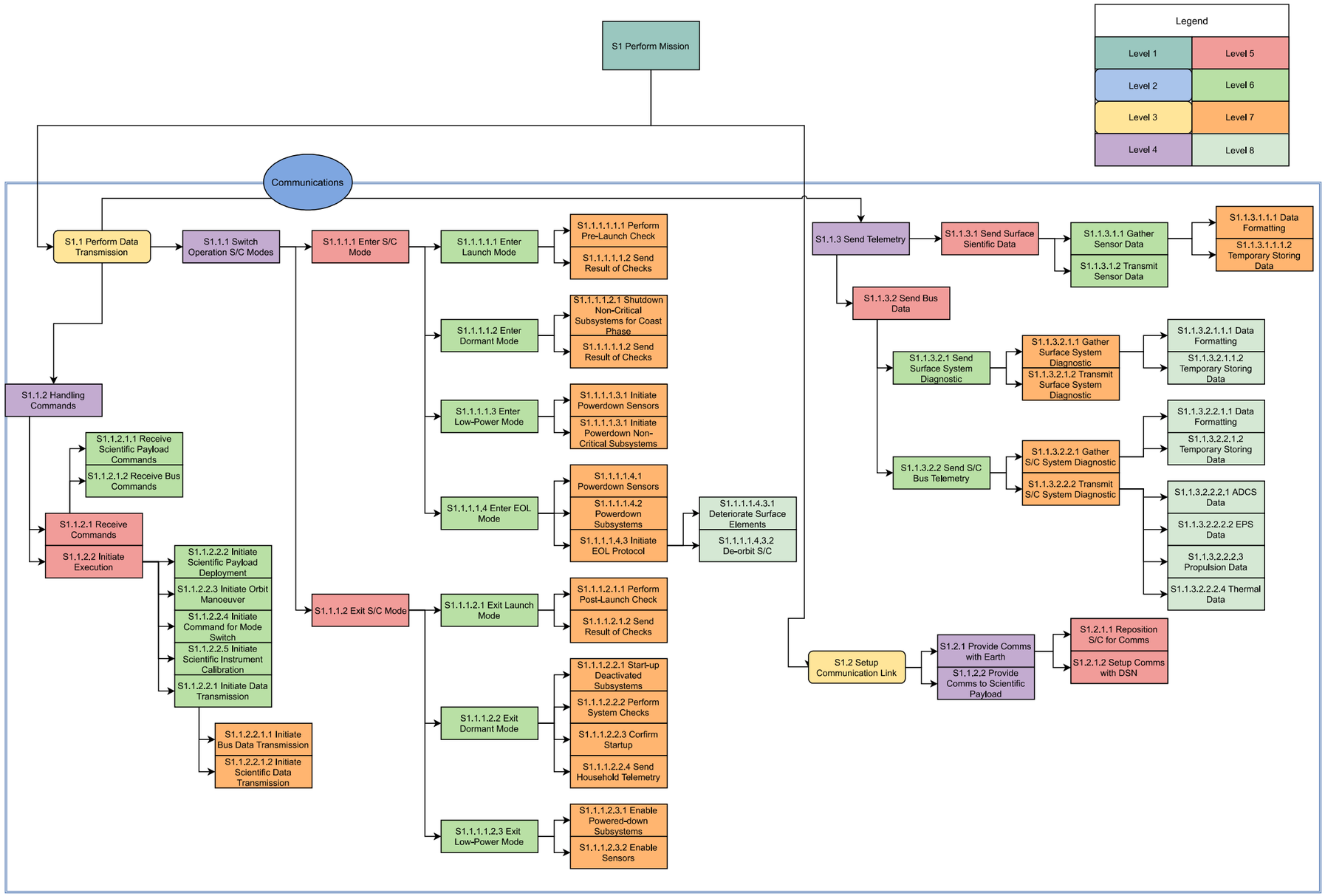

Figure B.3: *The Functional Breakdown Structure*

C High resolution CTX images of 11 landing ellipses

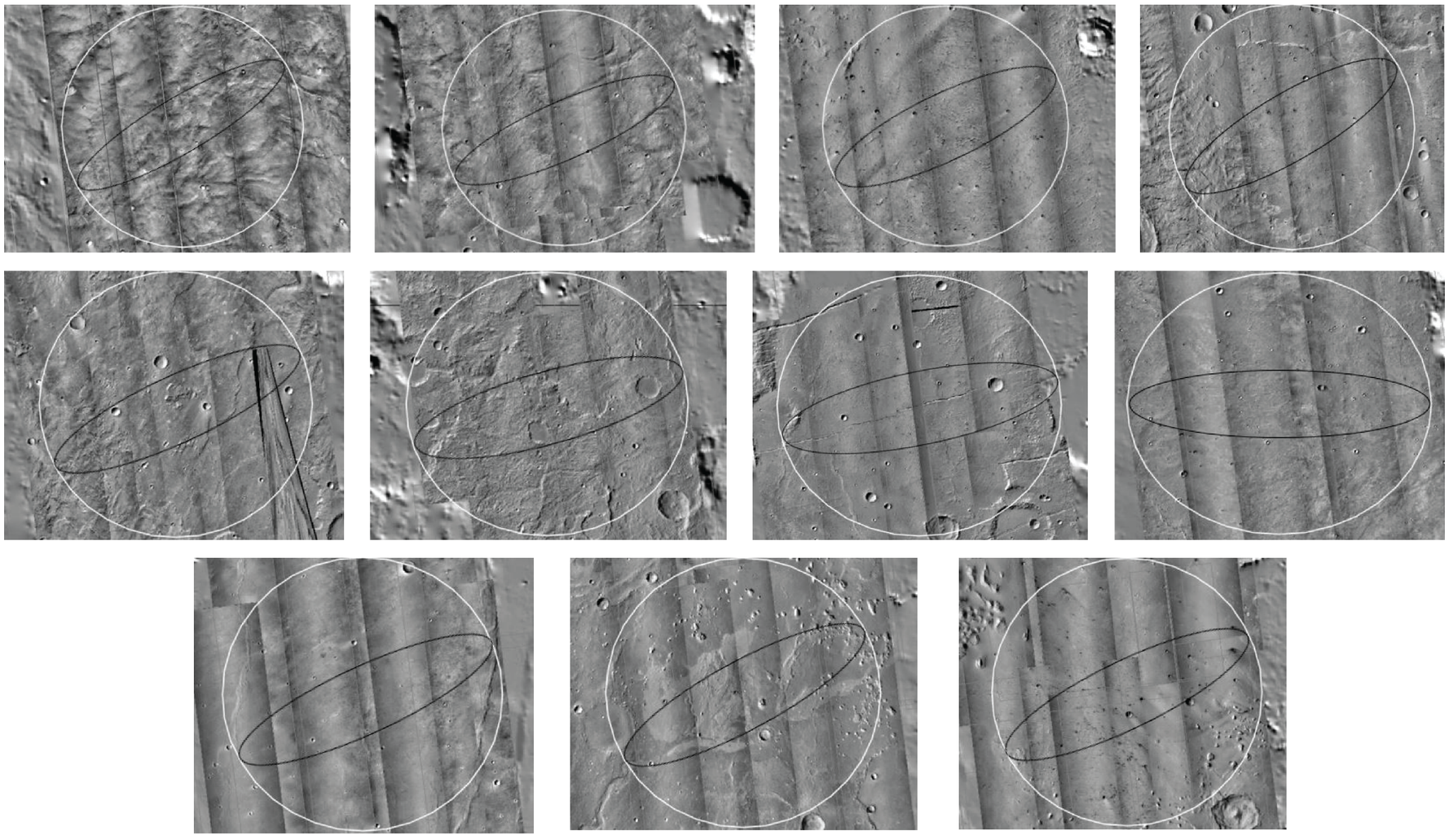

Figure C.1: *From left to right and top to bottom the eleven landing ellipses on the surface of Mars*

D Post DSE Gantt Chart

ID	Task Mode	Task Name	Duration	Start	Finish	Predecessors
1		Phase A	73,38 days	Mon 20-4-20	Thu 2-7-20	
2		**Phase B**	**2008 days**	**Thu 2-7-20**	**Wed 31-12-25**	
3		Preliminary Design	912 days	Thu 2-7-20	Sat 31-12-22	1
4		Detailed Design	1095 days	Sun 1-1-23	Wed 31-12-25	3
5		M-Class Proposal Deadline	0 days	Wed 31-12-25	Wed 31-12-25	4
6		**Phase C**	**1096 days**	**Wed 31-12-25**	**Sun 31-12-28**	
7		Building Models	9 mons	Wed 31-12-25	Mon 29-6-26	4
8		Testing Models	24 mons	Mon 29-6-26	Fri 22-10-27	7
9		Building Qualification Models	9 mons	Fri 22-10-27	Wed 19-4-28	8
10		Testing Qualification Models	12 mons	Fri 5-5-28	Sun 31-12-28	9
11		**Phase D**	**751 days**	**Sun 31-12-28**	**Tue 21-1-31**	
12		Flight Model	152,38 days	Sun 31-12-28	Sat 2-6-29	10
13		Testing Flight Model	598 days	Sat 2-6-29	Tue 21-1-31	12
14		**Phase E**	**1857 days**	**Wed 22-1-31**	**Fri 22-2-36**	
15		Launch Preparations	30 days	Wed 22-1-31	Fri 21-2-31	13
16		Launch	0 days	Sat 22-2-31	Sat 22-2-31	15
17		Interplanetary Transfer	258 days	Sat 22-2-31	Fri 7-11-31	16
18		Aerobraking Phase	60 days	Fri 7-11-31	Tue 6-1-32	17
19		Probe Deployment Phase	100 days	Tue 6-1-32	Thu 15-4-32	18
20		Orbit Circularization	0 days	Thu 15-4-32	Thu 15-4-32	19
21		Instrument Deployment	45 days	Thu 15-4-32	Sun 30-5-32	20
22		Probe Deployment Phase	1362 days	Mon 31-5-32	Fri 22-2-36	21

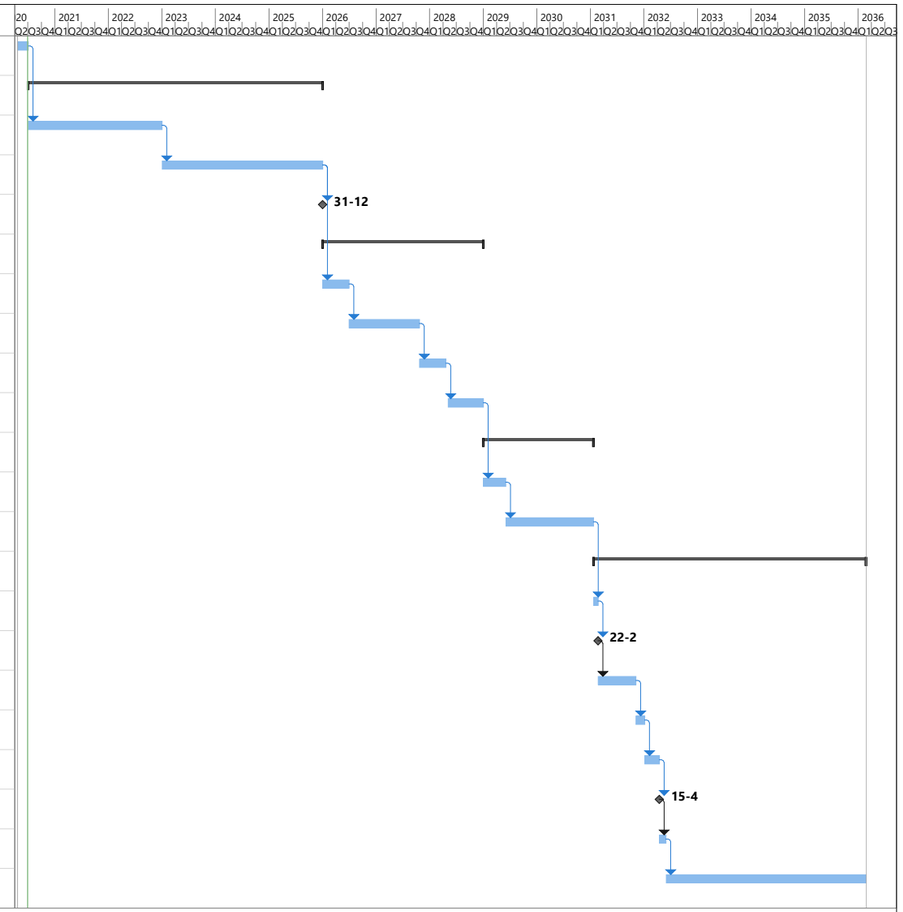

Project: PostDSE_final
Date: Tue 30-6-20

Task	Project Summary	Manual Task	Start-only	Deadline	
Split	Inactive Task	Duration-only	Finish-only	Progress	
Milestone	Inactive Milestone	Manual Summary Rollup	External Tasks	Manual Progress	
Summary	Inactive Summary	Manual Summary	External Milestone		

Page 1

Figure D.1: *Gantt chart for post DSE activities*

E Manufacturing, Assembly and Integration

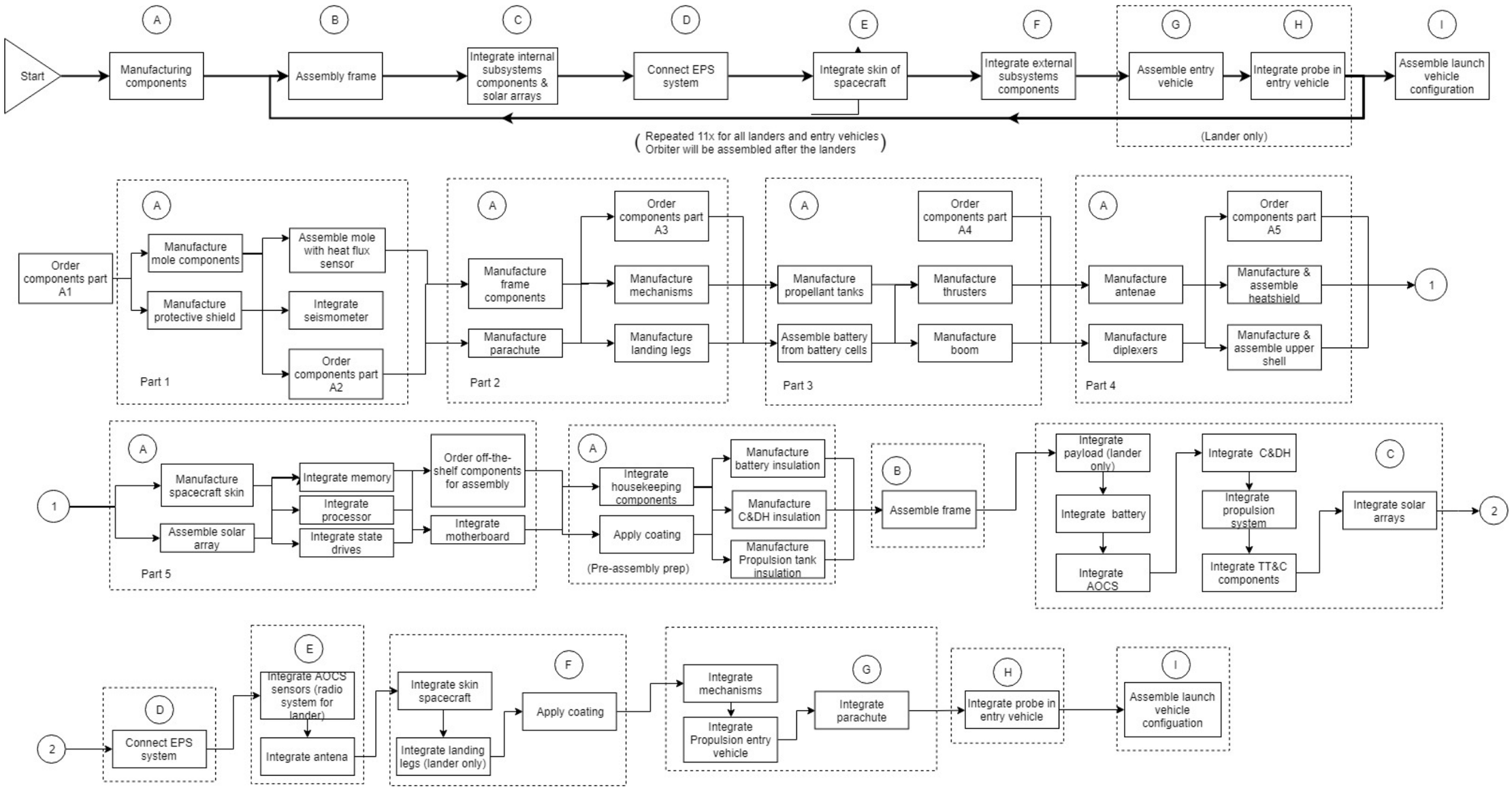

Figure E.1: *The Manufacturing, Assembly and Integration plan for both the lander and orbiter.*

F Cost breakdown structure

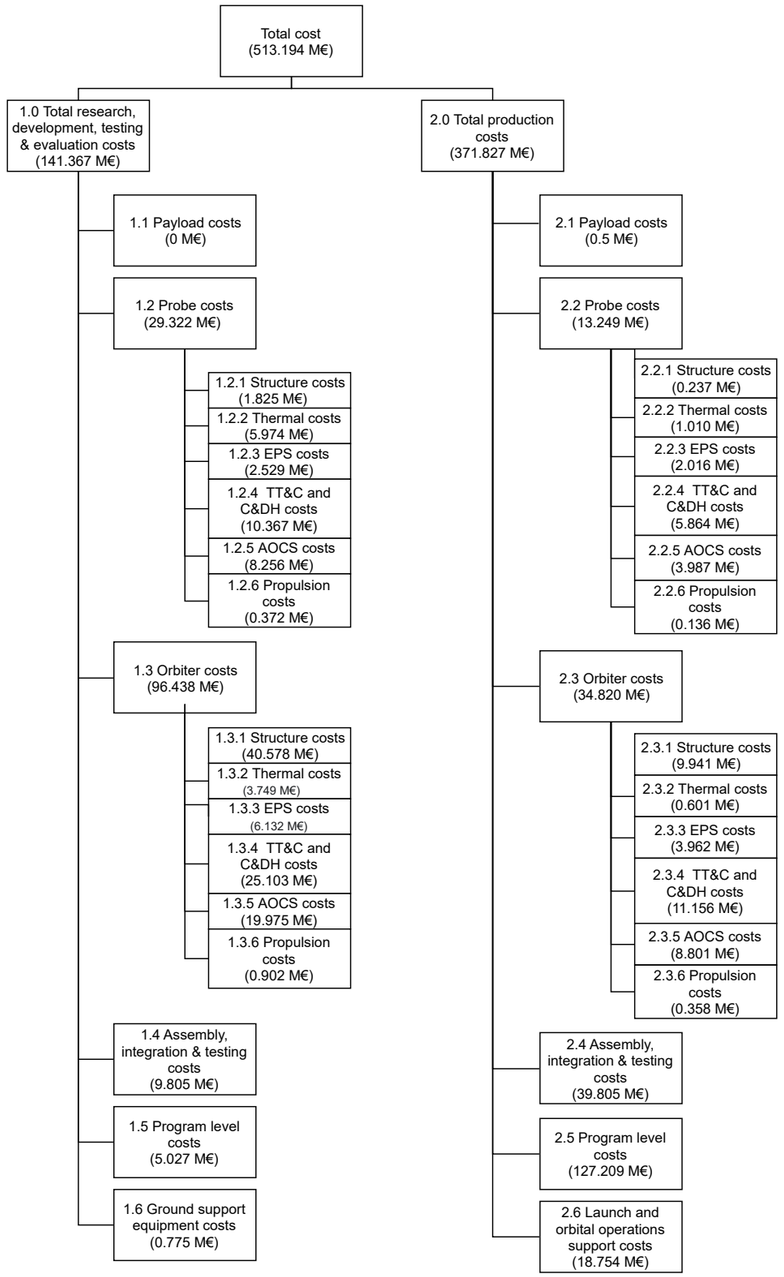

Figure F.1: *Cost breakdown structure of the product*